University of London

University College London

Mechanical Engineering Department

HUMAN INDUCED LOADING ON STAIRCASES

Stuart C. Kerr

Submission for Doctorate of Philosophy

1998

Abstract

Over the last decade it has become increasingly popular to provide large public areas with gracefully designed "flexible" staircases. One inherent characteristic of this type of construction is a low stiffness to mass ratio and hence a low natural frequency when compared to more traditional designs. A number of staircases have been found to be dynamically responsive to pedestrian traffic resulting in costly repairs. The objective of this thesis was to investigate the differences between human induced loading on floors with that on stairs.

Experimental work carried out on a purpose built staircase showed that forces up to 3 times the static body weight were generated during fast descents while forces up to 2.5 times the static body weight were generated during fast ascents. The work also showed that first harmonic values generated while ascending were slightly higher than for descending whilst second harmonic values were up to 3 times greater for fast descents than for fast ascents. When compared with floor testing, stair testing produced first harmonic values nearly 2.5 times greater with second, third and fourth harmonic values nearly 3 times greater. The harmonic results for the flat testing were also incorporated into a new mathematical expression to predict peak accelerations on simply supported floors and footbridges.

The experimental results were duplicated analytically by developing a computer program to calculate the vertical ground reaction forces from body segment positional data. Following a Newtonian approach, the predicted first harmonic values were 20% to 30% lower than actual while the second harmonic values were approximately the same. Monte Carlo simulation techniques were also used to model the effects of group loading on stairs. The simulations predicted enhancement factors (a multiplier on single subject loading) of 3 to 6 for smaller groups(< 9 people) and 4 for larger groups(> 25 people).

If the experimental/analytical results are combined with the group loading predictions, the harmonic values for groups ascending or descending flexible staircase could be substantially increased. These results demonstrate that loading data from floors is highly inappropriate for staircase design.

Acknowledgements

The author wishes to acknowledge and thank Dr. N.W.M. Bishop for his advice and guidance throughout the preparation of this thesis. The author also wishes to acknowledge and thank Dr. D. Brown, Dr. A. Halfpenny, Dr. R. Pumphrey, Dr. R. Wang, the RA's from G18, Andy at Stanmore, and all the students and staff who walked, ran, jumped and sometimes crawled through miles for force plate testing. Finally, the author wishes to thank Betty-Anne for her love, support, and understanding over the past 4 years.

Table of Contents

List of Figures

List of Tables

CHAPTER ONE 1

PREVIOUS WORK

1 THE NEED TO INVESTIGATE HUMAN INDUCED LOADING ON STAIRCASES

Many vibration textbooks published in the last 40 years make reference to the Tacoma Narrows Bridge collapse. The structure failed, in part, due to vortex shedding from wind blowing over the side of the bridge. Also referenced is the collapse of the Broughton Bridge in 1831 as 60 soldiers crossed the bridge marching in unison. The soldiers had unfortunately excited the natural frequency of the bridge causing excessive oscillations and eventually total failure. Hence, the message found on older bridges warning soldiers to break step while crossing. These are just two examples of catastrophic failures induced by different sources of excitation; yet not all excitation leads to failure.

In everyday life one can see many examples of casual vibrations caused by various external sources. A bridge can vibrate from a crossing lorry or train. A road sign can sway from side to side due to vortex shedding in high winds. A grandstand can rattle from the sounds of a concert or sways with the movements of a crowd. These are just a few examples of vibrations causes by traffic, wind, machinery, sound and humans.

The Broughton Bridge was an example of a structure dynamically excited by the co-ordinated movement of people. If a public structure is not designed with human excitation in mind, failures can and do occur. In recent history human induced vibrations have caused several disasters (or near disasters) because of the failure to recognise the dynamic consequences of crowd loading. In May 1992, a 1200 m^2 seated temporary grandstand collapsed at the Furiana football ground in Bastia, Corsica. The stand was able to support the static weight of the crowd but as the fans began to stomp and move in unison, the increased sway motion approached resonance and the stand collapsed within minutes. Seventeen people

were killed and 1400 injured (Bolton [1992]). In October 1994, a stand collapsed at a Pink Floyd concert at Earl's Court (London, England) due to the same type of crowd excitation. No one was killed but the failure resulted in many injuries. Near misses occurred in Edinburgh, Scotland during the 1986 Commonwealth Games and at the London Docklands Arena during a 'Take That' concert in 1995. In both cases pre-inspection recognised the impending failures and extra bracing was added.

The dynamic behaviour of these structures or was greatly influenced by structural stiffness. The construction techniques used for temporary and retractable stands typically creates structures with low stiffness values contributing to low natural frequencies (especially in sway). In 1988, Dr. James Dickie of Manchester University instrumented a stand at the London Docklands Arena during a pop concert. The natural sway frequency was 2.5 Hz when empty but reduced to 1.7 Hz during the concert (Fowler [1992]). In 1989, the Institute of Structural Engineers produced a guide entitled "Safety considerations for the design and erection of demountable grandstands". It suggested that structures with natural sway frequencies below 4 Hz be re-analysed to estimate the effects of the low frequency excitation induced by crowds. It also recommended that structures with natural frequencies between 4 and 6 Hz be subject to *"special considerations"* due to excitation harmonies. Structures with natural frequencies above 6 Hz were deemed more desirable and *"acceptable"* for normal use. The minimum natural vertical frequency was suggested to be 8 Hz.

It can be argued that these results are directly applicable to flexible staircases, i.e. staircases of light construction. As several references conclude, pop concert crowds move in rhythmic and co-ordinated motion (influenced by the beat of the music) which can excite the low natural frequencies of temporary and retractable stands. This co-ordinated motion can also occur as crowds ascend or descend stairs largely due to the fixed stride length imposed by the stair's geometry. As one steps forward the preceding person also tends to step forward, thus both footfalls occurs simultaneously creating a co-ordinated motion.

Staircases are normally designed to carry the same static loads as the floors to which they gives access (Smith [1988]). The effects of crowds are treated (nearly always) as equivalent static loads. For conventional designs this usually poses no

problem. However, recent trends towards slender construction have left modern staircases susceptible to the dynamic effects of human loading. The problem lies in the large reduction of system stiffness inherent in the light or supporting structures. This reduction lowers the natural frequencies, and in some cases, allows excitation by the users. It is now clear that designs based solely on aesthetic considerations can produce structures with increased probability of dynamic failure. For the designer however, there is little guidance for predicting human loading on staircases.

Recently, dynamic problems were evident after the construction of a slender staircase in a new shopping mall. The local district council raised concerns about the apparent 'liveliness' of the structure. It appeared that the staircase's natural frequency was low enough to be excited by the persons using it. An investigation was conducted which also looked at the effects of crowd loading on the staircase at different footfall rates with a group of 27 people (see Bishop *et al.* [1995]). Their results predicted a crowd load response up to 3 times that for an equivalent single person load. They also noted that the magnification effects of the crowd loading become minimal around 2.5 steps/sec possibly because the crowd was less likely to walk in unison at lower footfall rates. Other literature (Nilsson [1976] and Smith [1988]) showed that single person loading could be 4 to 5 times greater during normal descents on staircases than that experiences while walking on a floor. Hence, a large crowd rapidly descending a staircase could generate dynamic loads much higher than an equivalent crowd walking across a floor. Dr. Bishop's work emphases the need to promote an investigation into quantifying single person and multi-person loading on staircases which could be used as a future design guide.

In 1993, a 'Case for Support' was put forward by Dr. Bishop to the Engineering and Physical Sciences Research Council (EPSRC) to fund a three year research project on human induced loading and response of staircases. The project was approved and work was begun on November 1, 1994.

Chapters 1 through 4, as well as chapter 8, introduces the need to investigate human loading on staircases as well as the analytical tools and background information required to do the work. Chapter 5, 6, 7, and 9 contain the bulk of

the original work conducted by the author, while chapter 10 summarises the results of the thesis. These chapters are discusses in detail below.

Chapter 5 details extensive force plate experimental work conducted on a flat horizontal platform. This study was necessary in order to produce a benchmark set of measurement with which to compare the results from stair testing. The data gathered during this work constituted the most comprehensive collection of harmonic values found in recent literature. The work involved the sampling of over 1000 individual footfall traces from 40 subjects at various footfall rates. The results showed clear relationships between footfall rates, subject heights and harmonic values. These relationships were expressed in terms of mathematical formulae describing the maximum, minimum and mean expected harmonic values as a function of footfall rate (see Kerr and Bishop [1997]). These formulae were also incorporated into a new method for predicting peak accelerations on simply supported floor and bridge spans.

Chapter 6 details the extensive force plate experimental data collected from ascending and descending trials performed on a purpose built, specially designed staircase. Only 5 references were found in the literature that conducted testing on human induced loading of staircases prior to this work. Alcock and Lander [1987] and Morgan [1993] were undergraduate research projects involving a very limited number of subjects. Nilsson [1976] collected data for the Swedish Research Council using 15 subjects but a limited number of trials. His work, like the work of Smith [1988], only recorded peak load values and not force time histories. Thus, information required to calculate frequency content was not available. Bishop *et al.* [1995] conducted trials to determine staircase vibration levels for single subject and group loadings. His study also did not gather force time histories for individual subjects.

The data discussed in chapter 6 was generated from 600 individual ascending and descending force-time traces using 25 subjects and a variety of footfall rates. The trials were conducted using two different stair inclinations (22° and 33°), chosen to coincide with the limits imposed by BS5395 - "Stairs, Ladders and Walkways". This large amount of data produced first harmonic values with clear, footfall rate dependent regions. Also evident were clear limiting values for the harmonic

results. Based on this information, definitive conclusions were drawn about the harmonic results that could be expected from pedestrian traffic on staircases. This information should be used by staircase designers as a reference for determining the susceptibility of their structures to human induced vibrations. The information gathered in this chapter is summarised and detailed in Kerr and Bishop [1997].

Chapter 7 details the efforts to use Monte Carlo simulation techniques to simulate group loading on staircases. This topic has only limited reference in the literature, namely, Bishop *et al.* [1995]. He and his colleagues showed experimentally and analytically that group loading effects can cause an enhancement to the amount of loading impacting to a staircases. The work in this chapter builds on this reference and investigates further group loading effects in detail. Several loading conditions are examined to determine the limits of the response behaviour by varying the numbers of persons in the groups and their footfall rates. These results, like those of Chapter 6, are very important to the staircase designer and should be viewed in conjunction with the results of Chapter 5.

Chapter 9 deals with the prediction of the vertical ground reaction forces from body segment positional data; a topic often explored in the biomechanics field. Direct application of this approach has been found in the available literature on three occasions. Bobbert *et al.* [1991] and [1992] used the approach to determine ground reaction forces during running. Miller and Nissinen [1987] used the approach to determine ground reaction forces during a forward somersault. The approach used in these references was changed slightly to allow for the prediction of continuous force time histories generated while walking and negotiating stairs. The predicted results showed that, with properly sampled positional data, one can predict the vertical ground reaction forces and hence the harmonic components with reasonable accuracy. This can eliminate the need to use a force plate to calculate ground reaction forces.

Chapter 10 details and summarises the substantial work completed in this thesis and discusses how the results relate to the original objectives. This discussion is followed by Appendix A which contains flow charts and details of the custom C++ programs used in Chapter 5, 6, 7 and 9.

REFERENCES

British Standards Institution. (1992). BS5395 - Stairs, Ladders and Walkways.

Bishop, N.W.M., Willford, M., and Pumphrey, R. (1995). *Human Induced Loading of Flexible Staircases.* Safety Science. Pp. 261-276.

Bobbert, M.F., Schamhardt, C., and Nigg, M. (1991). *Calculation of Vertical Ground Reaction Force Estimates During Running from Positional Data..* Journal of Biomechanics. Vol.24. No.12. pp.1095-1105.

Bobbert, M.F., Yeadon, M.R., and Nigg, M. (1992). *Mechanical Analysis of the Landing Phase in Heel-Toe Running.* Journal of Biomechanics. Vol.25. No.3. pp.223-234.

Bolton, A. (1992). *Fatal Mix Caused Stand Fall.* New Civil Engineer Journal. May. pp. 5.

Fowler, D. (1992). *Unknown Frequency.* New Civil Engineer Journal. May. Pp.15.

Kerr, S.C. and Bishop, N.W.M. (1997). *Human Induced Loading of Flexible Staircases.* Innovation in Civil and Structural Engineering. Mouchel Centenary Conference Proceedings. ISBN 0-948749-50-4 Pp. 311-318.

Miller, D.I. and Nissinen, M.A. (1987). *Critical Examination of Ground Reaction Force in the Running Forward Somersault.* International Journal of Sport Biomechanics. Vol.3. pp.189-206.

Nilsson, L. (1976). *Impact Loads Produced by Human Motion.* Swedish Council for Building Research. Stockholm. Document 13, part A.

Smith, R.A. (1988). Vibrations of Structures. Chipman and Hill, London.

CHAPTER TWO 2

BEGINNING WITH FOURIER

2 FOURIER ANALYSIS AND THE FFT

2.1 INTRODUCTION

Due to the importance of this topic within this theses, this chapter deals exclusively with Fourier analysis and data sampling issues. Fourier analysis essentially began with Jean Baptiste Joseph Fourier. He was born in France on March 21, 1768 and worked as a mathematical physicist till his death on May 16, 1830. Fourier was mostly concerned with the flow of heat through objects and noted that the movement behaved like waves. He discovered that the heat waves were periodic, that is, they repeated themselves at a given time interval. He also discovered that a periodic wave was nothing more than the combination of many sine and cosine waves. A crude example is shown below (see Figure 1).

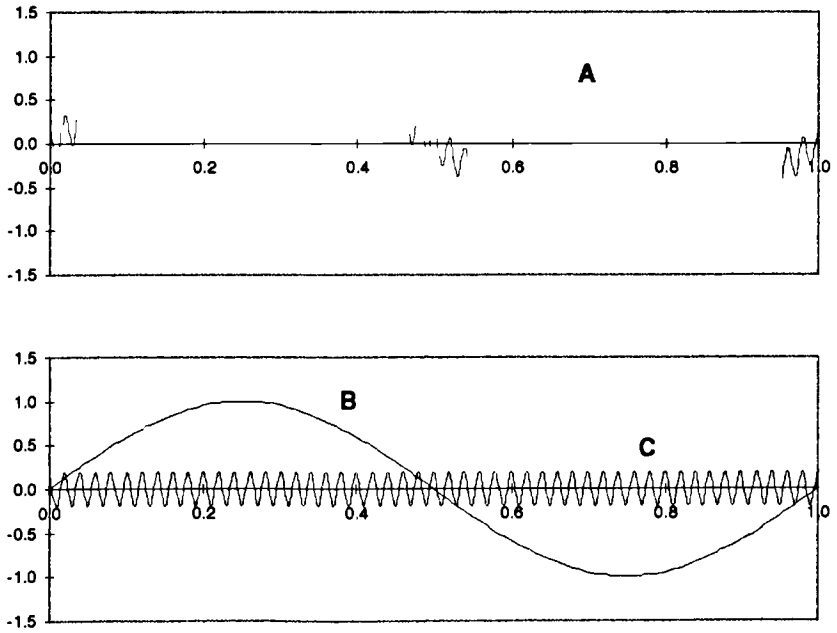

Figure 1 Complicated wave (A) made up of 1Hz sine wave (B) and 50 Hz cosine wave (C).

In this example the complicated wave (A) has the look of a sine wave but is outlined with a secondary higher frequency wave. A closer observation shows the complicated wave could be represented by two waves added together. One being a 1 Hz, 1 unit amplitude sine wave and the second being a 50 Hz, 0.2 unit amplitude cosine wave. Hence, like Fourier predicted, the complicated wave can be broken down into a series of sine and cosine waves.

The simplest periodic function that can be observed in nature with very little error is described by the following equation

$$F(t) = A\sin(2\pi ft + \phi)$$

where F(t) = the periodic function,
A = amplitude,
f = frequency,
ϕ = phase shift.

For example, the Romans observed the motion of the sun with sufficient accuracy to calculate the length of a year to be 364 ¼ days; the value used to construct the Julian calendar. A more complicated periodic function may have any number of sine wave contributions (as shown below)

$$F(t) = A_1\sin(2\pi f_1 t + \phi_1) + A_2\sin(2\pi f_2 t + \phi_2) + \ldots + A_n\sin(2\pi f_n t + \phi_n)$$

which may or may not be as evident as the example shown in Figure 1. This is where Fourier Series analysis becomes important.

2.2 DISCRETE OR FINITE FOURIER SERIES EXPANSION

2.2.1 Fourier Series and Fourier coefficients

Based on Fourier's discovery that a complicated wave can be broken down into its various wave components, an equation can be written to express this. Fourier predicted that the complicated wave will be made up of

a vertical offset from zero (a_0),

plus, a cosine wave that oscillates once per period,

plus, a cosine wave that oscillates twice per period,

plus, a cosine wave that oscillates three times per period, etc.,

plus, a sine wave that oscillates once per period,

plus, a sine wave that oscillates twice per period,

plus, a sine wave that oscillates three times per period, etc.,

or in other words, an infinite trigonometric series of the form

$$\begin{aligned} F(t) = a_0 &+ a_1 \cos(\omega t) + b_1 \sin(\omega t) \\ &+ a_2 \cos(2\omega t) + b_2 \sin(2\omega t) \\ &\vdots \\ &+ a_n \cos(n\omega t) + b_n \sin(n\omega t) \end{aligned}$$

where ω = angular frequency or $2\pi f$ or $2\pi/T$.

A more compact form for the series can be written as

$$F(t) = a_0 + \sum_{n=1}^{\infty} \left(a_n \cos(n\omega t) + b_n \sin(n\omega t) \right)$$

which is the standard *Fourier Series.*

Sine and cosine waves that oscillate once per period are said to be oscillating at the *fundamental frequency.* The remaining sine and cosine waves are said to be oscillating at multiples or *harmonics* of the fundamental frequency, i.e. a sine wave oscillating twice per period is said to be the second harmonic.

Fourier developed formulae to calculate the coefficients a_0, a_n, and b_n present in his series. They are

$$a_0 = \frac{1}{T} \int_0^T f(t) dt,$$

$$a_n = \frac{2}{T} \int_0^T f(t) \cos(n\omega t) dt, \text{ and}$$

$$b_n = \frac{2}{T} \int_0^T f(t) \sin(n\omega t) dt$$

where a_0 = signal offset from zero,
a_n = n^{th} cosine harmonic,

b_n = n^{th} sine harmonic,
T = period of the function.

So why does a_0 exist and b_0 not exist? If the Fourier series had been written

$$F(t) = a_0 \cos(0\omega t) + b_0 \sin(0\omega t) + a_1 \cos(1\omega t) + b_1 \sin(1\omega t) + a_2 \cos(2\omega t) + b_2 \sin(2\omega t) \\ \vdots \\ + a_n \cos(n\omega t) + b_n \sin(n\omega t)$$

regardless of the values for ω and t, $\cos(0\omega t)$ would always equal cos(0), which equals 1 and $\sin(0\omega t)$ would always equal sin(0) which equals 0. Therefore, a_0 exists and b_0 does not.

2.2.2 Fourier Expansion

A discrete Fourier expansion can be thought of as the decomposition (into sine and cosine waves) of a complicated time history sampled at such a frequency as to predict all the component waves. This is done by calculating the Fourier coefficients and substituting them into the Fourier series. This technique is use extensively in Chapter 5 and 6 to calculate the harmonic values present in the footfall traces for walking and ascending/descending stairs. The process will be explained with a simple example.

Figure 2 is a complicated, repeating wave form made up of a signal offset plus three sine waves and three cosine waves. It is not entirely obvious what individual sine and cosine amplitudes and frequencies exist in the trace, so it becomes necessary to conduct a discrete Fourier analysis on the signal.

To find a_o, the area under the repeating period *f(t)* must be calculated and divided by the period *T*. This was accomplished by using the "paper strip" method. The curve was divided into strips where the smaller the strip width, the greater the accuracy. For the work in Chapter 5 and 6, 200 strips per second were used which corresponded to the sampling rate at which the data was gathered. For this simple example only 10 strips were used as shown in Figure 3.

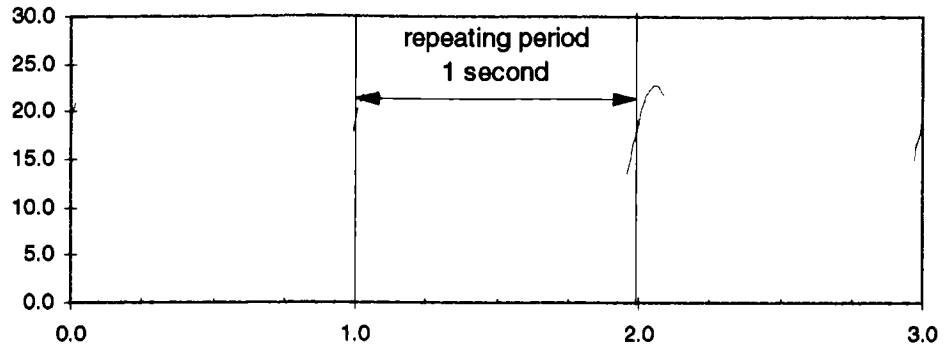

Figure 2 Complicated repeating wave form.

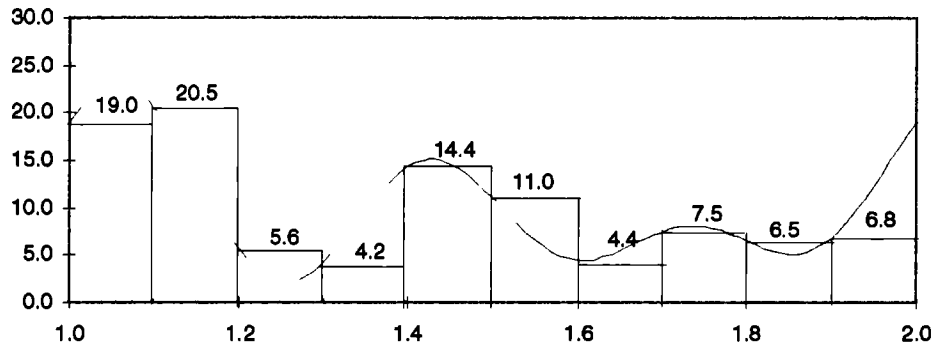

Figure 3 Repeating period divided into 10 strips.

Using all the strips the area was calculated at 9.99. Dividing through by the period (1 sec) gave a value of 9.99 for a_0. To find a_1, a_2, and a_3, the repeating trace was multiplied by a cosine wave in the form $\cos(n*2\pi ft)$ where n equalled 1,2 and 3. After each multiplication a new trace was generated on which the same strip method was applied. The values for a_1, a_2, and a_3 were found to be 2.99, 4.99 and 0.99, respectively. To find b_1, b_2, and b_3 the same method was applied but the trace was multiplied by $\sin(n*2\pi ft)$. The results were calculated as 1.99, 0.99, and 4.99, respectively.

Using these values for the coefficients, a predicted trace was generated which should have been identical to the original trace (see Figure 4). In this case the traces were slightly different indicating that the number of strips was not sufficient to accurately predict the Fourier coefficients.

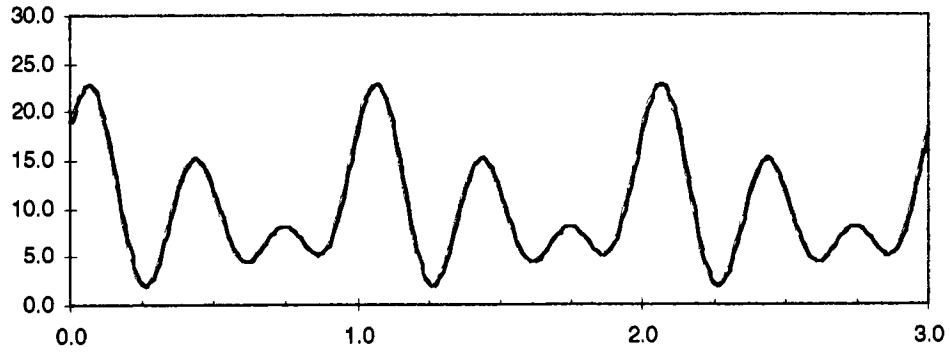

Figure 4 Predicted trace and original trace

The question now arises, what if we had selected a different repeating period, say, between t=0.5 and t=1.5 seconds; would the coefficients be different? The answer is that all the coefficients (except a_0) would be different. However, when combined to form a prediction of the original trace, the results would still be the same. Therefore, for every periodic time history there is an infinite number of Fourier coefficients which will reproduce the same signal. Hence, it is necessary to describe the Fourier series in such a manner as to remove the possible confusion.

The equation below describes the series in terms of a new coefficient, d_n, and a phase shift ϕ_n.

$$F(t) = a_0 + \sum_{n=1}^{\infty} d_n \sin(n\omega t + \phi_n)$$

The d_n coefficient is related to a_n and b_n in the following manner,

$$d_n = \sqrt{(a_n)^2 + (b_n)^2}\,.$$

The value for d_n remains unchanged regardless of which section of signal is selected. For the predicted trace a_1 equals 3 and b_1 equals 2. Hence, d_1 equals 3.61. As shown in Figure 5, d_n actually forms the radius of a circle. If a different

repeating period of time history were used the values of a_1 and b_1 would be in the range ± 3.61 and in such a combination as to produce the same radius arm.

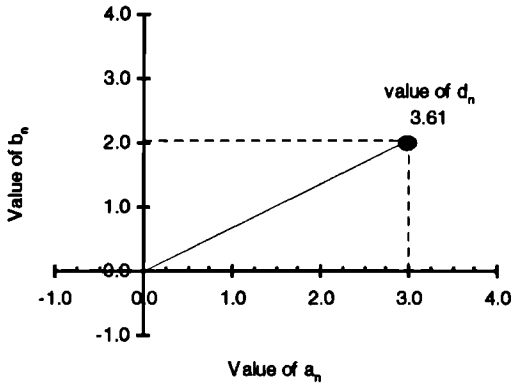

Figure 5 Combining a_n and b_n into d_n.

The phase shift is calculated from the formula

$$\phi_n = \tan^{-1}\left(b_n / a_n\right)$$

where ϕ_n = phase shift of the sine wave (radians).

Graphically, the phase shift is the counter clockwise angle from the positive X axis as depicted in Figure 6.

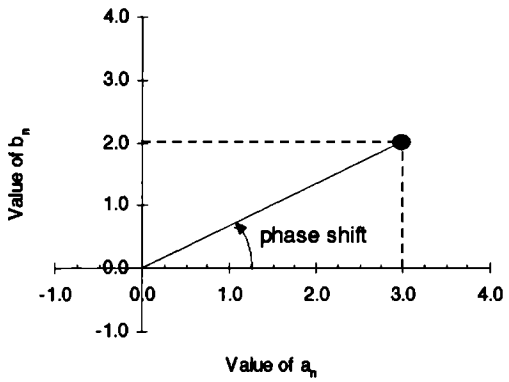

Figure 6 Depiction of the phase shift.

For this example, the coefficients could have been listed in two ways.

Original Coefficients (actual) a_n & b_n		or	New Coefficients d_n & ϕ_n	
$a_1 = 3$	$b_1 = 2$		$d_1 = 3.61$	$\phi_1 = -0.59$
$a_2 = 1$	$b_2 = 5$		$d_2 = 5.00$	$\phi_2 = -1.37$
$a_3 = 5$	$b_3 = 1$		$d_3 = 5.00$	$\phi_3 = -0.20$

Table 1 Coefficients a_n, b_n, d_n, and ϕ_n.

2.3 FAST FOURIER TRANSFORMS (FFT)

The probabilistic theories of time series were developed during the 1920s and 1930s with the concept of a *spectrum* of a time history being introduced. Throughout the 1940s and 1950s interest in Fourier methods grew steadily as their use found its way into electrical engineering applications, further advanced by the rapid development of the digital computers. This work provided a means of converting from the time domain (where the ordinate is in units of time) to the frequency domain (where the ordinate is in units of frequency). A frequency domain representation of a time series will typically be made as either an *amplitude spectrum* or a *power spectrum.*

Cooley and Tukey [1965] described an algorithm that significantly reduced the computational efforts involved in calculating Fourier coefficients. The routine made it possible to use Fourier analysis on vast amounts of data without loosing accuracy (as described by Brigham [1974]). The algorithm produced amplitude and phase information for a time signal at a chosen frequency interval. Figure 7 is the amplitude spectrum for the example used in the previous section.

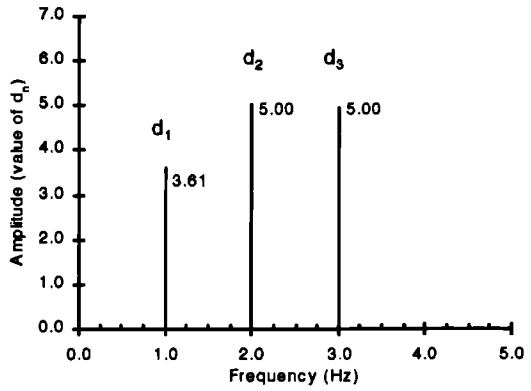

Figure 7 Example of an amplitude spectrum

Recall that the fundamental frequency for the original trace was 1 Hz. Therefore, the d_1 spike appears at 1 Hz and the second and third harmonics appear at 2 and 3 Hz. There is no fourth or higher harmonic in this case as the original trace was constructed with sine and cosine waves only oscillating up to 3 times the fundamental frequency. Also note that the amplitude spectrum does not indicate the phase relationships. It only displays the magnitudes of the harmonics.

The FFT algorithm described by Cochran [1967] gained its computational efficiency by separating the original time history into smaller and smaller groups of even numbers. When the groups could no longer be formed the process was stopped and the calculations begun. Start with the original Fourier Series equation but in a slightly altered form,

$$F(t) = a_0 + 2\sum_{n=1}^{\infty}\left(a_n \cos\left(\frac{n2\pi t}{T}\right) + b_n \sin\left(\frac{n2\pi t}{T}\right)\right).$$

In this case the transform equations for a_n and b_n are

$$a_n = \frac{1}{T}\int_0^T f(t)\cos\left(\frac{n2\pi t}{T}\right)dt$$

$$b_n = \frac{1}{T}\int_0^T f(t)\sin\left(\frac{n2\pi t}{T}\right)dt$$

where, n = 0,1,2, ... ∞. Note, the a_n equation now works for a_0 because the 2 has been removed to the outside of the summation sign.

If the continuous trace *F(t)* is only known at N equally spaced (sampled) points, a discrete series $\{x_s\}$ can be formed where S (the sample point number) equals 0,1,2 ... (N-1) and Δ equals the time between samples S. If the period (T) is replaced by NΔ, the time (*t*) replaced by sΔ, the integral signs replaced by summation signs and the sine and cosine terms combined using complex notation; the equations for a_n and b_n could be rewritten as

$$D_n = \frac{1}{N}\sum_{s=0}^{N-1} x_s e^{-i(n*2\pi*s\Delta/N*\Delta)}$$

or reduced further to,

$$D_n = \frac{1}{N}\sum_{s=0}^{N-1} x_s e^{-i\left(\frac{n2\pi s}{N}\right)}$$

where n = 0,1,2 ... (N-1).

The results given by the coefficient D_n for the discrete series are the approximate answers to the coefficient d_n used for the continuous series.

Suppose the discrete time series had an even number of sampled points. Split the series into two half-series $\{y_s\}$ and $\{z_s\}$ where the y series contained the even numbered samples and the z series contained the odd numbered samples (see below).

$$y_s = x_{2s} \qquad z_s = x_{2s-1}$$

where s = 0,1,2, ... (N/2-1).

If we develop a Fourier transform equation for the two half-series as was done for the original series, they would appear as follows

$$Y_n^{(N/2)} = \frac{2}{N}\sum_{s=0}^{(N/2)-1} y_s e^{-i\left(\frac{n4\pi s}{N}\right)}$$

$$Z_n^{(N/2)} = \frac{2}{N}\sum_{s=0}^{(N/2)-1} z_s e^{-i\left(\frac{n4\pi s}{N}\right)}$$

where the superscript {N/2} on the coefficients Y_m and Z_m denotes the number of points in the series. Now relate the Fourier expansion equations for the half-series with that for the full series (D_n) as follows

$$D_n = \frac{1}{N}\sum_{s=0}^{N-1} x_s e^{-i\left(\frac{n2\pi s}{N}\right)}$$

$$= \frac{1}{N}\left\{\sum_{s=0}^{(N/2)-1} x_{2s} e^{-i\left(\frac{n2\pi}{N}\right)(2s)} + \sum_{s=0}^{(N/2)-1} x_{2s-1} e^{-i\left(\frac{n2\pi}{N}\right)(2s-1)}\right\}$$

$$= \frac{1}{N}\left\{\sum_{s=0}^{(N/2)-1} y_s e^{-i\left(\frac{n4\pi s}{N}\right)} + e^{i\left(\frac{n2\pi}{N}\right)}\sum_{s=0}^{(N/2)-1} z_s e^{-i\left(\frac{n4\pi s}{N}\right)}\right\}$$

$$= \frac{1}{2}Y_n^{(N/2)} + \frac{e^{i\left(\frac{n2\pi}{N}\right)}}{2}Z_n^{(N/2)}$$

As can be seen, the Fourier coefficients D_n can be found from the Fourier expansions of the half-series, Y_n and Z_n. In fact, if the time series has 2^n points then the division process can be repeated until one obtains a half-series of only 2 points. As explained by Jenkins and Watts [1968], using the direct method to calculate the Fourier transform of a series of N points requires N^2 operations, whereas using the FFT algorithm requires only $2N\log_2 N$ operations. If one were sampling a time history at 4096 Hz for 32 seconds, they would gather 131,072 or 2^{17} sampled points. Using the direct method would require nearly 2 thousand billion operations, while using the FFT method would require just over 1 million operations. With today's computing efficiency that amounts to seconds compared with hours with no loss of accuracy. That makes the FFT algorithm the chosen method for performing Fourier analysis on large amounts of data.

2.4 SAMPLING THEOREM AND ALIASING

As a subject walks across a floor, the impact of their foot with the ground is continuous from heel strike through to toe push off (discussed in detail in Chapter 4). The force 'felt' by the floor is also continuous. However, if we wish to monitor the force felt by the floor we would have to acquire the data by taking repeated samples with some separation of time, say Δt. Between each sample, we

have no indication of the force so typically one assumes a linear relation between sample points. But, just how many points should be sampled per second?

Suppose one is trying to sample the 1 Hz sine wave shown in Figure 8 by taking one sample every second (as indicated by the black dots). In this case, if one draws a linear line between sample points it would construct a representation of a flat line, not a sine wave.

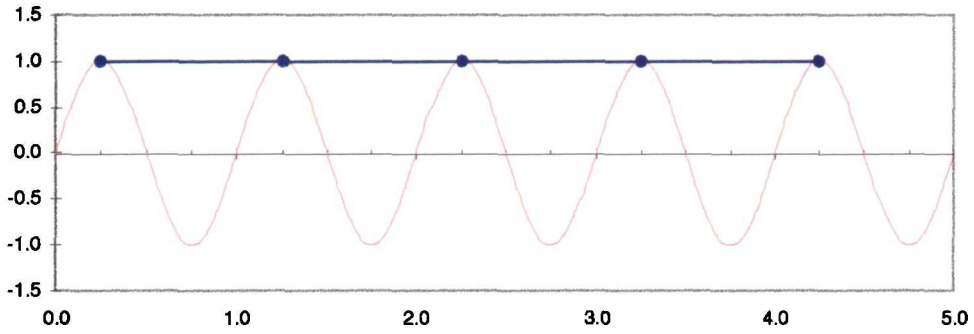

Figure 8 A 1Hz sine wave sampled at one point per second.

Suppose the sampling rate was increased to 2 samples per second. One would now see a saw tooth pattern and although not a perfect representation, it does give the correct period for the underlying sine wave (see Figure 9).

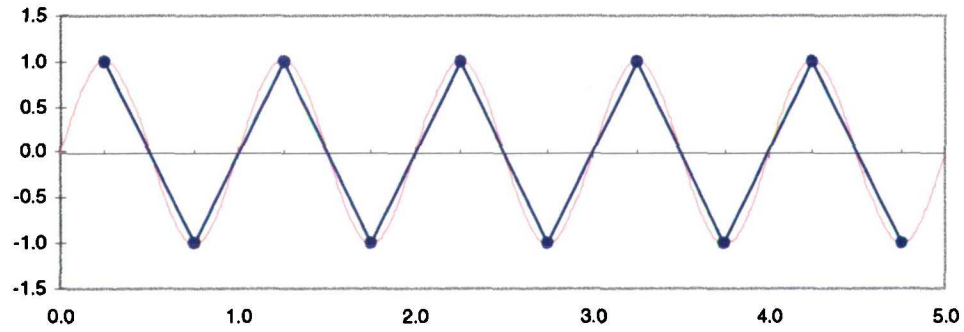

Figure 9 A 1Hz sine wave sampled at two points per second.

Therefore, from sampling theorem, one needs to sample at twice the frequency (minimum) of the sine wave in order to simulate it. Hence, two things have been learned from this discussion. First, a sampled trace is constructed from discrete observations of a continuous trace, or in other words, the sampled trace can be

regarded as having been derived from the continuous trace. Secondly, the sampling rate must be at least twice as high as the largest period of interest.

This can also be expressed mathematically. It was showed previously that the Fourier transform for a discrete (sampled) time history was

$$D_n = \frac{1}{N}\sum_{s=0}^{N-1} x_s e^{-i\left(\frac{n2\pi s}{N}\right)}$$

where n = 0,1,2, ... (N-1).

If the calculation was attempted for n>N, say n=N+1, the result would be

$$\begin{aligned} D_{N+1} &= \frac{1}{N}\sum_{s=0}^{N-1} x_s e^{-i\left(\frac{2\pi s}{N}\right)(N+1)} \\ &= \frac{1}{N}\sum_{s=0}^{N-1} x_s e^{-i(2\pi s)} e^{-i\left(\frac{2\pi s*1}{N}\right)} \\ &= \frac{1}{N}\sum_{s=0}^{N-1} x_s *1* e^{-i\left(\frac{2\pi s*1}{N}\right)} \\ &= D_1 \end{aligned}$$

Therefore, above N the values for D_n repeat themselves. In fact, if the values for n ranged from -N/2 to +N/2, the results would show that D_n is symmetric about zero. Hence, the only harmonic amplitudes that are unique are those calculated for n=0,1,2, ... (N/2). In other words, if the discrete trace was sampled at 1000Hz than the unique harmonic amplitudes will be cut-off after 500Hz.

This cut-off frequency is known as the *Nyquist frequency*. If frequencies exist in the signal above the Nyquist frequency, their harmonic amplitudes would be echoed or folded into the harmonic amplitudes below the Nyquest frequency creating distorted values. This process is called *aliasing* and can be avoided by ensuring the sampling rate is at least twice the highest significant frequency in the signal. If the frequency content of the signal is unknown, it is best to choose the highest

sampling rate available and collect a data sample. Repeat the process a second time at half the sampling rate first chosen. After performing a harmonic analysis on both time histories, compare the results. If they are identical, repeat the process at an even lower sampling rate until the harmonic amplitudes change. When the values change, it signifies that the last sampling rate was too low and aliasing had occurred. Hence, always filter above $f_{max}/2$. This procedure gives a rough guide as to what sampling rate to choose.

2.5 NARROW BAND, BROAD BAND AND RESOLUTION OF SIGNALS

Narrow and broad band are two extreme descriptions defining the shapes of the signals in the frequency domain. A pure narrow band signal is a distinctive time history which only has one peak for every zero crossing. An example of this is a sine wave, as shown in Figure 10.

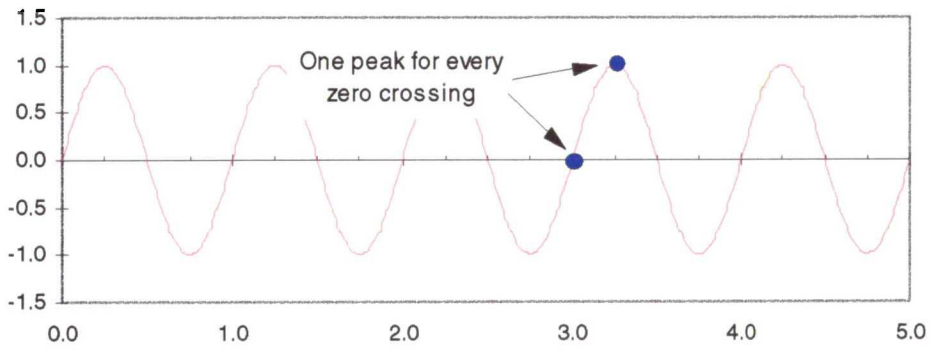

Figure 10 Narrow banded process - a sine wave.

If an FFT was done on an infinitely long version of this signal it would result in a *delta function*, i.e. a single "spike" located at 1Hz with a magnitude extending to infinity (see Figure 11). This means that the signal contains one specific frequency. At the other end of the spectrum, if an infinite signal contained components at all frequencies the FFT result would be a horizontal flat line with magnitude 1. This would be a pure broad band signal also referred to as "white noise". Most signals in nature are neither purely narrow banded or purely broad banded. Often the signal will tend toward one or the other but still retain elements of both. An FFT plot of this sort of signal will have the spikes replaced

by frequency distributions or a spectrum showing all the frequency content within the signal.

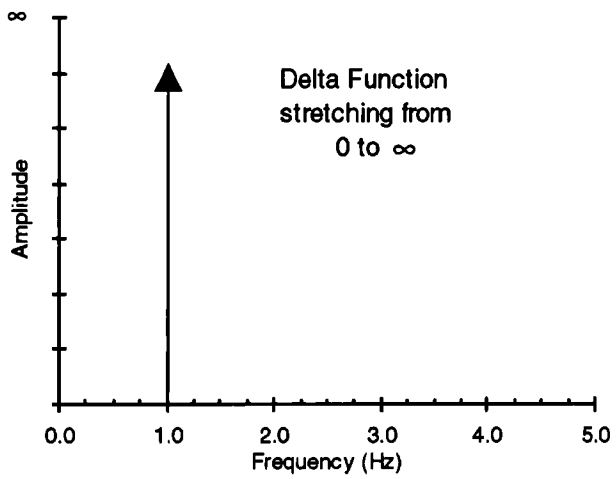

Figure 11 Result of FFT on 1Hz sine wave - Delta Function.

The *resolution* of the FFT is the number of points used to generate the frequency distribution plot. The more points, the finer the resolution and the better the accuracy of the predicted magnitudes. Resolution is determined by the sampling rate and the number of points in the signal. If a signal contains 5000 points and is sampled at 2000 Hz, the resolution will be

$$R = 2^* \text{ number of points / sampling rate, or}$$

$$R = 2 * 5000 / 2000 = 5 \text{ points/Hz}$$

The FFT plot would have a resolution of 0.2 Hz or 5 points per Hertz. If a finer resolution is required than the number of points sampled must be increased or the sampling rate decreased. Typically however, the sampling rate is fixed by the Nyquest frequency and cannot be lowered.

2.6 DISCUSSION

This chapter described in detail Fourier analysis and the Fast Fourier Transform. Both procedures are used extensively throughout this thesis as a means of calculating the harmonic components for various force-time histories. Several C++ programs have been written to exploit both methods with all thoroughly verified by hand calculations or by direct comparisons to established commercial

software. Care was also taken throughout the data acquisition process to avoid any problems associated with aliasing, and enough points were sampled to allow a very fine resolution in the FFT amplitude spectrum. A fine resolution was required for the modelling work conducted in Chapter 7.

REFERENCES

Brigham, E.O. (1974). The Fast Fourier Transform. Prentice-Hall, NJ.

Cooley, J.W. and Tukey, J.W. (1965). *An Algorithm for the Machine Computation of Complex Fourier Series.* Math. Comput. Vol.9. pp. 297-301.

Cochran, B.T. (1967). *What is the Fast Fourier Transform?. IEEE Transactions on Audio and Electroacoustics.* Vol.AU-15. No.2. pp. 45.

Jenkins, G.M. and Watts, D.G. (1968). Spectral Analysis and its Applications. Holden-Day Series in Time Series Analysis. Holden-Day, London.

CHAPTER THREE 3

BODY SEGMENT PARAMETERS

3 THE COLLECTION OF BODY SEGMENT PARAMETERS

3.1 INTRODUCTION

The work in Chapter 9 deals with the problem of defining the ground reaction forces analytically, during walking or ascending / descending a staircase. In order to accomplish this the mass of the body and the acceleration of the body must be known. Further to knowing the mass, knowing where the mass acts, or the position of the centre of gravity is also important. With this information, the ground reaction forces for the body as a whole can be calculated. If one wishes to know the contributions of particular body parts i.e. the legs, the trunk system, etc., knowledge of the *segmental* masses and accelerations is required.

There have been numerous methods developed for deriving or calculating the segmental properties of various body parts. The first and most often referenced method is from data collected during cadaver studies. Other approaches include mathematical modelling of the segments, photogrammetry, gamma mass scanning, computerised tomography and recently, magnetic resonance imaging or MRI methods. The following sections will look at these methods in more detail.

3.2 CADAVER STUDIES

The earliest work on cadavers was conducted by two German scientists, Braune and Fischer, in 1889. Their data was collected on three cadavers with an average height of 1.68m or 66.1 inches and an average weight of 64kg or 140.8 lb. To determine the centres of mass the cadavers were frozen and dismembered. The parts were balanced over a knife-edge and suspended in such a fashion as to allow free oscillation until equilibrium was reached. The locations of the centres of

mass were given in terms of percentage of the distance from proximal[1] to distal joint centres of the segments.

More comprehensive data was collected by Dempster in 1955. His study was conducted on eight male cadavers of "more or less medium build". This work addressed the problem that most joint centres change as the limbs are flexed and extended. This action alters (to a small degree) the length of the segments because the end points change and hence the centres of gravity. In Dempster's view, the most satisfactory division of the segments involved the sectioning of the body parts with the limbs partially flexed thus averaging the problems. The centres of mass were given in terms of percentages of the distance from the proximal to distal joint centres; the same as Braune and Ficher. Dempster's group later used this information to develop a drafting board mannequin of a seated male figure to use in cockpit design.

In 1969, Clauser and associates conducted a study in which they tried to predict segment characteristics of living subjects based on the information gathered from cadavers. Their study used thirteen male cadavers that were sectioned into 14 segments. Numerous measurements were taken or calculated including segmental weight, volume, centre of mass, length, circumference and breadth or depth. From these parameters, Clauser and his associates developed "three step" regression equations for predicting the anthropometric dimensions on living subjects. An example of which is given below for the estimation of leg mass.

Leg mass = 0.111 * calf circumference + 0.047 * tibial height + 0.074 * ankle circumference - 4.208 (where all length are measured in cm).

To validate their equations, Clauser and his associates took repeated observations on living subjects and found predicted errors to be between 3% and 5%. One major source of error quoted by Clauser was maintaining a subject's limb relatively motionless in an overflow tank (used to measure volume). Their final conclusions stated that the system of regression equations generated by their work allowed for the segmental parameters to be based more upon the

[1] Proximal denotes the part of an organ that is nearest to the organ's point of attachment. For example, the hip is at the proximal end of the leg.

individual's body size. Previous cadaver studies including Dempster, had not adequately considered this point.

Hinrichs [1990], identified a problem with the Clauser study and supplied adjustments to the calculated mass centres to compensate for the error. Hinrichs pointed out that Clauser and his associates dismembered the cadaver segments at the estimated joint centres but (typically) referenced the locations of the segmental mass centres to the bony landmarks at the proximal ends of the segments. This oversight prompted Hinrichs to make small adjustments to some of the mass centres predicted by Clauser.

Table 2 and Table 3 contains segmental parameter comparisons from the three studies mentioned above. One inherent flaw all cadaver studies have is that the data is based on a limited number of typically elderly male cadavers. Very little information exist for women, children, young adults and non-Caucasion subjects. Thus the database is not representative of all population bases.

3.3 MATHEMATICAL MODELLING

Many researchers have used mathematical modelling to predict the segmental masses and locations of the centres of gravity (see Amar [1920], and Hatze [1980]). This is done by representing the individual segments as regular geometric solids; i.e. a truncated cone for the upper arm, forearm, thigh, leg, and foot, two cylinders for the trunk, and elliptical spheres for the head and hand. The paper commonly cited by recent references is the work of Hanavan [1964]. He developed a computerised segmental model of the human body from which segmental parameters could be obtained from 25 standard anthropometric measurements of the individual.

Based on the references, a mathematical approach can predict the principal segmental parameters to within 5% of the actual values (Haze [1980]). This is about the same accuracy as the cadaver studies. However, the subjects studied must have similar segmental shapes to those in the modelling or the errors can be substantially higher (see Chandler *et al.*[1975] and Rodrigue and Gagnon[1984]).

Source	Braune and Fischer (1889)	Dempster (1955)	Clauser *et al.* (1969)
Sample size	3	8	13
Head	7.0%	8.1%	7.3%
Trunk	46.1	49.7	50.7
Upper Arm	3.3	2.8	2.6
Forearm	2.1	1.6	1.6
Hand	0.8	0.6	0.7
Total Arm	6.2	4.9	4.9
Forearm and Hand	2.9	2.2	2.3
Thigh	10.7	9.7	10.3
Calf	4.8	4.5	4.3
Foot	1.7	1.4	1.5
Total Leg	17.2	15.7	16.1
Calf and Foot	6.5	6.0	5.8

Table 2 Segmental weight as a percentage of subject weight (recreated from LeVeau [1977]).

Source	Braune and Fischer (1889)	Dempster (1955)	Clauser *et al.* (1969)
Sample size	3	8	13
Head	--%	43.3%	46.6
Trunk	--	--	38.0*
Arm	47.0	--	51.3
Forearm	42.1	43.6	39.0
Hand	--	43.0	48.0*
Total Arm	--	49.4	41.3
Forearm and Hand	47.2	--	62.6*
Thigh	44.0	67.7*	37.2*
Calf	42.0	43.3	37.1
Foot	44.4	42.9	44.9
Total Leg	--	43.3	38.2*
Calf and Foot	52.4	43.7	47.5
* These values are not directly comparable owing to variations in the definition of the segment length used by the different investigators.			

Table 3 Segmental centre of mass location as percentage of segment length from proximal end (recreated from LeVeau [1977]).

3.4 GAMMA SCANNING

Gamma scanning was developed at the Pennsylvania State University in a co-ordinated effort between the Nuclear Engineering Department and the Biomechanics Laboratory (Casper *et al.*[1971]). The basic premise of the approach, described by Zatsiorsky and Seluyanov [1983] and Brooks and Jacobs [1975], was that a gamma-radiation[2] beam in the energy range of 0.5 to 2.0 MeV (8.0e-14 to 3.2e-13 Joules) would interact with matter in such a way that its transmission is related to the mass traversed and was relatively independent of the elemental composition of the material traversed. From these experiments, regression equations were developed for the segmental mass and centre of gravity; an example of which is given below (from Zatsiorsky and Seluyanov [1983]).

$$\text{Leg mass} = -1.592 + 0.036 * \text{body mass} + 0.0121 * \text{body height}$$

(where mass is in kg and height is in cm).

This work has proven to be considerably accurate producing errors of only 1% on centre of mass locations and moments of inertia. However, research with gamma mass scanning has been limited because the required "specialised" facilities are scarce. Hence, the applications of this method are limited. Another disadvantage is the use of radiation as a measuring medium, although, the levels used are low.

3.5 PHOTOGRAMMETRY AND COMPUTERISED TOMOGRAPHY (CT) SCANNING

Photogrammetry has proven to be a fast and inexpensive method for determining segmental properties (Jensen [1978], Kaleps *et al.* [1984] and Sarfaty and Ladin [1993]). However, there are several shortcomings to the approach. The current limitations include the need to have the user input the segmental endpoints, the inherent assumption that the segments are symmetric outside the camera's field of view and the overestimation of the volume produced by the edge detection algorithms. The video-based system used by Sarfaty and Ladin produced volume (and hence mass) errors in the order of +5%.

Computerised tomography or CT scanning is better know for its use in the medical field. A CT scanner is a ring shaped X-ray machine that rotates through

---

[2] Gamma radiation is a form of electromagnetic radiation emitted by excited atomic nuclei during the process of passing to a lower excitation state. A common source is cobalt-60 (source Oxford science dictionary).

180° around the horizontal patient taking X-rays every few degrees. The data is fed into an onboard computer that displays the images as cross sections through the patient. The Oxford Science dictionary states that a patient undergoing a CT scan is typically exposed to a dose of X-rays some 20% of that used in a normal diagnostic X-ray.

Many researchers have commented on the use of CT scanning for determining segmental properties. Huang *et al.* [1979] and Hung and Suarez [1983], both report the use of CT scanning to determine the mass distribution of the body. They first defined the boundaries of the different tissues observed in the CT cross-section. Next, using tissue density data they were able to determine the inertial characteristics of the individual tissues and of the segments. They did not report, however, on the percentage error from their work.

Rodrigue and Gagnon [1983] also used CT scanning to estimate the forearm densities from 20 cadavers. They reported density estimates within 5% of values obtained from direct measurements showing that CT scanning is a promising tool for determining segmental properties. Unfortunately, a major drawback of this method is the need for specialised and expensive instrumentation and highly trained personnel. This makes CT as well as gamma scanning unavailable to a wide body of researchers.

3.6 MAGNETIC RESONANCE IMAGING (MRI)

Used in the medical field, magnetic resonance imaging is a sensitive form of nuclear magnetic resonance that detects the minute magnetic fields in the body's tissues to produce detailed cross-sectional images. Each tissue type shows up as a specific shade of brightness (white to black). This method unlike CT or gamma scanning does not use radiation yet produces images of equal or better quality (see Brady *et al.* [1982] and Alfidi *et al.* [1982]).

In 1990, Mungiole and Martin conducted a study to estimate segmental inertial properties using MRI and compared their results with existing methods. The research used twelve adult male distance runners as test subjects. Each person had their right lower leg imaged and the segmental properties computed from the images. The individual tissue densities (needed for the calculations) were obtained

from the work of Clauser *et al.* [1969]. Their results for segmental mass and centre of mass are compared with other methods and given in Table 4.

Method	Mass lower leg (kg)	Mass Location (% from proximal end)
MRI	3.44	41.6%
Clauser * (cadaver studies)	3.73	40.7
Hanavan ** (mathematical modelling)	3.21	42.4
Zatsiorsky and Seluyanov * (gamma scanning)	3.27	41.8
Mass: * Based on total body mass as the only predictor ** Based on Barter's regression equation.		
Mass Location: * Based on a constant % of segment length relative to proximal end. ** Based on the model of a frustum of a right circular cone.		

Table 4 A comparison of segmental mass and centre of mass for a right lower leg (Mungiole and Martin [1990]).

This study proved that the MRI approach produced reasonable segmental properties with no side effects. Unfortunately, at present very little research data is available for the segmental properties throughout the body.

3.7 DISCUSSION

This chapter discusses 6 methods used to calculate or measure the body segmental properties. These properties are required to analytically solve for the vertical ground reaction forces as discussed in Chapter 9. Based on preliminary work, the accuracy of the segmental properties is not critical to the force predictions, i.e. using a centre of mass location of 49.5% or 49.1% made little difference to the ground reaction force prediction and eventually the harmonic amplitude calculations. For this reason it was decided that the cadaver study information would be sufficiently accurate and the data from Clauser *et al.*[1969] was used in this thesis.

REFERENCES

Alifidi, R.J., Haaga, J.R., El Yousef, S.J., Bryan, P.J., Fletcher, B.D., LiPuma, J.P., Morrison, S.C., Kaufman, B., Richey, J.B., Hinshaw, W.S., Kramer, D.M., Yeung, H.N., Cohen, A.M., Butler, H.E., Ament, A.E. and Lieberman, J.M. (1982). *Preliminary Experimental Results in Humans and Animals with a Superconducting Whole Body Nuclear Magnetic resonance scanner.* Radiology. Vol.143. Pp.175-181.

Amar, J. (1920). The Human Motor. G. Routledge and Sons. London.

Braune, W. and Fischer, O. (1889). *Uber den Jschwerpunkt des menschlichen Korpers mit rucksicht auf die Austrustung des deutchen Infanteristen.* Abh. D. Math.-Phys. Cl. D. K. Sachs. Gesellsch. Der Wiss., Vol.26. Pp. 561-672. Also in : Krogman, W.M, and Johnston, F.E. (Eds) (1963). Human Mechanics - four monographs abridged. Wright-Patterson Air Force Base. Ohio. AMRL-TDR-63-123.

Brady, T.J., Gebhardt, M.C., Pykett, I.L., Buononno, F.S., Newhouse, J.H., Burt, C.T., Smith, R.J., Mankin, H.J., Kistler, J.P., Goldman, M.R., Hinshaw, W.S., and Pohost, G.M. (1982). *NMR Imaging of Forearms in Healthy Volunteers and Patients with Giant-Cell Tumor on Bone.* Radiology. Vol.144. Pp.549-552.

Brooks, C.B. and Jacobs, A.M. (1975). *The Gamma Mass Scanning Technique for Inertial Anthropometric Measurement.* Medical Science in Sports. Vol.7. Pp.290-294.

Casper, R.M. Jacobs, A.M., Kenney, E.S. and McMaster, I.B. (1971). *On the Use of Gamma Ray Images for Determination of Human Body Segment Parameters.* Presented at Quantitative Imagery in Biomedical Sciences. Huston.

Chandler, R.F., Clauser, C.E., McConville, J.T., Reynolds, H.M. and Young, J.W. (1975). Investigation of Inertial Properties of the Human Body. Wright-Patterson Air Force Base. Ohio. DOT HS-801-430.

Clauser, C.E., McConville, J.T., and Young, J.W. (1969). Volume and Center of Mass of Segments of the Human Body. Wright-Patterson Air Force Base. Ohio. AMRL-TR-69-70.

Dempster, W.T. (1955). Space Requirements of the Seated Operator. Wright-Patterson Air Force Base. Ohio. WADCTR-55-159.

Ellingwood, B. and Tallin, A. (1984). *Structural Serviceability: Floor Vibrations.* Journal of Structural Engineering. Vol.110. No.2.

Hanavan, E.P. (1964). A Mathematical Model of the Human Body. Wright-Patterson Air Force Base. Ohio. AMRL-64-102.

Haze, H. (1980). *A Mathematical Model for the Computational Determination of Parameter Values of Anthropomorphic Segments.* Journal of Biomechanics. Vol.13. Pp. 833-843.

Hinrichs, R.N. (1990). *Adjustments to the Segment Center of Mass Proportions of Clauser et al. (1969).* Journal of Biomechanics. Vol.23. No.9. Pp. 949-951.

Issaacs, A., Daintith, J. and Martin, E. (Eds). (1991). Oxford Concise Science Dictionary. Oxford University Press. Oxford.

Jensen, R.K. (1978). *Estimation of Biomechanical Properties of Three Body Types Using Photogrammetric Method.* Journal of Biomechanics. Vol.11. Pp. 349-358.

Kaleps, I., Clauser, C.E., Young, J.W., Chandler, R.F., Zehner, G.F., and Mcconville, J.T. (1984). *Investigation into the Mass Distribution Properties of the Human Body and its Segments.* Ergonomics. Vol.27. Pp.1225-1237.

Rodrigue, D. and Gagnon, M. (1983). *The Evaluation of Forearm Density with Axial Tomography.* Journal of Biomechanics. Vol.16. Pp. 907-913.

Rodrigue, D. and Gagnon, M. (1984). *Validation of Weinbach's and Hanavan's Models for Computation of Physical Properties of the Forearm.* Res. Q. Exercise Sport. Vol.55. Pp. 272-277.

Sarfaty, O. and Ladin, Z. (1993). *A Video-Dased System for the Estimation of the Inertial Properties of Body Segments.* Journal of Biomechanics. Vol.26. No.8. Pp.1011-1016.

Zatsiorsky, V.M and Seluyanov, V.N. (1985). *Estimation of the Mass and Inertia Characteristics of the Human Body by Means of the Best Predictive Regression Equations.* Biomechanics IX-B. Human Kinetics Publishers, Champaign, IL. Pp.233-239.

CHAPTER FOUR 4

A BACKGROUND TO HUMAN GAIT

4 THE FORCES AND MOTIONS INVOLVED IN WALKING AND ASCENDING / DESCENDING STAIRS

4.1 INTRODUCTION

This chapter is intended to give background information on the way humans walk and negotiate stairs as well as the vertical ground reaction forces generated during these activities. The chapter is laid out in 4 sections. The first two discuss the standard terms used by biomechanics in gait analysis of walking. These sections also discuss the vertical force traces typically expected during the contact phase and how the shape varies with the movements of the subject. The final two sections discuss the same topics but for ascending and descending stairs.

4.2 THE GEOMETRY OF WALKING

Motion is defined as a continuous change in body position. The change can be translational, where the points on the body are displaced along parallel lines; or rotational, where the points on the body are displaced along circles around the various body axes. The changes in body position associated with walking are a combination of both translational motion and rotational motion (see Figure 12).

Walking is a very familiar activity but it is doubtful that one could explain, in anatomical terms, the exact sequence of events that occur during a single gait cycle. In fact, the sequence of events occurs so quickly that it is very difficult, if not impossible, to explain the exact process viewing by eye alone. Hence, the greatest advances in analytical gait assessment have occurred with the development of photography. From still photos, scientists have described walking in terms of simple characteristics like stride length, step frequency, gait cycle duration, stance and swing phases and speed.

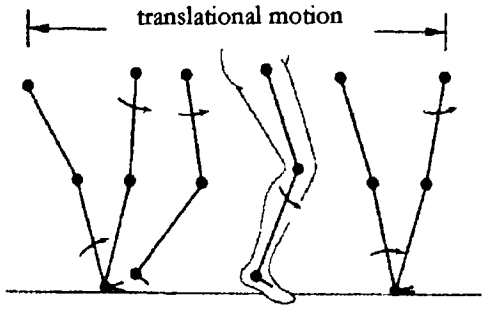

Figure 12 Rotation of the limbs to obtain translational motion (LeVeau [1977]).

These characteristics are related to the planes and axes used to describe motions of the body (see Figure 13). The most common plane used in the description of walking is the *sagittal* plane that divides the body into left and right halves. Nearly all photographic studies have been done from the side, perpendicular to the sagittal plane.

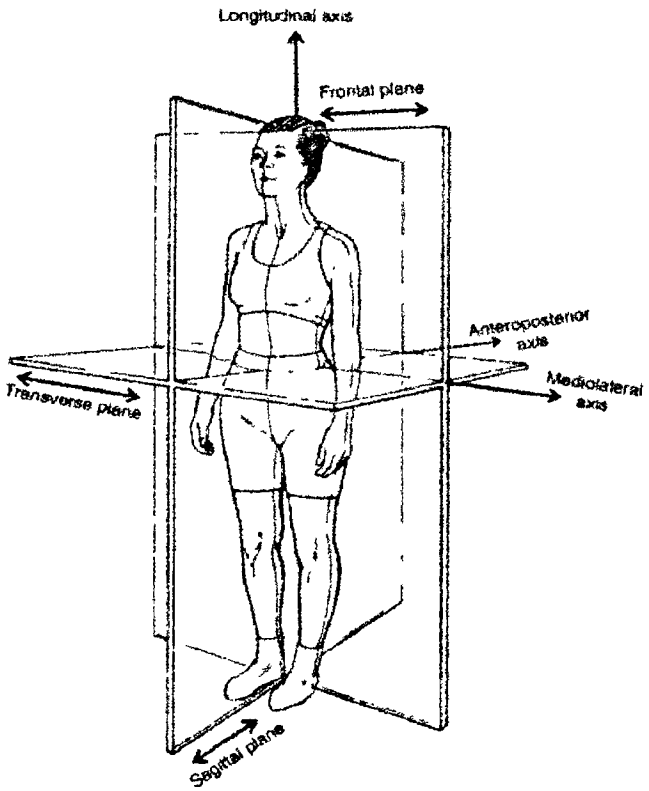

Figure 13 The planes and axes on the human body (Hamill and Knutzen [1995])

As stated by Ellingwood [1984], the average walking rate or step frequency is nearly 2 Hz or 2 steps per second. Unlike a running subject, a walking subject always maintains at least one foot in contact with the ground. That contact phase during walking is referred to as the *stance* phase while the opposite leg undergos the *swing* phase as it "swings" into position, ready to take up the next step. When the leg has gone through a stance and swing phase it is said to have completed a single *gait cycle*. During the stance phase the body is supported for a short time on both legs which is different to running where the body is only supported on one leg. This is an important point when attempting to analytically solve for the impact forces which is fully discussed in Chapter 9. Figure 14 illustrates the gait cycle during normal walking. During the double support phase two vertical ground reaction forces (VGRF) are created.

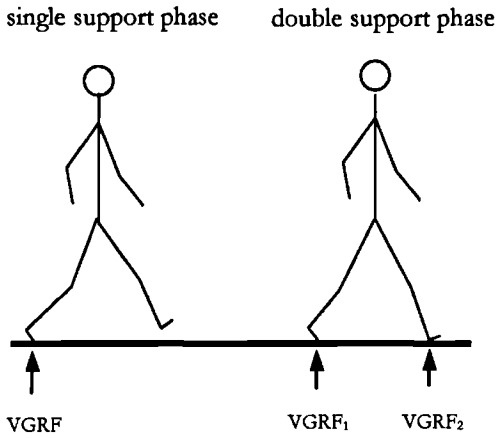

Figure 14 The gait cycle showing the double support and single support portions of the stance phase.

Figure 15 shows the detail sequence of events that occur during the gait cycle. When the heel strikes the floor the stance phase begins. As the foot rotates about the heel, it eventually falls flat (at approximately 15% of the gait cycle). The foot next rotates about the toes causing the heel to rise off the ground (at approximately 30% of the gait cycle). The toes then press into the floor to extend the step of the opposite foot (at approximately 45% of the gait cycle) and finally, after the opposite heel has made contact and is supporting the body weight, the toes leave the floor and the stance phase is ended (at approximately 60% of the gait cycle).

At this time the upper leg (quadriceps muscle) is lifting the lower leg/foot and beginning to extend it about the knee. During this manoeuvre the lower leg/foot

is raised and accelerated through 90°, allowing the toes to clear the floor as they swing through preparing for another heel strike. As the lower leg/foot is positioned, it is decelerated before dropping to the floor and making heel contact; ending the swing phase and the gait cycle. By placing sensors that measure vertical height on the toe and heel of a test subject, a graphical trace of the sequence of events during one gait cycle can be made (see Figure 16).

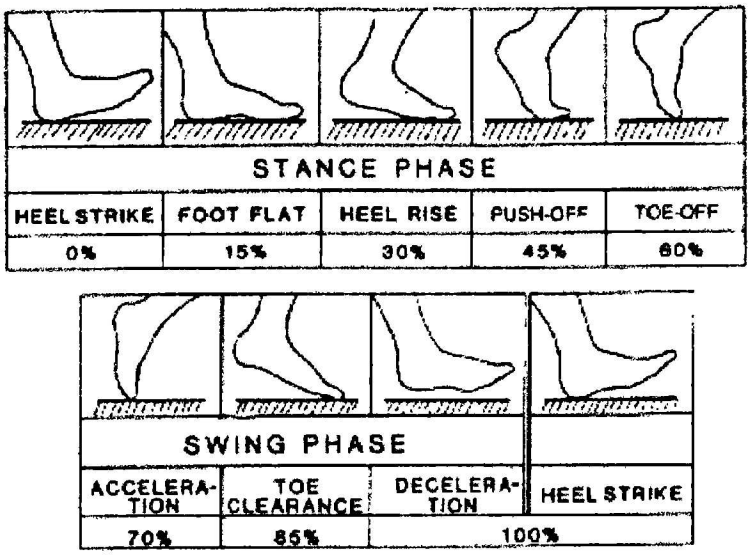

Figure 15 The gait cycle: one stance phase and one swing phase (Sammarco [1980]).

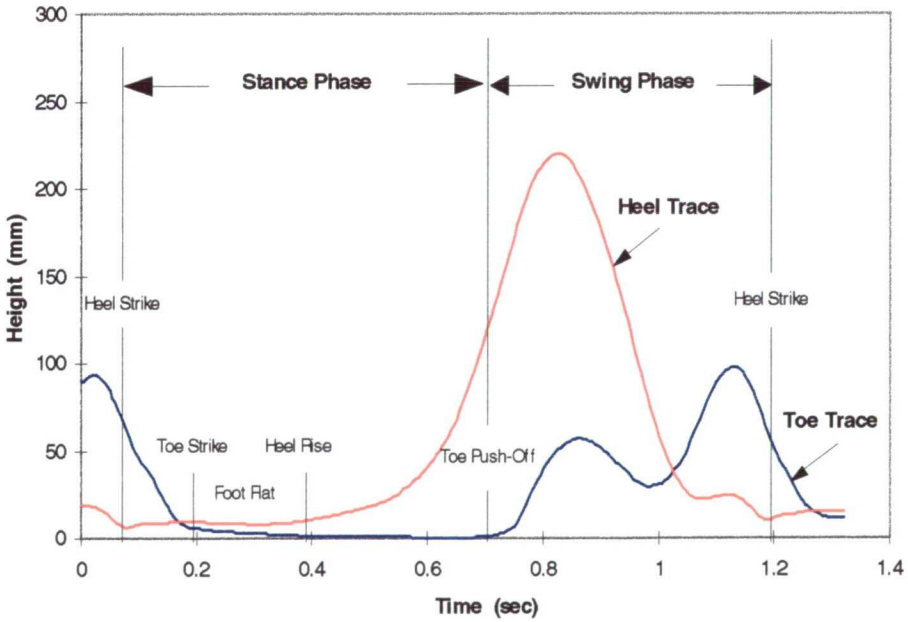

Figure 16 Graphical trace of event sequence for walking.

During the stance phase the progression of the load centre follows a curved path ending just under the big toe (see Figure 17).

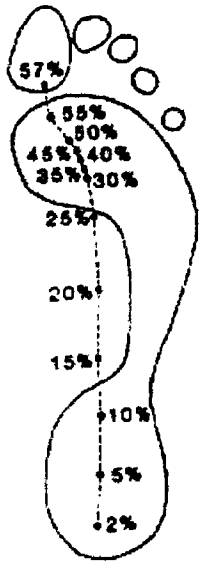

Figure 17 Progression of the load centre under the foot during the stance phase (Sammarco [1980]).

The step frequency, or footfall rate, is combined with the stride length to produce the speed at which a person walks. Grieve's [1969] generated data for a range of normal adult strides. For men, the average stride length was 0.45 to 0.58 times their height; while women ranged from 0.47 to 0.62 (these numbers conformed to ±1 standard deviation). This is evidence that our walking gait is continuously changing. We are constantly changing speed (whether by altering step frequency or stride length) to accommodate the situation, i.e. rushing to work, strolling along the river or walking with friends. However, countless gait studies have shown that we do maintain repetitiveness in our walking motions allowing comparisons between people.

4.3 IMPACT FORCES CREATED DURING WALKING

Characterising the forces exerted by normal walking or running has been the subject of numerous studies including; evaluation of surface abrasion properties (Harder *et al.* [1961]), structural vibration analysis (Wyatt [1989]) and the investigation of high frequency impulse loadings on the lower limbs used in the design of prosthetics (Simon *et al.* [1981]). In the normal walking gait as the heel strikes the surface it creates a reactionary force with a vertical component and two

shear components (in the plane of the contact surface). The research conducted in Chapters 5 and 6 only involved the vertical component that was considered to act in the Z direction.

Measuring the vertical component is generally accomplished directly with a *force plate* (see section 5.2.1) or indirectly using accelerometers or deflection measurements. Force plates are generally used to determine single trace, short duration impressions of the forces under the foot. They are typically constructed using piezoelectric force transducers or strain gauge proving rings. Accelerometers and deflection measurements are most often used for as-built structures to give an acceleration/deflection time history of loading. Provided the structure's mass, stiffness and damping characteristics are known, a force-time history can be produced from these acceleration / deflection time histories. Combinations of the two approaches can also prove successful. Rainer *et al.* [1986] described the use of piezoelectric force transducers inserted under temporary supports of an as-built office floor. This gave a direct force-time history of the loads applied to the floor.

Many papers including Rainer *et al.* [1986], Simon *et al.* [1981], and Wheeler [1982] have produced force time histories for foot-floor impacts. Figure 18 is a typical force time history produced during a slow walk. It shows a high initial impulse load occurring as the heel strikes the floor (A). The first hump (B) reflects the subject's weight plus an inertial component due to the subject's momentum while contacting the plate. This hump rises above the subject's static weight as the full combined force is measured by the plate. The trace then dips below the static weight (C) as the subject bends his knee, swings his opposite leg and transfers the body weight to the opposite limb. The final hump (D) occurs when the subject pushes off from the plate with the toes and finally (E), the subject ends contact with the plate entirely. This characteristic footprint is referred to as the *double camel hump*. Running tends to produce a single camel hump because the foot lands flat on the floor causing points B and D to blend together.

The impulse load at point A has a variable amplitude and contains frequency components between 10 and 75 Hz. The remaining trace contains frequency components up to 10 Hz (Simon *et al.* [1986]).

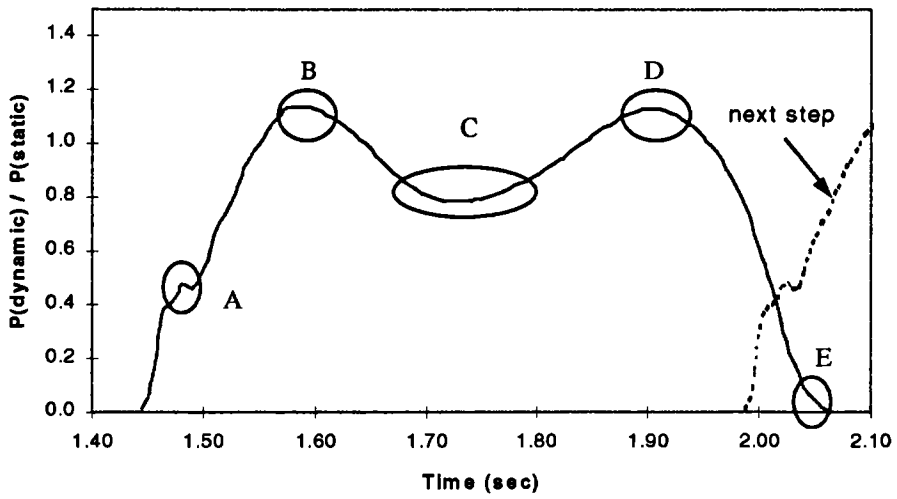

Figure 18 Typical force-time trace produced during a slow walk at 1.5 Hz (Wheeler [1982]).

4.4 THE GEOMETRY OF ASCENDING AND DESCENDING A STAIRCASE

When walking on the flat, a specific sequence of events occur (i.e. heel strike to toe push-off) which do not change regardless of the footfall rate used by the subject. For stair ascending and descending the sequence of events differs and is dependent on the footfall rate used by the subject.

Unlike walking, where one can choose the stride length, when ascending or descending the stride length is fixed by the geometry of the stair. Therefore the only way to attain a different speed is to change the footfall rate or alter the number of stairs used in a single step (i.e. take two steps at a time). Hence, a person walking briskly may chose to "run" up/down a set of stairs in order to maintain a brisk speed. The work carried out in Chapter 6 has provided interesting observations as to how we ascend or descend a staircase.

During a slow ascent (below 2 Hz), a subject typically takes one step at a time and does so in the same sequence of events as seen for walking, i.e. heel strike, flat foot, heel rise and toe push-off (see Figure 19 for graphical depiction of the gait cycle starting with the swing phase). When the footfall rate increases (between 2 Hz and 3.3 Hz), a subject may continue to "walk" up the stairs or may choose to "run". During a running ascent the sequence of events is slightly different. The subject first contacts the stair with their toes. Hence, the sequence of events is toe strike, flat foot, heel rise then toe push-off. As the footfall rate increases

further (above 3.3 Hz) a subject typically runs up the stairs so fast that the flat foot event cannot occur. Hence the sequence of events is toe strike and toe push-off. The change in elevation evident in Figure 19 and Figure 20 is due to the change in elevation of the steps.

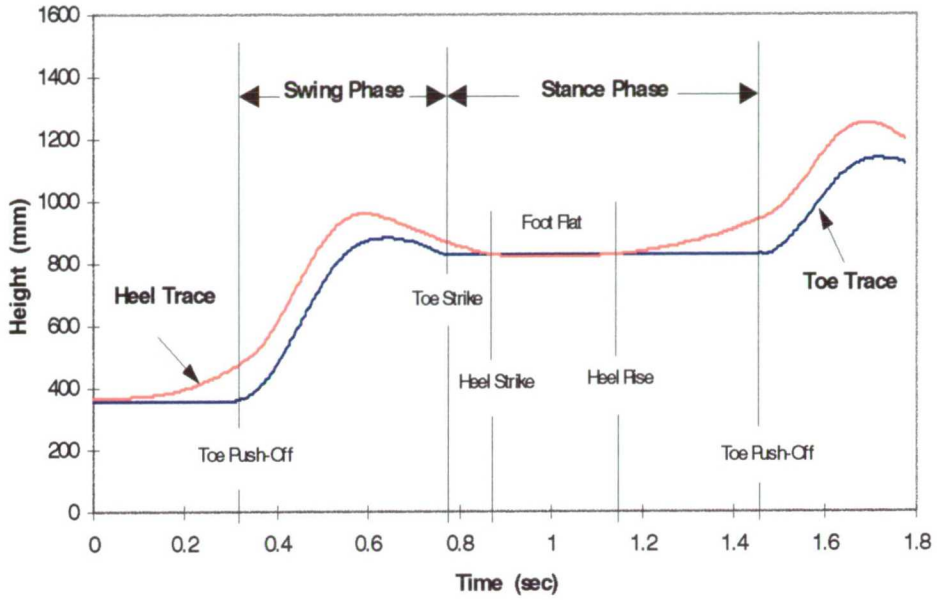

Figure 19 Graphical depiction of events for a slow ascent.

During a very slow descent (below 1.5 Hz), a subject typically takes one step at a time and does so with the same sequence of events as a slow ascent. However, at footfall rates between 1.5 Hz and 2.2 Hz, the sequence of events change to toe strike, flat foot, heel rise and toe push-off ascent (see Figure 20 for graphical depiction of the gait cycle). Above 2.2 Hz and below 3.3 Hz, the sequence of events remain the same except for the level of authority in the heel strike. Typically, the heel strike becomes less pronounced until the footfall rate increases above 3.3 Hz where, like ascending, there is insufficient time to permit the flat foot event and subjects typically run down stairs on their toes (i.e. toe strike and toe push-off). In fact, the toe push-off event can be so slight as to barely register on the force plate.

4.5 IMPACT FORCES CREATED DURING ASCENDING AND DESCENDING A STAIRCASE

As mentioned previously, during a slow ascent or descent the sequence of events is the same as that for walking. Hence, not surprisingly, the force-time history of the impact load has the same double camel hump shape. However, as the footfall rates increase the traces become very different. Figure 21 depicts the typical traces for a fast ascent and descent. The fast ascent shows a force-time history having the same shape as subjects running across a force plate on the floor. The humps labelled B and D in Figure 18 have merged as the contact time has become so short between toe strike and toe push-off as to produce a single hump. During a fast descent the initial toe strike produces a very large first peak while the toe push-off can be seen as a relatively small amplitude second peak. At very fast footfall rates the second hump is barely evident.

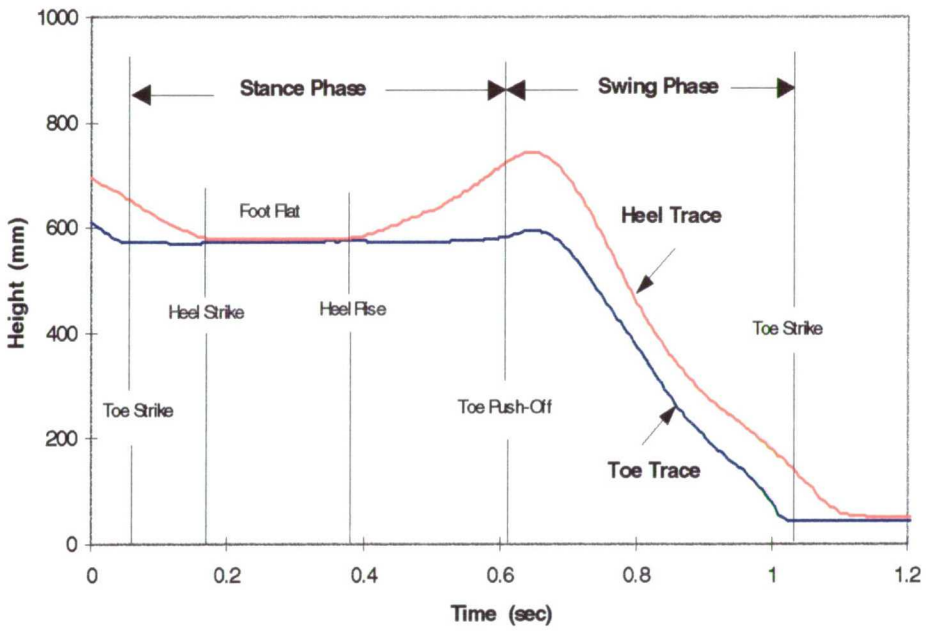

Figure 20 Graphical depiction of the gait cycle for a slow descent.

4.6 DISCUSSSION

This chapter was intended to give background information on the way humans walk and negotiate stairs as well as the vertical ground reaction forces generated during these activities. As discussed, the changes to the body positions are a combination of transitional and rotational motions that are typically analysed in

the sagittal plane. The walking gait, as well as the gait used during ascending and descending are made up of a stance phase and a swing phase. The impact loadings are measured with a force plate during the stance phase of the gait.

The force-time traces created during walking retained their distinctive "two camel hump" shape throughout all footfall rates and only varied in amplitude. The force-time trace created during ascending and descending varied in shape and amplitude depending on the footfall rate. This change in shape also substantially changed the harmonic components in the signal.

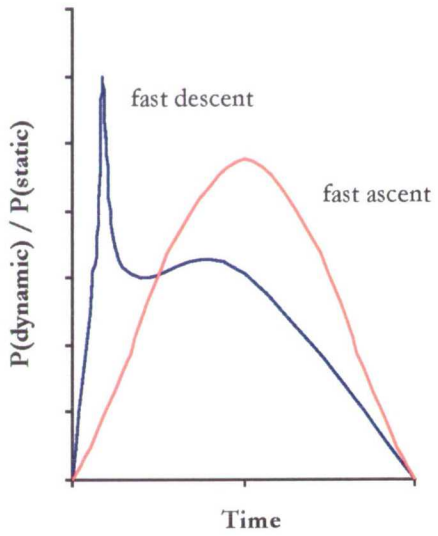

Figure 21 Typical traces for fast ascent and descent (reproduced from Smith [1988]).

REFERENCES

Ellingwood, B. and Tallin, A. (1984). *Structural Serviceability: Floor Vibrations.* Journal of Structural Engineering. Vol.110. No.2.

Harper, F.C., Warlow, W.J., and Clark, B.L. (1961). *The Forces applied to the Floor by the Foot in Walking.*. Building Research Station. National Building Studies research Paper No. 32, HMSO, London.

Hamill, J. and Knutzen, K.M. (1995). Biomechanical Basis of Human Movement. Williams & Wilkins. London.

Grieve, D.W. (1969). *The Assessment of Gait.* Physiotherapy. November.

LeVeau, B. (1977). Biomechanics of Human Motion. W.B. Saunders Company. London.

Rainer, J.H. and Pernica, B. (1986). *Vertical Dynamic Forces from Footsteps.* Canadian Acoustics. Vol.4. Part 2.

Sammarco, G.J. (1980). *Biomechanics of the Foot.* Basic Biomechanics of the Musculoskellital system. 2nd Ed. Chapter 9.

Simon, S.R., Paul, I.L., Mansour, J., Munro, M., Abernethy, P.J., and Radin, E.L. (1981). *Peak Dynamic Force in Human Gait.* Journal of Biomechanics. Vol.14. No.12. Pp. 817-822.

Smith, J.W. (1988). Vibrations of Structures. Chipman and Hill. London.

Wheeler, J.E. (1982). *Prediction and Control of Pedestrian Induced Vibration in Footbridges.* Journal of the Structural Division, Proceedings of the American Society of Civil Engineers. Vol.108. Pp.2045-2065.

Wyatt, T.A. (1985). *Floor Excitation by Rhythmic vertical Jumping.* Engineering Structures Journal. Vol.7.

CHAPTER FIVE 5

FLOOR LOADING

5 EXPERIMENTAL WORK CONDUCTED ON THE FLAT

5.1 INTRODUCTION

5.1.1 What are Vibrations?

There are two important reasons for investigating the forces generated under a foot during walking or running. The first is to gather human loading data to use in the field of structural engineering; especially in the design of structures susceptible to human induced vibrations, i.e. floors, footbridges, and staircases. The second is to gather human loading data to use in the field of biomechanics, which is discussed in Chapter 9.

Within structural engineering, vibration analysis has become increasingly important with the increased use of lightweight dynamically sensitive structures. This has been especially true with the move towards slender structures for cost saving and to aid in more 'adventurous' designs. In some cases the problems caused by vibrations can lead to fatigue cracking, dynamic instability or plastic deformation (Bolton [1978]). Since these results can be devastating and even life threatening, a designer should have a clear understanding of vibration mechanics. So, what are vibrations?

Any engineering system that has mass and has some form of elasticity is capable of relative motion. Once started, if this motion repeats itself it becomes known as a *vibration.* Vibration is a form of energy transfer that is typically undesirable. To eliminate the effects of vibrations or to at least lessen them, structural engineers study the *equation of motion* for systems under investigation. A single degree of freedom system has an equation of motion as given below.

$$m\ddot{x} + c\dot{x} + kx = 0$$

where k = stiffness of the system
c = damping coefficient
m = mass to be vibrated
$x, \dot{x}, \ddot{x}$ = displacement, velocity and acceleration

From this formula yields the equation for a system's *damped natural frequency*

$$f_d = (1/2\pi)\sqrt{k/m} * \sqrt{1 - \{c^2/(4mk)\}}$$

where f_d = damped natural frequency of the system

If the system has little or no damping the natural frequency can be approximated by the undamped natural frequency equation given below

$$f = (1/2\pi)\sqrt{k/m}$$

where f = undamped natural frequency of the system

The natural frequency of a system is the frequency of oscillation that occurs when the system is set in motion by some internal/external force. The equation above can give an approximate result for many applications. For example, suppose a large container is being moved across a simply supported massless floor as shown in Figure 22.

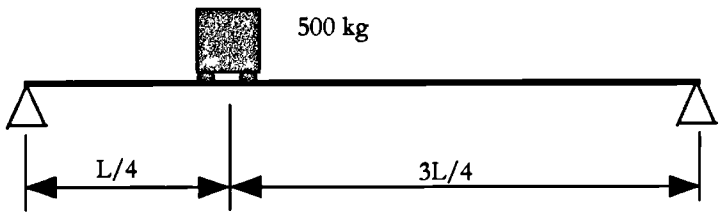

Figure 22 Example of a mass being moved across a floor.

Now assume that a computer model calculated the deflection of the floor at the ½ span to be 1 mm per 1 kN force. Therefore, the floor stiffness is

= 1000 N / 0.001 m
or 1.0×10^6 N/m

Inserting into the undamped natural frequency equation

$$f = (1/2\pi)\sqrt{1.0x10^6/500}$$

yields a natural frequency of 7.1 Hz.

5.1.2 Harmonic Content in Human Gait Applied to the Design of Floors

Although structural vibrations can be caused by a variety of sources, (e.g. machinery, external traffic, wind) floors typically vibrate when people walk on them. Floors and framing systems are designed to well known stiffness criteria such as limiting the static deflection due to normal live loads to the length of floor span, l, divided by 360; or, limiting the length to depth ratio of supporting steel beams to $l/20$. These simple criteria have been used by designers for nearly 100 years and have obviously worked well owing to the fact that little guidance can be found in available literature on controlling vibrations in buildings.

In recent decades however, these criteria have not worked so well. Structural analysis methods have become more refined allowing the use of lighter, high strength steel members and materials. Floor construction has used longer spans and lighter coverings. Open floor plans have reduced the use of partitioning walls and non-structural members, removing the additional stiffness and damping they had provided. All these factors have created multi-story buildings that are increasingly sensitive to the dynamics effects of human motion.

The static strength of the floor systems in these buildings is not in question. It is simply that the floor systems now have significantly reduced natural frequencies that can be excited by normal human activities. Once set in motion, these floors often exhibit levels of vibrations which, at the very least, are annoying, and are often intolerable. Unwanted vibration can reduce work efficiency and even quality of life.

Much investigation has gone into the effects of human exposure to vibrations and acceptable tolerance levels (Ellingwood and Tallin [1984], Wyatt [1985], Pernica and Allen [1983], Allen and Rainer [1976]). ISO 2631 [1985] is a guide to human

exposure to whole body vibrations which has close ties to BS6472 [1984], human exposure to vibrations in buildings.

Section 4.2 of BS6472 was entitled "Satisfactory vibration magnitudes in buildings" and presented a base curve of vibration levels in the Z direction (foot to head), measured in structural RMS acceleration (m/s^2) between frequencies of 1 Hz to 80 Hz (see Figure 23). This curve represents the minimum perceptible acceleration levels for critical working areas, i.e. hospital operating theatres, precision laboratories. Other buildings such as residential, office or workshops are permitted to have acceleration levels based on multiples of the curve. For example, a general office may have perceptible or acceptable acceleration levels of 4 to 8 times the base curve.

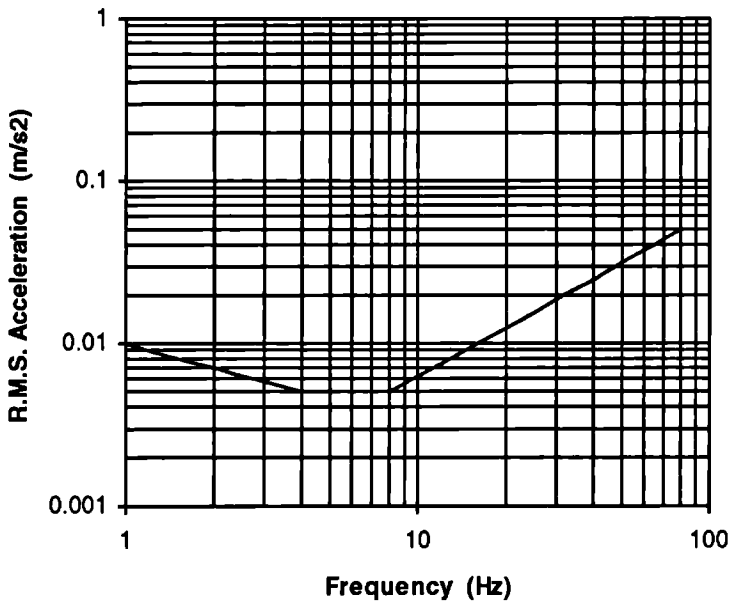

Figure 23 Base perception curve for vertical accelerations - BS6472

A substantial document was also produced by the Steel Construction Institute in association with the Construction Industry Research and Information Association. The SCI/CIRIA guide to vibration of floors [1989], was written " ... to provide a practical method for assessing the likely vibrational behaviour of floors in steel framed buildings". The guide essentially provides a formula for calculating the response of a floor system to the Fourier components of a walking force-time history. The *response factor*, R, given by the formula is a multiplier to the vertical

acceleration base curve presented in BS6472. In the calculation of the response factor, the authors of the guide make several assumptions as to the type and magnitude of the harmonic loading.

Firstly, only the first three harmonic components of the walking pace were considered in the calculations. Above the third harmonic, the amplitudes were considered too low to cause excessive vibration in the floor system by walking. Secondly, the amplitudes for the second and third harmonics were based on the value of a *Fourier component factor*, C_f. The first harmonic amplitude was given as 240N based on an average male subject (weight, 700N) walking at the average footfall rate (approximately 2 Hz). This produced a first harmonic amplitude of 0.34 or 34% of the subject's weight. The second harmonic amplitude was based on a C_f value of 0.40 or 40% of the first harmonic, giving an amplitude of 0.14. The third harmonic was based on a C_f value of 0.20 giving an amplitude of 0.07. These ratios were fixed and woven into the response factor equation for floors with natural frequencies less than 7 Hz.

$$R = \frac{68000 C_f}{m S L_{eff} \zeta}$$

where	R	=	response factor
	C_f	=	Fourier component factor
	m	=	floor mass (kg/m^2) **[3]
	S	=	floor effective width (m) **
	L_{eff}	=	floor beam effective span (m) **
	ζ	=	structural critical damping ratio

The guide also gave general considerations for the design of floors. That is, floors systems should not normally be designed with natural frequencies under 3Hz. Hence, the first harmonic frequency (typically, 1.6 to 2.3 Hz) should not excite the floor. If the floor system is subjected to rhythmic activities, i.e. dancing, concerts, exercises, etc., it should not normally have a natural frequency under 5 Hz. Hence, the floor will not be excited by the first or second harmonic frequencies.

Literature on acceptable vibration levels typically quotes structural acceleration values directly or as a multiplier to a base curve. Care must be taken to understand which base curve is being referenced. Allen and Rainer [1976]

presented a base curve for continuous vertical vibration as shown in Figure 24. Note the ordinate was measured as peak acceleration as a percentage of g and not RMS acceleration. The curve is identical in shape to the BS6472 curve (above 4 Hz) with an ordinate value 10 times greater.

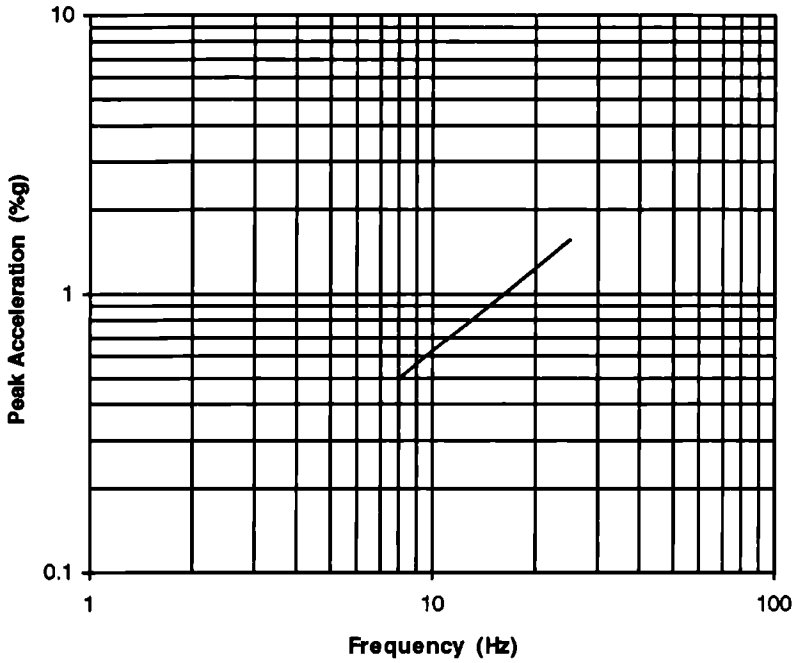

Figure 24 Base curve for vertical vibration - Allen and Rainer [1976].

5.1.3 Harmonic Content in Human Gait Applied to the Design of Footbridges

BS 5400, Part 2 [1978] deals with the vibration serviceability requirements of footbridges in appendix C, section 3. The standard gives two methods for determining the maximum acceptable vertical acceleration. The first method was based on static deflection, a configuration factor, and a dynamic load factor as shown below,

$$a = (2\pi f_o)^2 y_s K \psi$$

where a = maximum vertical acceleration,
f_o = natural frequency of footbridge (Hz),
y_s = static deflection at midpoint (mm),

[3] See section 7.2, Wyatt, T.A. (1989) "Design guide on the vibration of floors", SCI. for a description of terms.

K = configuration factor, and
ψ = dynamic response factor.

The amount of static deflection was based on a 700N person standing at the centre of the main span which can be calculated with standard FEA packages or from empirical formula (for a 3 span footbridges, the deflection is taken at the centre span). The configuration factor was based on the number of spans (up to 3) and the dynamic response factor was based on the span length and the *logarithmic decrement of decay of vibration*, δ (see BS5400 [1978] for further details). This method produced a single figure for the predicted vertical acceleration and did not consider loading functions from higher harmonics.

The second method was applied to footbridge configurations other than those used in the previous method. It was based on a dynamic, pulsating point load, F, moving across the main span of the footbridge at a constant footfall rate of V_t. The loading was applied by an average male pedestrian weighing 700N. The load, F, and the footfall rate, V_t, were given by the equations

$$F = 180\sin(2\pi f_o t)$$

$$V_t = 0.9 f_o \ .$$

Also, the maximum acceleration should not exceed

$$a_{\max} = 0.5\sqrt{f_o} \ .$$

If the value of f_o is greater than 4Hz, the calculated maximum acceleration can be reduced by an amount varying linearly from zero reduction at 4Hz to 70% reduction at 5Hz.

This method assumed a first harmonic amplitude of 26% of the subjects weight or 0.26 (i.e.180/700). It also assumed this dynamic force was exciting the footbridge at all footfall frequencies up to 4 Hz. This seems unlikely as the average walking footfall rate (2 Hz) will excite a footbridge (having a natural frequency of 4 Hz) with the second harmonic, not the first. The amplitude of the second harmonic will be much smaller. Hence, the procedures layout in BS5400 (which are the

same in the Ontario Highway Bridge Design Code, OHBDC [1983]) do not take into account the loading functions from the higher harmonics.

Rainer *et al.* [1988] understanding the deficiencies in BS5400 and the OHBDC, proposed a new design procedure for evaluating the maximum allowable peak accelerations at resonance for simply supported bridge spans. Their expression (given below) was a function of a *dynamic amplification factor,* Φ, and allowed the prediction of peak accelerations for any harmonic component.

$$a = (2\pi f_o)^2 \frac{\alpha P}{k} \Phi$$

where	a	=	maximum vertical acceleration,
	f_o	=	natural frequency of footbridge (Hz),
	α	=	harmonic amplitude as fraction of body weight
	P	=	subject body weight
	k	=	measured stiffness of span at centre
	Φ	=	dynamic amplification factor

The dynamic amplification factors required for the formula were calculated by Rainer and his colleagues as functions of damping ratio and the number of cycles per span (i.e. the number of steps required to cross the span times the harmonic number of the loading function). The plot has been reproduced as Figure 25. As the number of cycles are increased the values of the amplification factors increase monotonically until their values reach the steady state amplitude for long, continued excitation, i.e.

$$\Phi \cong \frac{1}{2\xi}$$

where	ξ	=	critical damping ratio.

Rainer and his colleagues used this method to predict the peak results for two purpose built bridge spans. Their predictions compared favourably with the results from experimental tests and from BS5400 and the OHBDC. They were also able so show a significant contribution from a second harmonic loading function which was not accounted for in BS5400 and OHBDC.

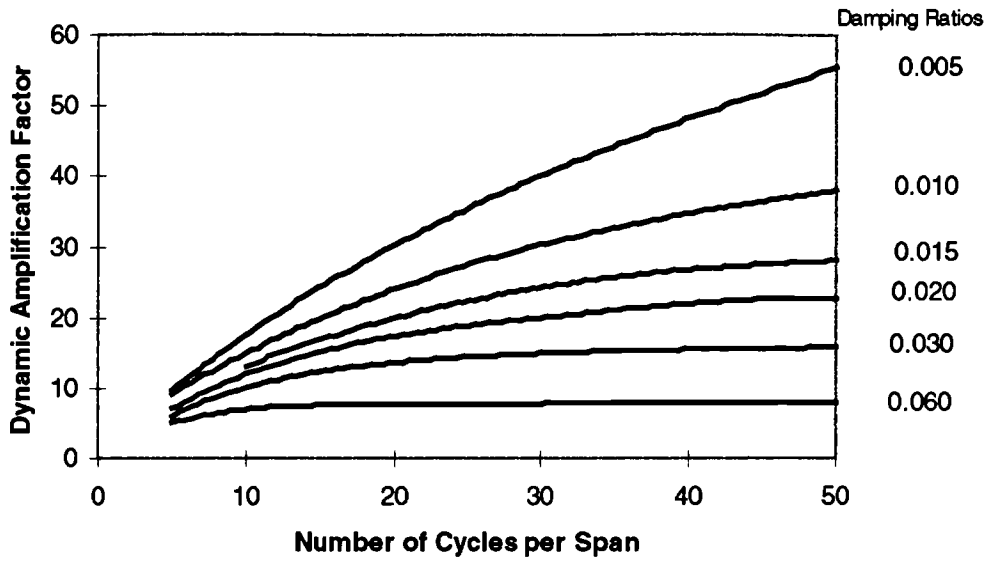

Figure 25 Dynamic amplification factor at resonance verse number of cycles per span and damping ratio (reproduced from Rainer et al.[1988].

5.2 TECHNICAL BACKGROUND INFORMATION

5.2.1 Force Plates

The study of human motion has a long history but only in the recent past, with the invention of the force plate, has a researcher had the tools to study first hand the forces generated by the motion, or in other words, the ground reaction forces.

In 1965, Skorecki designed an apparatus for measuring the ground reaction forces exerted by both feet when walking along an 11ft or 3.5m platform (see Skorecki [1966]). His device, referred to as a 'gait machine', was installed at the Wrightington Hospital near Wigan in Lancashire, England. Although there had been force plates developed prior to the Skorecki's machine (Bresler and Frankel [1950], Cunningham and Brown [1952]), his was considered a vast improvement and provided data in a dynamic response range of 0 to 30 Hz. For walking, this amounted to an accuracy in force prediction to within 1% or better (according to Skorecki). After Skorecki, came a flood of devices to measure reaction forces and with them came a greater awareness of the special care needed during the design of force plates from the static and dynamic point of view. For the plate to be accurate it must be rigid enough to withstand deflection that would cause "cross talk" among the transducers (static requirement). However, the plate must be as

light as possible to increase its natural frequency well beyond those transmitted through the body on contact with the plate (dynamic requirement). Force plates are generally used to determine single trace, short duration impressions of the forces under the foot and are constructed in the form of a flat plate which is lowered into a recess to make it level with the floor. The plate is typically a section of composite material supported by four piezoelectric force transducers or strain gauge proving rings.

A transducer is a device for converting non-electrical signals, i.e. sound or light, into electrical signals or visa versa. A piezoelectric transducer operates on the principle of *piezoelectric effect* which is the generation of a potential difference across the opposite faces of non-conducting piezoelectric crystals through the application of mechanical stress between the faces. The potential is proportional to the stress and will change direction if the stress changes from compression to tension. The most common type of piezoelectric crystal is quartz although a another crystal called Rochelle Salt is sometimes used for its greater potential forming ability. However, it does not have the greater strength of quartz.

Strain gauge proving rings operate on the same principle of generating a potential difference but across a pair of strain gauges. A strain gauge is a small mechanical device used to measure small deformation. The most widely used devices are metal wires or semiconductor materials such as silicon crystals. These devices are attached to a proving ring as shown in Figure 26-A and as they are stretched under tensile stress the resistance of the wires or semi-conducting materials increases. The strain gauges are then used as elements in a Wheatstone-bridge[4] electrical circuit (see Figure 26-B). As the proving ring is compressed the outside strain gauges labelled T_1 and T_2 increase in resistance while the gauges labelled C_1 and C_2 decrease in resistance causing an electrical potential to build up across V_{out}. If the ring is stretched, the reverse will occur and the potential will build up with an opposite sign.

Typically strain gauges need to be calibrated by placing a series of known weights on the force plate and recording the output voltage. The calibration process is usually linear which allows either interpolation or extrapolation of the data.

[4] Popularised though not invented by Sir Charles Wheatstone(1802-1875) it is an electrical circuit typically used to measure the value of a resistor.

Piezoelectric transducers typically have a factory set calibration factor. The outputs obtained from the transducers are amplified, summed (in the case of vertical loads) and, typically, recorded by a data acquisition system.

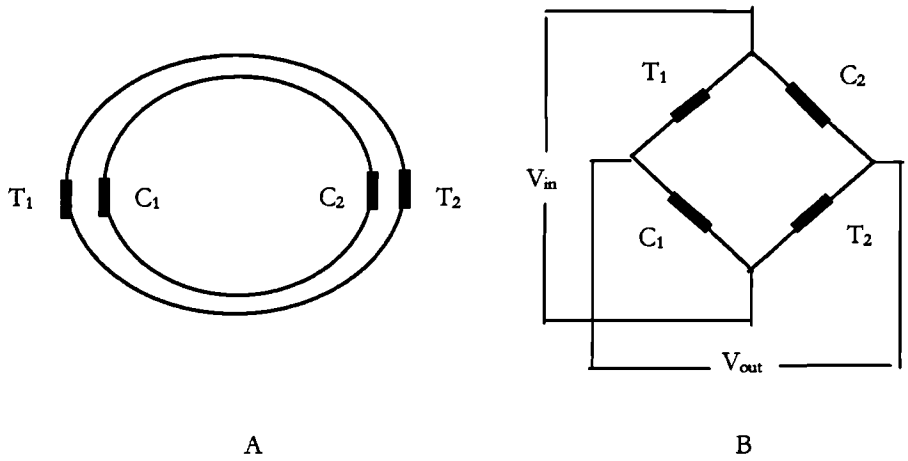

Figure 26 (A) Location of strain gauges on a compressed proving ring (B) a Wheatstone-bridge electrical circuit.

The force plate used for this thesis operated with piezoelectric transducers that detected impact force in the vertical (Z), fore-aft (X), and anterior-posterior (Y) directions although the work in this thesis was only concerned with the vertical direction. If the vertical forces measured at each transducer were labelled F_1, F_2, F_3, and F_4, the total force was simply $F_z = F_1 + F_2 + F_3 + F_4$. If all 4 forces were equal then the centre of pressure, i.e. the point of application was at the exact centre of the plate (length/2, width/2). If the forces were not equal than the point of application could be calculated by the following equations

$$x = \frac{length}{2}\left[1 + \frac{(F_2 + F_4) - (F_1 + F_3)}{F_z}\right]$$

$$y = \frac{width}{2}\left[1 + \frac{(F_3 + F_4) - (F_1 + F_2)}{F_z}\right]$$

It is also vitally important that the force plate itself had a natural frequency well above the frequencies to be measured. If not, there could have been a possibility that the plate's fundamental frequency was excited to resonance causing the plate to deflect significantly, thus giving false output. Modern force plates are typically

made of composite materials with light mass and high stiffness to avoid this problem. This combination of mass and stiffness will produce a very high natural frequency for the force plate.

5.2.2 Data Acquisition Systems

The analogue voltages generated by the force plate transducers are typically recorded with a computer via a data acquisition system. The main purpose of the system is to convert the analogue voltage signals into digital signals through an A/D (analogue to digital) converter. The analogue signals coming from the transducers can be either in *polar* or *bipolar* mode. Polar signals have a range of 0 Vdc to X Vdc where X is a positive number. Bipolar signals have a range of +/- X Vdc. All A/D converters allow input in either mode.

5.2.2.1 Resolution and accuracy

Typically an A/D converter has a resolution of between 8 and 16 bits and a maximum range of +/- 10 Vdc; or in other words, a 12 bit converter has a range 2^{12} or 4096 bits (4095 actually) with which to represent +/- 10 Vdc. The converter is typically set up that

+10 Vdc	=	4095 bits,
0 Vdc	=	2048 bits, and
-10 Vdc	=	0 bit.

For a 12 bit card, the smallest reading of full scale is 1 bit in 4095 bits. This bit is referred to as the *least significant bit* or LSB and is the term used to specify accuracy. In most cases the converters will be accurate to +/- 1 LSB. Therefore if a transducer is not putting out any voltage, i.e. 0 Vdc, the 12 bit converter will read 2048 +/- 1 bit.

5.2.2.2 Conversion speed

A data acquisition system operates by sampling points from the continuous analogue signal. Most systems will allow the sampling of up to 16 analogue signals (channels). This is not to say that all 16 channels are sampled at the same time. A typical A/D converter and the sample & hold circuits can capture and digitise a sample in 10 μs (microseconds). Therefore it would take 160 μs to

sample all channels just once. In terms of throughput per second; sampling 1 channel allows a maximum sample rate of 100 kHz, whereas sampling 16 channels allows a maximum sample rate 100/16 or 6.25 kHz. The actual sample rate is user specified and if it is less than the maximum throughput allowed, the system will simply wait until the appropriate times to take the samples.

All data acquisition systems allow the user a second stage of amplification when the analogue signals enter the A/D converter. This user specified gain amplifier is usually located as a "front end" to the A/D chip along with the sampling circuitry and a multiplexor. All A/D chips have a fixed input range, typically +/- 10 Vdc. It is the analogue front end that amplifies low level signals or adjusts unipolar signals to match the chip. A poorly designed front end will allow fast throughput at certain ranges but will greatly reduce the input at other ranges. A well designed front end will sustain the maximum throughput for all ranges.

5.2.2.3 Single ended and differential channels

A signal coming in from a transducer will consist of a *signal high* and a *signal low*. A 16 channel "single ended" A/D card will have analogue inputs for 16 signal high connections and one analogue ground connection (referred to as low-level ground). An 8 channel "differential" A/D card will have analogue inputs for 8 signal high and 8 signal low connections and the low level ground. Usually the A/D card will be set-up to handle both types of input and merely requires a jumper setting to be made.

When using a single ended type card to capture the analogue signals, certain precautions must be followed to ensure the A/D converter is receiving a good clean signal. Firstly, all signal lows coming from the transducers must be at the same potential or in other words, if a volt meter is connected between any two signal lows the reading would be zero. Also, there must be no potential between the signal lows and the chassis ground. Unfortunately, this can be a problem if the A/D card is installed within a laptop that is running off battery power. In such a case the chassis ground of the computer is "floating" with respect to the earth ground and therefore a potential can exist with the signal low. When the computer is grounded, there must not be a potential between the signal ground

and the PC ground. If a potential does exist it is called a "ground loop" and will be added to the signal input.

When using a differential type card these concerns can be avoided; however, the card is typically restricted to inputs from only 8 channels. Since the signal high and signal low coming from each channel is independent of the other channels, a potential can exist between the various signal lows without affecting each other. The analogue signal measured for each channel is taken as the potential between the high and low for that channel, only. The ground from the transducers must now be hooked to the low level ground which in turn is connected to the chassis ground. A potential can exist between the signal lows and the low-level ground (chassis ground) but it cannot be greater than +/- 10 Vdc, typically. This allows the use of a laptop on battery power without the worry of signal interference. A differential type A/D card is useful to have in areas of electromagnetic interference (EMI) or radio frequency interference (RFI) that cross the signal wires. These interferences will equally affect the signal high and signal low wires causing a net potential of zero. On a single ended A/D card the interference would affect the signal high wire while the signal low wire would remain grounded. Thus, voltage spikes could appear in the data.

5.3 EXPERIMENTAL SET-UP AND EQUIPMENT

For these experiments, each subject was asked to walk along a raised platform and step onto a calibrated force plate. The voltage signals delivered from the piezoelectric transducers were recorded by a data acquisition system and stored on a laptop computer. The data files were then converted into a suitable binary format for post-processing. Figure 27 is a picture of the equipment set-up used for experiments conducted on the flat. Each item of interest has been labelled and a detailed description given below.

Item A: Force plate with 4 quartz piezoelectric transducer units

The force plate was originally constructed in 1969 by the Composite Structures Division of Rolls-Royce plc for the Biomechanical Research and Development Unit (BRADU) of the Department of Health and Social Security. It was made of a sandwich construction with a central layer of aluminium honeycomb bonded

between two sheets of a carbon filament filled resin material and topped with a non-slip walking surface. It had dimensions of 610mm x 380mm x 30mm (24" x 15" x 1.2").

The force plate had a very high stiffness to mass ratio that produced a fundamental natural frequency in excess of 650 Hertz. This eliminated any concerns of inducing higher order harmonic resonance from the experiments into the plate since the highest loading frequencies expected were around 50 to 70 Hertz.

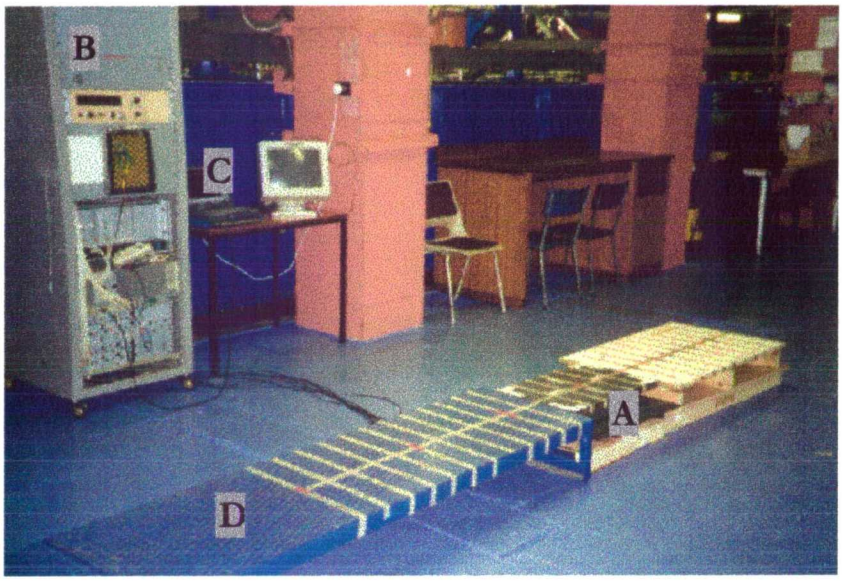

Figure 27 View showing force plate, amplifiers and computer/ data acquisition system.

The underside of the plate had four small cast iron pads bonded to the surface and ground to a flatness tolerance of 0.005mm. Their locations formed a grid 460mm x 230mm (18" x 9") positioned symmetrically under the plate. To each pad was attached a Kistler quartz piezoelectric transducer, type 9251A which provided a small output voltage to an amplifier. The signals were amplified to prevent transmission losses. The system was designed to provide forces and moments in/about the X, Y and Z directions although, for these experiments only the Z (vertical) direction forces were stored. Figure 28 is a sketch and photo of a transducer.

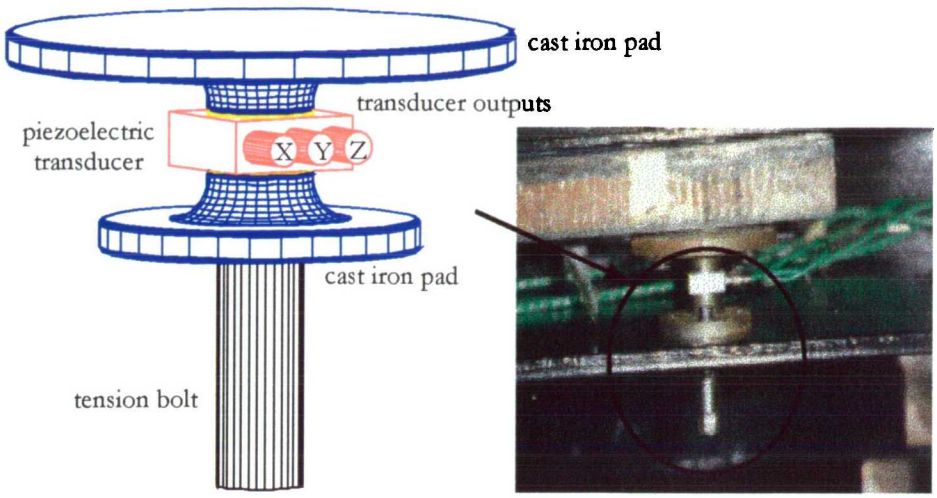

Figure 28 Piezoelectric transducer

Item B: Amplifier unit

The four Z direction inputs were each fed into separate Kistler charge amplifiers of type 5001. At each amplifier the sensitivity setting was altered to produce the same output voltage for a given static load. This checking procedure was performed on the force plate by moving a 20kg load over each transducer and recording the voltage from the F_Z BNC output connection on the amplifier case. Each amplified signal was fed into a Kistler summing amplifier that (in the case of the Z force inputs) simply added the voltages to produce a single output voltage.

Item C: PCMCIA data acquisition system

The data acquisition equipment chosen was a "Datagate" data acquisition and evaluation system created by nCode International of Sheffield. The output voltages from the summing amplifier were routed through a 16 channel breakout box and captured by a PCMCIA 16 channel, single ended, A/D card of type PCM-DAS16 (manufactured by Computer Boards Inc., Mansfield, MA, USA). Within this system, a real time display could be viewed, but the individual data file could not be stored on the hard drive unless the 'data transfer' sub menu was used. The data files can be viewed for post processing within the Datagate program by using the sub menu 'graphical display' which also allows the file to be exported in an ASCII format. To convert the stored data to binary format

require an nCode program called 'dgdmx' which was found in nCode's 'nSoft' suite of programs.

Item D: Raised walkway

To facilitate the use of the force plate a metal walkway was used as a 'lead-in' and a platform built to bring up the force plate height to the level of the walkway. A second walkway also served to provide a 'lead-out' from the force plate so the subject's normal stride was achieved when he/she made contact with the plate.

5.4 PROCEDURE

5.4.1 Capturing the Force Data from a Footfall Trace

Section 4.3 of the previous chapter discussed the expected forces from a single footfall trace whether from the left foot or right foot. Also discussed was the frequency content expected in such a trace i.e. anything up to approximately 75 Hz. Therefore, based on standard sampling theory, an acquisition rate of 200 Hz was chosen to capture all frequency content in the trace up to 100 Hz.

Available literature agreed that pace and subject stature (weight and height) were the most influential variables relating to the shape of the footfall trace. Other factors also suggested were stride length (typically a function of height), age, sex, physical abnormalities, and shoe apparel. All may be valid factors affecting the shape of the footfall trace so it was necessary to quantify their effects through targeted testing.

A breakdown of participating subjects, grouped according to age and sex is given in Table 3. All the subjects had 'normal' walking patterns, unaffected by physical abnormalities. An undergraduate study by Martin [1995] (in which the author participated), revealed that shoe apparel altered the high frequency content of the footfall trace i.e. soft soled shoes attenuated the higher frequencies. As the high frequency content related to the higher harmonic content in the trace, it was determined early on that it would not be necessary to record the type of shoe

apparel worn by the subjects (although nearly all subjects wore soft sole shoes by choice).[5]

Age	Male	Female
Under 20	6	2
20 to 30	23	3
Over 30, but <45	3	3
Total	**32**	**8**

Table 5 Breakdown of participating subjects in walking tests by age and sex.

For each test, a subject was asked to "follow" the tones generated from an electronic metronome. By starting at the beginning of the walkway and walking at a comfortable "natural" stride, the stride length achieved just prior and just after contact with the force plate was noted. These lengths were then averaged and recorded as the subject's stride length for that particular test. The impact information, produced when contact was made with the force plate, was recorded by the data acquisition system in the form of a footfall trace sampled at 200 samples per second (see Figure 29).

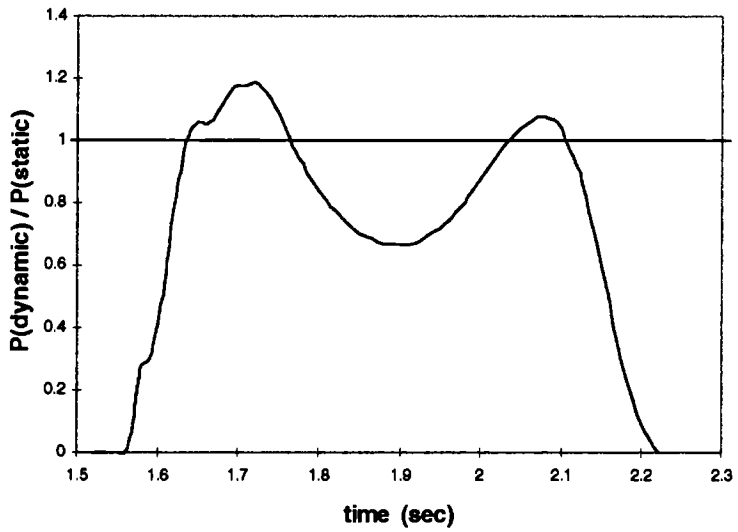

Figure 29 Typical footfall trace - the "double camel hump".

To facilitate comparisons between individuals, it was necessary to normalise each footfall trace by the individuals body weight, P (static), hence removing body

[5] To recreate an approximate force time history from the harmonics only requires the initial harmonics (i.e. the first 10 harmonics). The higher harmonics are not necessary.

weight as a factor affecting the shape of the footfall trace. This was accomplished by having each subject stand on the force plate so a 'weight' in volts could be recorded. A plot of a typical weight trace is shown in Figure 30.

By averaging the values near the centre of the trace (where the subject was stationary on the plate) and subtracting any non-zero offset, a normalising weight was achieved. This normalising process ensured that each subject had a body weight of 1.0 volts and thus variations about this mean value could be compared on the same basis for each subject.

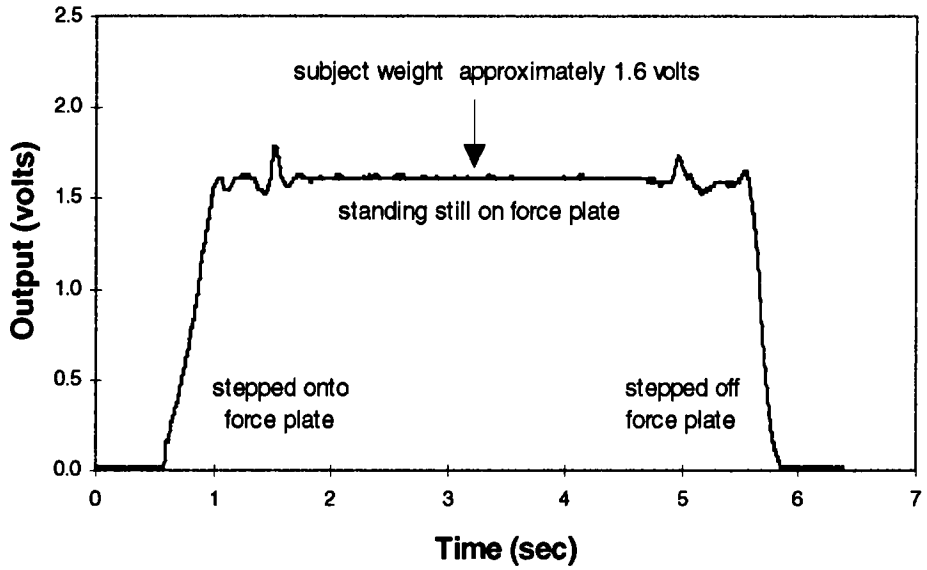

Figure 30 Voltage trace of a test subject standing on the force plate.

The range of footfall rates chosen for the experiments was determined using the many "normal walking" rates cited in various papers. Matsumoto *et al.* [1978], conducted an experiment where 505 persons were sampled as they walked naturally down a road. The distribution of walking paces closely followed a normal distribution with a mean value of 2 Hz and a standard deviation of 0.175. Ellingwood's [1984] work however, sited a mean walking footfall rate of 112 steps per minute or 1.86 Hz. Hence, a range was chosen between 1 and 3 Hz, although in practice all subjects found it extremely difficult to walk beyond 2.6 Hz. This author also found that the Ellingwood and Tallin prediction more closely matched the observed normal walking footfall rates seen during the tests.

5.4.2 A C++ Program for the Production of a Continuous Force Time History from a Footfall Trace

Over 1000 individual tests were conducted producing single footfall traces over a range of walking rates varying between 1 and 3 Hz. Since a Fourier analysis can only be conducted on a repetitive time history, it was necessary to modify the single footfall traces into continuous traces. However, there are some important issues concerning how this should be done. Ohlsson [1982] and Ellingwood and Tallin [1984] both concluded that in order to construct a single time history one must assume the footfall traces for the left and right foot are essentially identical. But are they?

Jacobs *et al.* [1972] used the Skorecki gait machine in his analysis of the vertical forces exhibited in normal and pathological gait. Figure 31 shows example footfall traces as captured by Jacobs on the Skorecki gait machine. Although the traces show some variations between the left and right foot, Ohlsson [1982] and Ellingwood and Tallin [1984] conclude that one can assume the footfall traces for the left and right foot agree well enough that one could represent the other.

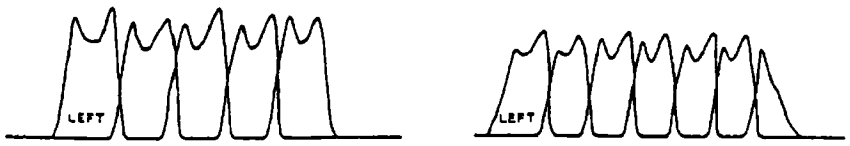

Figure 31 Examples of 'left-right' footfall traces as measured by Jacobs[1966].

As discussed earlier, the trace information gathered for each test was in the form of a single footfall trace. For the above reasons, no attempt was made to record which foot (left or right) created the trace.

To develop a continuous force time history from the single foot fall trace (see Figure 32) each trace was overlapped by the exact period between heel strikes. Determining the exact period was crucial to the calculation of the harmonics.

Initially, the period was calculated by viewing video of the walking experiments. A Sony Hi8 video camera recorded the images at 25 frames per second. An estimate of the time at heel strike was accurate to ± 1 frame or $^1/_{25}$ of a second. Considering an average period of ½ second between heel strikes, the ± 1 frame

error created nearly a ± 10% variation on the actual period. This affected the harmonic calculations by nearly as much; therefore, a better solution was needed for calculating the period.

To produce a finer estimate of the period, a simple assumption was made. Since the subjects' footfall traces were normalised, the signal offset for the continuous trace must be equal to 1 volt. Based on previous discussions of Fourier Series, this 1 volt offset equals A_0. Hence, if one assumes a starting period (say 0.5 seconds) and iterates the A_0 expression, eventually a period will be found that produces a value of 1. This period is the overlap period between traces.

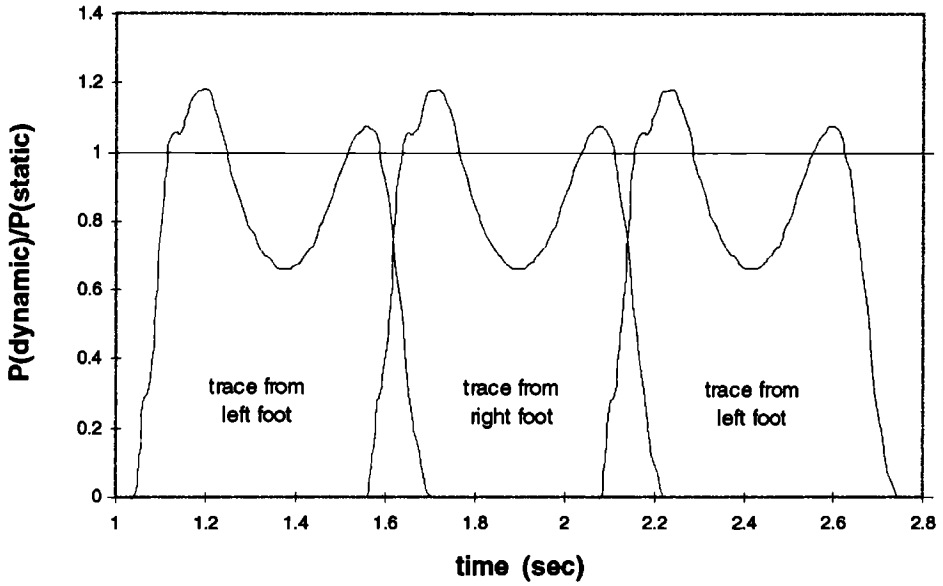

Figure 32 Left - Right - Left : Overlapping the footfall traces

A C++ program called *harmonic.cpp* was written to do this work automatically. It operated by reading a raw data file (see Figure 33) along with the subject weight (in volts). The data file was divided by the weight to produce a normalised data trace. Each trace was then reduced by the amount of signal offset, (labelled A in Figure 33). Typically, all raw data files contained a signal offset because no attempt was made to zero the force plate system prior to each test.

The program then read through and compared the data values to determine the start and end points for the trace, labelled "start" and "end" on Figure 33. Three copies of the trace between the start and end points were then inserted into an array with an offset between each trace of 0.5 seconds or 2 Hz. This was the

initial default footfall rate used in the program. Pictorially, this process looked like Figure 32. Once overlapped, the three traces were added together at each point to produce a continuous time history (see Figure 34). The repeating period shown on the plot was the trace on which the "a_0" calculation was done. The calculation was repeated with the overlap between the three signals increased or decreased until the a_0 result fell within the range 0.995 to 1.005. Once completed the period of the overlap became the period of the continuous trace, which in turn became an accurate measure of the subject's footfall rate.

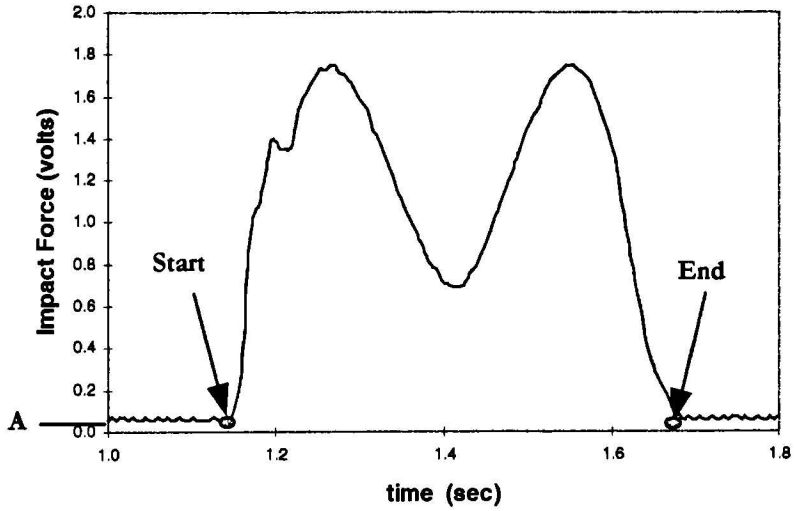

Figure 33 Typically raw data trace - direct from data acquisition system.

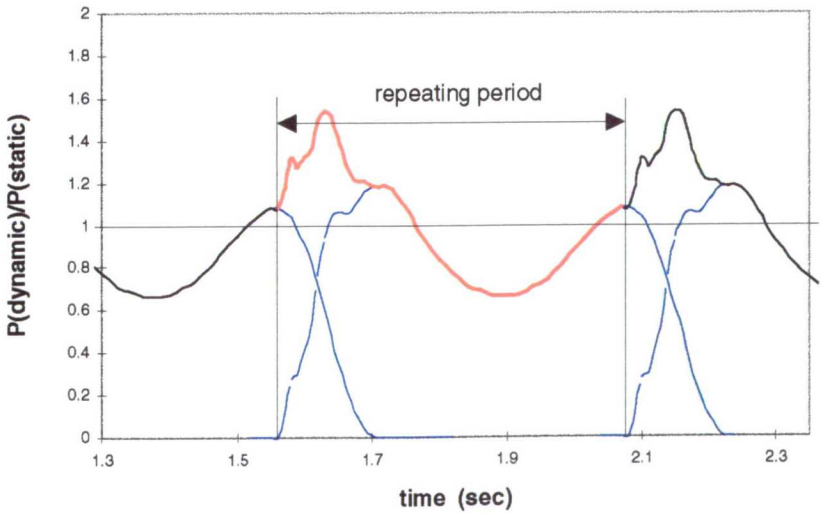

Figure 34 Summing the individual traces to form a continuous trace.

5.4.3 A C++ Program for the Calculation of Normalised Harmonics and the Regeneration of the Time History

Employing the foundations laid in Chapter 2, the next step was to perform a discrete Fourier analysis on the combined time history. This was accomplished with an addition to the *harmonic.cpp* program. The procedures explained in section 2.2.2, were followed to produce the harmonic results up to 100 Hz. The calculated d_n's and phase shifts were written to an ASCII file for comparisons.

To prove the validity of the results, the program also worked in reverse, i.e. taking the harmonic results and reassembling the complicated time history from the component sine waves. Table 6 shows the first 10 harmonic amplitudes (d_n's) and phase angles calculated for the continuous trace shown in Figure 34. The trace was reconstructed using 5 and 10 harmonics (see Figure 35). Although the 5 harmonic trace was a close match, the 10 harmonic trace was virtually identical to the original. This reconstruction proved the validity of the program as well as the number of harmonics required to accurately simulate the original trace.

Figure / Pace	Units	Harmonic Amplitudes and Phase Angles									
		1	2	3	4	5	6	7	8	9	10
Figure 34	Fraction of weight	0.35	0.04	0.04	0.04	0.03	0.02	0.01	0.01	0.02	0.01
(1.92 Hz)	Degrees	79	39	2	79	15	88	8	69	50	9

Table 6 First 10 harmonic values and phases calculated for Figure 34.

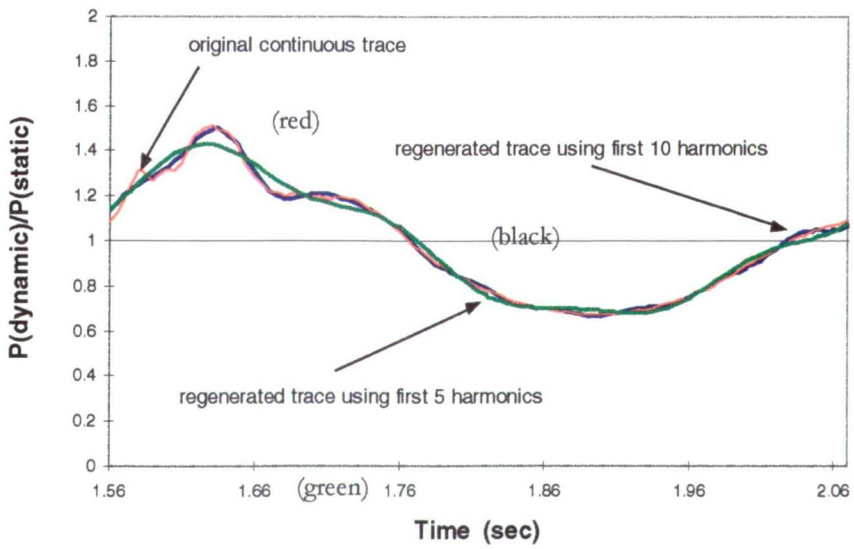

Figure 35 Reconstructed force-time history compared with original.

5.5 RESULTS

5.5.1 Typical Example of Recorded Traces

As stated in the previous section, over 1000 individual footfall traces were recorded utilising 40 subjects walking at a variety of footfall rates. For each footfall trace a combined time history was produced by overlapping the single traces in a "left-right-left" pattern with an accurate period inserted between heel strikes. Finally a discrete Fourier analysis was conducted on the combined time history to calculate the harmonic values.

Figure 36 is a typical example of a calculated combined time history superimposed over a single footfall trace. Harmonic amplitude data generated from this continuous trace is shown in Table 7.

Test No.	Pace (Hz)	Max Force	1st Harmonic	2nd Harmonic	3rd Harmonic	4th Harmonic
119n09	1.92	1.20	0.35	0.03	0.03	0.04

Table 7 Typical harmonics data from a subject.

The values shown for the harmonics are given as a fraction of the static or body weight. Hence, 0.35 represents the first harmonic sine wave with an amplitude of 35% of the subject weight. Note that the magnitude of the first harmonic is over 10 times greater than that of the second.

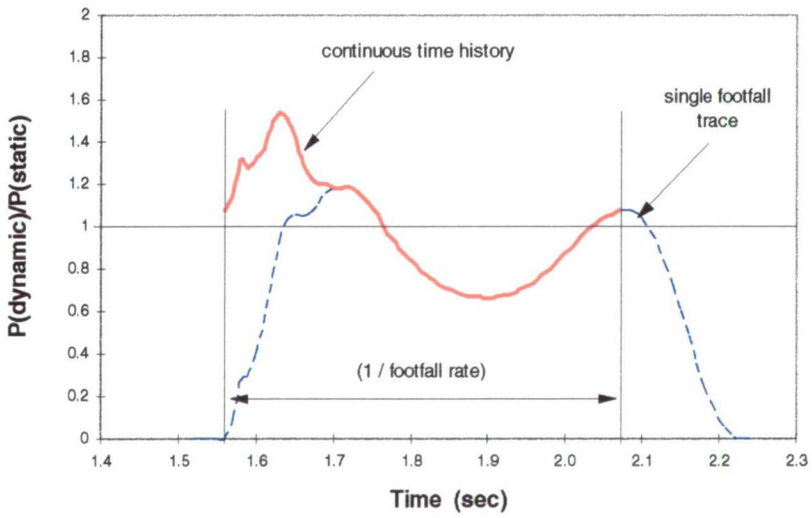

Figure 36 Single footfall trace and continuous time history - test 119n09.

5.5.2 The first harmonic data

Figure 37 is a plot of all first harmonic values for each test. It is apparent that there was significant scatter in the data especially near the average footfall rate of 2 Hz. As discussed earlier, several factors affected the shape of the continuous time history and hence the magnitudes of the harmonic values. One such factor was the subject's stature, i.e. weight and height. The data in Figure 37 is presented with amplitudes that were normalised to subject weight but not to subject height.

The (blue) circles indicate tests where the stride lengths measured were greater than 0.81m, typically belonging to subjects with heights greater than 5ft 9ins or 1.75m. The (red) crosses indicate stride lengths less that 0.81m belonging to subjects with heights less than 5ft 9ins or 1.75m. In Figure 37, a separation between the two groups is evident which creates scatter in the points. If the two groups are looked at separately, the harmonic data for the shorter subjects (Figure 38-B) follows a distinctive linear pattern (as indicated by the approximate mean line) with the scatter nearly proportional to the footfall rate. The data for the taller subjects (Figure 38-A) shows the same pattern (up to 2.3 Hz) with the approximate mean line having a slightly greater slope. Above 2.3 Hz the data levelled off as the taller subjects reduced their stride lengths in order to maintain the required footfall rate. Shorter subjects did not seem to have this difficulty.

The increased slope of the mean line along with the taller subject's difficulties above 2.3 Hz, indicated and the data was also a function of subject height and or stride length. To achieve a normalisation by height, each subject's data was divided by his/her height. The resulting plot shows less reduction to the scatter that initially expected (see Figure 39). However this can be explained from events observed during testing.

As each subject was tested, he/she was asked to walk "naturally" at a set footfall rate. As the stride lengths were recorded it was noted that the lengths changed with pace (discussed in detail in section 5.5.2.1). Hence, it is best to divide the amplitudes by normalised stride lengths (i.e. subject stride length/subject height) which varied with each test, as opposed to the subject's height which remained constant.

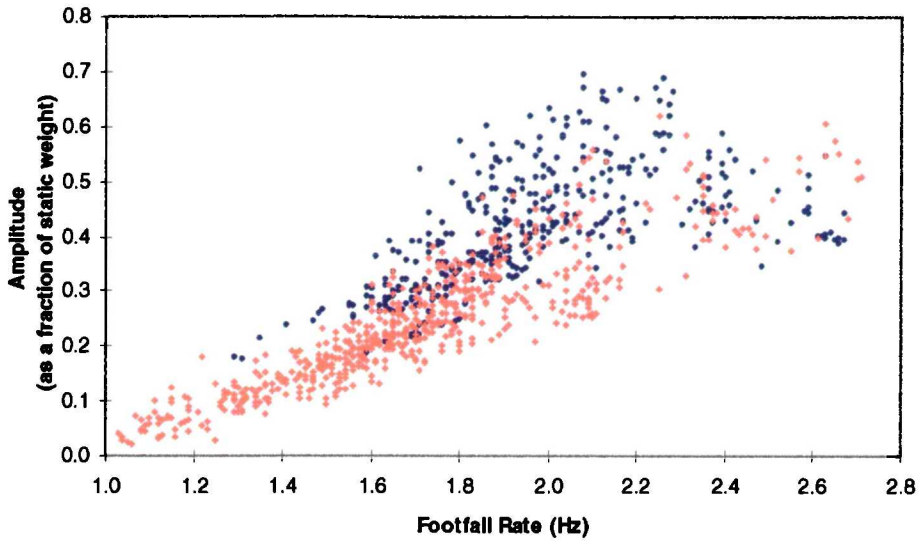

Figure 37 All first harmonic data from walking tests.

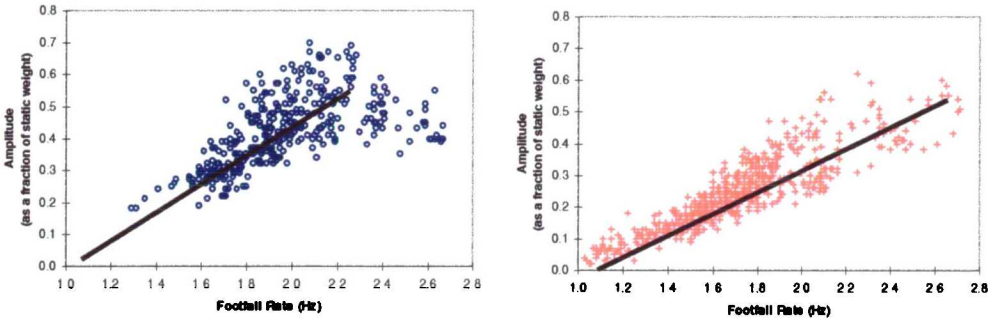

A **B**

Figure 38 (A) harmonic data typically for subjects taller than 1.75m (B) harmonic data typically for subjects shorter than 1.75m.

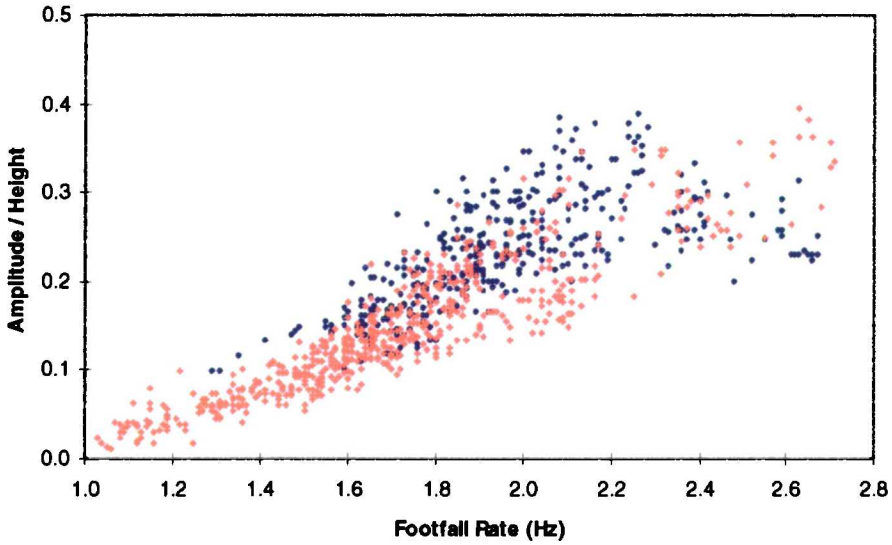

Figure 39 All first harmonic data normalised to subject height.

Figure 40 is a plot of harmonic amplitudes divided by normalised stride lengths. Note that the scatter is significantly reduced in the 2 Hz region as compared to the original plot. Therefore, the scatter in the original data was artificial and a function of normalised stride length.

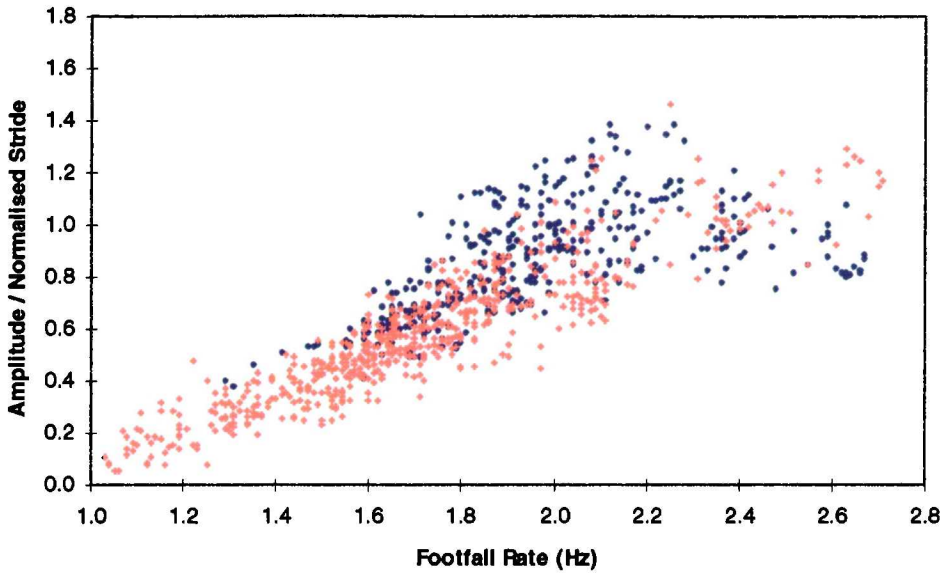

Figure 40 All first harmonic data divided by normalised subject stride length.

5.5.2.1 Distribution of stride lengths.

The data displayed in Figure 40 is not helpful if information is not known about population stride lengths. Therefore, efforts were made to quantify normalised stride lengths to footfall rates. Figure 41 represents all the normalised stride data. The normal footfall rate range of 1.6 to 2.2 Hz, is indicated between the two vertical lines.

The plot shows significant scatter, however, if the data from a single subject is removed and plotted (see Figure 42) a trend becomes obvious. This data was gathered from a male subject of height 5ft 9in or 1.75m; the mean height between taller and shorter subjects in these tests. The line running through the data represented the normalised stride length expected for the subject. At the average footfall rate of 2 Hz the normalised stride expected was 0.46. This value ties up nicely with the work of Grieve [1969], (see section 4.2).

If the data in Figure 40 is multiplied by the values from Figure 42 the results would be the predicted average harmonic values expected for an average person walking at a normal footfall rate. A plot of this is shown in Figure 43.

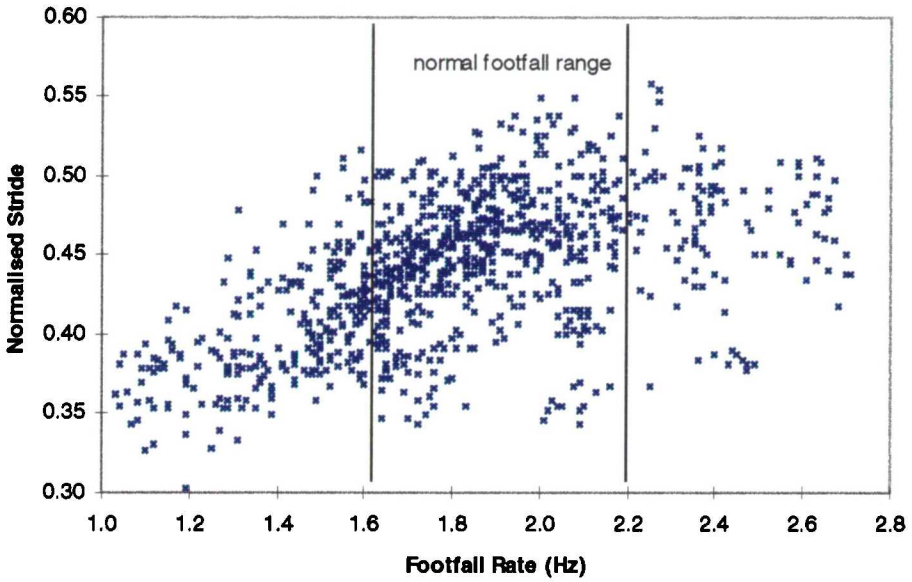

Figure 41 Subject stride length as a percentage of height when walking at normal paces.

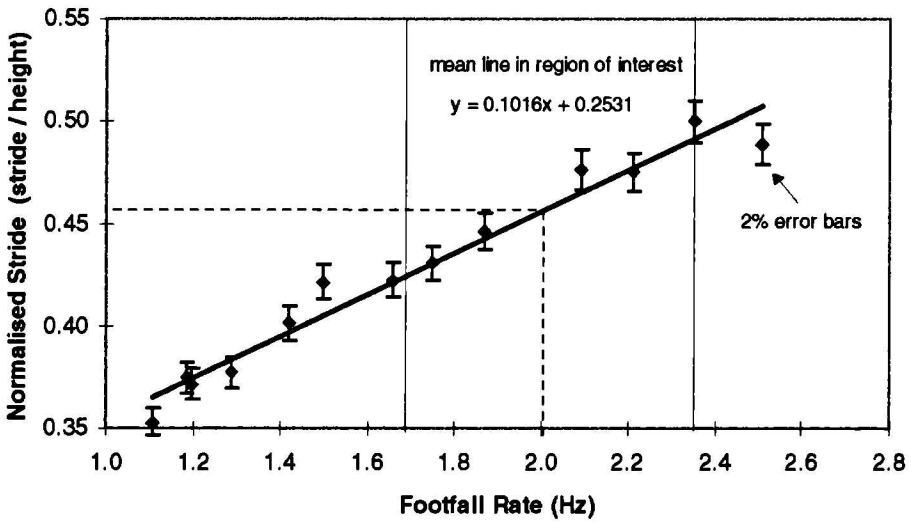

Figure 42 Single subject stride lengths (as fraction of height) for various footfall rates.

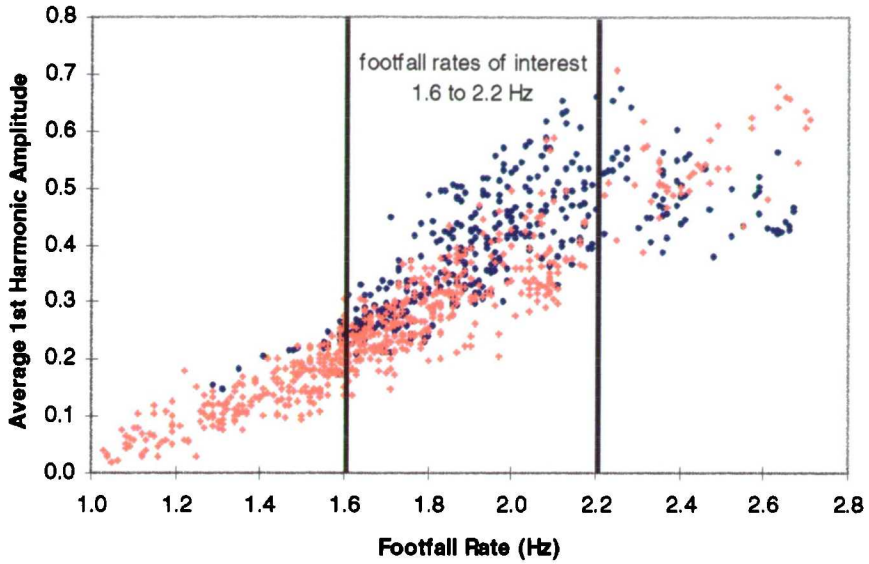

Figure 43 Predicted first harmonic values for an average subject walking normally .

5.5.2.2 Quantifying the data spread.

The data in Figure 43 has an average which tends to follow a third order polynomial although, due to the problems encountered by some subjects walking above 2.3 Hz, the upper end should be viewed with caution (see Figure 44). Below 2.3 Hz, the equation for the polynomial can be used with confidence (especially at the footfall rates of interest, 1.6 to 2.2 Hz).

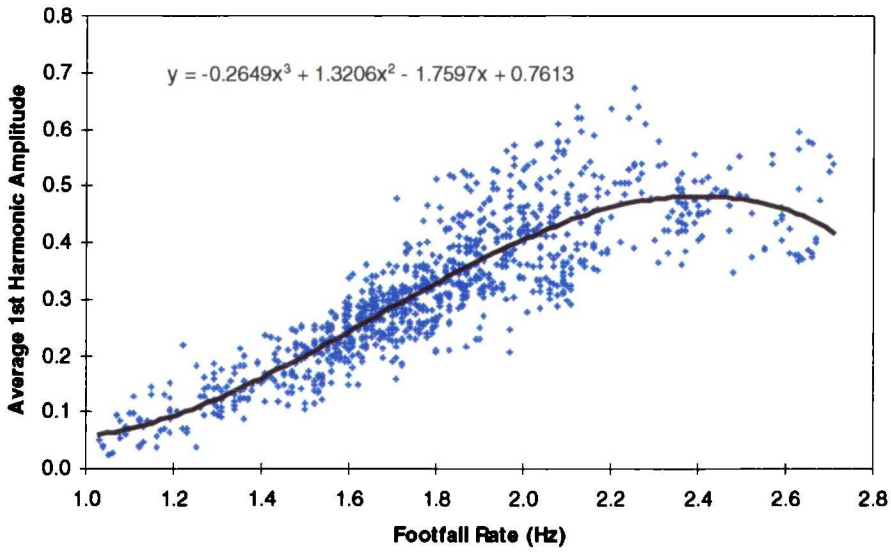

Figure 44 Third order polynomial fit to first harmonic data.

To quantify the spread of the data upper and lower bands can be calculated from the percentage difference of each point to the polynomial line. This calculation was done for data between 1.6 to 2.2 Hz, thus eliminating the scatter outside this footfall range. Figure 45 is a plot of the percentages from the mean with a ±2 sigma or 95% confidence band placed over the points. The plot shows the ±2 sigma limit confidence band extends by ±32% from the mean. Figure 46 shows the original data points with a ±2 sigma confidence band described by an upper and lower third order polynomial equation.

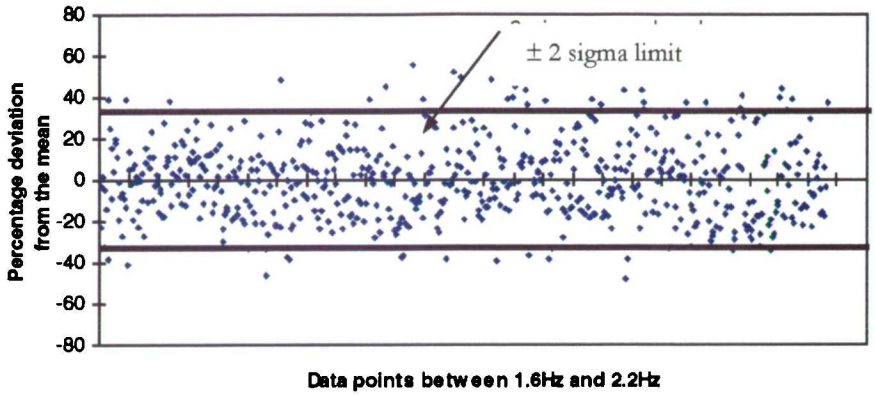

Figure 45 ±2 sigma band placed through percentage differences from mean.

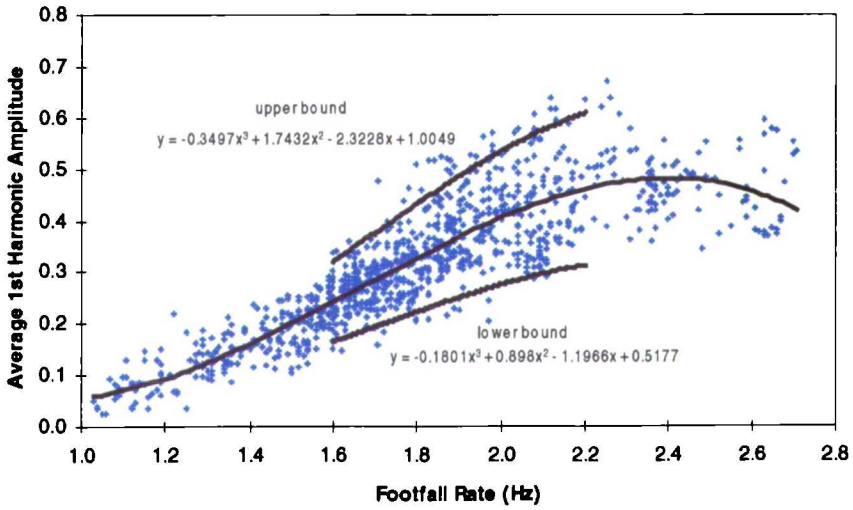

Figure 46 Third order polynomial upper and lower bounds to first order harmonic data.

The ±2 sigma confidence bands and the mean curve could also be approximated by the equation Y = mX + B as shown in Figure 47 (only in the region of interest).

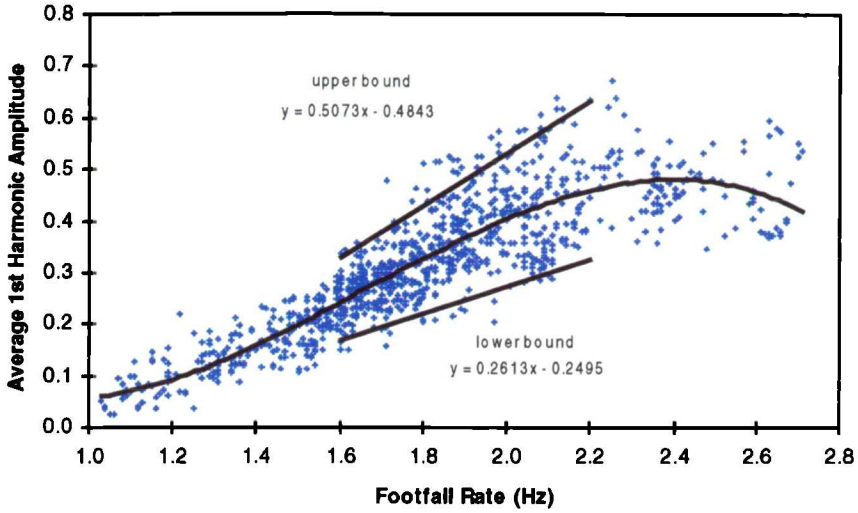

Figure 47 Approximate linear equations for upper and lower bounds.

5.5.3 The second harmonic data.

Figure 48 is a plot of all second harmonic data normalised to subject weight and average normalised stride length. Viewing the figure, unlike the first harmonic data, there is no discernible pattern in the data. The values are scattered throughout all walking paces with an average value of 0.07 and the ±2 sigma limit located between 0.0 and 0.13.

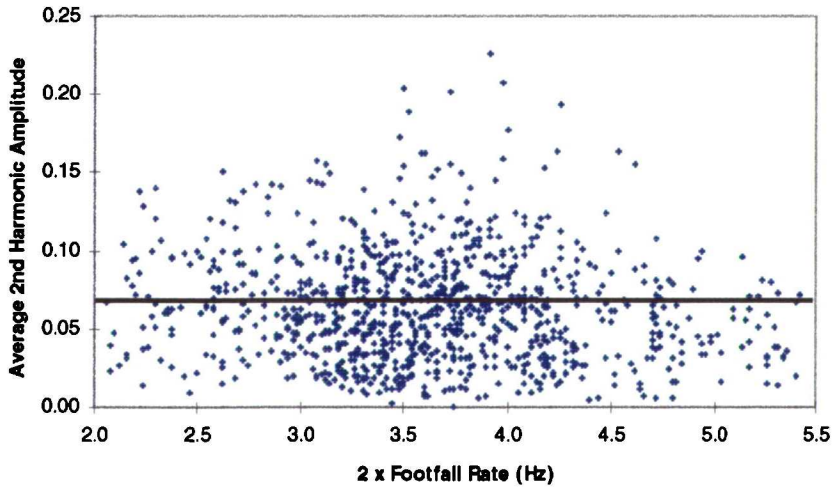

Figure 48 Second harmonic data from walking tests.

5.5.4 The higher harmonic data.

Figure 49 and Figure 50 are plots of the third and fourth harmonic data normalised to subject weight and average normalised stride length. In a similar way to the second harmonic, there is no discernible pattern in the data. The mean line on both plots is approximately 0.05 with a ±2 sigma limit band between 0.01 and 0.09. Beyond the fourth harmonic the values become very small and are approximately zero by the fifth harmonic.

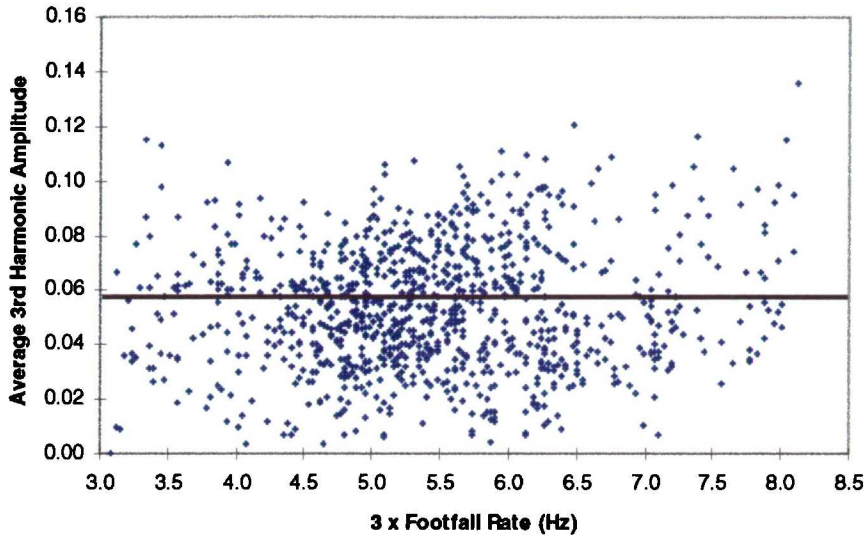

Figure 49 Third harmonic data from walking tests.

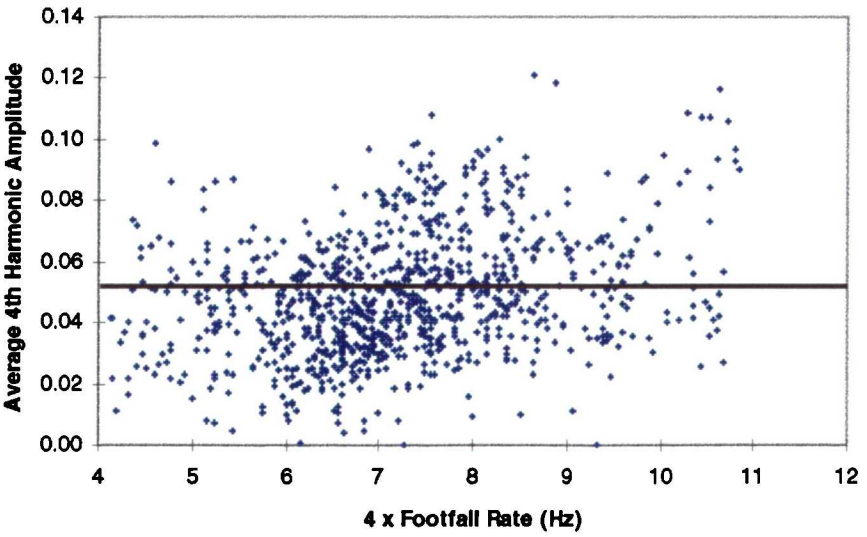

Figure 50 Fourth harmonic data from walking tests.

5.6 APPLICATION OF RESULTS TO A NEW METHOD FOR PREDICTING PEAK ACCELERATIONS ON FOOTBRIDGES AT RESONANCE

Rainer *et al.* [1988] introduced a new method for predicting the peak accelerations at resonance on simply supported bridge spans based on a 'dynamic amplification factor'. Although Rainer gave a plot of the amplification factors for various critical damping ratios (see Figure 25) he did not give an indication of the harmonic loadings expected for various footfall rates. The new method proposed, expands on the work of Rainer by introducing an equation to describe the harmonic loading as a function of bridge natural frequency as well as a series of equations to predict the dynamic amplification factors based on Rainer work.

Below is the maximum peak acceleration expression used in Rainer's work.

$$a_p = (2\pi f_o)^2 \frac{\alpha P}{k} \Phi$$

where
a_p = peak vertical acceleration at resonance
f_o = natural frequency of footbridge (Hz),
α = harmonic amplitude as fraction of body weight,
P = subject body weight (N),
k = measured stiffness of span at centre (N/m),
Φ = dynamic amplification factor obtained from plot.

The new method (which is given by the following expression) can be incorporated into a spreadsheet or computer program since it does not require data obtained directly from the Rainer graph.

$$a_p = (2\pi f_o)^2 \frac{FHA_m P}{k} \left\{ Cr_{(0.005)} - \left(\left(a\xi^{-b} \right) * (\xi - 0.005) \right) \right\}$$

where
a_p = peak vertical acceleration at resonance
f_o = natural frequency of footbridge (Hz),
FHA_m = expression for the mean first harmonic amplitude
P = body weight (N)
k = measured stiffness of span at centre (N/m)
$Cr_{(0.005)}$ = expression for critical damping ratio curve at 0.005
ξ = critical damping ratio for footbridge
a, b = expressions for constants

The FHA (first harmonic amplitude) expression that takes the place of Rainer's α is simply the mean third order polynomial equation given in Figure 44. Using the

natural frequency of the footbridge instead of the pace frequency ensures the peak acceleration is predicted at resonance.

$$FHA_m = -0.265 f_o^3 + 1.321 f_o^2 - 1.760 f_o + 0.761$$

where f_o = natural frequency of the footbridge.

The equation yields the mean expected first harmonic value for a footfall rate equivalent to the natural frequency of the footbridge. This allows a broader and more accurate use of the equation. If the upper or lower two sigma limits are required, than the expression could be replaced as shown below (see Figure 46)

$$FHA_{+2\sigma} = -0.350 f_o^3 + 1.743 f_o^2 - 2.323 f_o + 1.005$$

or

$$FHA_{-2\sigma} = -0.180 f_o^3 + 0.898 f_o^2 - 1.197 f_o + 0.518.$$

If the loading function is not the first harmonic, the expression should be replaced by the values shown in Table 8.

Loading Function	Mean	$+2\sigma$
2nd harmonic	0.07	0.13
3th harmonic	0.05	0.09

Table 8 Values to use for FHA if the loading function is not the 1st harmonic

The latter half of the new peak acceleration equation, namely,

$$\left\{Cr_{(0.005)} - \left(\left(a\xi^{-b}\right) * \left(\xi - 0.005\right)\right)\right\}$$

is a mathematical formulation which calculates the value of the dynamic amplification factor at resonance based on Rainer's curves in Figure 25. The expression for $Cr_{(0.005)}$, as shown below, is a fifth order polynomial fit to the critical damping curve (ξ = 0.005) taken from Rainer's plot.

$$Cr_{(0.005)} = -(1.22E-6)CPS^5 + (1.73E-4)CPS^4 - (8.81E-3)CPS^3 + (0.18)CPS^2 - (0.14)CPS + 7.17$$

where CPS = number of cycles per span (as described by Rainer).

The expressions for the constants "a" and "b" were derived through a chain of steps. First, the values from each curve were recorded for 'cycles per span' numbers 5, 10, 15, 20, 30, 40, and 50. Then, at each cycle number the differences between the value at each curve and the base curve (ξ=0.005) were recorded. These values were then normalised by the differences between the critical damping ratios. Table 9 is an example of the data taken from the dynamic amplification curves corresponding to 40 'cycles per span'.

Data taken at 40 cycles per span		
A Difference between the value at base curve (i.e. 48.0 @ ξ = 0.005) and the values at remaining curves.	**B** Difference between ξ for the base curve (i.e ξ=0.005) and ξ for remaining curves.	Normalising **A / B**
48.0 - (35.0 @ ξ = 0.01) = 13.0	0.010 - 0.005 = 0.005	2600
48.0 - (27.0 @ ξ = 0.015) = 21.0	0.015 - 0.005 = 0.010	2100
48.0 - (22.0 @ ξ = 0.02) = 26.0	0.020 - 0.005 = 0.015	1733
48.0 - (15.5 @ ξ = 0.03) = 32.5	0.030 - 0.005 = 0.025	1300
48.0 - (7.9 @ ξ = 0.06) = 40.1	0.060 - 0.005 = 0.055	729

Table 9 Example of values used to develop the mathematical expressions for predicting Rainer's dynamic amplification curves.

The normalised values were then plotted for each 'cycles per span' (see Figure 51). Between the data points, curves were formed by linear interpolation. The linearly interpolated curves were then approximated by a 'power' curve fit algorithm following the equation shown below and depicted as an example for the 40 'cycles per span' curve in Figure 51.

$$y = ax^b$$

Once a curve fit was made to each set of data, the "a" and "b" terms were noted and plotted (a graph of the "a" constant is shown in Figure 52). The plots reflected the changes in the curve fit shapes (see Figure 51) as the 'cycles per span' was lowered from 50 to 5. A fifth order polynomial was then placed over each curve to produce an equation to predict the values of the "a" and "b" constants throughout the 'cycles per span' range (i.e. 5 to 50). The fifth order polynomial equations which form the expressions for "a" and "b" are given below

$$a = (6.36E-6)CPS^5 - (1.01E-3)CPS^4 + (0.06)CPS^3 - (1.51)CPS^2 + (19.09)CPS - 35.50$$

$$b = -(8.03E-8)CPS^5 + (1.17E-5)CPS^4 - (6.16E-4)CPS^3 + (1.42E-2)CPS^2 - (0.12)CPS + 0.79$$

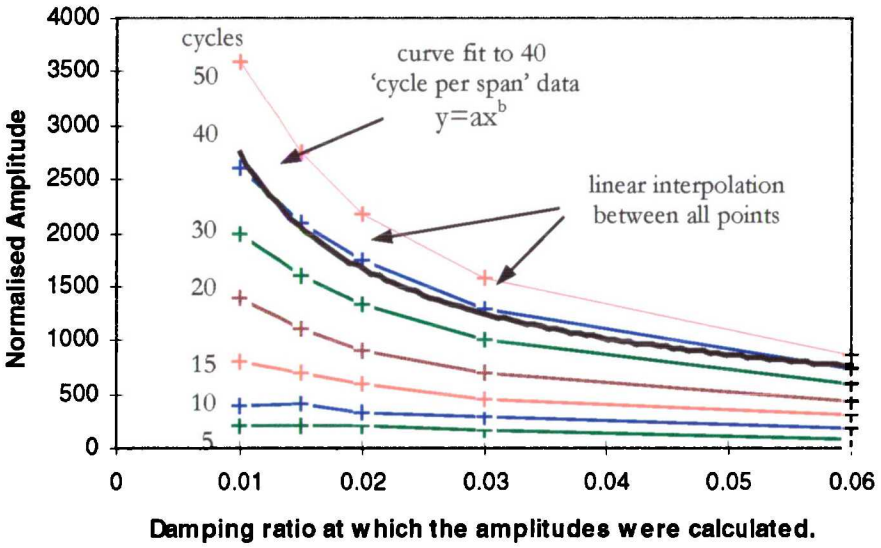

Figure 51 Example of curve fit to data from Table 9.

This new formulation allows the prediction of peak accelerations at resonance on simply supported bridge spans without the need to refer to look-up tables. The inputs required for the program are the natural frequency of the footbridge, the weight of the subject, the stiffness of the bridge span, the critical damping ratio and the number of cycles per span.

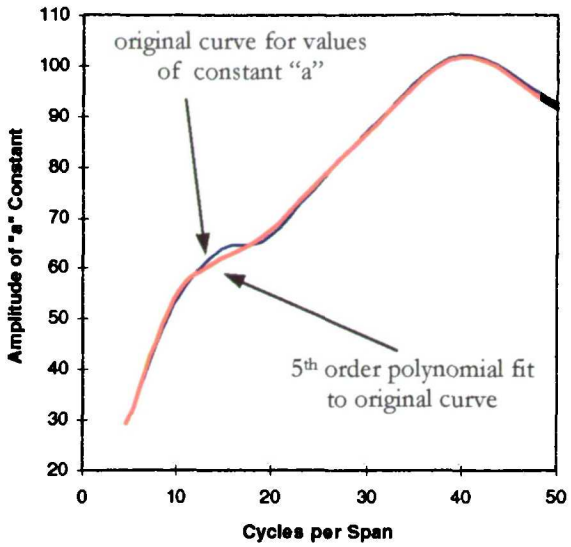

Figure 52 Fifth order polynomial fit to constant 'a' from curve fit.

5.7 DISCUSSION

Information on harmonic content of walking force on the flat has been published by Rainer and Pernica [1986] on data recorded from 3 subjects walking along an instrumented 17m long floor strip. For the first harmonic, their peak value and location was 0.52 at 2.4 Hz which closely matches that shown in Figure 34, i.e. 0.46 at 2.35. For the second harmonic however, Rainer and Pernica show relative values nearing 45% of the first harmonic at 2.4 Hz, which did not compare with the 10% at 2.35 Hz shown in Figure 34. The third and fourth harmonic values compare identically. It is possible that the use of an instrumented floor as opposed to a force plate altered the second harmonic results although it must be stressed that their results came from a limited sample size.

Jacobs *et al.* [1972] using the Skorecki gait machine, produced harmonic values from testing with 25 subjects. The results were given in relative terms to the magnitude of the first harmonic. Their calculations produced a second harmonic relative value of 20% at 1.85 Hz and a third harmonic value of 40% also at 1.85 Hz. At these same paces, Figure 34 shows a second harmonic of 22% and a third harmonic of 16%. Unlike Rainer and Pernica, Jacob's work predicted higher third harmonic values and relatively lower second harmonic values. In fact, the predicted third harmonic values of Jacob's were on average 2.5 times greater than those found in this work. Only 2% of the flat testing traces had third harmonic values as high. Although Jacob used a large number of subjects, he only gathered

a small number of traces; 50 in fact. This represented ony 5% of the traces gathered for this work and could explain the large discrepancies in the higher harmonic values. The harmonic results form these tests were summarised and presented in Kerr and Bishop [1997].

The new peak acceleration formula (partly based on Rainer's work) was developed for easy incorporation into a spreadsheet or computer program. The formula was used to re-evaluate the examples in Rainer's paper with virtually the same results obtained. If the average first harmonic value is not required, the FHA formula can be replaced by formulas for the ±2 sigma limits. The FHA can also be replaced by harmonic values representing the effects of the higher harmonics making sure to double or triple the number of cycles per span corresponding to the harmonic chosen.

REFERENCES

Allen, D.E. and Rainer, J.H. (1976). *Vibration Criteria for Long-Span Floors.* Canadian Journal of Civil Engineering. Vol.3. No.2. Pp.165-173.

British Standards Institution. (1978). *BS5400 - Steel, Concrete and Composite Bridges. Part 2 - specification for Loads.* BSI.

British Standards Institution. (1984). *BS6472 - Evaluation of Human exposure to Vibration in Buildings (1Hz to 80Hz).* BSI.

Bolton, A. (1978). *Natural Frequencies of Structures for Designers.* The Structural Engineer. Vol.56A. No.9. Pp.245-253.

Bresler, B. and Frankel, J.P., (1950). *The Forces and Moments in the Leg During Level Walking. ASME Transactions.* Vol. 72. pp. 27-36.

Charnley, J. (1972). *Analysis of the Vertical Component of Force in Normal and Pathological Gait.* Journal of Biomechanics. Vol.5. pp. 11-34.

Cunningham, D.M. and Brown, G.W. (1952). *Two Devices for Measuring the Forces Acting on the Human Body During Walking.. Proc. SESA XIV. Vol.2* pp. 75-90.

Ellingwood, B. and Tallin, A. (1984). *Structural Serviceability: Floor Vibrations.* Journal of Structural Engineering. Vol.110. No.2.

Grieve, D.W. (1969). *The Assessment of Gait.* Physiotherapy. November.

International Standards Organisation. (1985). *ISO2631- Guide to the Evaluation of Human Exposure to Whold body Vibration.* ISO.

Jacobs, N.A., Skorecki, J., and Charnley, J. (1972). *Analysis of the Vertical Component of Force in Normal and Pathological Gait.* Journal of Biomechanics. Vol.5. Pp.11-34.

Kerr, S.C. and Bishop, N.W.M. (1997). *Human Induced Loading of Flexible Staircases.* Innovation in Civil and Structural Engineering. Mouchel Centenary Conference Proceedings. ISBN 0-948749-50-4 Pp. 311-318.

Martin, D.G. (1995). *Measurement of Dynamic Properties of Insole Materials.* Third Year Engineering Project. Mechanical Engineering Department. University College London.

Matsumoto, Y., Nishioka, T., Shiojiri, H., and Matsuzaki, K. (1978). *Dynamic Design of Footbridges.* International Association for Bridge and Structural Engineering (IABSE), Proceedings P-18/78.

Ontairo Highway Bridge Design Code (1983). Canadian Ministry of Transportation and Communications. Toronto, ON.

Ohlsson, S. (1982). *Floor Vibrations and Human Discomfort.* Doctoral Thesis at Chalmers University of Technology, Division of Steel and Timber Structures. ISBN 91-7032-0777-2. Goteborg.

Pernica, G. and Allen, D.E. (1982). *Floor Vibration Measurements in a Shopping Centre.* Canadian Journal of Civil Engineering. Vol.9. Pp.149-155.

Rainer, J.H. and Pernica, G. (1986). *Vertical Dynamic Forces from Footsteps.* Canadian Acoustics. Vol.4. Part 2.

Rainer, J.H., Pernica, G., and Allen, D.E. (1988). *Dynamic Loading and Response of Footbridges.* Canadian Journal of Civil Engineering. Vol.15. Pp.66-71.

Skorecki, J. (1966). *The Design and Construction of a New Apparatus for Measuring the Vertical Forces Exerted on Walking: A Gait Machine.* Journal of Strain Analysis. Vol.5. pp.429.

Wheeler, J.E. (1982). *Prediction and Control of Pedestrian Induced Vibration in Footbridges.* Journal of the Structural Division, Proceedings of the American Society of Civil Engineers. Vol.108. pp. 2045-2065.

Wyatt, T.A. (1985). *Floor Excitation by Rhythmic Vertical Jumping.* Engineering Structures. Vol.7. Pp.208-210.

CHAPTER SIX 6

STAIRCASE LOADING

6 EXPERIMENTAL WORK CONDUCTED ON THE STAIRS

6.1 INTRODUCTION

6.1.1 Previous Work

Over the last decade it has become increasingly popular to provide large public areas with gracefully designed "flexible" staircases. Figure 53 is an example of a flexible staircase spanning the atrium of a shopping mall.

Figure 53 Example of a slender staircase.

Two inherent characteristics of this type of design are a low stiffness to mass ratio and a (typically) long span. This can create a low natural frequency when compared to more traditional staircase designs. Without satisfactory guidance,

designers rely on experience gained from footbridge and floor designs. However available literature has shown that experience gained in these areas cannot be safely applied to staircases because footfall rates and harmonic amplitudes can be vastly different.

For example, Nilsson [1976] performed a number of experiments on a 42° incline staircase for the Swedish Council for Building Research in an attempt to quantify the loading due to a variety of human motion patterns. His work used 15 subjects who each conducted 3 trials (typically) for each motion pattern. Hence, 45 recorded responses were made for each pattern. The relevant results of his work are summarised in Table 10. Unfortunately, Nilsson only measured peak loads and not force-time histories so frequency contents could not be determined. Nilsson also did not give an indication of the footfall rates used in his experiments except to characterise the trials as "walking" and "running". Assuming a normal ascent / descent rate of 2 Hz for walking, Nilsson showed that average peak forces of approximately 1.5 times the body weight can be expected during normal ascents and average peak forces of approximately 2 times the body weight can be expected during normal descent.

Motion Patterns	Mean P(dyn)/P(stat)	Maximum P(dyn)/P(stat)
Walking at 1 stair / step, ascending	1.40	1.96
Walking at 1 stair / step, descending	1.95	2.82
Running at 1 stair / step, descending	2.65	5.26
Walking at 2 stair / step, ascending	2.22	4.78
Running at 3 stair / step, ascending	2.22	5.65
Walking at 2 stair / step, descending	3.92	6.34
Running at 3 stair / step, descending	4.97	8.34

Table 10 Summary of results from Nilsson [1976].

Alcock and Lander [1987] conducted similar experiments on a 27° incline staircase for an undergraduate project at Bristol University. They used 13 subjects with 6 motion patterns and retained only the peak values. Table 11 presents a summary of their results.

Motion Patterns	Mean P(dyn) / P(stat)
Walking slowly at / step, 1 stair ascending	1.30
Walking fast at 1 stair / step, ascending	2.05
Walking fast at 1 stair / step, descending	2.21
Running at 3 stair / step, descending	5.01

Table 11 Summary of results from Alcock and Lander [1987].

Morgan [1993] as part of an undergraduate project at University of Sheffield, designed and constructed a portable load plate to use on an existing staircase. During calibration trials with 2 test subjects, he recorded peak loading results that are summarised in Table 12. Unfortunately, Morgan made no mention of the stairs/steps used by his subjects or the incline angle of the staircase, so comparisons are difficult.

Motion Patterns	Footfall Rate	Mean P(dyn) / P(stat)
Walking fast ascent	3.3	1.32
Walking fast descent	3.3	2.25
Running descent	5.0	1.60

Table 12 Summary of results from Morgan [1993].

The force plate was later used by Gething [1994] to conduct the same type of experiments as Alcock and Lander. In her work she used 5 subjects and 6 motion patterns. Each subject conducted 2 trials for each pattern. The maximum results obtained are summarised in Table 13. Gething, like Morgan, also made no mention of the staircase inclination.

Motion Patterns	Footfall Rate	Mean P(dyn) / P(stat)	Maximum P(dyn) / P(stat)
Walking slow at 1 stair/step, ascending	1.02	1.77	2.24
Walking slow at 1 stair/step, descending	1.11	1.79	2.31
Walking normal at 1 stair/step, ascending	1.84	1.98	2.27
Walking normal at 1 stair/step, descending	2.24	1.98	2.86
Walking fast at 1 stair/step, ascending	3.43	2.32	3.30
Walking fast at 1 stair/step, descending	3.78	2.39	3.07

Table 13 Summary of results from Gething [1994].

In 1992 an independent structural investigation was conducted by Dr. Neil Bishop (University College London) on a slender staircase exhibiting "lively" behaviour during use. Recognising the lack of empirical data on human loading of staircases, Dr. Bishop took the opportunity to conduct single person and multiple person loading trials. The multi-person tests were carried out using a group of 27 subjects ascending and descending the staircase with varying footfall rates. Dr. Bishop and his colleagues instrumented the staircase to measure mid-span vertical accelerations. Their work (see Bishop *et al.* [1995]) produced a plot of R value verses footfall rate where the R value was a multiplier on the base curve in BS6472; as described in section 5.1.2 (see Figure 54). The result showed a crowd load response up to 3 times that for an equivalent single person. Also noted by Bishop was that the magnification effects of the crowd loading became minimal around 2.5 steps/sec; because the persons in a crowd were (possibly) less likely to

walk in unison at lower speeds. Hence, based on this and previous references, a large crowd descending a staircase rapidly could possibly generate 10 times the load of an equivalent crowd walking across a floor. The work of Dr. Bishop and his colleges emphases the need to promote an investigation into quantifying single person and multi-person loading on staircases.

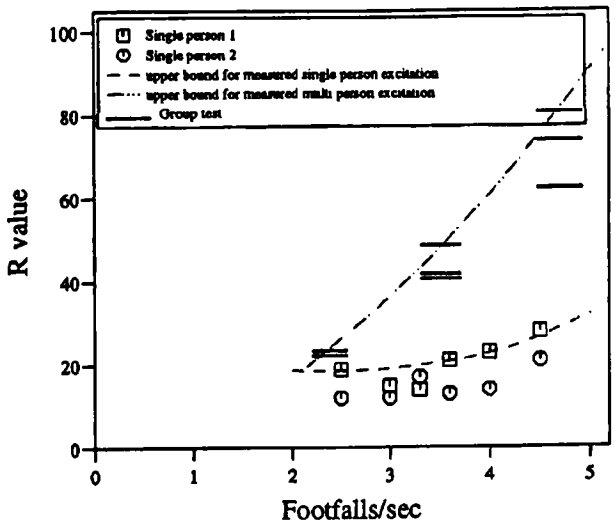

Figure 54 Variation of response with footfall rate (Bishop et al. 1995]).

Based on his research, Bishop was able to describe the design of modern flexible staircases as a three-fold problem. Firstly, the loading applied to the staircase is not clearly defined and data from floor testing appears to be inadequate. Secondly, little data can be found to quantify the loading effects from groups. Lastly, setting appropriate acceptance levels for vibration is difficult because guidelines do not specifically cater for this type of structure. This chapter has addressed the first problem identified by Bishop.

6.1.2 Harmonic Content in Human Gait Applied to the Design of Staircases

The British Standards Code of Practice CP3: Chapter V - Loading [1967] divides the loading applicable to structures as *dead loads*, *imposed loads*, and *wind loads*. Dead loads are defined as:

> *"The force due to the static weight of all walls, partitions, floors, roofs, and finishes including all permanent construction".*

Imposed loads are defined as:

> *"The load assumed to be produced by the intended occupancy, or use, including distributed, concentrated, impact, inertial, and snow loads but excluding wind loads".*

Wind loads are defined as:

> *"All loads due to the effects of wind pressure or suction ".*

The Code of Practice makes no mention of dynamic loads except for the possible dynamic effects of gantry cranes and rotating machinery. Therefore, under CP3, human induced dynamic loading is not mentioned.

For a structural engineer, BS5395 [1977] is the standard that must be followed when designing stairs, ladders, and walkways. It details such things as dimensions, clearances, serviceability requirements, and loads. However, the loading requirements are actually those described in CP3 and are purely static requirements. The standard does have a vibration criteria, but it is vague as shown below.

> *"The uncomfortable sensation from vibration should be considered for the confidence of users. Methods of determining how to forecast it are not yet available, but research is in hand".*

Hence, BS5395 does not give guidance on human induced dynamic loading or place limits on acceptable vibration limits forcing the staircase designer to rely on information and guidance intended for floors and footbridges.

6.2 EXPERIMENTAL SET-UP AND EQUIPMENT

Each subject was asked to ascend and descend a purpose built staircase erected outdoors at University College London. The staircase incorporated a calibrated force plate in place of the fourth or middle step. The impact voltages generated by the piezoelectric transducers located under the force plate were recorded with a data acquisition system and stored on a laptop computer. Figure 55 is a picture

of the equipment set-up used for the experiments conducted on the staircase. Each item of interest has been labelled and a detailed description given below.

Figure 55 Equipment set up for staircase testing.

Item A: Force plate with 4 piezoelectric transducer units

The force plate used in the flat testing was removed from its mounting plate and attached to a false step which was incorporated into the staircase as the fourth step. The force plate and transducer units themselves remained unchanged from the floor testing.

Item B: Amplifier unit

The amplifier unit used for the staircase testing remained unchanged from the flat testing. However, because the testing was outdoors the amplifier equipment was set-up and removed on each day of testing. This required calibration measurements to be undertaken before each day of testing.

Item C: PCMCIA data acquisition system

The data acquisition system remained unchanged from the flat testing.

Item D: Staircase - 22 degree and 33 degree inclines

One result from the observation conducted on actual stairs was that the inclination of the stair might affect the loading. Therefore, it was the intention of the author to use a staircase that could be assembled at one inclination then dismantled and reassembled at another inclination. This kind of flexibility ruled out the purchase of a prefabricated staircase leaving the structure to be designed and fabricated in-house at University College London.

Part K of the Building Regulations - Stairs, ramps and guards [1992] was used as a design guide for the staircase. For the required testing, the staircase was designed to follow the criteria for an institutional or assembly stair. Referring to Figure 56, the minimum and maximum rise specification was 135mm to 180mm whereas the minimum and maximum going specification was 280mm to 340mm. Using these values the testing staircase had a minimum incline of 22° and a maximum incline of 33°. These values fall in line with the pitch requirements from BS 5395 - Stairs, ladders and walkways, Part 1 [1977], i.e. optimum 27° with maximum at 33°.

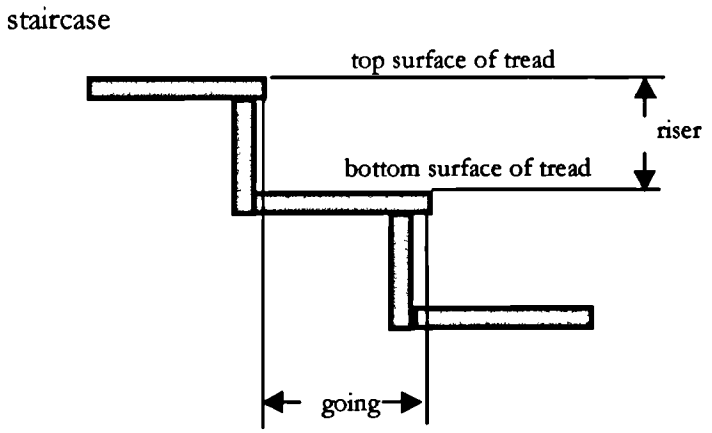

Figure 56 Details for rise and going of an institutional stair.

A location for the staircase was found in a 1m alley between two adjacent buildings just outside the Engineering Department. The plan was to attach a

10mm steel stringer to each wall onto which the steps would be attached through a bolted connection. To achieve the desired flexibility, the stringers were drilled with holes to attach the steps at both inclines, along with three pilot holes through which concrete anchor bolts were used to attach the stringers to the walls. Receiving holes were drilled into each wall at 5 locations; 3 for the 22° incline and 2 for the 33° incline (the third location was a duplicate hole used for the 22° incline). Figure 57 is a sketch detailing the hole locations and incline flexibility of the stringers. Receiving holes were also drilled to support the upper platform (discussed later).

Like the walkway in the flat testing, there was a need to have a lead-in and a lead-out from the force plate to ensure normal stride patterns were used by each subject. To accomplish this the staircase was designed with 3 steps before and after the force plate. Unlike the flat testing, efforts were also made to disguise the force plate by bonding a false step to the top of the plate and using risers to hide its location. This was done to make the experimental set-up appear as natural as possible to the tested subjects.

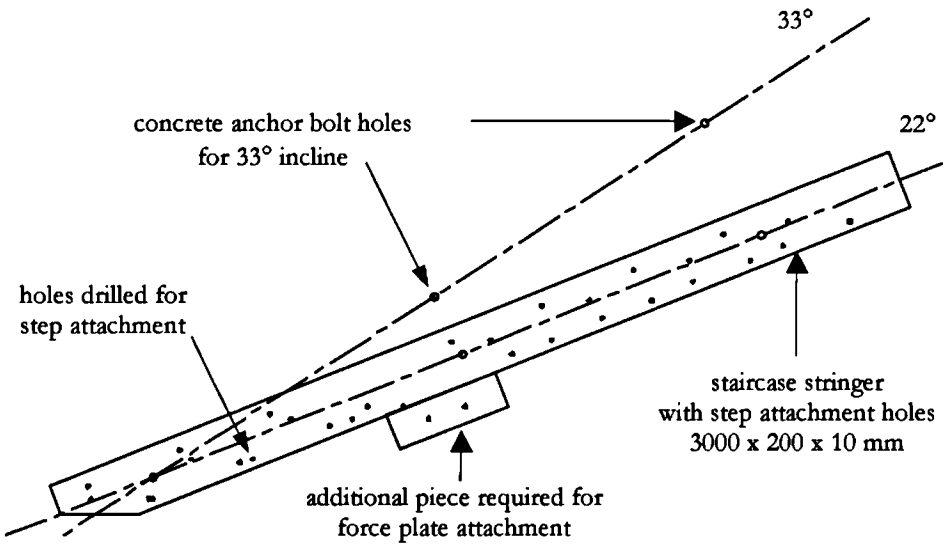

Figure 57 Staircase stringer with step attachment holes.

The 6 steps were constructed using 1040 x 365 x 10mm steel plate with a 960 x 25 x 10mm steel stripe welding on the under side for support (see Figure 58). Angles 25 x 25 x 5mm (270mm long) were also bolted to either side of the step to serve as attachment points to the stringers. Also welded to the step were two 960 x 60

x 3mm steel plates to serve as "half" risers. The purpose of the half risers was to hide the underside of the staircase at both testing inclinations.

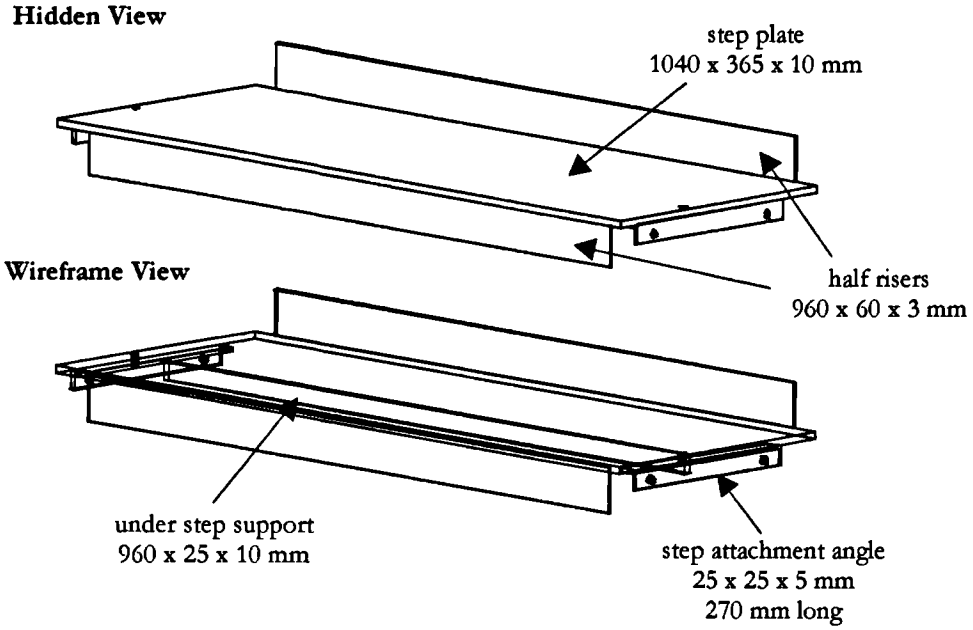

Figure 58 Lead-in and lead-out step details

The force plate was attached to the support step which had the same details as an actual step but excluded the riser plates (see Figure 59). Once in place, a false step was bonded (with silicon) to the top of the force place to disguise its presence. The false step also had the same details as an actual step but excluded the underside support and attachment angles.

At the top of the staircase was a platform that served as a starting location for descent tests (see Figure 60). It was constructed of 10mm plate with 2 supporting steel strips welded underside. The platform also used angles for attachment to the stringers and walls.

Prior to assembly, the entire staircase was coated in black hammerite and a strip of non-slip rubber glued to each step to act as a tread. Figure 61 is a hidden view of the staircase fully erected at an incline of 22°. Note, at this lower incline the half risers align to hide the underside of the staircase.

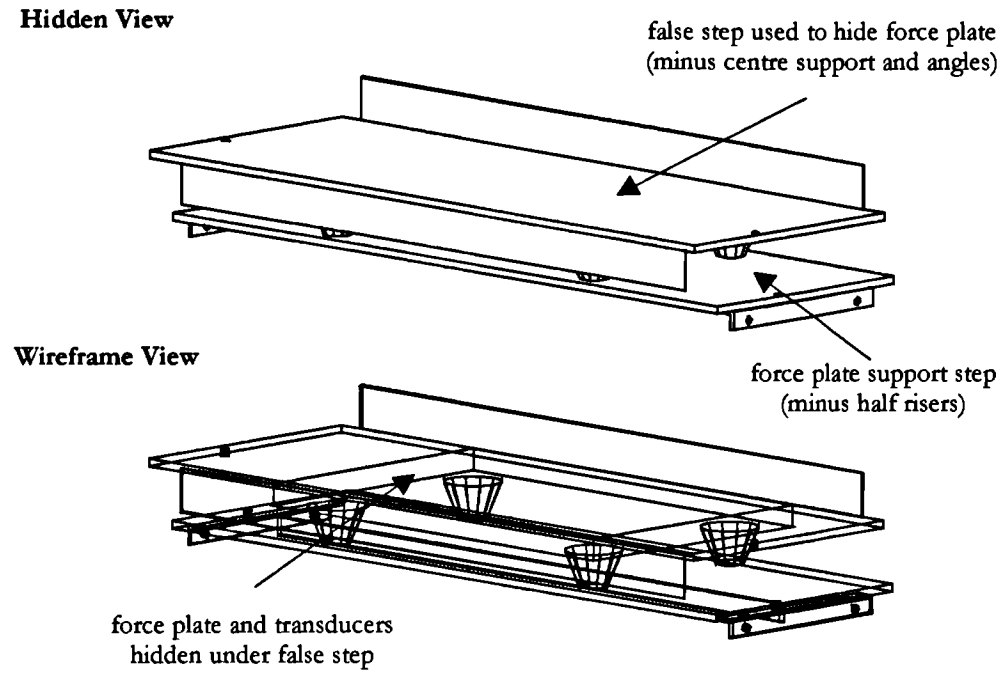

Figure 59 False step incorporating the force plate.

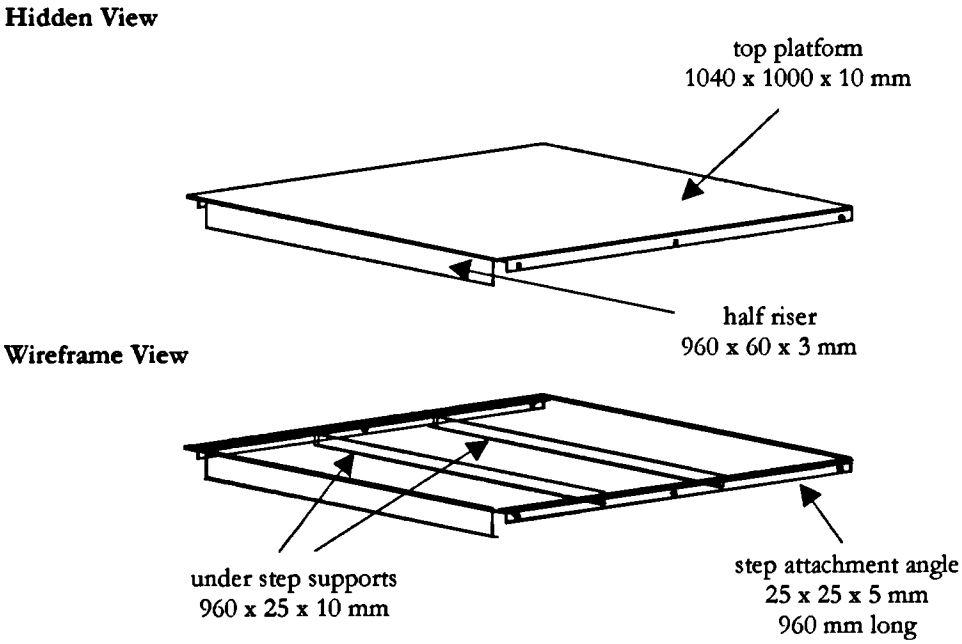

Figure 60 Platform details

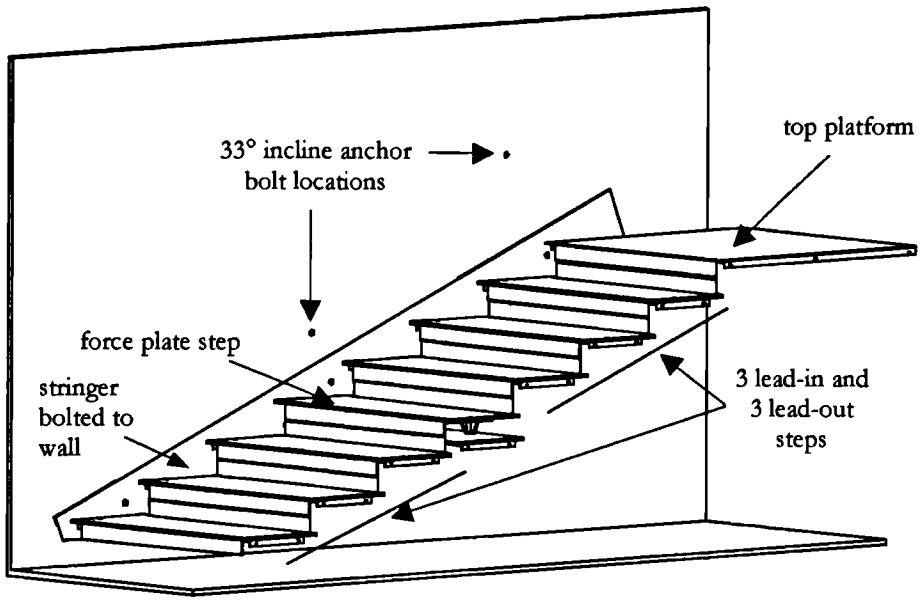

Figure 61 Sketch of staircase inclined at 22°.

6.3 PROCEDURE

6.3.1 What is 'normal' ?

Section 5.4.1 of the previous chapter discussed the expected force trace of a single footfall while walking on the flat. As seen from the data generated in Chapter 5, the double camel hump shape remains more or less the same regardless of the walking pace, i.e. hump - hollow - hump. It is only when a subject attempts to run across the plate does one see the characteristic single camel hump shape. As walking is considered the 'normal' method of locomotion for the majority of people going about their daily lives, the base case study dealt with only the walking harmonics. However, for ascending and descending stairs the distinction between normal and abnormal is not so clear. One may walk normally on a floor but when faced with a set of stairs, one may decide to run up or down in the interest of saving time. One may also decide to use one step at a time or use two or more. Different combinations can vastly affect the shape of the force-time history and hence the harmonics. Therefore, it was necessary to observe normal ascending and descending patterns before deciding what experimental procedures to follow for the staircase testing.

Throughout a period of several months, observations were made on actual staircases at several locations including rail stations, shopping centres, university common areas and hospitals. Observations at these locations lead to the prediction of several factors affecting the way we negotiate stairs. These factors can be broadly broken down into stair congestion, subject age, inclination of stairs, time of day, and purpose. Each are explained below.

Stair Congestion - When the stairs were heavily congested the pace slowed to typically less than 2 Hz and everyone use of a single stair/step pattern. It was also noted that the phasing between heel strikes seemed to develop coherence while the subjects negotiated the stairs. This was likely brought on by the forced stride length imposed by the staircase. Bishop's work [Bishop *et al.* 1995] noted that when a group of 27 students were asked to descend a staircase "fast", their footfall rates began to take on coherence. So coherence in footfall rates seemed to occur at slow and fast ascent and descent speeds.

Subjects Age - On non-congested stairs, it was observed that the elderly typically negotiated all staircases at one stair per step and usually at a pace approximating their normal walking pace or slower. The youth (mid teens or less) more than half the time used two stairs on ascents and descents with an elevated pace. Some negotiated more that two stairs at a time but this was very rare. The twenty and thirty something age group seemed content on negotiating stairs one step at a time but with varying speeds and quite often used two stairs for ascending but only one stair for descending. The forty plus age groups tended to use a single stair for ascending and descending but used a variety of paces.

Inclination of the Stairs - It was observed that low inclination staircases encouraged the teen to thirty something age groups to negotiate the stairs more rapidly than steeper staircases.

Time of Day - As one might expect, the greatest variation to pace and number of stairs was observed during the morning and evening rust hours (especially at the rail stations). Off peak observations produced the slower results in all age groups.

Purpose - At any time of day, some pedestrians would negotiate a staircase at great pace. These subjects were atypical of the generally observed pedestrian motions. In most cases, subject motions were at comfortable, average footfall rates.

6.3.2 Capturing the Force Data From a Footfall Trace

The observations above have led to this generalisation. Most people under everyday conditions negotiate stairs one at a time but at different footfall rates. Some rates, which if used on the flat, would be considered running. Therefore, the ascending and descending experiments would be conducted using one step at a time and have footfall rates varying from the slowest deemed reasonable to as fast as comfortably possible. The data acquisition rate for the system remained at 200 Hz as the higher frequency contents in the signal was not expected to change.

As with the flat testing, a number of variables were expected to influence the harmonics. The single most important was the footfall rate of ascent and descent. As Bishop *et al.* [1995] showed in his paper, during ascending the shape of the time history varied from the familiar double camel hump at lower footfall rates to a single camel hump at faster footfall rates. During descending the shape of the force trace showed a large initial hump and a second smaller hump. Their relative heights remained somewhat the same although their spacing decreased as the footfall rate increased.

A second influencing variable was the stride length. On a staircase, the stride length is fixed by the geometry of the stair. If the staircase geometry forces the use of a stride length that is much shorter than one is accustomed to, he or she may wish to increase their footfall rate to avoid the feeling of 'being held up'. Perhaps this also triggers a change in ascending/descending pattern from using one stair/step to using two or more, especially during ascent. It was observed that the younger crowds (typically during the morning's rush) often resorted to these two variations in their ascending patterns although typically only an increase in footfall rate was observed during descending (these observations were made at a rail station where passengers had to use a footbridge to change platforms).

Subjects participating in the staircase testing were grouped according to age and sex as given below. All subjects had 'normal' walking patterns, unaffected by any

physical abnormalities. For each test the subjects were asked to ascend the staircase at various footfall rates. They were then asked to descend with the same rates. By having the force plate as the fourth step in a seven step staircase, it allowed the subjects to attain a natural rhythm as they contacted the plate. Each subject was also asked to comment on what pace felt 'normal'. This definition actually produced two values. One while 'walking' up the stairs and a second while 'running' up. The participants in the experiments felt two 'normal' speeds gave a better description as to how they felt. Since little information could be found to predict expected paces, it was decided to forgo the electronic metronome and allow the subjects to choose the footfall rates for themselves. The only stipulation from the test organiser was that some ascents should be 'slow' and some should be 'fast'. The other rates were to be variations on what the subject considered normal, i.e. slower than normal or faster than normal.

Age	Male	Female
Under 20	1	-
20 to 30	21	2
Over 30	1	-
Total	**23**	**2**

Table 14 Breakdown of participating subjects in walking tests by age and sex.

To facilitate comparisons between individuals, it was necessary to normalise each footfall trace by the individuals body weight (hence removing body weight as a factor affecting the amplitude of the footfall trace). As on the flat, this was accomplished by having each subject stand on the force plate so a 'weight' in volts could be recorded. By averaging the values near the centre of the trace (where the subject was stationary on the plate) and subtracting any non-zero offset, a normalising weight was achieved. This normalising process ensured that each subject had a body weight of 1.0 volts.

6.3.3 Production of a Continuous Force Time History

Over 600 individual trials were conducted for both the ascending and descending on two different staircase inclinations. As explained in the previous chapter the development of a continuous force time history from a single foot fall trace was

relatively straight forward. By making the assumption that the left foot produced the same force trace as the right foot, and with an accurate calculation of the footfall rate, one could simply add the overlapped footfall traces for each time increment as was done for walking. The program *harmonic.cpp* also conducted a Fourier analysis as described in Chapter 2.

6.4 RESULTS

6.4.1 Ascending Stairs

6.4.1.1 Typical examples of recorded traces

As expected, the harmonics varied widely depending on the footfall rate at which the subject negotiated the stairs. Figure 62 shows typical examples of the force-time traces observed from subjects during stair ascent at 3 different footfall rates.

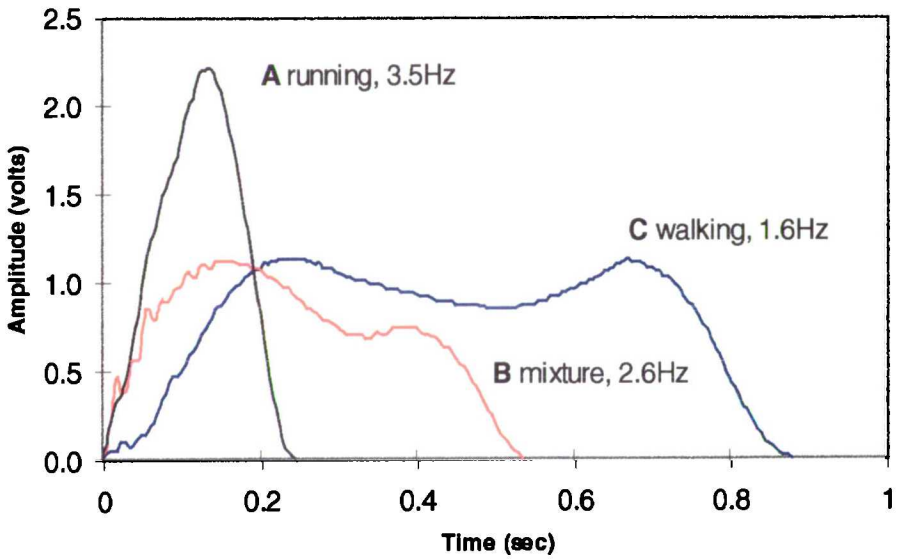

Figure 62 -A,B,C Single footfall traces for stair ascent at various footfall rates (33° incline).

The trace labelled 'walking' referred to the method of ascent which produced this trace i.e. each subject walked up the stairs hitting the balls of their feet first then touching down their heels before lifting them again and pushing off with the toes. The trace labelled 'running' was produced by subjects running up the stairs using only the balls of their feet. The 'mixture' trace was a trace of indecision, with the heels touching down only slightly; causing a small second hump in the force trace. This trace was produced mostly in the transition region between walking and

running. It is interesting to note that all subjects felt that near 2 Hz was the most comfortable rate at which to walk up the stairs and near 3.3 Hz was the most comfortable rate at which to run up. Attempting to walk or run in the mixture region made most subjects feel 'uncomfortable' and would not normally be the footfall rate range they would use to ascend the stairs. The harmonic data generated from the plots in Figure 62 are shown in Table 15.

Test No.	Pace (Hz)	Max Force	1st Harmonic	2nd Harmonic	3rd Harmonic	4th Harmonic
A-c6u17 (62-A)	3.5	2.2	1.12	0.11	0.05	0.03
B-b5u13 (62-B)	2.6	1.11	0.29	0.12	0.05	0.01
C-a8u04 (62-C)	1.6	1.10	0.25	0.07	0.03	0.02

Table 15 Typical harmonics data from subjects ascending a staircase at a 33° incline.

As with the flat testing data, the values displayed for the harmonics are given as a fraction of the static or body weight. Hence, 1.12 represents the first harmonic sine wave with an amplitude of 112% of the subject weight. The general shapes of the 3 figures did not change with the change in stair inclination, but did change slightly in amplitude.

6.4.1.2 The first harmonic results

Figure 63 is a plot of all first harmonic values from each ascending test. The (red) circles represent data gathered on the 22° incline staircase whereas the (blue) crosses represent data gathered on the 33° incline staircase. As expected, the harmonic values attained were typically higher for the 33° incline.

The data in Figure 63 was presented in the customary form which is normalised to subject weight but not to subject height or stride length. The stride length for ascending (and descending) was fixed by the geometry of the staircase and hence, was the same for each subject. Normalisation to subject height (which is calculated and shown in Figure 64) shows little reduction in scatter when compared to Figure 63. Therefore, one can assume subject height had little effect on the harmonic values while ascending.

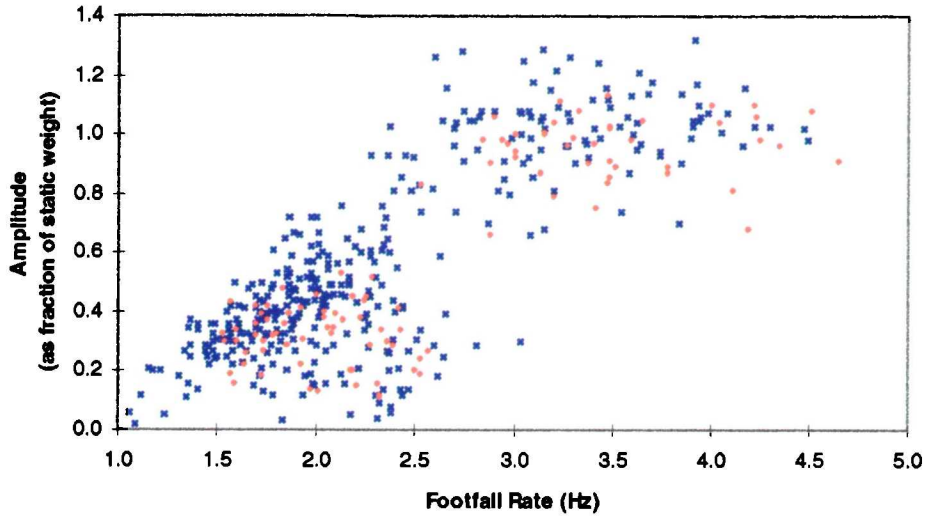

Figure 63 All first harmonic data from ascending tests.

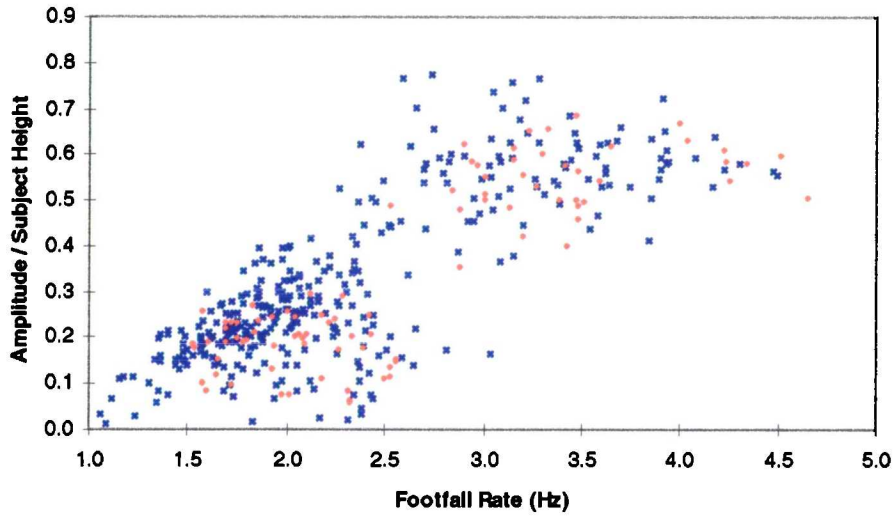

Figure 64 First harmonic data divided by subject height.

Closer analysis of the data presented in Figure 63 also revealed a second pattern (see Figure 65). The (blue) diamonds represent data for which the subject ascended the stairs with sufficient pace to generate a clearly defined single hump force trace (like Figure 62-A). The (green) crosses represent data where the subject ascended the stairs at a slow pace generating a clearly defined double hump trace (like Figure 62-C). The (red) triangles represent data which produced force shapes somewhere in between i.e. neither truly a single hump or double

hump (like Figure 62-B). These divisions also fall nicely in line with subject comments that the most "comfortable" footfall rates for ascending were at 2.0 Hz and 3.3 Hz. As can be seen in the data, the mixture range was the transition between a slow steady walk up the stairs and a fast energetic run. It was also the most "uncomfortable" range at which to ascend as the subjects found it difficult to choose between walking or running.

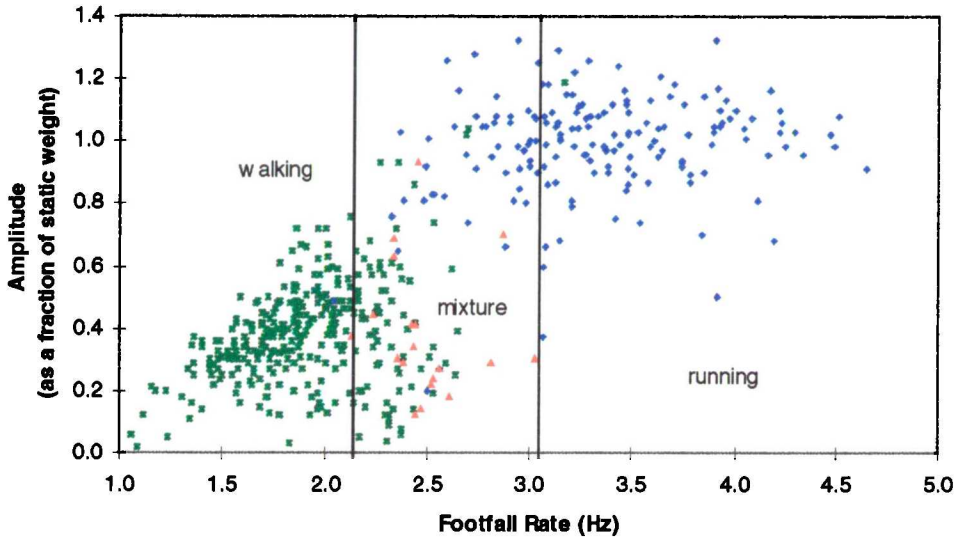

Figure 65 First harmonic data divided into walking, running and mixture regions.

6.4.1.3 The second harmonic data

Figure 66 is a plot of the second harmonic values calculated from all the ascending tests on both sets of stairs. Like the first harmonic data, the values were significantly higher for the 33° incline, shown by the (blue) crosses, when compared with the 22° incline shown by the (red) circles. All values were widely scattered in amplitude throughout the frequency range with a decreasing mean value. At 4 Hz the average value was approximately 0.13 declining to approximately 0.07 at 7 Hz. The ±2 sigma limit for the entire data range was approximately between 0.00 and 0.22. Normalisation by subjects' height had little effect in reducing the scatter.

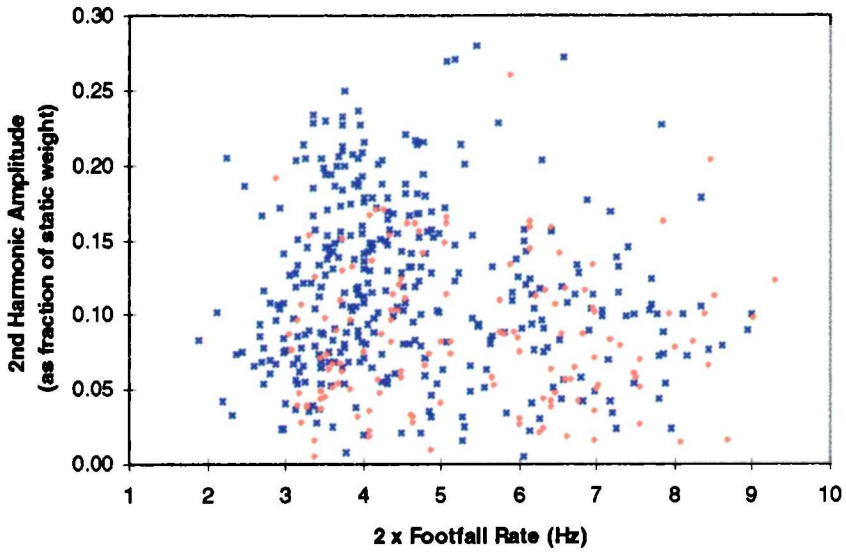

Figure 66 Second harmonic values for ascending stairs.

6.4.1.4 The higher harmonic data

Figure 67 and Figure 68 are plots of the third and fourth harmonic values respectively. Like the second harmonic, the values are scattered in amplitude throughout the frequency range. The third harmonic has a mean value of approximately 0.06 of the subject's static weight with a ±2 sigma range between 0.00 and 0.11. The fourth harmonic has a mean value of approximately 0.03 with a ±2 sigma range between 0.00 and 0.07.

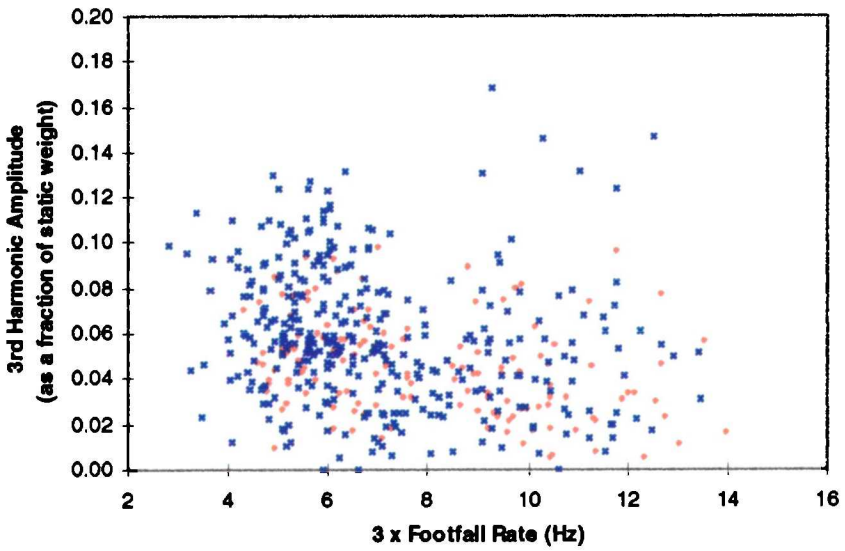

Figure 67 Third harmonic amplitudes from ascending traces.

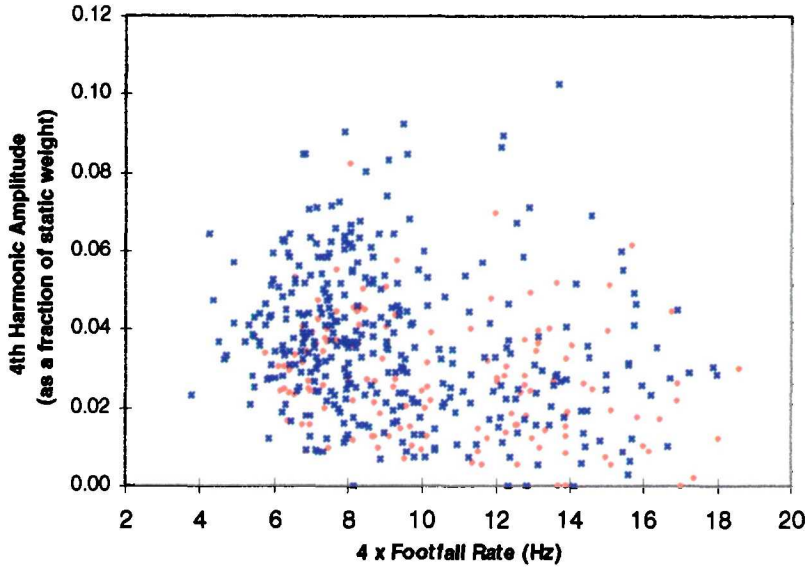

Figure 68 Fourth harmonic amplitudes from ascending traces.

The remaining harmonics (above the fourth) are very small. Two typical traces have been selected to illustrate this point. Figure 69 is an FFT frequency spectrum calculated from a trace generated by a subject walking at 2.0 Hz. The trace would have the same shape as Figure 62-C. Figure 70 is an FFT frequency spectrum calculated from a trace generated by a subject walking at 3.3 Hz. This trace would have the shape of Figure 62-A.

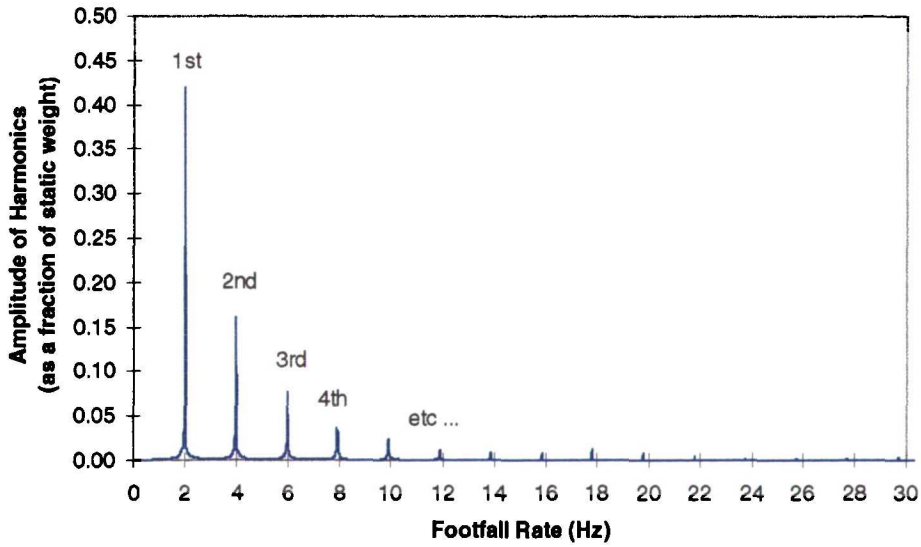

Figure 69 Typical harmonic amplitudes for ascending footfall rates around 2 Hz.

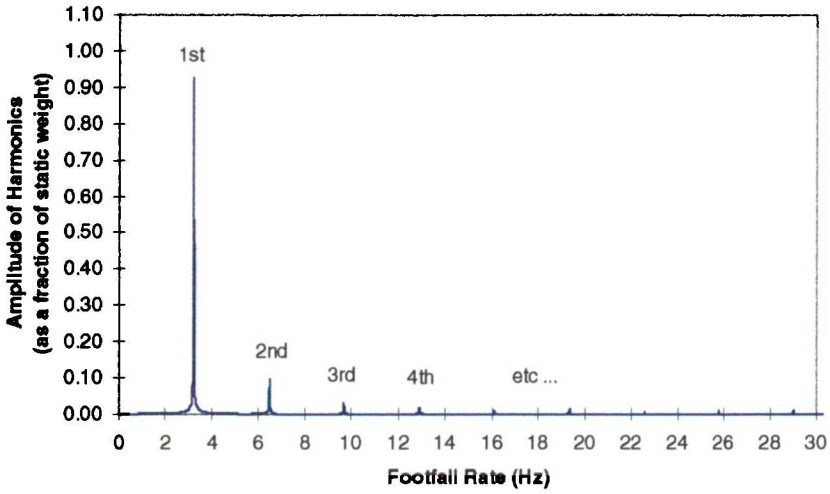

Figure 70 Typical harmonic amplitudes for ascending footfall rates around 3.3 Hz.

Although both traces vary significantly in the values of the first 4 harmonics, from the 5 harmonic onwards the values are virtually zero.

6.4.2 Descending Stairs

6.4.2.1 Typical examples of recorded traces

As expected the harmonics varied widely depending on the footfall rate at which the subject negotiated the stairs. Figure 71-A,B,C are typical examples of the force- time traces observed from the subjects during stair descent at three different footfall rates.

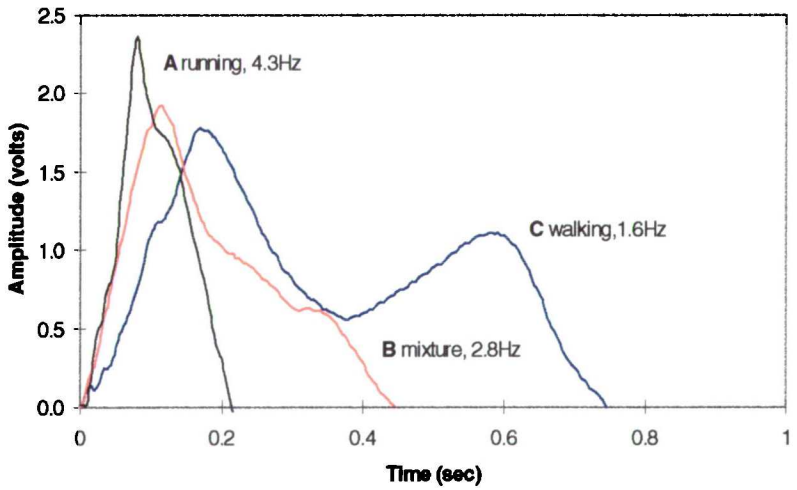

Figure 71 -A,B,C Single footfall traces for stair descent at various footfall rates (33° incline).

The harmonic data generated from these plots are displayed in Table 16. As with the flat testing data, the values displayed for the harmonics are given as a fraction of the static or body weight. Hence, 1.00 represents the first harmonic sine wave with an amplitude of 100% of the subject weight. The general shapes of the three figures did not change with the change in stair inclination.

Test No.	Pace (Hz)	Max Force	1st Harmonic	2nd Harmonic	3rd Harmonic	4th Harmonic
A-b2d18 (71-A)	4.3	2.4	1.00	0.18	0.10	0.11
B-a2d04 (71-B)	2.8	1.9	0.55	0.21	0.07	0.02
C-b2d05 (71-C)	1.6	1.7	0.36	0.26	0.10	0.03

Table 16 Typical harmonics data from a subject descending a staircase with 33° incline.

6.4.2.2 The first harmonic data

Figure 72 is a plot of all first harmonic values from each descending test. The (red) circles represent data gathered on the 22° incline whereas the (blue) crosses represent data gathered on the 33° incline. Again, the harmonic values attained are typically higher for the 33° incline although not to the extent shown on the ascent trials.

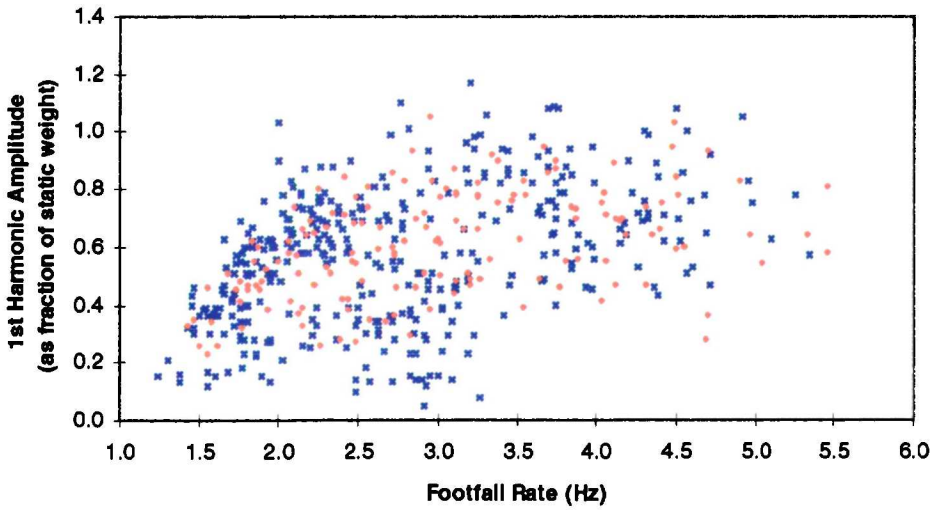

Figure 72 All first harmonic data from descending tests.

Closer analysis of the data also revealed a second pattern (see Figure 73). The (blue) diamonds represent data for which the subject ascended the stairs with sufficient pace as to generate a clearly defined single hump force trace (like Figure 71-A). The (green) crosses represent data for which the subject ascended the stairs at a slow pace generating a clearly defined double hump trace (like Figure 71-C). The (red) triangles were tests which produced force shapes somewhere in between, i.e. neither truly a single hump or double hump (like Figure 71-B).

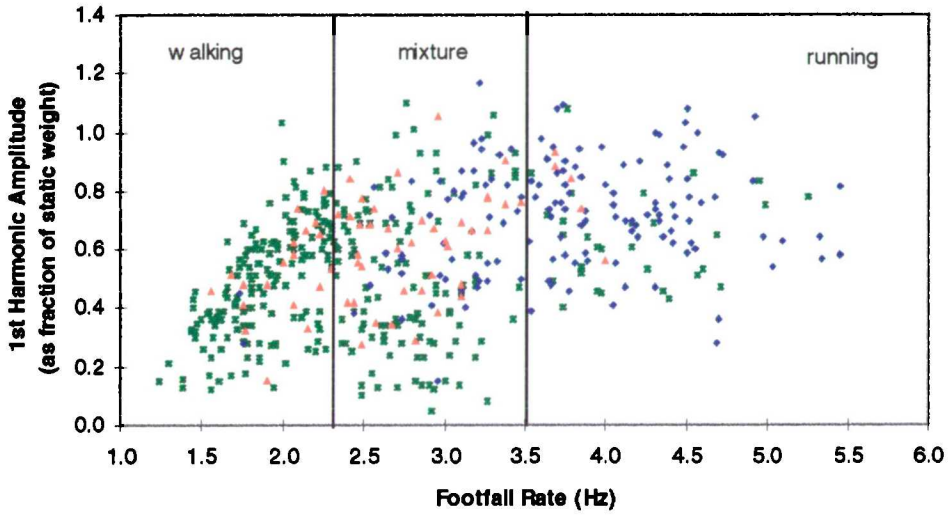

Figure 73 First harmonic amplitudes divided into walking, running and mixture regions.

In this case the divisions are much more arbitrary although one can certainly see the division between the walking region and the running region. The comments from the subjects (typically) indicated that all footfall rates below 4 Hz felt "comfortable" during descent, which was indicated by the large spread in the (red) triangle indicators. These comments were different from the ascending trials where two distinct footfall rates were singled out.

6.4.2.3 The second harmonic data

Figure 74 is a plot of the second harmonic values calculated from all the ascending tests on both stair inclines. Like on the flat, the values were widely scattered in amplitude throughout the frequency range with an average value around 0.2 of the subjects' static weight. The ±2 sigma limit for the data varies approximately

between 0.03 and 0.33. Normalisation by subjects' height, as with the first harmonic data, had little effect in reducing the scatter.

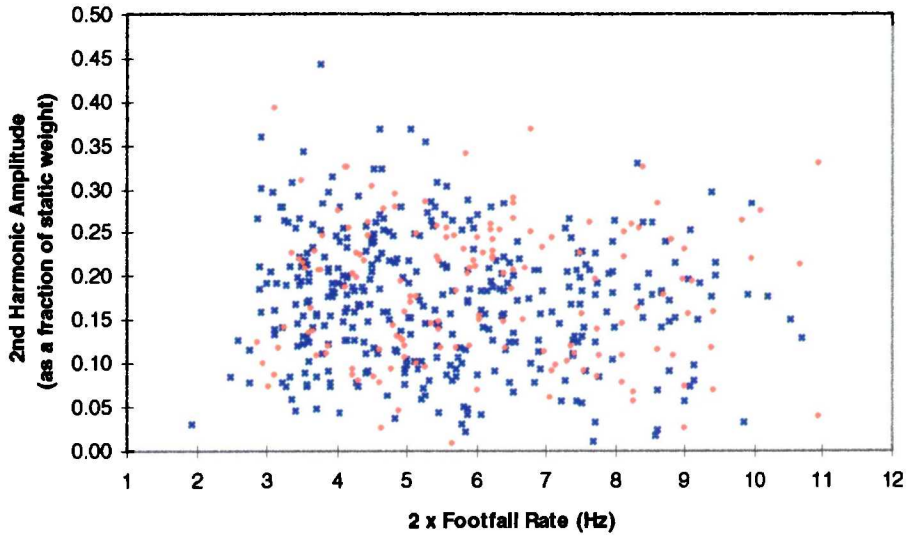

Figure 74 Second harmonic values for descending.

6.4.2.4 The higher harmonic data

Figure 75 and Figure 76 are plots of the third and fourth harmonic values respectively. Like the second harmonic data, the values were scattered in amplitude throughout the frequency range. The third harmonic had a mean value of approximately 0.09 with a ±2 sigma range between 0.00 and 0.16.

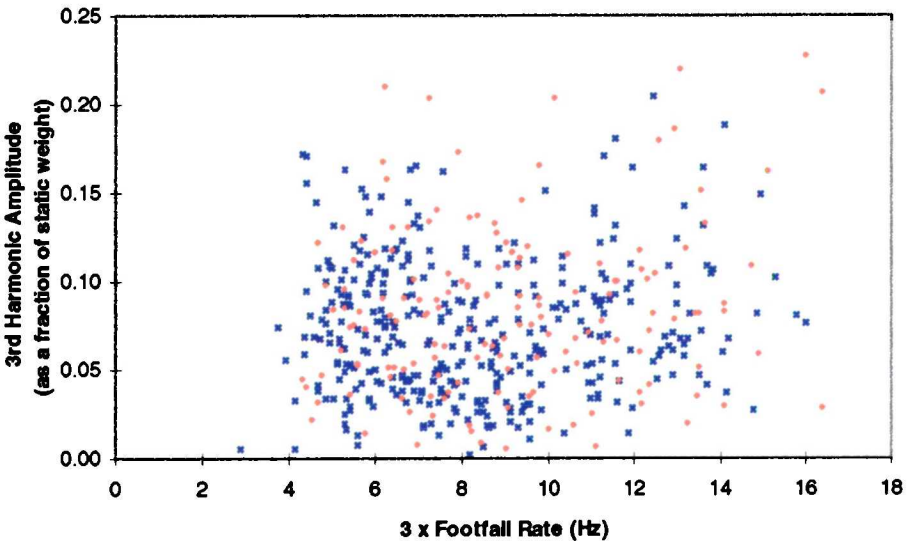

Figure 75 Third harmonic values for descending.

The fourth harmonic had a mean value of approximately 0.06 with a ±2 sigma range between 0.00 and 0.13.

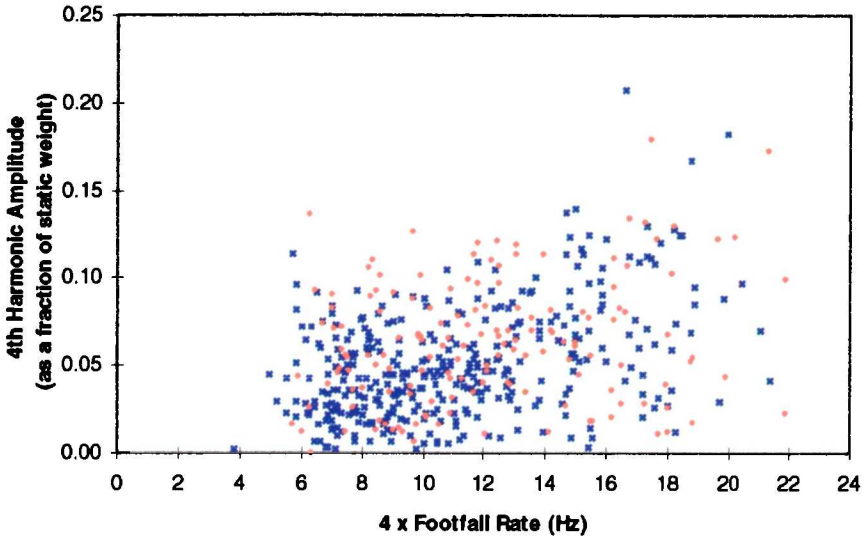

Figure 76 Fourth harmonic amplitudes for descending.

The remaining harmonics (above the fourth) were small. Two typical traces have been selected to illustrate this point. Figure 77 is an FFT frequency spectrum calculated from a trace generated by a subject walking at 2.0 Hz. The trace had the same shape as Figure 71-C. Figure 78 is an FFT frequency spectrum calculated from a trace generated by a subject walking at 3.3 Hz. This trace had the shape of Figure 71-A.

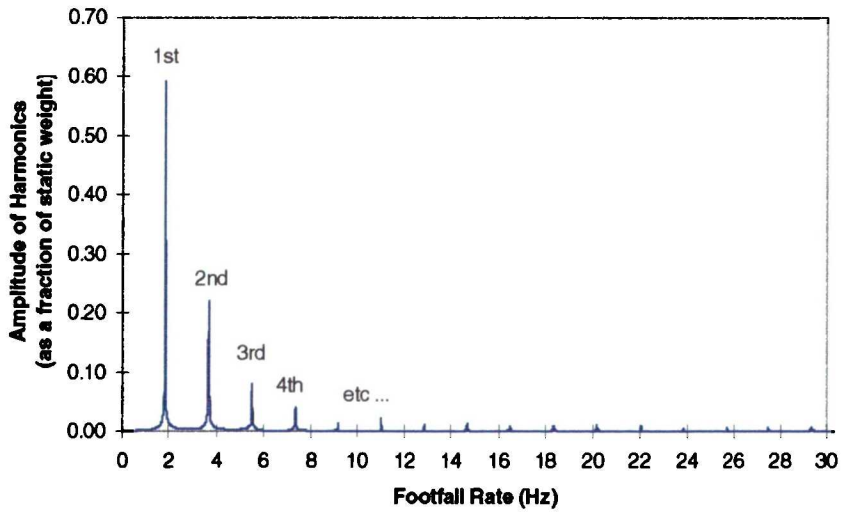

Figure 77 Typical harmonic amplitudes for descending traces around 1.8 Hz.

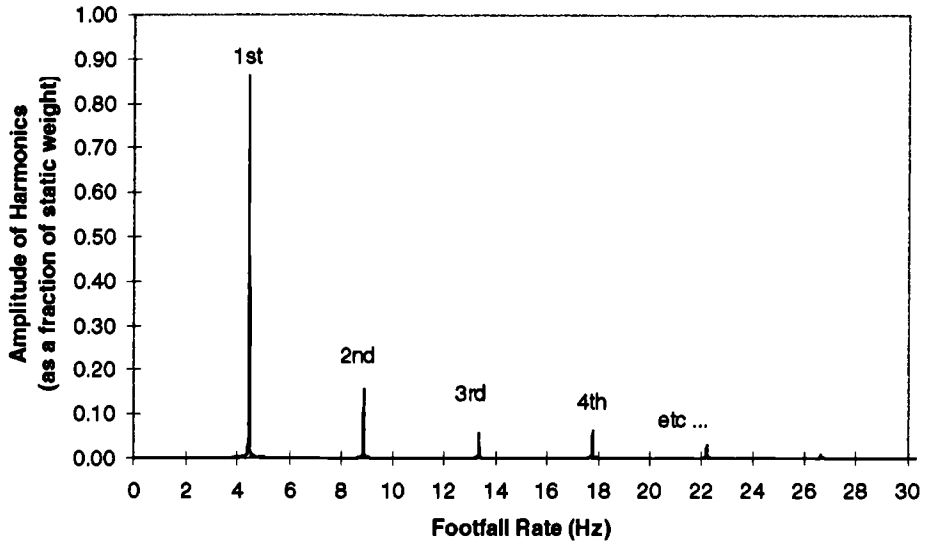

Figure 78 Typical harmonic amplitudes for descending traces around 4.3 Hz.

Although both traces vary in the values of the first 4 harmonics, from the fifth harmonic onwards the values were virtually zero.

6.5 DISCUSSION

As previously discussed, the amount of information available on human loading of staircases is minimal. Therefore, the purpose of this chapter was to accurately quantify the impact loading caused by subjects ascending and/or descending a staircase. In order to conduct this analysis, a specially designed seven step staircase was erected at University College London incorporating a force plate in place of the fourth step. The staircase was specially designed so that it could be used at a 22° and 33° incline. Over 600 impact traces were collected at both inclines using 25 subjects all ascending or descending at one stair per step. The traces were post-processed to determine both maximum and average impact loads as well as harmonic content.

The ascending results showed a maximum impact load of approximately 2.5 times subject body weight with an average impact load of approximately 1.3 times body weight when ascending at 2 Hz. Table 17 compares these values to those mentioned in section 6.1.1.

Author	Mean	Maximum
Kerr	**1.30**	**2.50**
Nilsson	1.40	1.96
Alcock and Lander	1.30	--
Morgan	1.32	--
Gething	1.84	3.3

Table 17 Mean and maximum impact loads from ascending traces.

The maximum footfall rates observed during the ascending trials were approximately 4.5 Hz with an average "walking" footfall rate of 2.0 Hz and an average "running" footfall rate of 3.3 Hz. The harmonic components found in the force time history traces are detailed in Table 18. The values were very small beyond the fourth harmonic.

Harmonic	Mean at 2.0 Hz	Mean at 3.3 Hz	Max
1st	0.40	1.00	1.30
2nd	0.13	0.09	0.28
3rd	0.06	0.04	0.16
4th	0.04	0.03	0.10

Table 18 Maximum and mean harmonic components calculated from ascending traces.

The descending results showed a maximum impact load of approximately 3.0 times body weight with an average load of approximately 2.1 times body weight when descending at 2 Hz. Table 19 compares these values to those mentioned in section 6.1.1. All values (except the maximum Nilsson results) are consistent with each other.

Author	Mean	Maximum
Kerr	**2.10**	**3.00**
Nilsson	1.95	5.26
Alcock and Lander	2.21	--
Morgan	2.25	--
Gething	2.24	3.07

Table 19 Mean and maximum impact loads from descending traces.

The maximum footfall rates observed during the descending trials were approximately 5.5 Hz. The harmonic components found in the force-time history

traces are detailed in Table 20. Like the ascending traces, the values were very small beyond the fourth harmonic.

Harmonic	Mean at 2.0 Hz	Mean at 3.3 Hz	Max
1st	0.45	0.77	1.15
2nd	0.21	0.18	0.37
3rd	0.08	0.07	0.22
4th	0.05	0.05	0.18

Table 20 Maximum and mean harmonic components calculated from descending traces.

The harmonic results showed that slightly larger first harmonic values can be expected for ascending traces although descending traces showed much larger amplitudes for the higher harmonics. In fact, second harmonic amplitudes during very fast descents (greater than 4.0 Hz) were nearly 3 times greater than for ascents.

Overall, ascending and descending produced first harmonic values nearly 2.5 times greater (at 3.3Hz) than that experienced on the flat (at 2.0 Hz) whilst second harmonic values were up to 3 times greater (at 2.0 Hz). The third and forth harmonic values were approximately 2 to 3 times that calculated on the flat but remained low with values rarely greater than 0.10. The substantial increase in first and second harmonic amplitudes coupled with the larger impact loads should concern staircase designers who presently rely on guidance from floors and footbridges. Based on the data gathered in this chapter, any staircase having a natural frequency less than 10 Hz may be dynamically responsive to the pedestrian traffic and produce unacceptable levels of vibration. The results gathered from this chapter are summarised in Kerr and Bishop [1997].

REFERENCES

Alcock, N.J. and Lander, L.E. (1987). *Vibration of Staircases.* Undergraduate Project Thesis. University of Bristol.

Bishop, N.W.M., Willford, M., and Pumphrey, R. (1993). *Multi-Person Excitation of Modern Slender Staircases.* Engineering for Crowd Safety. Elsevier Science Publishers. Amsterdam. Pp.399-408.

Bresler, B. and Frankel, J.P., (1950). *The Forces and Moments in the Leg During Level Walking. ASME Transactions.* Vol. 72. pp. 27-36.

Building Regulation Part K. (1992). Stairs, Ramps and Guards. Department of the Environment and The Welsh Office. HMSO.

Charnley, J. (1972). *Analysis of the Vertical Component of Force in Normal and Pathological Gait.* Journal of Biomechanics. Vol.5. pp. 11-34.

Cunningham, D.M. and Brown, G.W. (1952). *Two Devices for Measuring the Forces Acting on the Human Body During Walking.. Proc. SESA XIV. Vol.2* pp. 75-90.

Ellingwood, B. and Tallin, A. (1984). *Structural Serviceability: Floor Vibrations.* Journal of Structural Engineering. Vol.110. No.2.

Kerr, S.C. and Bishop, N.W.M. (1997). *Human Induced Loading of Flexible Staircases.* Innovation in Civil and Structural Engineering. Mouchel Centenary Conference Proceedings. ISBN 0-948749-50-4 Pp. 311-318.

Martin, D.G. (1995). *Measurement of Dynamic Properties of Insole Materials.* Third Year Engineering Project. Mechanical Engineering Department. University College London.

Matsumoto, Y., Nishioka, T., Shiojiri, H., and Matsuzaki, K. (1978). *Dynamic Design of Footbridges.* International Association for Bridge and Structural Engineering (IABSE), Proceedings P-18/78.

Morgan, G. (1993). *Dynamic Load Measurement Technique for Staircases.* Undergraduate Report Thesis. Department of Mechanical Engineering. Sheffield University.

Nilsson, L. (1976). *Impact Loads Produced by Human Motion.* Swedish Council for Building research. Stockholm. Document 13:Part1.

Ohlsson, S. (1982). *Floor Vibrations and Human Discomfort.* Doctoral Thesis at Chalmers University of Technology, Division of Steel and Timber Structures. ISBN 91-7032-0777-2. Goteborg.

Rainer, J.H. and Pernica, G. (1986). *Vertical Dynamic Forces from Footsteps.* Canadian Acoustics. Vol.4. Part 2.

Rainer, J.H., Pernica, G., and Allen, D.E. (1988). *Dynamic Loading and Response of Footbridges.* Canadian Journal of Civil Engineering. Vol.15. Pp.66-71.

Skorecki, J. (1966). *The Design and Construction of a New Apparatus for Measuring the Vertical Forces Exerted on Walking: A Gait Machine.* Journal of Strain Analysis. Vol.5. pp.429.

Wheeler, J.E. (1982). *Prediction and Control of Pedestrian Induced Vibration in Footbridges.* Journal of the Structural Division, Proceedings of the American Society of Civil Engineers. Vol.108. pp. 2045-2065.

CHAPTER SEVEN 7

SIMULATION OF GROUP LOADING

7 MONTE CARLO SIMULATION OF FORCES GENERATED DURING MULTI PERSON LOADING ON STAIRS

7.1 INTRODUCTION

7.1.1 Previous Work

When walking across a floor, one can choose a footfall rate and stride length to suit the speed one wishes to walk. When negotiating stairs, however, one can only choose a footfall rate since the stride length is fixed by the geometry of the staircase. Observations by the author on actual staircases have shown that this can lead to coherence in the footfall rates when a staircase becomes crowed with pedestrians. So how does this affect the loading?

Bishop *et al.* [1995] raised the concern that multi-person loading conditions on flexible staircases will cause an enhancement to the applied force which would not normally be seen for multi-person loading conditions on a floor. Bishop and his colleagues attempted to quantify these concerns analytically through Monte Carlo simulation techniques. They chose to model group loading conditions using groups of 9, 18 and 27 pedestrians descending a staircase with uniform spacing and the same footfall rate. The only variable was a randomly selected phase shift in their dynamic forces. Since the same footfall rate was used, Bishop simplified the process by using a single force time history (i.e. a single subject) in the groups. The simulation results were expressed as a probability density function verses multi-person force enhancement factor, or in other words, a ratio of maximum group modal force to single person modal force. Therefore, if the dynamic effects from a group of pedestrians were twice as large as a single pedestrian, the enhancement factor would be 2. See Figure 79 for the results of Bishop's work.

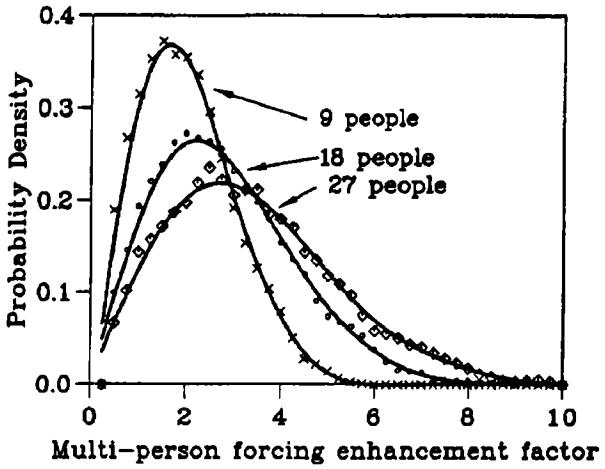

Figure 79 Modal force enhancement factor for multi-person excitation (Bishop et al. [1995])

Their efforts predicted enhancement factors most likely around 2.0, 2.4 and 3.1 for groups of 9, 18 and 27 subjects respectively. However, as Bishop pointed out, a large number of subjects on the stairs increased the damping value that reduced the dynamic effects; therefore, a likely enhancement value of 1.5 to 3 seems more reasonable for the group of 27 subjects.

The purpose of this chapter is to duplicate the work of Bishop as well as show the dynamic effects of several other loading conditions involving groups of pedestrians. This was accomplished by writing two C++ programs to simulate groups of pedestrians ascending and descending a staircase with various phase shifts. One program was written for pedestrians travelling at the same footfall rate while the second was written for pedestrians travelling at different footfall rates.

7.1.2 What is Monte Carlo Simulation

Mathematics has been defined as the science of space, number and quantity (Oxford Dictionary). Mathematicians have been described as either theoretical or experimental. A theoretical mathematician deduces conclusions from postulates. An experimental mathematician infers conclusions from observations. Monte Carlo simulation techniques are tools used by the experimental mathematician.

The methods are typically used on experiments with random inputs. The name and development of the method dates back to 1944 as a research tool in the

development of the atom bomb. It was used to simulate problems concerned with neutron diffusion in fissile material. In recent history, Monte Carlo techniques have found additional favour in the fields of operational research and nuclear physics where problem solving can be beyond the theoretical mathematician (Hammersley and Handscomb [1967]). The types of problems solved through Monte Carlo simulation can either be *probabilistic* or *deterministic.*

A simplistic example of a probabilistic problem might be the prediction of the number of descendants created by a family for 10 generations. Starting with a single couple, a random whole number could be generated to represent the number of children that the couple might have based solely on population statistics. For each child a further random number could be generated to create the next generation, and so on, until 10 generations have been completed. To make things slightly more realistic, other statistical factors could be taken into consideration such as death rates, marriage statistics, income statistics, demographic movements, etc. Each time the simulation is run a different number will be generated. After several thousand simulations, a distribution can be generated to reveal the most likely number of offspring (the mean) as well as the simulation spread (the standard deviation). This data could have been collected from painstaking research into past historical records but simulation is easier.

Another example of a more practical nature is the use of Monte Carlo simulation in the telephone industry. The demand for telephone service is dependant on the decisions of it customers and is therefore a random event. The demand can be predicted using an average call rate per hour plus some random fluctuation described by a known probability distribution. The telephone companies can make special allowances for the predicted demands before it happens.

On the surface, using Monte Carlo simulation techniques to solve deterministic problems makes little sense. After all, deterministic problems have no connection to the theory of probability. However, if a deterministic problem is closely connected with the characteristics of a random process, then simulating the random process can indicate the outcome of the deterministic problem. Tee [1966] describes the use of Monte Carlo simulation to solve Laplace's equations and the parabolic equations describing heat-conduction problems which are

closely connected with certain diffusion-type processes which can be simulated to give a prediction of the heat-conduction problem.

7.2 C++ GROUP SIMULATION PROGRAMS

7.2.1 Background

The force generated by a single person negotiating a staircase can be expressed mathematically by the following,

$$F(t) = P + \sum_{n=1}^{N} \alpha_n \sin(n2\pi ft + \theta_n),$$

where $F(t)$ = force as a function of time,
P = subject weight,
N = total number of harmonics,
α_n = amplitude of n^{th} harmonic sine wave,
f = footfall rate, and
θ_n = phase shift of n^{th} harmonic sine wave.

If two people are negotiating a staircase at the same footfall rate and in phase, the total force is expressed as

$$F_T(t) = P_1 + \left\{\sum_{n=1}^{N} \alpha_n \sin(n2\pi ft + \theta_n)\right\}_1 + P_2 + \left\{\sum_{n=1}^{N} \alpha_n \sin(n2\pi ft + \theta_n)\right\}_2$$

or in general terms,

$$F_T(t) = \sum_{m=1}^{M} P_m + \sum_{m=1}^{M}\sum_{n=1}^{N} \alpha_{n_m} \sin(n2\pi ft + \theta_{n_m})$$

where M = total number of subjects.

If the generalised equation is normalised to subject body weight, the equation is expressed as

$$F_T^*(t) = M + \sum_{m=1}^{M} \sum_{n=1}^{N} \frac{\alpha_{n_m}}{P_m} \sin\left(n2\pi ft + \theta_{n_m}\right)$$

where $F_T^*(t)$ = refers to normalised force.

This equation calculates the total normalised force expected for subjects ascended or descended a staircase simultaneously, i.e. in phase and at the same footfall rate. If the subjects also produced identical force time histories, then the equation is simplified further as shown below

$$F_T^*(t) = M\left\{1 + \sum_{n=1}^{N} \beta_n \sin\left(n2\pi ft + \theta_n\right)\right\}$$

where β_n = normalised amplitude of the n^{th} harmonic sine wave i.e. α_n / P.

Equation 1 Normalised general equation for multiple same-subject Monte Carlo simulation with no phase shift between time histories.

As can be seen by equation 1, when any number of identical subjects ascend or descend simultaneously, the total force is simply one plus the normalised force for a single subject multiplied by the total number of subjects.

Suppose two identical subjects are negotiating the stairs at the same footfall rate but not in phase, i.e. their steps are slightly out of sync (see Figure 80). If the impact forces generated by the two subjects are plotted using the same time scale (see Figure 81), the phase shift can be clearly seen. In this case, the impact loads cannot be simply added together. The phase shift must be taken into account.

Starting with the equation

$$F_T(t) = P_1 + \left\{\sum_{n=1}^{N} \alpha_n \sin\left(n2\pi ft + \theta_n\right)\right\}_1 + P_2 + \left\{\sum_{n=1}^{N} \alpha_n \sin\left(n2\pi ft + \theta_n\right)\right\}_2$$

it can be altered to reflect the difference between the two subjects by inserting a phase shift in the time component of the second subject, as shown on the following page.

$$F_T(t) = P_1 + \left\{ \sum_{n=1}^{N} \alpha_n \sin\left(n2\pi ft + \theta_n\right) \right\}_1 + P_2 + \left\{ \sum_{n=1}^{N} \alpha_n \sin\left(n2\pi f\left(t + \phi_2\right) + \theta_n\right) \right\}_2$$

where ϕ_2 = time shift for the second subject trace.

Therefore, the normalised general equation for any number of identical subjects walking at the same footfall rates but out of phase can still be expressed as equation 1 with only slight alterations, as indicated with the dotted circles

$$F_T^*(t) = M + \sum_{m=1}^{M} \sum_{n=1}^{N} \beta_n \left\{ \sin\left(n2\pi f\left(t + \phi_m\right) + \theta_n\right) \right\}$$

where ϕ_m = phase shift between subject strides.

Equation 2 Normalised general equation for multiple same-subject Monte Carlo simulation with phase shifts between time histories used to verify Bishop et al.[1995].

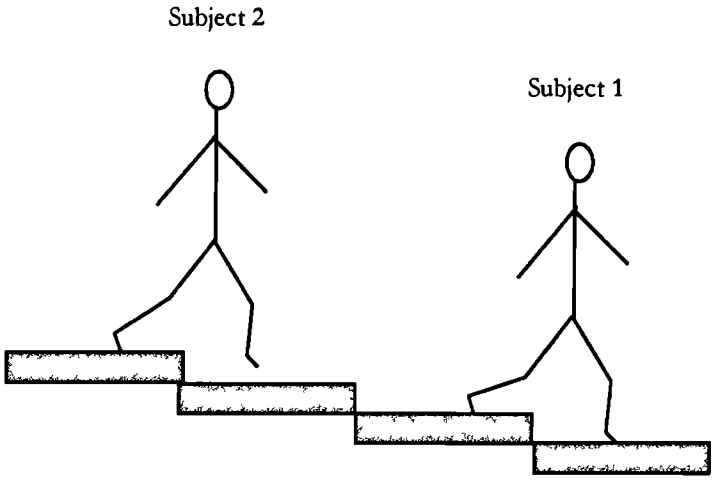

Figure 80 Pictorial of subjects descending at the same footfall rate but slightly out of phase.

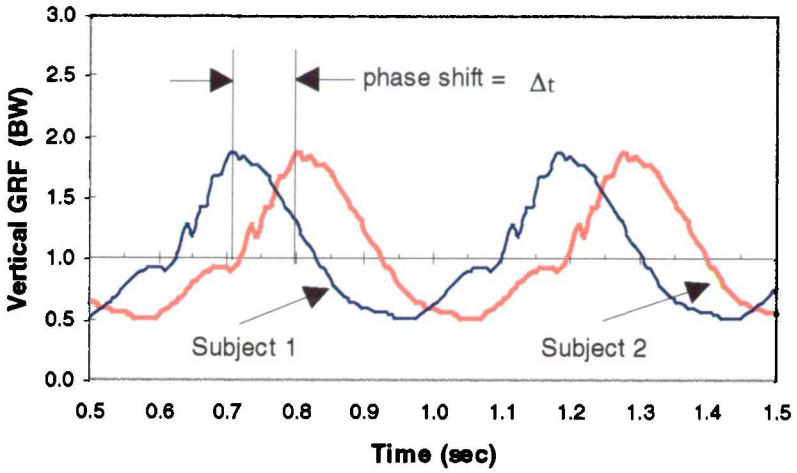

Figure 81 Impact forces from subjects shown slightly out of phase.

Finally, in a real life situation, the subjects would be ascending or descending the stairs at different footfall rates with different phase shifts and likely producing very different force time histories. For this situation equation 2 can be altered by including the individual subject time histories characteristics into the equation i.e. adding the subscript "m" to various parts of the equation.

$$F_T^*(t) = M + \sum_{m=1}^{M}\sum_{n=1}^{N} \beta_{n_m} \left\{\sin\left(n2\pi f_m (t+\phi_m)+\theta_{n_m}\right)\right\}$$

where

$F_T^*(t)$	=	total normalised force as a function of time,
M	=	total number of subjects,
N	=	total number of harmonics,
β_{nm}	=	normalised amplitude of the n^{th} harmonic sine wave for the m^{th} subect,
f_m	=	m^{th} subject footfall rate,
ϕ_m	=	phase shift of force time history for m^{th} subject (at m=1 … ϕ_m=0),
θ_{nm}	=	phase shift of the n^{th} harmonic sine wave for the m^{th} subject.

Equation 3 Normalised general equation for multiple subject Monte Carlo simulation with phase shifts between time histories.

This is the normalised general force equation that serves as the basis for the Monte Carlo simulation work in this chapter.

7.2.2 Operational Flow Chart and Program Description

Two programs have been written to simulate the various group loading conditions investigated in this chapter. The first program, *ms_harmonic.cpp*, was designed to calculate the total force and harmonics generated for groups of pedestrians travelling at the same footfall rate with a phase shift between their force time histories. It operated by reading in user specified raw data files from the staircase testing experiments and proceeded to normalise and convert the data in the same manor as described in Chapter 5.

The heart of the program was the *MULSUBJECTS* function that performed a number of tasks. Firstly, it utilised the random number generator provided within C++ and altered the output to provide a phase shift number between 0 and X, where X equals the sampling frequency of the data files, i.e. 200 Hz, divided by the footfall rate. This phase shift was then applied to the first data file by moving each point to a new time index and storing the results in a two column array of time indexes and data points (a crude example is shown in Table 21). Since the traces were repeating, there was no continuity problem between the start and finish points of the trace.

Time Index	**0**	**1**	**2**	**3**	**4**
Original Data File	1	2	3	4	5
Applying Phase Shift of 2	4	5	1	2	3

Table 21 Application of phase shift to data file.

This process of determining and applying a phase shift was repeated for each file (subject) in the group. Upon completion the two column arrays were added together at every time index producing a combined, continuous time-history for the group.

This trace was then passed on to the Fourier analysis functions (as described in Chapter 5) for determining the group trace harmonics. Once completed, the first harmonic value was divided by the average first harmonic value calculated from the individual subject traces. The result was a group amplification or enhancement factor which was stored in a specific bin depending on it value. The

process was repeated thousands of times and upon completion, the bins were converted into a probability density function (pdf). The program then converted the pdf into a two column ASCII file of enhancement factor verses probability density. This program was used to duplicate the work of Bishop *et al.* [1995].

The second program, *ms_thistory.cpp*, was written with the same functionality as the first program (i.e. to calculate the group loading and harmonics) but for groups of subjects ascending or descending at different footfall rates. The key difference with this program was in the calculation of the harmonics. After the data files were normalised and converted into continuous traces, each had a different length corresponding to the footfall rate. Therefore, the fundamental period lengths were not the same for all files as it was for the first program where the footfall rates were the same. This problem did not allow the calculation of the harmonics using traditional Fourier series analysis. Instead, the program used a Fast Fourier Transform (FFT) algorithm to produce an amplitude spectrum of the continuous trace.

After each data file was read, normalised and converted into a continuous trace, it was sent to the MULSUBJECTS function where a phase shift was applied and the points altered to new time indexes (no summing together of the files occurred at this point). Once complete all files were extended to a common length of 131,072 points or 2^{17} by duplicating the file X times until the correct length was reached. Recall from Chapter 2 that an FFT algorithm operates fastest when the number of points in the data file are 2^N. At this point, the data files were added together at every time index just as they were for the first program. The combined, group data file was then sent to the FFT algorithm which returned a frequency spectrum containing 65,536 points spanning a range of 100 Hz, or half of the original sampling rate due to aliasing (see Chapter 2). This created a resolution of 655.36 points per second or a point every 0.0015 seconds. This fine resolution was required to get an accurate depiction of the peak heights in the spectrum. The flow charts and code for both programs are contained in Appendix A.

7.2.3 Validation of the Programs

To validate the first program an attempt was made to duplicate the work of Bishop *et al.* [1995] shown previously in Figure 79. For this task a time history

from a subject descending a staircase at 2.1 Hz was chosen from the data collected in Chapter 6. The initial part of the program normalised the force plate data (see Figure 82-A) and converted it into a continuous force-time history (see Figure 82-B) following the same procedures used in section 5.4.2.

The continuous time history was added to itself in groups of 9, 18 and 27 with the time phase shifts randomised between 0 and 2π. This process was repeated one million times per group. The results were displayed as a plot of probability density verses enhancement factor (see Figure 83). Note the distributions obtained were slightly different than those predicted by Bishop. The most likely enhancement factors were calculated as 2.2, 2.8, and 3.8 with 9, 18, and 27 subjects respectively. Bishop's work showed likely enhancement factors of 1.8, 2.2 and 3.1 respectively. The heights of the curves were smaller than Bishop's, indicating flatter, broader distributions.

The enhancement factors presented by Bishop and his colleges were calculated based on increased modal shape with an increasing distribution of subjects. Since their subjects were distributed across the staircase (i.e. from start to end) it was expected that their modal enhancement factors would be slightly smaller since the mode shape is only being affected by the subjects standing closest to he middle of the stair. The subjects at the start and end have little effect on the deflection on the span.

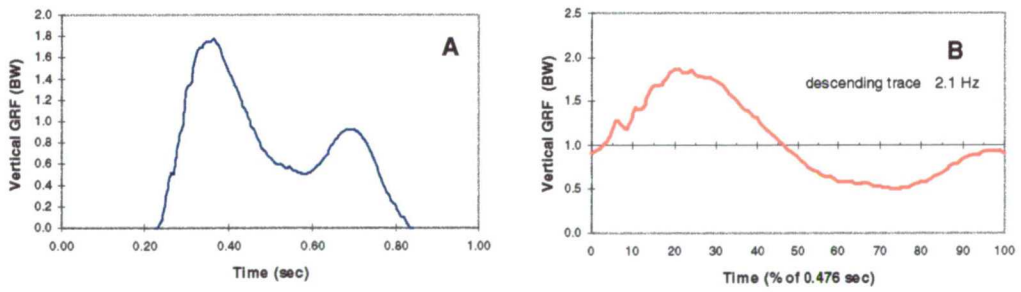

Figure 82 Single (A) and continuous (B) force-time histories generated by a subject descending a staircase at 2.1 Hz.

Further discrepancies may also be due to the number of simulations used to define the probability density curves. This work used one million simulations to produce a smooth representation of the enhancement factors whereas Bishop's

work used far less. The enhancement results calculated in this work are presented in Figure 83. These results validate the operation of the computer program.

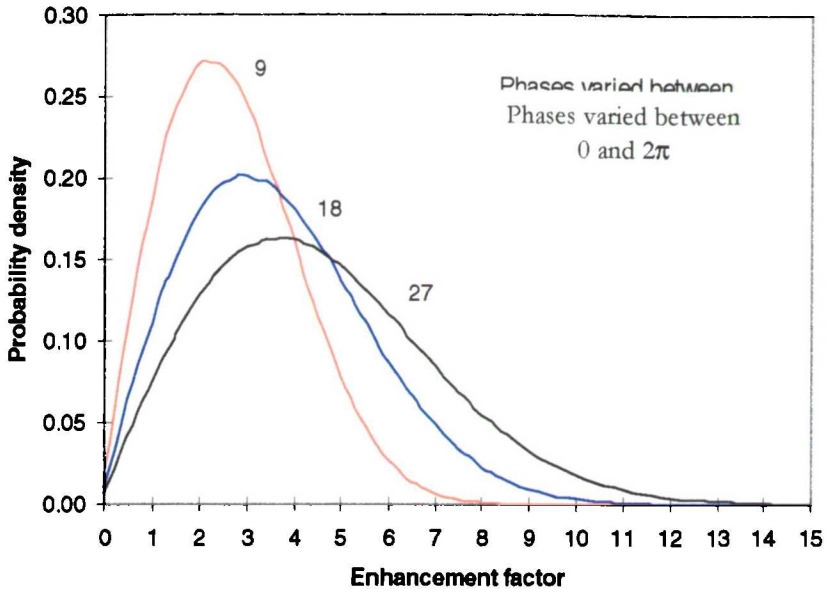

Figure 83 Probability density verses enhancement factor for 'same subject' excitation.

Carrying the analysis slightly further, Figure 84 is a plot of probability distribution functions (PDF's) for the three groups of subjects. Note that there is a 5% chance that the enhancement factors will exceed 5, 7 and 8.5 for groups of 9, 18 and 27 subjects respectively.

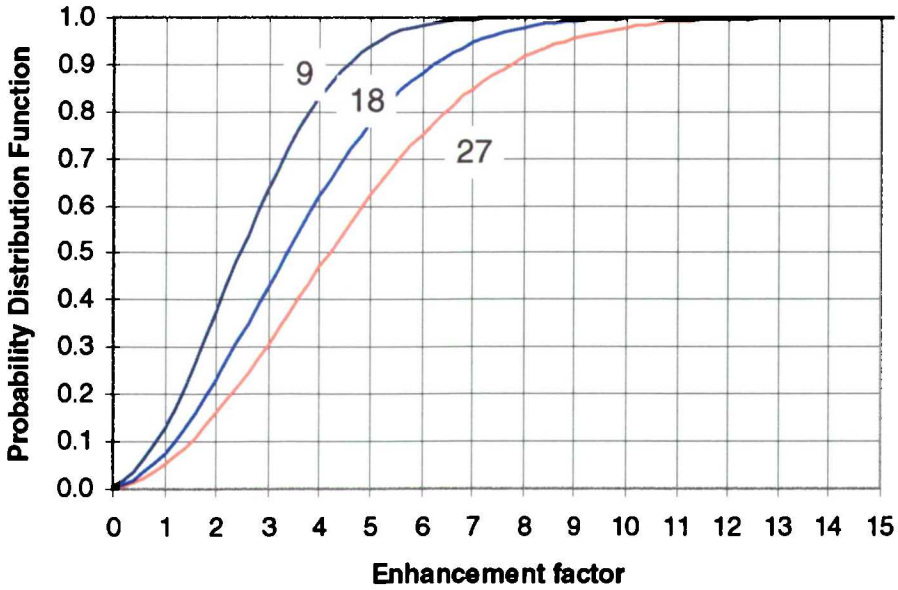

Figure 84 Probability Distribution Functions of enhancement factors for the three groups.

These values constitute significant enhancements to the single subject harmonics and would therefore create a substantial dynamic loading increase to the stairs (Bishop also pointed out, that the increased structural damping created as the number of subjects increases will limit the enhancement factors for the larger groups). Although these results show enhancement factors well above the single person excitation, there are other group loading conditions that could produce enhancement factors even greater.

To validate the second program, two ascending traces were selected with footfall rates of 1.22 Hz and 2.10 Hz (spaced far enough apart as not to influence each other). The first harmonic values for each file was 0.21 and 0.49, as calculated through a commercial Fourier analysis program. If operating correctly, the second program would generate a frequency spectrum showing harmonic peaks at 1.22 Hz and 2.10 Hz (and multiples thereof) with the first harmonic peaks extending to heights of 0.21 and 0.49. Figure 85 is a close up of the output produced by the program. It was run twice with a buffer size of 131,072 points or 2^{17} and 8,192 points or 2^{13}. At 8,192 points the spectrum resolution is 40.96 points per second or 0.0244 Hz between points. Note that this resolution is 1600% less refined than for the larger buffer size.

After viewing Figure 85, it is obvious that the lower buffer size is inadequate to produce the correct peak height. The spectrum distributions are flatter and spread out. Running the program with the higher resolution produced the correct peak heights and peak locations, therefore verifying the operation of the program and validating the use of a large buffer size.

7.3 SIMULATION OF MULTIPLE SUBJECTS WITH DIFFERENT FOOTFALL RATES

This situation can be thought of as a group of people randomly ascending (or descending) a staircase at very different footfall rates which is similar to a group of persons walking along a floor at different footfall rates. However, on a staircase the subject's stride length is fixed by the geometry of the stair and cannot be varied unlike walking on a floor.

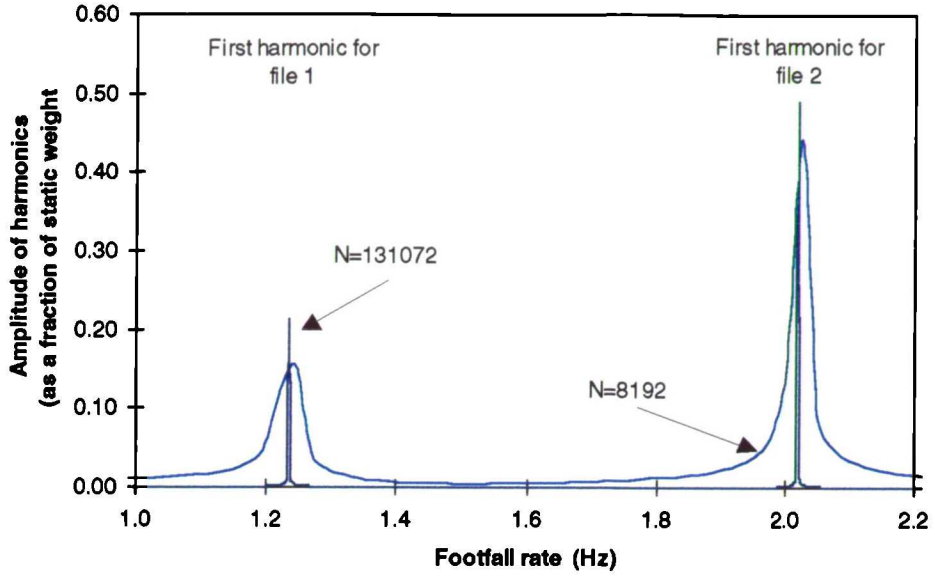

Figure 85 First harmonic peaks from two ascending traces showing necessity to have large FFT buffer size.

Ellingwood and Tallin [1984] describe the dynamic amplification for groups walking on a floor. They state that there is no magnification of the harmonics when a group walks across a floor as compared with a single subject walking across a floor. Therefore, one might also expect no magnification of the harmonics while ascending (or descending) stairs assuming that the stride restriction has no effect in the loading.

To model this situation a group of 9 ascending traces were selected varying in footfall rate by approximately 0.25 Hz per trace, i.e. Figure 86 is a frequency spectrum for one of the ascending traces created at 2 footfalls per second. These traces were then added together with randomly selected phase shifts between 0 and 2π, to produce a new time history from which the harmonics were calculated. This procedure was repeated thousands of times to produce an average plot of predicted harmonic amplitudes verses footfall rates (see Figure 87).

The taller peaks were the first harmonic values for each trace while the smaller peaks represent the higher harmonics present below 5 Hz. The dotted line in the background (labelled "actual") was a compilation of the nine traces, each expanded into its component harmonics and added together, representing the actual heights of the individual harmonics before the simulation. There was no

appreciable difference between the two plots nor was there any difference when the simulation was rerun for descending traces. Therefore, if the footfall rates are widely spaced there will be no group amplification effects impacted to the staircase which was the same result predicted by Ellingwood and Tallin [1984] for a floor. The restriction on the stride length had no effect provided the footfall rates were spaced far enough apart as not to effect each other.

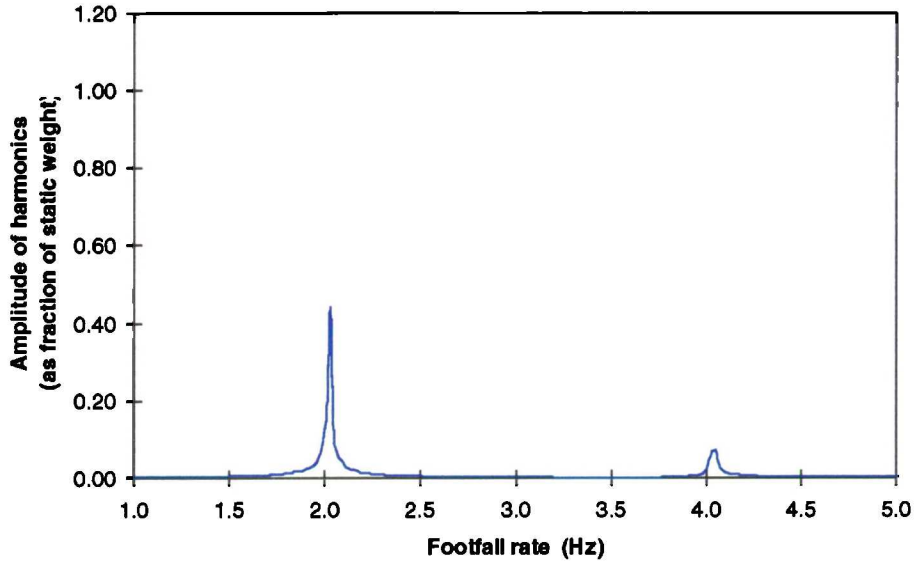

Figure 86 Frequency spectrum for ascending trace at 2Hz.

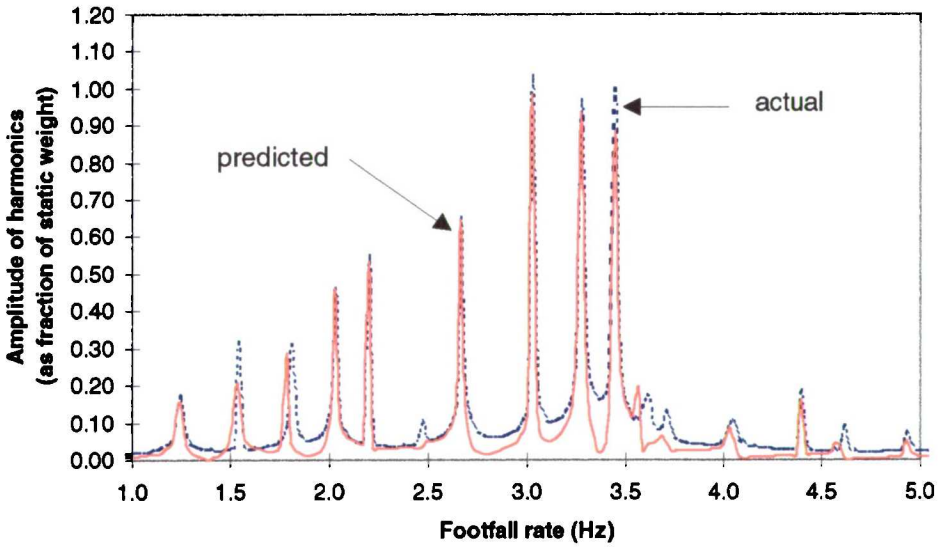

Figure 87 Actual and predicted frequency spectrums using 9 combined traces.

7.4 SIMULATION OF MULTIPLE SUBJECTS WITH CLOSELY SPACED FOOTFALL RATES

Observations on actual staircases have shown that as a staircase becomes crowded, pedestrian motions find coherence. It was common to see a subject mimic the person in front of them while ascending or descending a staircase i.e. as one person stepped forward so did the next and so on. This action caused two things to happen. First the footfall rates became closely spaced, and secondly, the phase shifts tended to develop coherence (for smaller groups).

To model closely spaced footfall rates, a group of 9 ascending traces were randomly selected with a variation across their rates of 10%. As before, these traces were added together with time index phase shifts varying between 0 and 2π to produce a combined time history. After several thousand simulations the average values were calculated and are shown in Figure 88. The average first harmonic value from all 9 traces prior to the simulation was 0.37. As can be seen, the simulation produced a first harmonic peak near 0.70, creating an enhancement factor of approximately 2 on the averaged first harmonic value. The enhancement factor also applied to all higher harmonics. These results indicated that an increase in the harmonics amplitudes can be expected if the footfall rates are closely spaced.

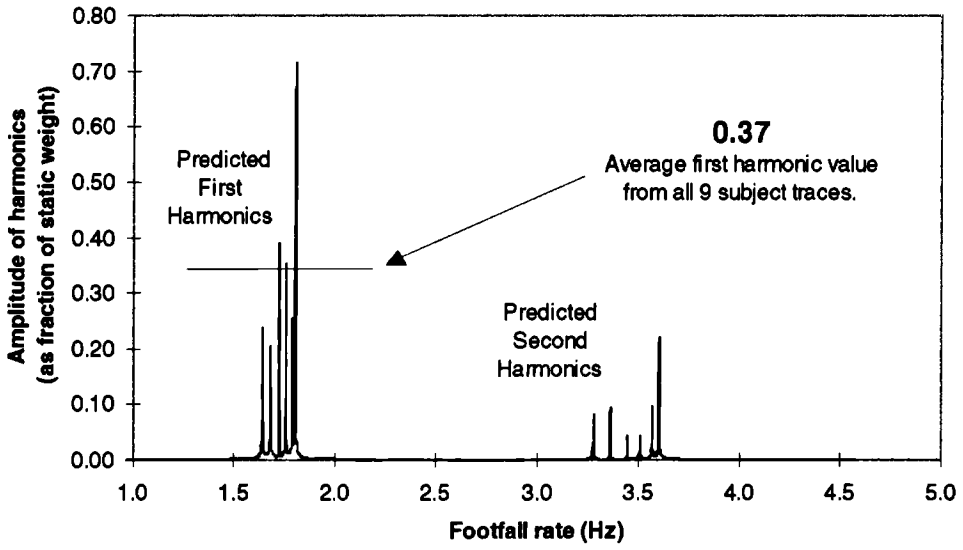

Figure 88 Predicted harmonic results from a group of 9 subjects with closely spaced footfall rates.

An effort was also made to model the coherence in the phase shifts to show what difference it made to the predicted results. The question is, however, what amount of coherence occurred? Suppose 2 people were walking down a crowded staircase. From observations at London underground stations, it was seen that as the first person stepped down so did the second person, with only a small delay or phase shift in their steps. For 3, 4 and 5 persons this same pattern occurred although by the 8th and 9th person the delay or phase shift amounted to approximately half a step. Therefore for smaller groups, say up to 9 subjects, coherence in the motions tended to make the phase shifts vary between 0 and π, not 0 and 2π.

The simulation was rerun using the reduced phase shift range and the results are shown in Figure 89. The simulation produced a first harmonic peak near 1.10 creating an enhancement factor of approximately 3 on the original value 0.37. This order of magnitude could only be expected for smaller groups (< 9 people) provided their footfall rates only varied by 5 or 10%. Therefore, a small group could produce enhancement factors between 2 and 3 on the original averaged harmonic value and the magnitude of enhancement holds whether ascending or descending.

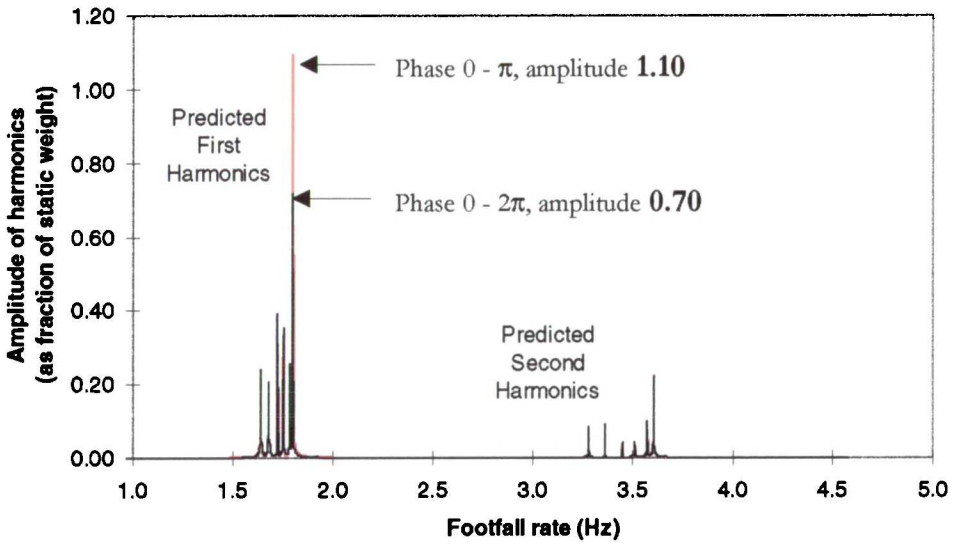

Figure 89 Predicted harmonic results from a group of 9 subjects with closely spaced footfall rates and phase shifts varying from 0 to π and 0 to 2π.

7.5 SIMULATION OF MULTIPLE SUBJECTS WITH THE SAME FOOTFALL RATE

Observations at underground stations showed that as people filed onto and up (down) stairways they tended to walk at the same footfall rate. To model this situation 9 descending traces were selected having the same footfall rate. From these traces a second group of 4 traces was also created. The two groups were run through *ms_harmonic.cpp* over thousands of simulations each varying the phase shifts between 0 and 2π. This simulation was the same as the validation work conducted in section 7.2.3 except that 9 individual subject traces were used as opposed to a single trace. The simulation results were presented as a probability density verses enhancement factor on the averaged first harmonic value (in this case the average harmonic value for both groups was 0.45, see Figure 90). As seen from the plot, likely enhancement factors were 1.6 for the group of 4 and 2.2 for the group of 9. The value for the group of 9 ties up exactly with the value for a group of 9 using the same subject. This result provided evidence that the selection of a single subject to represent groups of subjects was an accurate simplification by Bishop *et al.* [1995].

Figure 91 is the probability distribution plot for the two groups. It showed a 5% chance that the maximum enhancement value could exceed 3.5 for a group of 4 subjects and 5.5 for a group of 9. The enhancement factors and distribution plots were identical when the simulation was rerun using ascending traces.

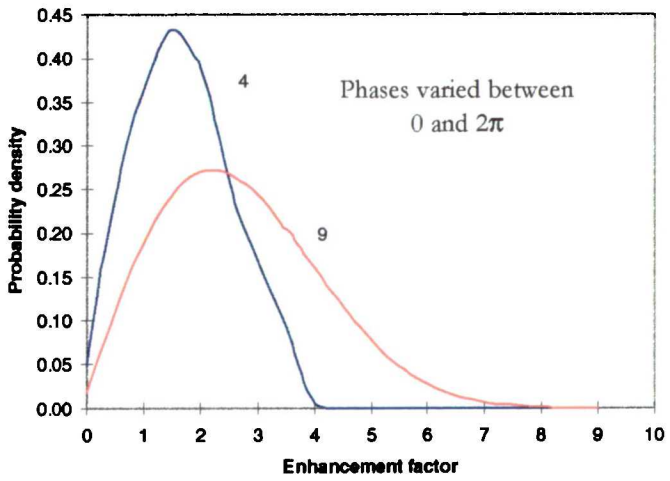

Figure 90 Enhancement factor on first harmonic for multi-subject groups of 4 and 9 people.

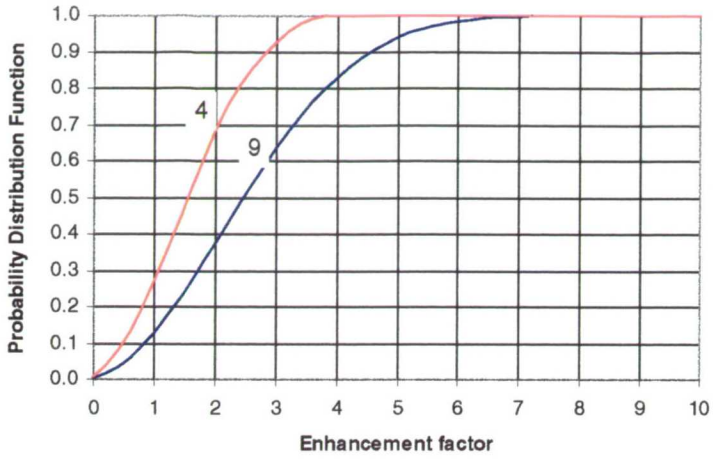

Figure 91 Probability Distribution Functions of enhancement factors for the two groups.

As stated previously, for smaller groups there was coherence in the phase shifts between subjects. To model this the program was rerun with a phase shift varying between 0 and π (see Figure 92). The most likely enhancement factors were 3 for the group of 4 subjects and 6 for the group of 9. Looking at the probability distribution plot (Figure 93), there is a 5% chance that the enhancement factors could exceed 3.8 for a group of 4 subjects and 7.5 for a group 9.

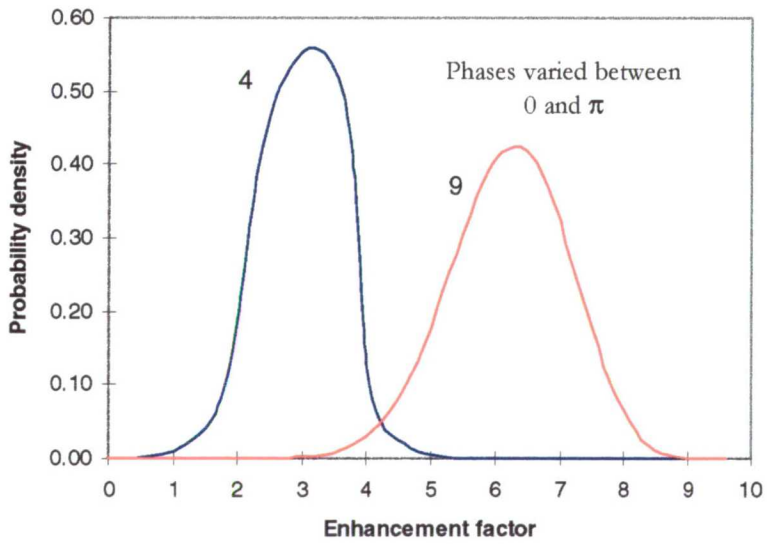

Figure 92 Enhancement values for groups of 4 and 9 subjects with phases varying between 0 and π

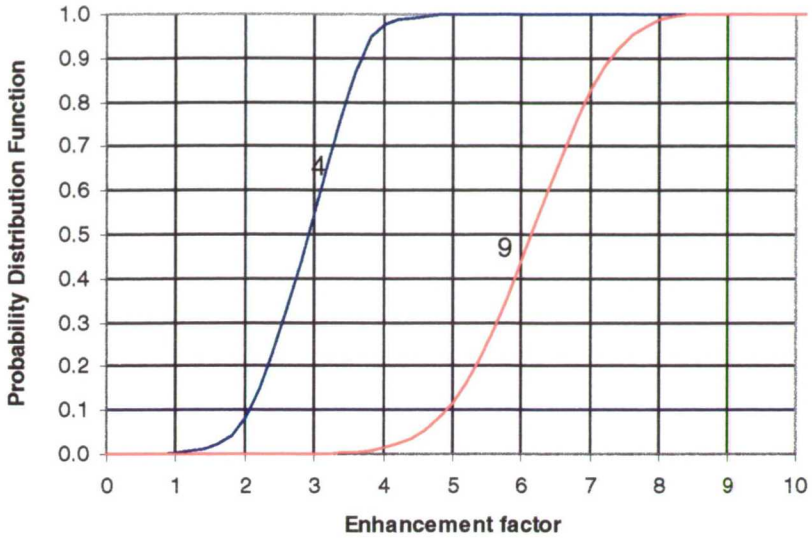

Figure 93 Probability distribution plots for groups of 4 and 9 subjects with phases varying between 0 and π

7.6 DISCUSSION

Kerr and Bishop [1997] have shown that impact forces up to 2.5 times the body weight would load a staircase during the fast ascents of a single subject with impact forces up to 3 times the body weight expected for fast descents (this paper is based on the work presented in Chapter 5 and 6). Also, they pointed out that first harmonic values were slightly higher during ascents than descents although the second harmonic values during descents are nearly 3 time larger at faster footfall rates than that for ascents. Overall, they showed that ascending and descending produced first harmonic values nearly 2.5 times greater than that experienced while walking on a floor with second harmonic values up to 3 times greater.

Couple these findings with the substantial increases in harmonic amplitudes produced from groups of pedestrians ascending and descending and it is understandable that some modern flexible staircases are encountering human induced vibration problems. The Monte Carlo simulation work in this chapter has shown an enhancement factor of 4 for a group of 27 subjects ascending at the same footfall rate with phase shifts varying between 0 and 2π. If one accepts the possibility of coherence in the phase shifts for smaller groups, enhancement

factors of between 3 to 6 are predicted for groups of less than 10 people with phase shifts varying between 0 to π.

These results concur with the field work conducted by Bishop *et al.*[1995] on a slender staircase in a shopping mall. He directed a group of 27 subjects descending a staircase repeatedly using different footfall rates. The results showed a response of nearly 3 times the equivalent single person response during fast descents which ties up nicely with the predicted response of 4 times. The difference can be probability attributed to the increase in structural damping observed during the larger group tests. A damping value of 2.2% was calculated for the staircase during the single person descents, while a damping value of 6% was calculated for the large group descents. Bishop also pointed out that the group loading effects diminished with footfall rate and became negligible at around 2.5 footfalls per second. This would suggest that the Monte Carlo simulation work conducted in this thesis should only be applicable to the higher footfall rates, i.e. greater than 2.5 footfalls per second during ascending and descending.

Combining the Monte Carlo simulations with the work of Kerr and Bishop [1997] would suggest that a group of pedestrians rapidly ascending or descending a staircase could produce first harmonic values nearly 10 times greater than that experienced on a floor while second harmonic values could be 15 times greater. The higher harmonics, which showed little increase in Kerr and Bishop's work, could also be influenced by the group effects and be 3 to 5 times greater. Therefore, any staircase having a natural frequency less than 10 Hz will likely be susceptible to human induced resonance which would probably produce unacceptable levels of vibration. This simulation work has produced valuable information for the staircase designer that was not available prior to the completion of this thesis.

REFERENCES

Bishop, N.W.M., Willford, M., and Pumphrey, R. (1995). *Human Induced Loading of Flexible Staircases.* Safety Science. Pp. 261-276.

Ellingwood, B. and Tallin, A. (1984). *Structural Serviceability: Floor Vibrations.* Journal of Structural Engineering. Vol. 110. Pp. 401-418.

Hammersley, J.M. and Handscomb, D.C. (1967). Monte Carlo Methods. Methuen & Co Ltd. London.

Kerr, S.C. and Bishop, N.W.M. (1997). *Human Induced Loading of Flexible Staircases.* Innovation in Civil and Structural Engineering. Mouchel Centenary Conference Proceedings. ISBN 0-948749-50-4 Pp. 311-318.

Tee, G.J. (1966). The Mone Carlo Method. Pergamon Press. London.

CHAPTER EIGHT 8

OBTAINING GAIT DATA

8 OBTAINING POSITIONAL DATA FOR THE BODY DURING WALKING AND ASCENDING / DESCENDING STAIRS

8.1 INTRODUCTION

Papers such as Bobbert *et al.* [1991], Bobbert *et al.* [1992], Miller and Nissinen [1987], and Thornton-Trump and Daher [1975] describe a mathematical approach (using Newton's Laws of Motion) for predicting the vertical ground reaction forces generated as a body makes contact with the ground. Using this method it is possible to analytically predict/confirm the results obtained during the experimental work. By doing so, it may give the staircase designer an optional method for generating vertical ground reaction forces without the need for a forceplate. The procedure is fully discussed in Chapter 9 but in summary, it relies on the accurate prediction of limb kinematics during motion as well as anthropometric data like that discussed in Clauser *et al.* [1969] or Dempster and Gaughran [1967].

To acquire the kinematics data required subject testing using a motion analysis system. For this thesis the testing was conducted at the Stanmore Orthopaedics Centre which is part of University College London (England). The object of the testing was to gather kinematic data that described the motions of the limbs as the subject walked across the laboratory floor and ascended/descended a small custom built staircase. During the floor testing, actual vertical ground reaction forces were gathered utilising the same force plate and set up described in Chapter 5 (the system was moved from UCL to Stanmore for the testing). The force plate data was used to validate a computer program written to calculate the vertical ground reaction forces (VGRF) from body segment positional data.

8.2 MOTION ANALYSIS SYSTEMS ... A BRIEF HISTORY

8.2.1 Video Based

Up to the mid-nineteenth century, only direct visual observations had provided any data on animal and human motions. With the advent of photography, non-contact methods of gait analysis began to flourish. In 1872 British photographer, E. Muggeridge used a system of 12 cameras with shutters activated by trip wire to produce a series of photos of trotting horses. His work provided proof of the unsupported phase which occurs during a horse's trot (and settled the famous wager concerning the number of hooves in contact with the turf, see Willmann [1882]). Between 1872 and 1884 he developed over 100,000 pictures of animal and human motion.

The first sprocketed film camera, the Kinetoscope, was built by W.K.L. Dickson at the Edison factory in 1891. His camera used a 70mm celluloid film developed by George Eastman for a Kodak camera, but cut in half and perforated at the edges, thus giving rise to the 35mm format used in the cinemas and cameras of today. Cinematography further progressed with the development of high speed flashing, slow motion and single frame playback but extraction of marker co-ordinates took longer to develop. It was the late 1960's before a manually operated film analyser was made for numerical co-ordinate extraction from cinematography records. An experiment performed at the University of Strathclyde (see Paul [1967]) used two orthogonal Bolex 16mm cameras synchronously running at 50 frames per second to film walking subjects. The participants wore 6mm white paper dots as markers on darkened skin areas. At the same time force plate data was also collected and the two were synchronised by pulses fed to flash bulbs within the camera field of view. Two operators spent 9 hours digitising the film with the analyser and another 5 hours were spent on punching paper tape for computer input. The use of paper tape also signified the arrival of the digital computer.

The late 1960's and 1970's saw the development of several approaches to data acquisition and film analysing. Most analysers were simply pointers used to pick out markers viewed within a frame of film for which the co-ordinates would be fed directly into a computer or used to produce punch cards. Eventually,

processors were developed which could extract the marker positions directly from video signals and the basic TV based motion analysis system was born.

Today, positional data is typically obtained through the use of medium or high speed video camera systems consisting of a video camera(s), a computer for data acquisition and analysis, a series of contrasting markers placed on the subject and, a processor for extracting the marker co-ordinates from the video signal. The camera is typically placed perpendicular to the object of interest (a force plate, perhaps) at a distance of approximately 10m. The subject to be filmed wears a number of reflective or contrasting markers at various points on their body. These points are typically on the joints and other specific areas of interest. Within the field of view, a number of calibration markers are also placed to allow the determination of position as the subject's markers appear within the field of view of the camera. The control markers can also be removed in favour of a grid system usually marked on a wall and oriented perpendicular to the camera. The camera is typically zoomed in on the area of interest to maximise the number of pixels picking up the targets and thus provide the greatest accuracy.

To further improve accuracy more than one camera can be used. Bobbert *et al.* [1991] described the use of a video based system utilising 4 high speed cameras placed around a force plate (see Figure 94). The cameras were zoomed into a field of view 2 m in the X direction, 1 m in the Y direction and 2 m in the Z direction. The system was calibrated using 16 control markers. The maximum speed of the camera was 200 Hz, hence the positional data was collected at 200 frames per second.

Other video based systems can use slightly different apparatus, i.e. instead of reflective or contrasting markers, miniature lights can be attached to a subject and the filming conducted in near darkness. In this case the control markers would also be lights but of a different colour.

Regardless of the apparatus used, the essence of a video based system is the camera (preferably high speed), the reflective markers and the control system within the field of view from which to calibrate the marker positions. In all cases the sampling rate of the system is fixed by the speed of the camera. To accurately predict the forces occurring during human gait, it is necessary to have a camera

operating in excess of 200 frames per second (a sufficient sampling rate as described by Bobbert [1991]).

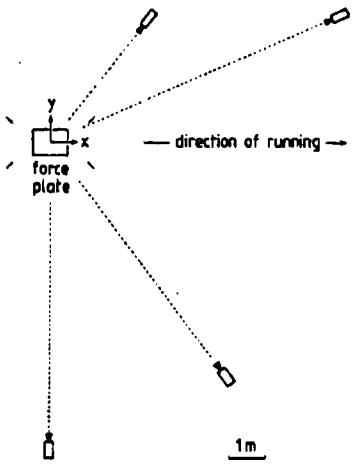

Figure 94 Positions of cameras used for collecting positional data in Bobbert et al.[1991].

8.2.2 Optoelectronic Based

These systems are not TV based and rely on light sensors to operate. The work carried out in Chapter 9 has made use of such a system located at Stanmore Hospital called the Cartesian Optoelectronic Dynamic Antropometer system or CODA for short.

The CODA system first came on the market in 1975 with very limited success. It was entirely revamped in 1981 and marketed as the CODA-3. It then saw another radical change in 1993 and is now on the market as the CODA-mpx30. The Stanmore system is comprised of 2 sub-systems; the scanner unit and a number of LED markers.

The LED markers (shown in Figure 95) are attached to the skin with 2 way tape and powered through a small cable attached to a rechargeable power cell. After receiving a timing signal from the scanner unit the individual markers flash in sequence revealing their positions.

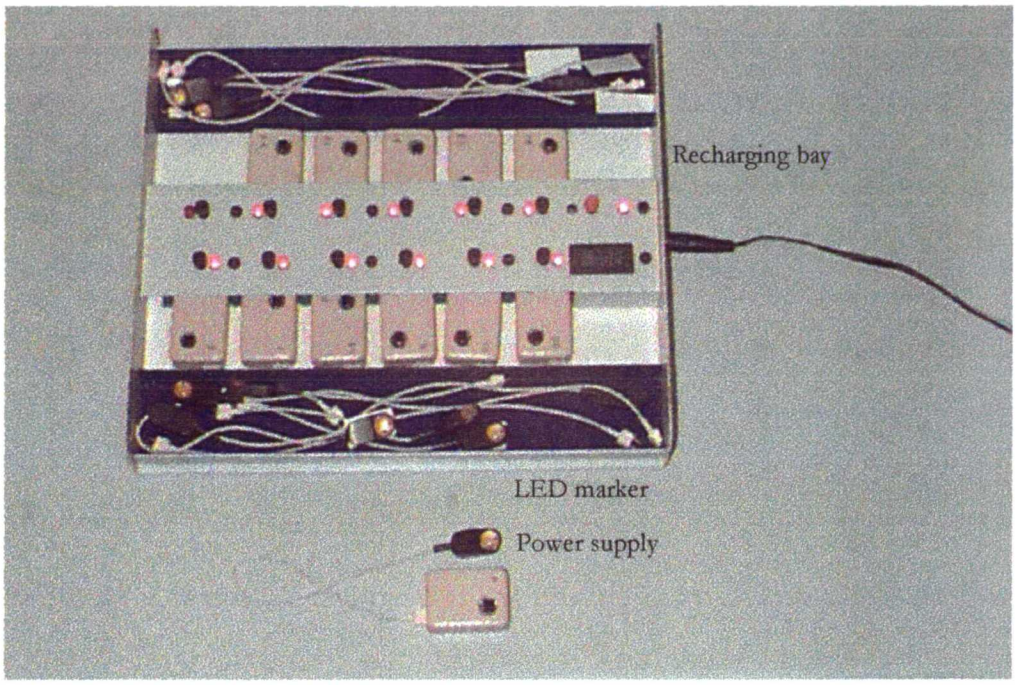

Figure 95 LED markers and power supplies used by the CODA system for collecting positional data.

The scanner unit (shown in Figure 96) receives the emitted light flashes through three sensor openings shown as large black squares in the picture. As the light entered through the openings it passed through a beam splitter which cast a shadow on a system of photodiode sensors. When the LEDs change position and emit another light pulse the shadows move across the photodiode sensor according to the angle of the incoming light. The sensors pick up these changes in the shadow pattern and through cross-correlation techniques calculate the positions of the LED markers.

8.3 COLLECTING THE DATA

8.3.1 Preparation

The CODA system at Stanmore utilised a single scanner that was placed perpendicular to the force plate at a distance of approximate 2.5 m. The system as a whole was set up and collecting data in a very short period of time (approximately 10 minutes). Unlike video systems, the CODA required no field calibration as the system was factory calibrated. Prior to configuring the

computer the test subject was outfitted with the LED markers at the various locations on his body as indicated in Figure 97.

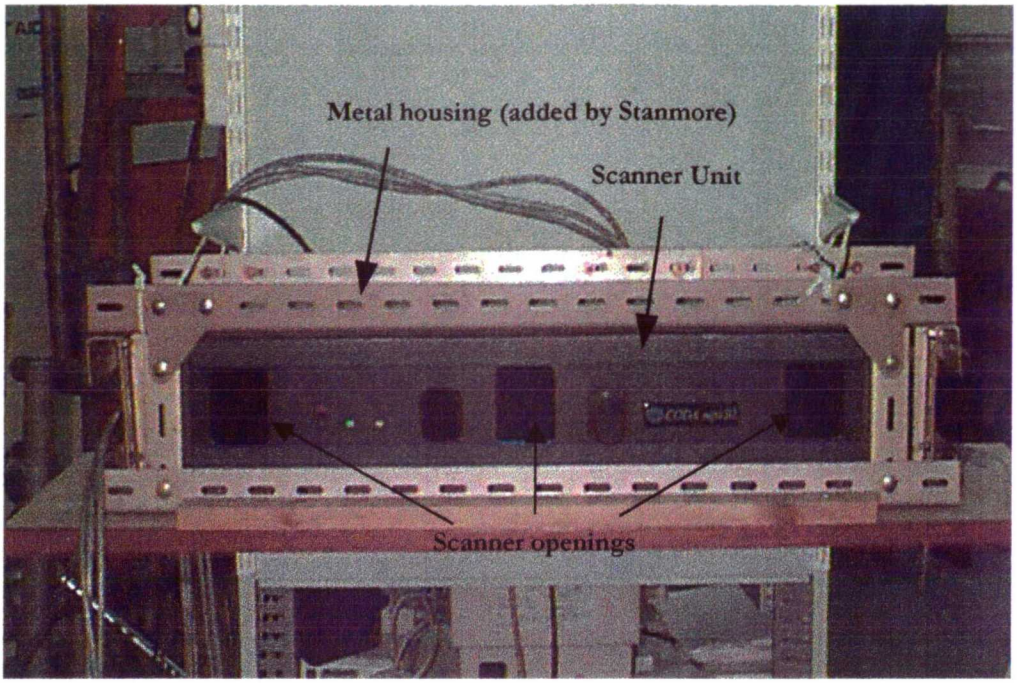

Figure 96 The CODA mpx30 scanner unit.

The markers were affixed to the skin with two sided tape which was found to give adequate adhesion. Care was taken to avoid placing the markers on bony protrusions as these areas of skin have a high relative motion compared to the bone and underlying tissue and would therefore give a false indication of the movements of the limbs. By gathering the positional data for each marker, it was possible to predict the motions of the limbs by assuming a rigid linked model for the body. Therefore, the nine markers outlined the movements of the head/neck system, trunk (shoulder to pelvis), upper arm (shoulder to elbow), lower arm (elbow to wrist), upper leg (pelvis to knee), lower leg (knee to ankle), and foot (heel to toe). An image obtained from the CODA sales brochure (see Figure 98) shows how the markers would be placed if one were interested in the motions of the entire foot. The marker locations used in the Stanmore work have been circled to reflect the ankle, heel and toe (aligned to the fifth metatarsal) positions.

Setting up the computer software for the system required a small number of steps. Firstly, the rigid link model was entered into the computer by inputting the location of each LED marker. The system recognises each marker individually as

number 1, 2, 3, ... n where n at present is 28; the maximum number of markers which can be tracked simultaneously. The input procedure tells the computer that, for example, LED number 1 in on the knee, LED number 2 is on the ankle, and so on. Afterwards, the individual links were also described by inputting which two markers constitute a link and the name of that link. For example, LED number 1 is connected to LED number 2 and is called the 'lower leg'. This portion of the set up is called 'generating the stick figure'. Following this an acquisition rate of 200 Hz was selected for the timing flashes and the force plate, although any value between 1 Hz and 800 Hz could have been chosen (200 Hz was selected based on Bobbert's papers). Finally, the system was set up to trigger on for a period of 5 seconds as the subject walked into the field of view of the scanner.

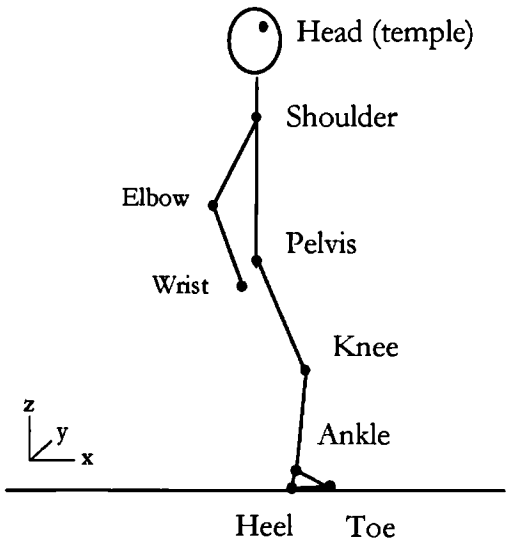

Figure 97 Positions of LED markers on test subject.

8.3.2 Procedure

The time available on the system was limited by a busy testing schedule. Hence, only a single male subject (1.73m, 85kg) was used for the trials. The markers were positioned along the right side of the subject using 2 sided tape. The positive X direction was in the direction of travel with the positive Y axis pointed away from the scanner and the positive Z axis pointed vertically upwards (this corresponds to the right hand rule).

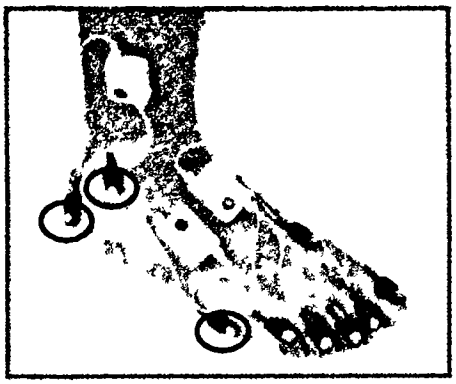

Figure 98 Example of the CODA LED markers placed on a foot (taken from CODA sales brochure, Charnwood Dynamics Ltd., Barrow on Soar).

The subject was asked to perform a number of walking trials at a footfall rate of approximately 2 Hz. In Bobbert *et al.* [1991] they performed the same type of trials for running, utilising a video based system with an acquisition film rate of 200 Hz. In their experiments they added an LED to the force plate set-up that would activate when a force greater than 20 Newtons was applied to the plate. The activated LED was captured on film (along with the running motion) and was used as a synchronisation tool between the film and the force plate data. To minimise their synchronisation errors they operated the force plate at an acquisition rate at 1000 Hz. Unlike Bobbert's work the CODA system allowed the direct input of the force plate data at the same acquisition rate as the timing flashes from the LED's (200 Hz). Therefore no synchronisation errors occurred.

During the walking trials the subject was asked to swing his arms freely as well as bend them at a 90° angle to avoid hiding the pelvis marker. In the trials where the arms were freely swinging, the pelvis marker was monetarily hidden by the hand as the arm swung pass the hip. For these situations the CODA system linearly interpolated for the missing pelvis data from the points just before and just after the interruptions. Post processing work in Chapter 9 indicated that these small approximations have very little effect on the final predictions.

For the trials involving ascending and descending, a small set of stairs was constructed in the testing laboratory utilising scaffolding poles. Due to height restrictions in the laboratory the number of stairs was limited to 4 and the force

plate could not be incorporated into the staircase. For these trials the subject was asked to ascend and descend the stairs in a normal fashion at approximately 2 Hz.

8.3.3 Results and Filtering

As mentioned previously the sample rate used for the CODA work was 200 Hz for a duration of 5 seconds. Hence each trial consisted of 1000 individual data points for each LED marker. This was sufficient to capture several strides of the subject. Figure 99 is a plot of the marker location trajectories as the subject took two walking strides with his right leg (in this case the subject was holding his arm at 90 degrees). From this plot one can see the typical sinusoidal oscillation patterns of the various body markers as the subject walked. One can also see the interaction of the various markers attached to the foot as the stride occurs.

Although these marker trajectories indicate the true position of the markers they do not necessarily depict the true positions of the limb segments. Although care was taken to avoid areas of large skin motion relative to the bone and underlying tissue, this situation could not be completely avoided even through elaborate means (see Bobbert *et al.*[1991]). Therefore the trajectories of the markers do contain small sinusoidal oscillations due to the skin movements, especially during heel contact. The area circled in Figure 99 is an example of a 'rough' area which is not the true movement of the toe. To compensate for this problem the CODA system incorporates a filtering tool which allows the raw data to be low pass filtered at a user specified boundary. Figure 100 depicts the results of passing the data through a 9 Hz filter. The task was to determine which filtering value(s) would eliminate the unwanted sinusoidal oscillations of the skin yet retain the movements which reflected the motions of the limbs. This is discussed in detail in Chapter 9.

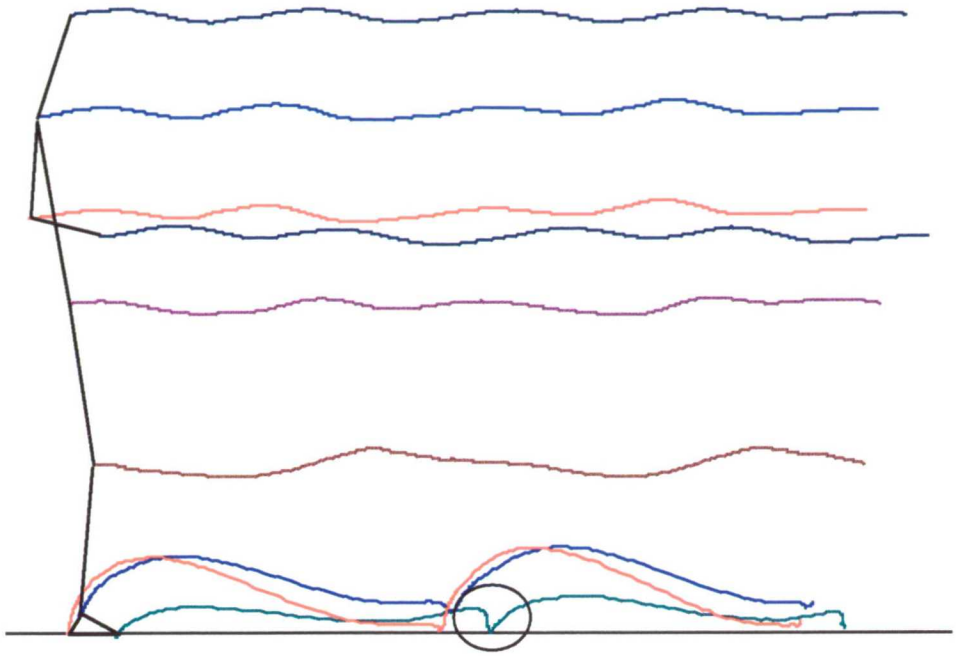

example of rough transition

Figure 99 Z verses X plot of raw displacement data with no filtering applied.

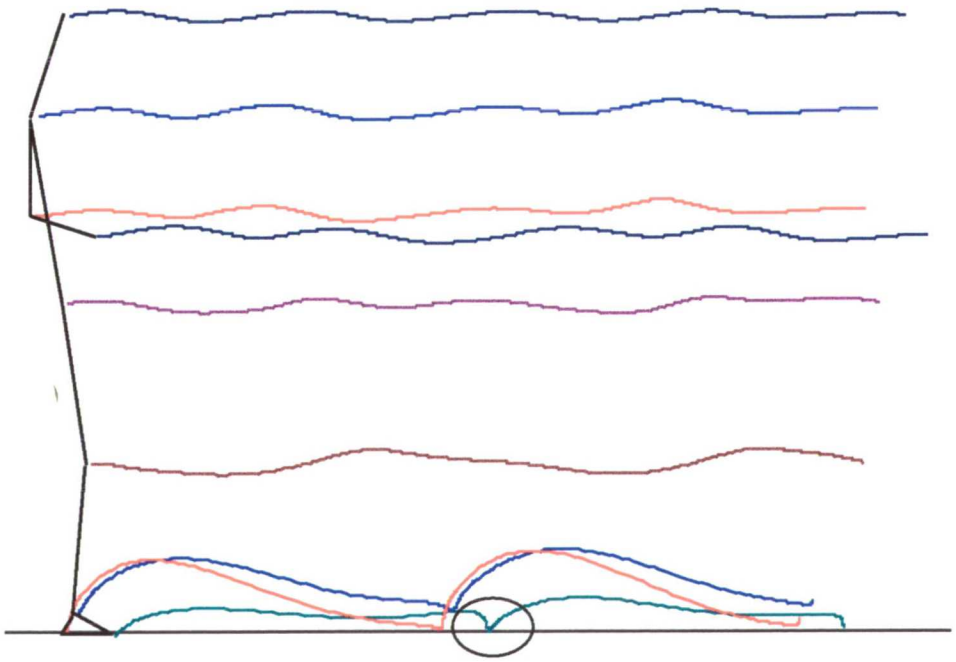

transition has lower peak through filtering

Figure 100 Z verses X plot of displacement data low pass filtered at 9 Hz.

8.3.4 Other Information Available from the CODA System

The CODA system has a number of other features that were used in this work. Based on the data (whether raw or filtered), the software calculated translational velocity and accelerations at the marker positions. These velocities and accelerations were used to verify the correct operation of the C++ programs used in section 9.8. The CODA software also allowed the definition of joint angles. For example, the knee joint angle was defined as pelvis to knee to ankle with a clockwise positive rotation as viewed in the sagittal plane. From the defined joint angles, the software calculated the rotational velocities and accelerations that were also used to verify the correct operation of the C++ programs used in section 9.8.

A final CODA feature used in post processing was the calculation of the distance between markers. By entering two chosen markers, say at the knee and ankle, the software could calculate the distance giving the lower leg limb length. This allowed for quick checks on limb lengths used in the conversion of the rotational velocities and accelerations into their equivalent linear values.

8.4 DISCUSSION

The aim of this chapter was to introduce the optoelectronic motion analysis system called CODA. The system was used in this thesis to collect body segment positional data. This data was post processed (as detailed in Chapter 9), to calculate the vertical ground reaction force created due to the motions. The tests were conducted at Stanmore Orthopaedic Centre and utilised a force plate to record the impact force created during walking. The set-up and procedures used in the tests have also been fully detailed in this chapter.

REFERENCES

Bobbert, M.F., Schamhardt, C., and Nigg, M. (1991). *Calculation of Vertical Ground Reaction Force Estimates During Running from Positional Data.*. Journal of Biomechanics. Vol.24. No.12. pp.1095-1105.

Bobbert, M.F., Yeadon, M.R., and Nigg, M. (1992). *Mechanical Analysis of the Landing Phase in Heel-Toe Running.* Journal of Biomechanics. Vol.25. No.3. pp.223-234.

Clauser, C.E., McConville, J.T. and Young, J.W. (1969). *Weight, Volumn and Center of Mass of Segments of the Human Body.* Wright-Patterson Air Force Base, OH (ARML-TR-69-70). pp.59-60.

Dempster, R. and Gaughran, G.R.L. (1967). *Properties of Body Segments based on Size and Weight.* American Journal of Anatomy. Vol.120. pp.33-54.

Paul, J.P. (1967). *Forces Transmitted by Joints in the Human Body.* Proceedings of the Institute of Mechanical Engineers. Vol.181. pp.8-15.

Miller, D.I. and Nissinen, M.A. (1987). *Critical Examination of Ground Reaction Force in the Running Forward Somersault.* International Journal of Sport Biomechanics. Vol.3. pp.189-206.

Thornton-Trump, A.B. and Daher, R. (1975). *The Prediction of reaction Forces from Gait Data.* Journal of Biomechanics. Vol.8. pp.173-178.

Willimann (1882). *The Horse in Motion as Shown by Instantaneous Photography.* Turner. London.

CHAPTER NINE 9

CALCULATING VGRF FROM GAIT DATA

9 ESTIMATING THE VERTICAL GROUND REACTION FORCE (VGRF) USING CODA POSITIONAL DATA

9.1 INTRODUCTION

Estimating the ground reaction forces from positional data can be examined through the principles of biomechanics. Like engineering mechanics, that can be broken down into the study of statics and dynamics, biomechanics can be broken down into the study of kinematics and kinetics. Kinematics is concerned with motion characteristics from a spatial and temporal perspective and is unconcerned with the forces causing the motions. Kinetics, on the other hand, is concerned with the forces causing the motions. Therefore, it can be stated, biomechanics evaluates the motions of living organisms and the effects that forces have (whether internal or external) on the motions of that organism.

9.2 CONDUCTING A KINEMATIC STUDY WITH POSITIONAL DATA

When conducting a kinematic study one may be interested in many aspects of the motion. Thus, understanding a body's position, velocity, and acceleration are vitally important. However, like in mechanics, these positional derivatives exist both in a linear sense (translational) and an angular sense (rotational). Figure 101 gives examples of each. Note, the motions are two dimensional, and lie in the XY plane. When referring to a three dimensional human body however, the XY plane is the sagittal plane and this, technically speaking, would relate to the XZ plane using positive X as the direction of travel and applying the right hand rule for axis orientation. When dealing with body segment motions and the calculation of ground reaction forces, one is essentially interested in the sagittal plane motions analogous to example D in Figure 101.

Each limb typically needs both a translational and a rotational component to describe it's motion although during the stance phase, when the body is rotating about the heel, the lower limb motion can be described by rotation alone.

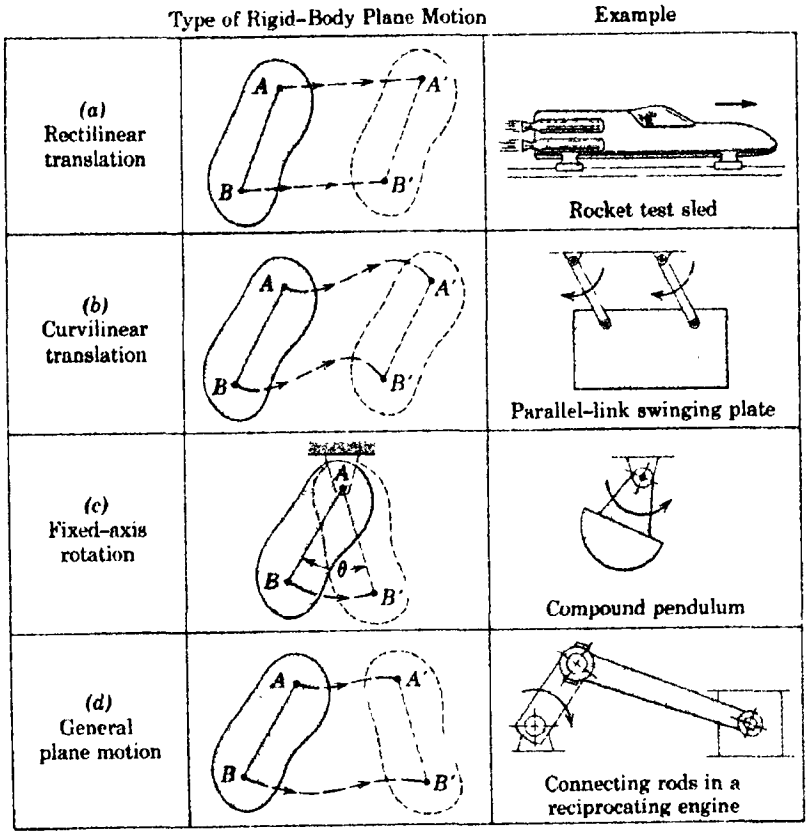

Figure 101 Examples of linear kinematics (a,b), angular kinematics (c), and a combination of both (d). (from J.L. Meriam, "Dynamics", 1980)

9.2.1 Linear Kinematics

Describing linear or translational motions is usually conducted in the Cartesian coordinate system although any spatial reference system can be used. Typically, for walking and running studies, coordinates of the limb joints in the sagittal plane are used to describe the body's motion during the activity. Figure 102 shows an example of the heel and toe positions, in the sagittal plane, as a subject walks across a floor. As pointed out in section 8.3.1, the toe marker was located on the outside of the right foot, just behind the fifth metatarsal. In the figure the toe begins to rise prior to the swing phase. Since the swing phase technically begins after the entire foot breaks contact with the floor, the toe marker begins to rise

prior to the start of the swing phase because the big toe is still making contact with the floor.

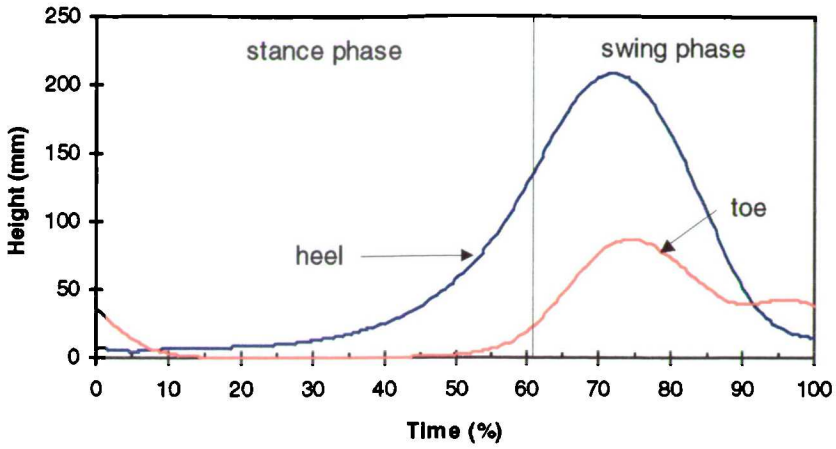

Figure 102 Heel and toe marker positions during walking.

The marker velocities can be calculated by differentiating the plot with respect to time, or in other words, finding the slopes of the curves at every point. One must be careful however, not to calculate the slope between adjacent points as this will produce the velocity between points and not at the points themselves. The procedure for calculating the velocities using the "first central differences" method is described by the equation

$$\dot{X}_i = \frac{X_{i-1} - X_{i+1}}{2 * \Delta T}$$

where $\dot{X}_i$ = velocity at X_i,

X_{i-1} = displacement at X_{i-1},

X_{i+1} = displacement at X_{i+1}, and

ΔT = time interval between points.

Figure 103 is a graphical representation of this method. As can be seen, the first central differences method gives the velocities at the points rather than between the points. Once the velocity profile has been calculated, the accelerations can be determined at each point in exactly the same manner using the velocity curves.

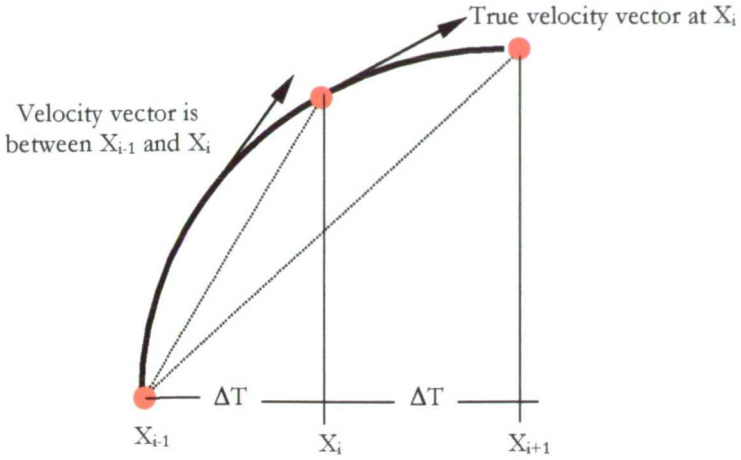

Figure 103 Use of the first central differences method.

As an example, Figure 104 depicts the velocity and acceleration profiles calculated from the heel marker positions shown of Figure 102.

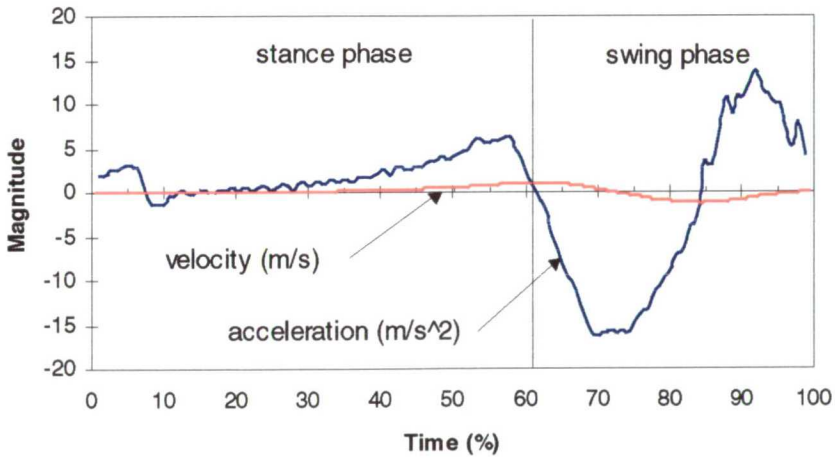

Figure 104 Velocity and acceleration profiles from heel marker positions.

9.2.2 Angular Kinematics

Angular kinematics are typically described using a cylindrical co-ordinate system. Therefore, it is vitally important that one adheres to the right hand rule for axis orientation so that the sign convention for the angular measurements remain consistent. Figure 105 depicts the sign convention and axis orientation used throughout this work.

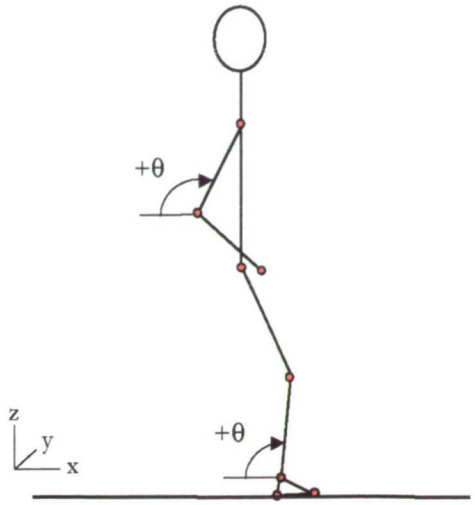

Figure 105 Description of limb angles in the sagittal plane.

For each data sample the angles of the various segments can be calculated and the first central differences method used to calculate the angular velocities (ω) and the angular accelerations (α) for each limb.

The angular velocity can be converted to a linear (tangential) velocity (v_t) through the formula

$$v_t = r * \omega$$

where, v_t = tangential velocity,
r = radius of rotation,
ω = angular velocity.

Figure 106 gives a graphically representation of this expression. The angular accelerations, unlike the angular velocities, produce two linear accelerations, i.e. a tangential acceleration (a_t) and a normal acceleration (a_n) directed towards the centre of rotation. The formulae are given below:

tangential acceleration, $$a_t = r * \alpha$$

normal acceleration, $$a_n = r * \omega^2$$

where, a_t = tangential acceleration,
a_n = normal acceleration,
r = radius of rotation,

α = angular acceleration,
ω = angular velocity.

Figure 107 give a graphically representation of this expression.

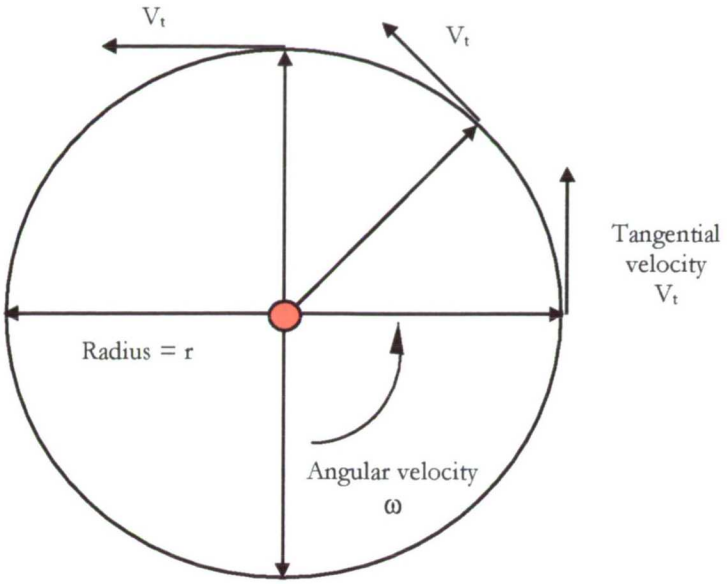

Figure 106 Graphically representation of tangential velocity.

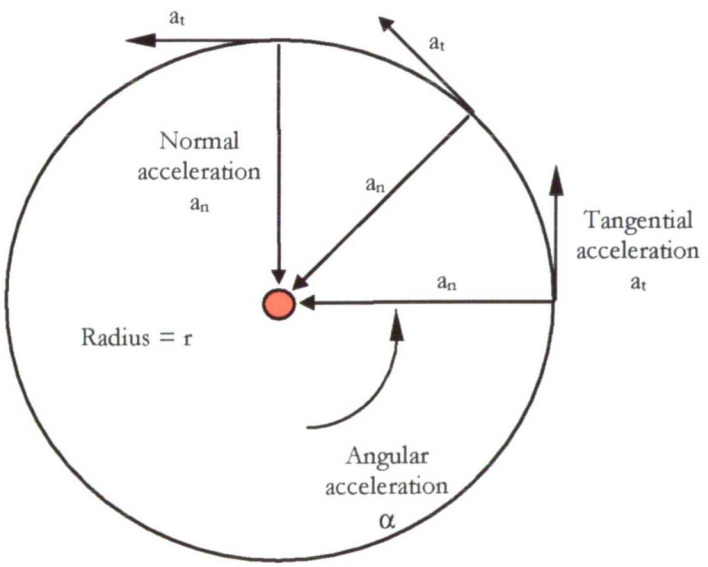

Figure 107 Graphical representation of tangential and normal accelerations.

9.3 CONDUCTING A KINETIC ANALYSIS BASED ON A KINEMATIC STUDY

As discussed earlier, kinetics is concerned with the forces causing the motion. The forces which act on a body can be non-contact forces (gravity) or contact forces (ground reaction, joint reaction, inertial and muscle) (see Hamill and Knutzen [1995]).

9.3.1 Non-Contact Forces

Gravity is by far the most important non-contact force. Our understanding of gravity stems from the contributions of Newton and his "Law of Gravitation" presented in his work *Principia.*

9.3.2 Contact Forces

Contact forces have several important contributors. The ground reaction force is the force provided by the surface upon which one is moving. It is a direct application of Newton's third law of motion concerning the principle of action and reaction and is typically separated into components along the X, Y, and Z directions. As described in previous chapters, the ground reaction force is typically measured with a *force plate.*

The joint reaction force is the force provided across the joint of two body segments. In most analysis the magnitude of this force is unknown. However, given the kinematic data, ground reaction force and appropriate anthropometric data describing limb characteristics, the joint reaction force can be calculated (see Bobbert, *et al.* [1992]).

Inertial forces obey Newton's first law and typically occur in human movement when one body segment causes a second body segment to move solely through the muscle action of the first segment. A prime example of this occurs during the swing phase of the gait cycle. As the hip and thigh muscles propel the upper leg through a counter clockwise rotation, the lower leg and foot also swing through with virtually no muscle activity about the lower joints. Hence the upper leg is said to have impacted an inertial force on the lower leg and foot (Hamil and Knutzen [1995]). Muscles can only offer a pulling force. To flex and extend a

limb requires the interaction of at least two opposing muscles, i.e. the biceps brachii flexes the lower arm at the elbow while the triceps brachii extends arm. The muscle force is thought of as the net muscle force because in many situations more than one muscle aids in the flexing or extending of a limb. Also the point of application of the muscle force is typically not at the joint but applied at the point of attachment to the bone. Muscle forces are very difficult to measure as it requires the placement of force transducers on the muscle tendons. Therefore many researchers have developed mathematical models to approximate the muscle forces although a number of assumptions must be made concerning point of application, force direction and whether co-contraction occurs or not (Scott and Winter, [1991]). Figure 108 shows a free body diagram of the contact and non-contact forces involved in a simple forearm curl.

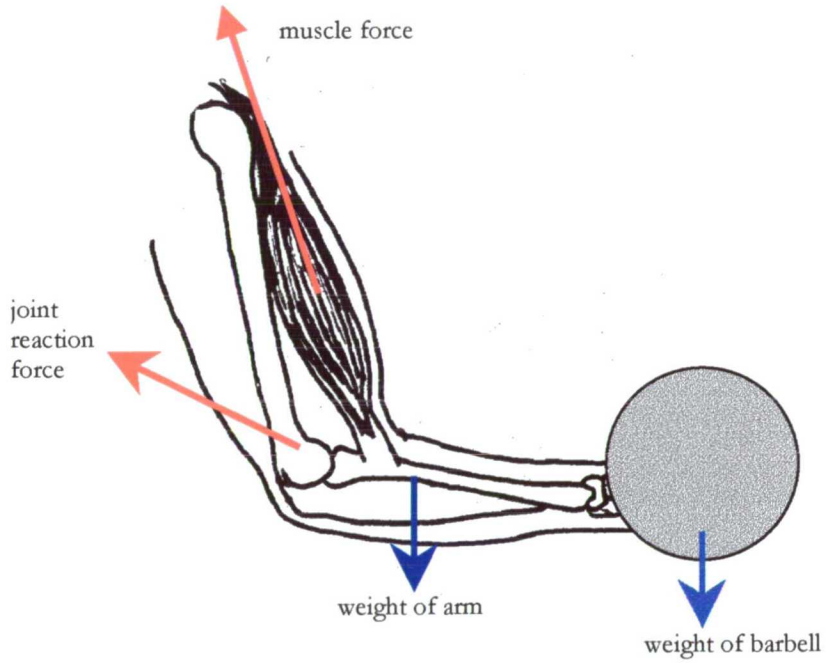

Figure 108 A free body diagram of the forearm during a biceps curl.
(Reproduced from Hamill and Knutzen, "Biomechanical Basis of Human Movement", 1995)

9.3.3 Direct and Inverse Dynamic Problem Approach

In the biomechanics literature, there are numerous papers on the attempts to simulate human gait. Most often this is done by manipulating the internal forces (joint reaction and muscle) on a segmented human model until the required kinematics are produced (Beckett and Chang, [1968], Huston, *et al.* [1976],

Onyshro and Winter, [1980], Pandy and Berme, [1988], Ju and Mansour, [1988]). These papers solve what is referred to as the "direct dynamic problem" which typically does not involve a resolution of the ground reaction forces since they are not required to develop the kinematics. However, if one already has the segmental kinematics (or has previously calculated the data through the direct dynamic problem approach) one can choose to solve the "inverse dynamic problem". This approach calculates the ground reaction forces and joint reaction forces (and moments) from the known movements of the segments by differentiating the displacements to obtain velocities/accelerations and applying a Newtonian approach (discussed later) to each set of sampled kinematics (McGhee, *et al.*[1976], Hardt and Mann [1980], Koopman, *et al.* [1995], Thornton, *et al.*[1975], Cappozzo, *et al.*[1975], Seireg, *et al.*[1975]). When calculating the joint forces, this type of analysis makes several assumptions as to the distribution of ground reaction forces under each foot during the double support phase of the walking gait. These assumptions can be eliminated if measured ground reaction forces are available (Brand, *et al.* [1982], Eng and Winter, [1995]).

9.4 METHODS FOR CALCULATING THE GRF

Whether following the direct or inverse dynamic approach, typically three types of mechanical analysis can be applied to link the kinematics and kinetics to solve for the ground reaction forces. If the effects of the forces are applied at an instant of time than a direct application of Newton's second law (called the force-acceleration method) may be more appropriate. If the effects of the forces are applied over a period of time than the equations of impulse and momentum may be more appropriate. Finally, if the effects of the forces are applied over a distance than the equations of work and energy may be more suitable. All three have advantages and disadvantage depending on the situations.

9.4.1 Newtonian Approach

Newton's second law of motion in its familiar form

force = mass * acceleration

can be applied to both static and dynamic systems and is by far the most widely used analysis technique for calculating ground reaction forces from positional data. A static analysis is conducted on a human body when there is little or no translational or rotational accelerations, i.e. the subjects is standing still or is moving so slowly as to assume a steady state condition exist (Winter, [1983]). When the accelerations are non-zero, like during walking or running, a dynamic analysis must be used. Several researchers have specifically used this method to calculate ground reaction forces, as it is the most applicable method for determining the force at each time sample of positional data (Thornton-Trump and Daher [1975], Miller and Nissinen [1987], Bobbert *et al.* [1991]).

9.4.2 Impulse and Momentum Approach

The impulse and momentum approach is simply a manipulation of Newton's second of motion to generate a relationship between momentum of an body and the force (applied over a period of time). Starting with the familiar 'force equals mass times acceleration' and knowing that acceleration is the time derivative of velocity, the equation can be rewritten as

$$F = m * \frac{dv}{dt}$$

or

$$F = \frac{d(m * v)}{dt}$$

and finally,

$$F * dt = d(m * v)$$

or in the more familiar forms,

$$F * dt = mv_{final} - mv_{initial} \qquad \text{(for the translational case)}$$

$$T * dt = I\omega_{final} - I\omega_{initial} \qquad \text{(for the rotational case)}$$

where F or T = force or torque
m or I = mass or moment of inertia
v or ω = linear velocity or angular velocity
dt = time interval

The left side of the equation is known as the *impulse* and is a measure of what is required to change the motion of a body. The right side of the equation describes the change in *momentum*. This approach is typically used in collision analysis such as a body falling to the floor. Dowling and Vamos [1993] also used this method to evaluate vertical jump performances from a number of subjects. Dillman [1970] used this approach to analysis the momentum change in the swing leg while running. Only two references were found in the literature that discussed the use of impulse and momentum in the analysis of ground reaction forces while walking. Elftman [1939], who compared results using a momentum approach to those using a Newtonian approach and Perry [1967], who did not provide any calculations but simple discussed the use of impulse and momentum in gait analysis.

9.4.3 Work and Energy Approach

The work and energy approach is very useful in biomechanics to analysis human motion (Hamill and Knutzen [1995]). The general form of the work - energy equation can be written as

work = change in energy .

When analysing the locomotion of a body there are two forms of work to consider; *internal* and *external*. Internal work is the total work done from the motion of all the body segments during locomotion. It is the summation of the work done on all single segments as shown below.

$$W_s = \Delta KE + \Delta RE + \Delta PE$$

where W_s = work on a segment
ΔKE = change in linear kinetic energy of the segment
ΔRE = change in rotational kinetic energy of the segment
ΔPE = change in potential energy of the segment

or

$$W_s = \Delta\left(\frac{1}{2}mv^2\right) + \Delta\left(\frac{1}{2}I\omega^2\right) + \Delta(mgh)$$

where
W_s = work on a segment
m or I = mass or moment of inertia
v or ω = linear velocity or angular velocity
h = height above base line
g = acceleration due to gravity
Δ = delta (change in)

Figure 109 shows the relationships between the various internal energies occurring for the foot during a typical walking stride.

Unfortunately, this basic formulation does not account for all the energy of the segment. For example, the strain energy due to the deformation of tissue is not considered (Hammill and Knutzen [1995]). Many researchers have developed algorithms to calculate internal work taking into account factors not included in the above equation (Winter [1979], Pierrynowski *et al.* [1980], Williams and Cavanagh [1983], White and Winter [1985]).

External work is defined as the work done by the body on an object. For example, if a body is walking uphill than external work is being done by the body to raise the centre of mass. If the body is walking along a level surface then no external work is being done to raise the body. Cavagna *et al.*, [1976] explored several other possible sources of external work in level walking and running.

Onyshro and Winter [1980] described the use of the work and energy approach coupled with Lagrangian mechanics to produce equations of motion for individual body segments. Within their mathematical model they were able to adjust the joint moments to closely simulate the kinematics of walking. Although not the focus of the paper, Onyshro and Winter could have used the kinematics to predict the ground reaction forces based on a Newtonian approach. Therefore, if one does not have kinematic data, ground reaction forces can still be calculated (in a round about way) based on the work-energy and Newtonian approaches.

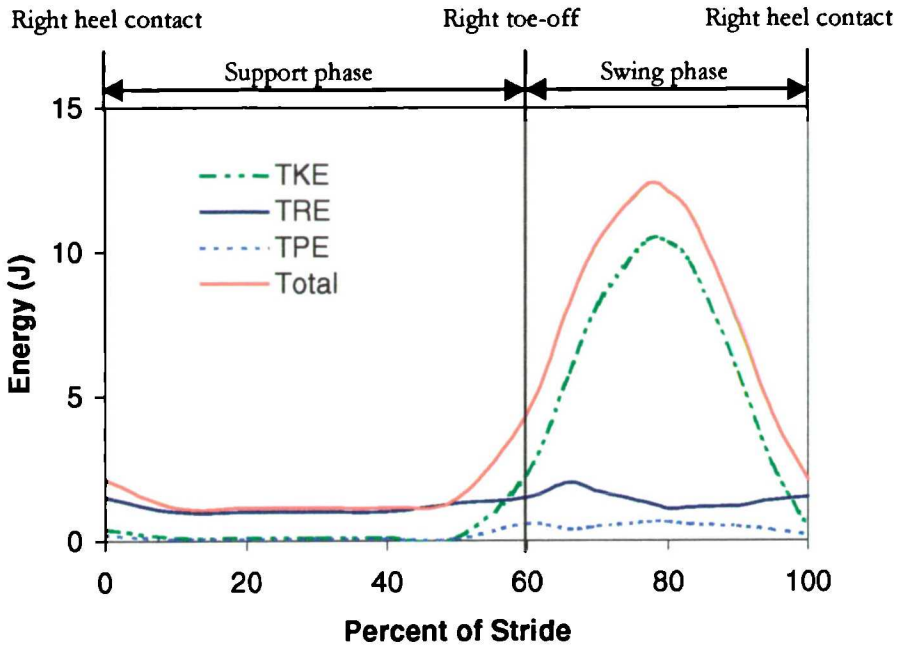

Figure 109 The relationship between linear (TKE), rotational(TRE)and potential energy (TPE) for a foot during a typical walking stride.
(reproduced from Hamill and Knutzen, "Biomechanical Basis of Human Movement", 1995)

9.5 VALIDATION OF THE NEWTONIAN APPROACH

9.5.1 Thornton-Trump and Daher, The Prediction of Reaction Forces from Gait Data, 1975.

Thornton-Trump and Daher describe one of the earliest attempts to predict ground reaction forces from kinematic information. The gait data used in their study was gathered from the research of Bresler *et al.* [1950], Murray *et al.* [1964], Murray *et al.* [1966] and Murray [1967]. From these studies they acquired the velocities and accelerations for the centres of mass of the head-arms-trunk (HAT) system and the hip, knee, and ankle joints; all in the sagittal plane. From this data they wrote a computer program to mimic the kinematics of normal walking. Unfortunately the information relating the centre of mass of the HAT to the femur position was not available in the literature so a phase shift for the HAT's centre of mass was introduced into their computer program.

The anthropometric data needed for the work was gathered from Dempster [1955], while the predictions of ground reaction force were compared to Cunningham [1950]. Their study did not make any direct mention of the

sampling rate although the comment " ... the 1 per cent intervals of the walking cycle (stride) used in the computer program may be necessary for data collection if details of the data are not to be lost in smoothing", would suggest that the sampling rate was somewhat less that 100 Hz (assuming an average walking speed of 2 Hz). Figure 110 is a plot of the predicted vertical forces compared to Cunningham. The results were somewhat crude in shape and did not show the high frequency components at the beginning of each footfall trace. This was likely due to the very low sampling rate of the kinematic data.

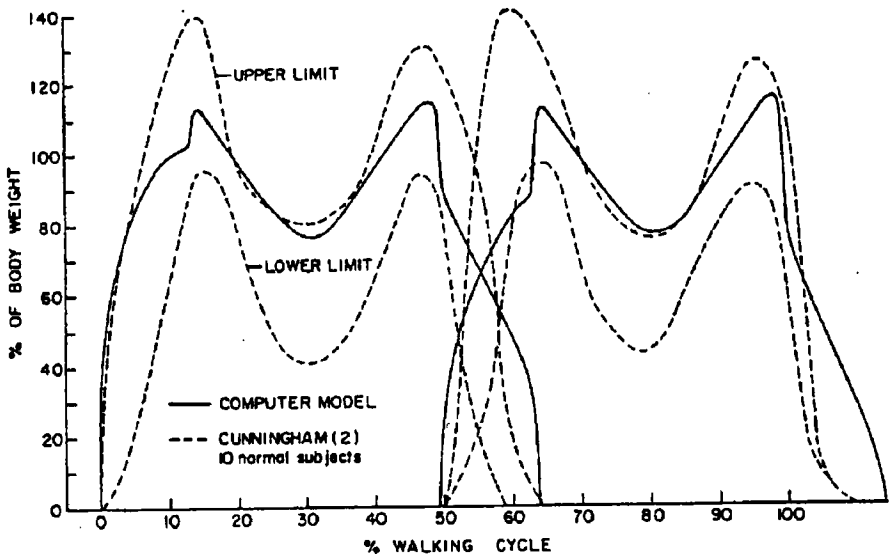

Figure 110 Vertical reaction forces predicted by Thornton-Trump and Daiber. (from Thornton-Trump and Daiber, "The Prediction of Reaction Forces from Gait Data", 1975)

9.5.2 Miller and Nissinen, Critical Examination of Ground Reaction Force in the Running Forward Somersault, 1987.

Although this paper did not deal with walking or running, it did discuss in detail the procedures used to predict the ground reaction forces. Miller and Nissinen, unlike the previous paper, utilised kinematic and force plate data captured specifically for their study. The kinematic data was gathered through the use of a single camera system placed orthogonal to the force plate at a distance of 11m. The sample rate achieved with the video film was approximately 197 Hz. The impact force data was gathered from a Kistler force plate (type 9261A) at a sampling rate of 1000 Hz. No mention was made as to how the kinematic data

and force plate information was synchronised. The anthropometric data was gathered from Dempster [1955] and Dempster and Gaughran [1967].

Miller and Nissinen modelled each subject as a system of seven rigid links rotating about frictionless, pinned joints. Although they did not mention what the seven links were, one might assume they refer to the HAT, two upper legs, two lower legs and two feet. The captured kinematic data was first smoothed through a symmetric, second-order Butterworth digital filter at a cut-off frequency ranging between 7 and 9 Hz (depending on the subject). Once complete, the displacements were differentiated with respect to time using the first order central finite differences method to produce velocities and accelerations.

The choice of cut-off frequency was derived using the work of Jackson [1979]. Unfortunately, Miller and Nissinen failed to appreciate the higher frequency components generated during the initial impact which were removed by the low cut-off frequency. As a result, their predicted results for vertical ground reaction force completely missed the large initial impact spike (see Figure 111).

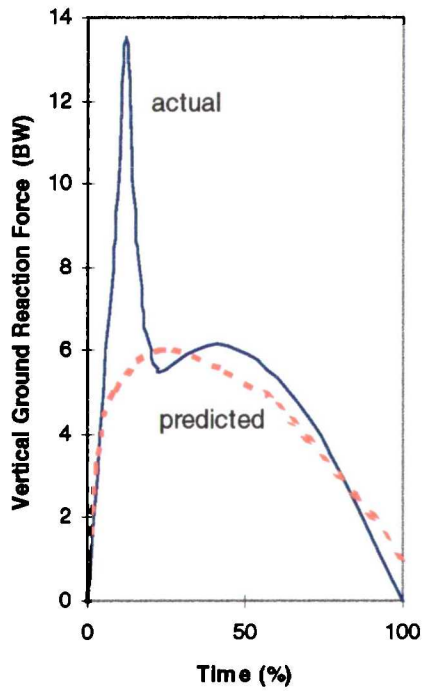

Figure 111 Reproduction of actual and predicted vertical impact results from Miller and Nissinen.

9.5.3 Bobbert, Schamhardt and Nigg, Calculation of Vertical Ground Reaction Force Estimates During Running from Positional Data, 1991.

Bobbert *et al* [1991] (and Bobbert *et al* [1992]) tackled the problem of estimating the ground reaction force during running. The kinematics were gathered with a video system consisting of 4 cameras placed within 10m of the force plate through an arc of approximately 170 degreess. The sample rate for the system was 200 Hz. The impact force information was gathered with a Kistler force plate (type 9287) and sampled at 1000 Hz. The two systems were synchronised using and LED (in view of the cameras) which was energised when the impact load exceeded 20 N. The required anthropometric data was gathered from Clauser *et al.* [1969]. Each of three subjects was modelled by seven segmental links connected with frictionless pins. The segments comprised a HAT, two upper legs, two lower legs, and two feet.

Bobbert's work was specifically aimed at reproducing the high frequency transient loading experienced in the first 50ms of ground contact (Light *et al.* [1980]). Of particular concern in their study was the movement of the skin relative to the underlying tissue. They argued that reflective markers placed directly on the skin would introduce a major source of error into the kinematics as the markers, especially on the lower extremities, moved with the sinusoidal oscillations of the skin during initial heel impact. These additional oscillations would not depict the motion of the segmental centres of gravity and hence, the limb dynamics would not be accurately described by the velocities and accelerations of the markers. Bobbert attempted to eliminate the sinusoidal accelerations by attaching the markers, with long straps of athletic tape, to large areas of skin. After unsuccessful trials Bobbert devised a device consisting of two light wooden rods connected by a hinged joint. The joint was aligned to the knee and the upper and lower rods were fastened to the leg with tape and elastic bandages. The markers were then attached to the rods. The device maintained the correct distance between markers and attempted to provide the support needed to eliminate the unwanted accelerations. Unfortunately, the results indicated that the high frequency oscillations were still present in the kinematics despite their efforts.

Based on this research, Bobbert and his colleagues identify three conditions to satisfy for a reasonable prediction of the ground reaction force. First, the change

in marker positions must reflect the change in the segmental centre of mass. Secondly, the position data must be sufficiently sampled as to retain the higher order frequencies generated during heel strike. Lastly, the positional data must be properly processed to extract these higher frequencies.

The first condition specifically identified the problem of locating the centre of mass. Since the muscle mass contributes a great deal to the segmental mass and the muscle is a soft tissue that typically move relative to the bone, it is quite reasonable to expect that the actual acceleration of the mass centre be somewhere between the bone acceleration and the muscle (soft tissue) acceleration. A further problem was that the skin on which the markers were attached moved relative to the soft tissue and bone. This study took elaborate measures to eliminate the relative skin movement and failed. Therefore, it appeared that only the bone mounted markers would be successful. One might then argue that the bone accelerations are still not truly indicative of the mass centre accelerations.

To satisfy the second condition, Bobbert and his associates studied the frequency content of a typical running trace. As well, they selected a trace captured with the force plate (sampled at 1000 Hz) and integrated twice to generate a displacement time history. By selecting every fifth point and differentiating, they reconstructed a force trace as if it were sampled at only 200 Hz. The results showed some attenuation of the initial high frequency force peak but the peak itself was sufficiently preserved; indicating a footfall rate of 200 Hz was high enough to predict the initial peak in the vertical ground reaction force.

The last condition dealt with the filtering cut-off frequency. Initially, the marker data was smoothed through a Butterworth second order digital filter with a cut-off frequency of 50 Hz. The velocities and accelerations were calculated by differentiating the positional data using the first central differences method. Prediction of ground reaction forces showed high fluctuations at this cut-off frequency indicating that the sinusoidal oscillations of the skin were not entirely removed. The positional data was re-filtered at 10 Hz which, although producing a smoother predicted force, completely missed the initial high frequency force spike (effectively, the same results produced by Miller and Nissinen). The best results were obtained by filtering the individual segment with different cut-off frequencies. In the final assessment, a 50 Hz cut-off was used for the legs and

feet, a 20 Hz cut-off was used for the hips and a 15 Hz cut-off was used for the HAT (see Figure 112).

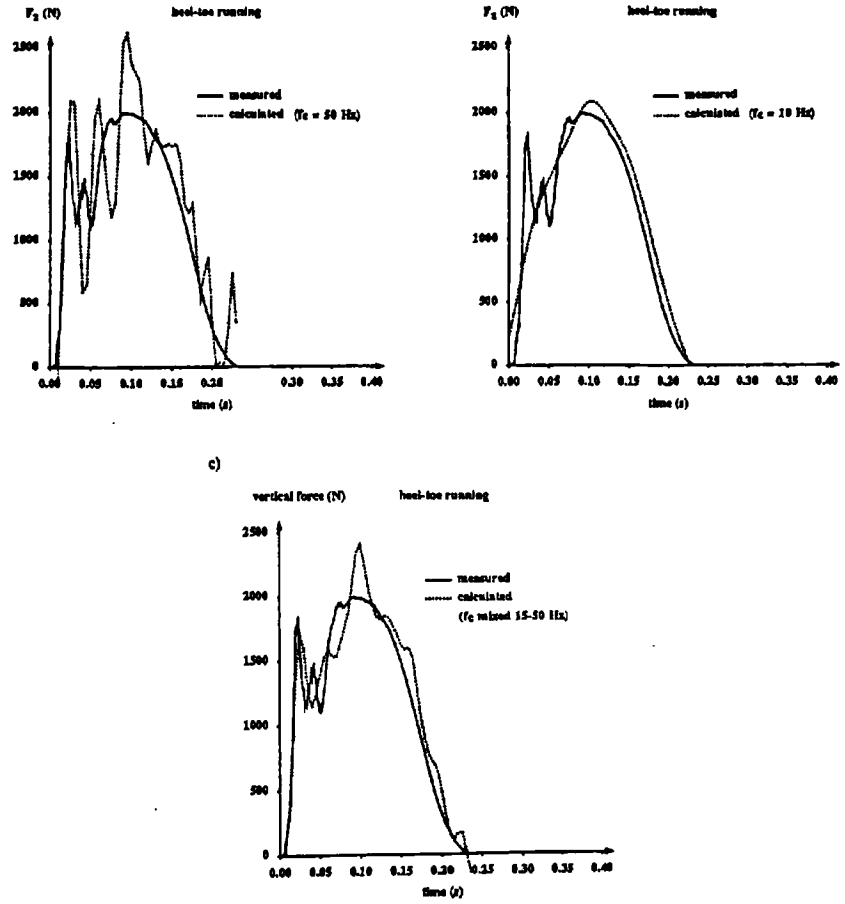

Figure 112 Effects of changing the filtering frequency.
(from Bobbert et al., "Calculation of Vertical Ground Reaction Force Estimates During Running from Positional Data", 1991

9.6 ADJUSTMENTS REQUIRED FOR CALCULATING THE VERTICAL GRF DURING WALKING AND ASCENDING/DESCENDING STAIRS

The papers by Bobbert *et al.*[1991 & 1992] as well as the paper by Miller and Nissinen [1987] predicted ground reaction forces directly from kinematic data gathered during running and somersault experiments. The question is, can the vertical ground reaction force also be calculated for walking or ascending / descending stairs. To answer this question for walking, perhaps it is best to compare the initial phase of the gait cycle (see Figure 113) just before and just after heel strike for running and walking.

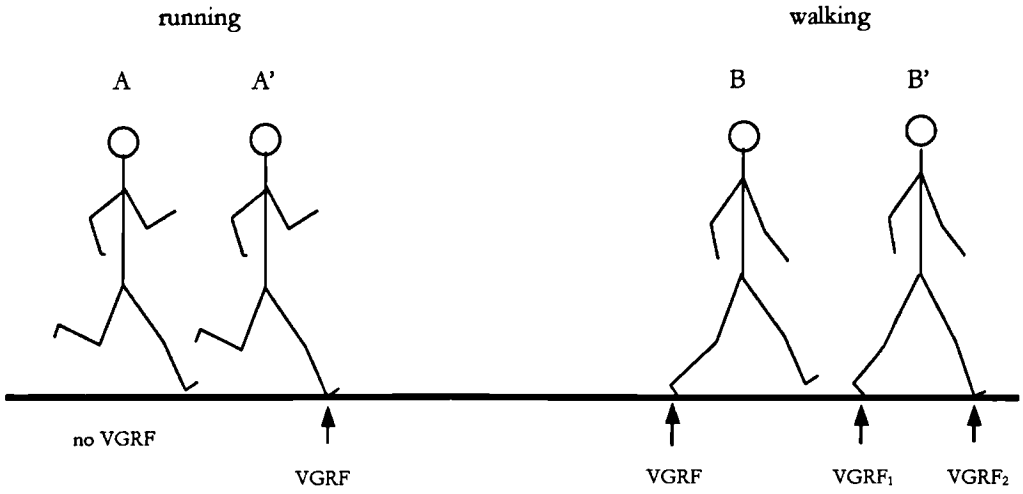

Figure 113 Running and walking subjects just before and just after initial heel contact.

Just before the running heel strike (A) no contact is made with the ground hence, no vertical GRF exists. Using Newton's equation,

$$\Sigma F = ma$$

the only forces present are that due to gravity. Therefore,

$$-mg = ma$$

or, in other words, the body is in a free fall accelerating downwards with the force of gravity. Just after the heel strike (A') the vertical GRF begins to build, hence

$$VGRF - mg = ma$$

and the body begins to decelerate proportional to the increase in vertical GRF. This simple analysis shows that at any stage in the running gait the vertical GRF can be calculated by

$$VGRF = \Sigma\, m(a + g)$$

where $\Sigma\, m(a + g)$ is the summation of all the segmental mass times acceleration terms. For walking, however, it is a different story.

Just before the initial walking heel strike (B) there is an existing vertical GRF under the toes of the rear foot. Hence,

$$VGRF - mg = ma$$

already exist and the vertical GRF under the foot can be calculated. However, just after heel strike (B') the rear foot is still making contact with the ground so two vertical GRF's exist. Substituting into the Newton formula,

$$VGRF_1 + VGRF_2 - mg = ma$$

cannot be solved since there is one equation and two unknowns. This period in the gait cycle is referred to as the double support phase that was discussed in Chapter 4. Figure 114 shows the double and single support phases overlapped on a plot of the vertical GRF's generated by left-right-left contact with the floor. During the double support phase the individual vertical GRF's from each foot cannot be calculated and therefore a compromise method must be used.

If one combines the $VGRF_1$ and $VGRF_2$ into a total vertical ground reaction force ($VGRF_{total}$) then the previous equation

$$VGRF_1 + VGRF_2 - mg = ma$$

can be rewritten as

$$VGRF_{total} - mg = ma$$

which can now be solved. Graphically, the predicted $VGRF_{total}$ would reflect summation of the overlapped traces in the double support phase and is shown in Figure 115. This is the same overlap trace that was produced in section 5.4.2.

When negotiating a staircase, the same overlapping situation that applied to walking would apply to slow and medium pace ascents and descents. If the subject touches one step while his trailing foot still makes contact with the previous step, than the vertical GRF's will overlap and the $VGRF_{total}$ will be the result of the force prediction.

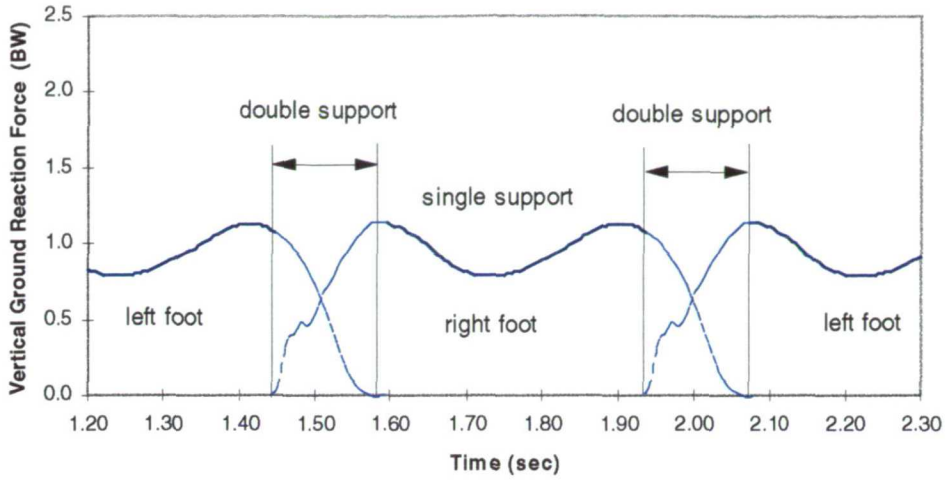

Figure 114 Overlapping vertical GRF traces occurring during walking.

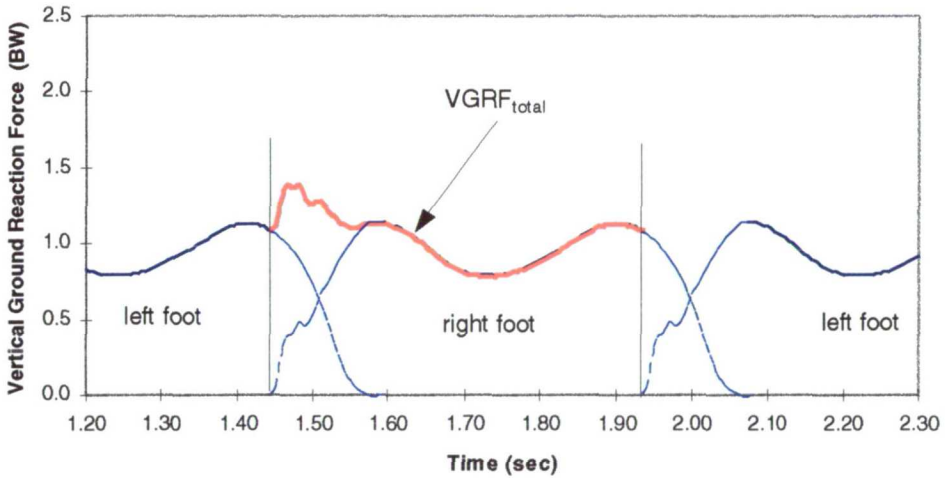

Figure 115 Summing the overlap values to produce the $VGRF_{total}$ trace.

9.7 CALCULATING THE VERTICAL GRF FOLLOWING THE NEWTONIAN APPROACH

9.7.1 Model Description

For the purposes of this research the body was assumed to be segmented into 12 rigid links held together by frictionless pins at the joints, i.e. rigid body mechanics apply. The placement of the LED's in the CODA experiments outline the segment locations. With reference to Figure 116, the segments were: (1) neck - linking the head to the shoulder, (2) trunk - linking the shoulder to the hip, (3 &

4) left and right upper arm - linking the shoulder to the elbow, (5 & 6) left and right lower arm - linking the elbow to the wrist, (7 & 8) left and right upper leg - linking the hip to the knee, (9 & 10) left and right lower leg - linking the knee to the ankle, and finally, (11 & 12) left and right foot - linking the heel to the fifth metatarsal.

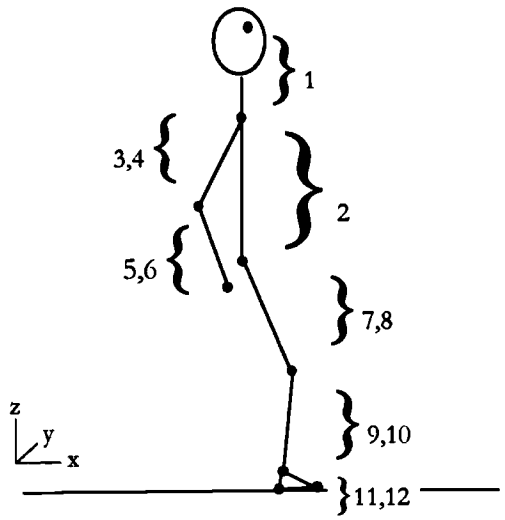

Figure 116 Description of segmental model in the sagittal plane.

The anthropometric data used for the model was gathered from Clauser *et al.* [1969] and is shown in Table 22.

Segment Description	***Segment Weight (as a % of body weight)***	***Segment Centre of Mass (as a % of segment length)***
neck	7.3	57% from shoulder
trunk	50.7	46% from hip
upper arm	2.6	48% from shoulder
lower arm (including the hand)	2.3	44% from elbow
upper leg	10.3	41% from hip
lower leg	4.3	43% from knee
foot	1.5	47% from heel

Table 22 Clauser's anthropometric data for 12 segment model.

9.7.2 Force Plate Data

The ground reaction forces were gathered in the identical manner as done for the experimental work conducted on the flat and on the stairs. The only variation was the requirement of the subject to be bare foot so markers could be attached to the foot area. This increased the initial impact loading which increased the magnitudes of the upper harmonics.

9.7.3 Segmental Position Data

The CODA data was gathered as described in section 8.3.

9.7.4 Calculation Procedure: Translational verses Rotational Method

Newton's second law of motion described the basic relation between force and acceleration. Its verification was entirely experimental and is depicted in its usual form as

$$\Sigma \mathbf{F} = \mathbf{m} * \mathbf{a}$$

or sum of the forces equals mass times acceleration. When generating the vertical ground reaction force from positional data it is rewritten as

$$F_Z = \sum_{I=1}^{N} m_i \left(\ddot{Z}_I - g \right)$$

where F_Z = vertical component of the ground reaction force
m_i = mass of the ith body segment
$\ddot{Z}_I$ = vertical acceleration of the ith body segment
g = acceleration due to gravity.

The positional data captured by the CODA system contained X, Y and Z co-ordinates for each marker position attached to the subject's body. The selected rate for data acquisition was 200 Hz or 0.005 seconds between samples. The positional data was differentiated with respect to time, using the first central differences method as described in section 9.2.1, to produce the linear velocities and accelerations of the markers. The angular velocities and accelerations were

calculated by deriving the segmental angles at each time sample and differentiating with respect to time using the first central differences method once again.

When using the differences method, a small problem occurs at the boundaries of the gait. Referring to Figure 117, t_0 is the first sample of data acquired during the test. To calculate angular velocity from the formula (revised from the linear case)

$$\dot{\theta}_i = \frac{\theta_{i-1} - \theta_{i+1}}{2 * \Delta T}$$

where $\dot{\theta}_i$ = angular velocity at θ_i,
θ_{i-1} = segment angle at θ_{i-1},
θ_{i+1} = segment angle at θ_{i+1},
ΔT = time interval between points,

suggest the earliest angular velocity that can be calculated for the gait is at t_1 (because of the θ_{i-1} term). The earliest angular accelerations would therefore be at t_2. Hence, to calculate the linear and angular velocities and accelerations the sampled data must extend at least two frames before and after the gait cycle.

At this stage the linear and angular velocities and accelerations are scalar values, i.e. magnitudes only. To predict the vertical components the direction of the scalar must also be known, i.e. vector form.

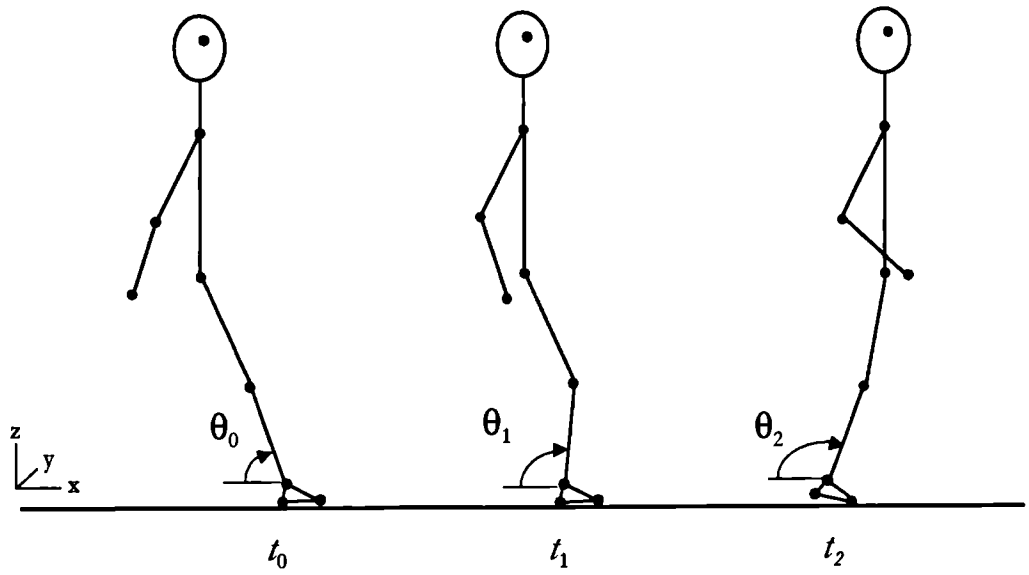

Figure 117 Three time segments from the position data showing the change in lower leg limb angle..

Figure 118 illustrates graphically the reasoning for this. The rigid link is moved from point A to B. The movement is an example of general plane motion, combining a translation from A to A' and a rotation A' to B. The acceleration vector of the complete movement is from i to k, which is composed of the translation vector from i to j and the rotation vector from j to k.

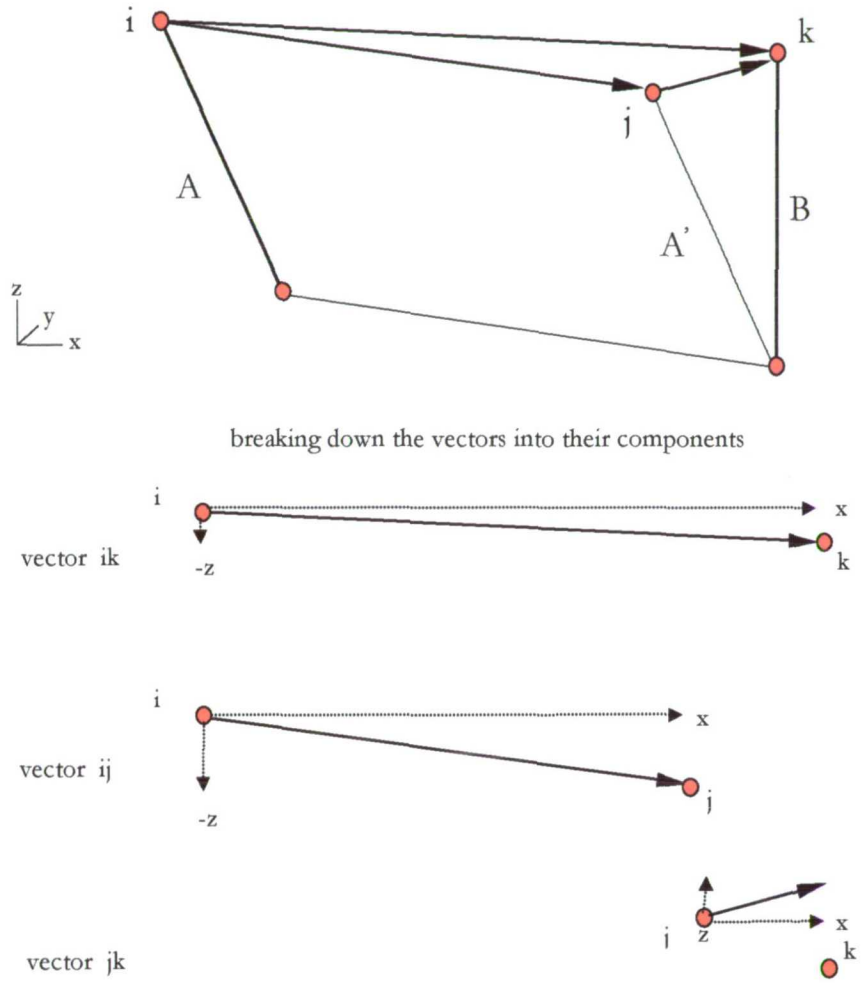

Figure 118 Example of translational and rotational motion.

From the breakdown of the vectors, it is clearly seen that vertical acceleration experienced in the movement from A to B can be calculated in two ways: either by obtaining the Z component of the vector ik or added the Z components from vector ij and vector jk. This is an important point as it provides two avenues for predicting the ground reaction forces: the *translational* method or the *rotational* method. Figure 119 is used to illustrate an example.

A subject has moved from a position at t_0 to a position at t_1. The move occurs just after heel impact where the body has rotated about the ankle. During the motion the lower limb has undergone rotation only, whereas the rest of the body (except the foot) has undergone a rotation and a translation. If the legs are looked at in closer detail (see Figure 120) one can see that the knee's translational vector ik is the same as the rotational vector jk. Hence the knee's acceleration can be calculated as a linear translation or an angular rotation (producing a linearised tangential and normal acceleration vectors, see section 9.2.2).

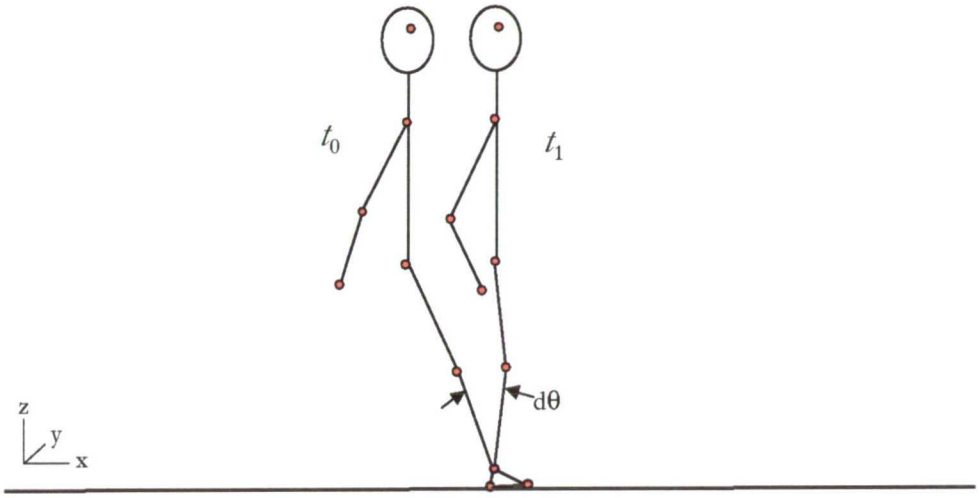

Figure 119 Adjacent gait samples during support phase in normal walking.

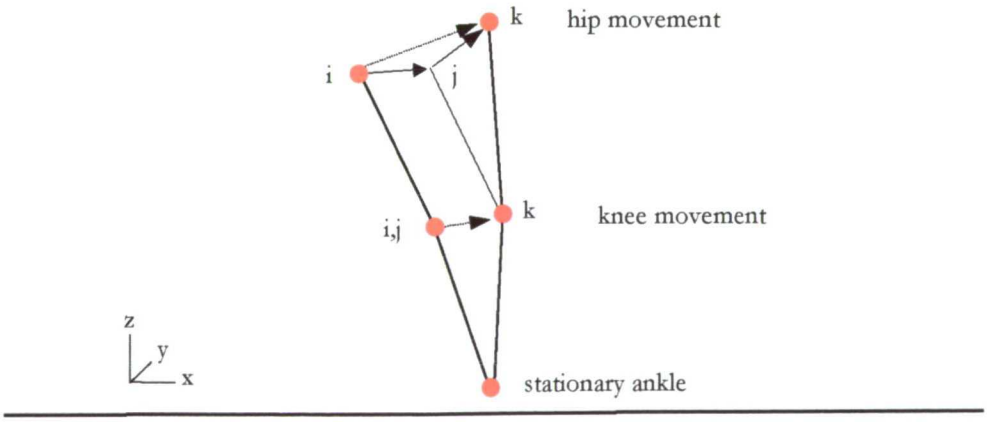

Figure 120 Detail of legs during movement ftom t_0 to t_1.

The hip acceleration can now be calculated solely as the translational vector ik or as the combination of two rotational vectors; jk for the knee plus jk for the hip. Using this manner, the accelerations of the entire body can be calculated based

solely on either the translational motions or the rotational motions. When the ankle is not stationary the sole use of the translational motions will still produce the desired accelerations, however, sole use of the rotational motion required a small compromise.

To use only the rotational motions the calculations must start at the heel. When looking at the heel's movement about the toe, it produces a rotational component (jk) about the toe and a translational component (ij) which equals the translation acceleration of the toe. If these two components are added together they fully describe the motions of the heel as well as form the translational (ij) component for the ankle movement. Add this to the rotational movement of the ankle relative to the heel (vector jk) and it forms the translational component (ij) of the knee. Therefore, to calculate the acceleration components for the entire body would require a link to link calculation which is "seeded" with the translational acceleration of the toe.

9.7.5 Accuracy: Translational verses Rotational Method

Suppose one wishes to know the relative acceleration of the knee compared with the ankle at a moment in time. Starting with the following equation

$$Z_{knee} - Z_{ankle} = l * \sin\theta$$

where
Z_{knee} = vertical displacement of the knee
Z_{ankle} = vertical displacement of the ankle
l = length of the lower leg
θ = angle of the lower leg with the horizontal
(see Figure 121)

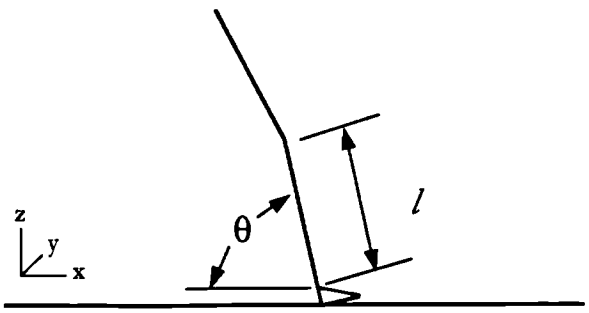

Figure 121 Depiction of the leg at an instant of time.

Double differentiation of both sides with respect to time gives the equation

$$\left(\ddot{Z}_{knee} - \ddot{Z}_{ankle}\right)^T = l\ddot{\theta}\cos\theta - l\dot{\theta}^2\sin\theta + \ddot{l}\sin\theta + 2\dot{l}\dot{\theta}\cos\theta$$

where T = refers to translational approach
$\cdot$ = single time derivative
$\cdot\cdot$ = double time derivative

Therefore, the translational vertical acceleration for the knee minus the vertical acceleration for the ankle can be calculated by solving the four terms on the right hand side of the equation. If one looks closely at the right hand side however, two terms use a time derivative of the limb length which is an experimental error as the limb length remains unchanged with time. If one assume the limb length does not change with respect to time, the right hand side will reduced to

$$\left(\ddot{Z}_{knee} - \ddot{Z}_{ankle}\right)^R = l\ddot{\theta}\cos\theta - l\dot{\theta}^2\sin\theta$$

where R = refers to the rotational approach

The first term on the right hand side refers to the tangential acceleration that is a function of the angular acceleration. The second term refers to the normal acceleration that is a function of the angular velocity squared. Subtracting these two terms gives a better prediction of the relative acceleration of the knee to the ankle than the translational approach.

9.8 PREDICTED RESULTS FOR VERTICAL GRF

9.8.1 Program Validation: Predicted Vertical GRF for a Walking Gait

Figure 122 is an example of the marker positions projected on the sagittal plane as a function of time. The figure depicts a complete gait as the subject walks from left to right. The beginning of the trace represents the heel strike of the right foot. The subject then proceeds through the stance and swing phases and produces a second right foot heel strike at the end of the trace. For purposes of clarity the images are separated by 0.1 seconds although the actual sampling rate was 200 Hz.

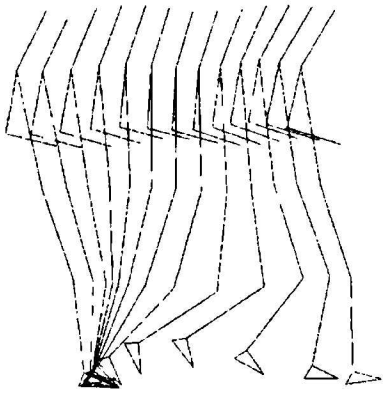

Figure 122 Example of marker positions, projected on the sagittal plane as a function of time. The subject is walking from left to right (in the direction of positive X).

As discussed in section 8.3.2, the measured vertical ground reaction forces and the positional data were simultaneously recorded by the CODA system eliminating any synchronisation errors. Figure 123 is the vertical force trace that corresponds to Figure 122. The trace shows the vertical force time history produced as the right foot makes contact with the plate at the beginning of the trace until the toes push off from the plate to begin the swing phase.

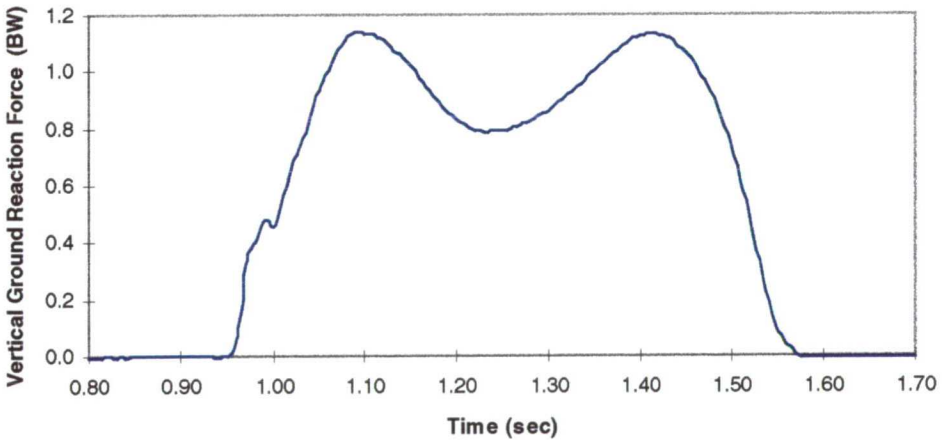

Figure 123 Measured vertical ground reaction force data.

The trace represents the force felt under a single foot. The aim of this work was to model the vertical ground reaction force produced from the whole body, i.e. a combined trace, and to make a comparison of the harmonic values from the predicted trace with those from the real trace. The combined force-time history was constructed by simply overlapping the single trace at the exact walking period. This procedure was unchanged from that conducted in section 5.4.2. Figure 124 depicts the combined trace produced from the single trace in Figure 123. The

repeating period was the time history on which the Fourier analysis was conducted.

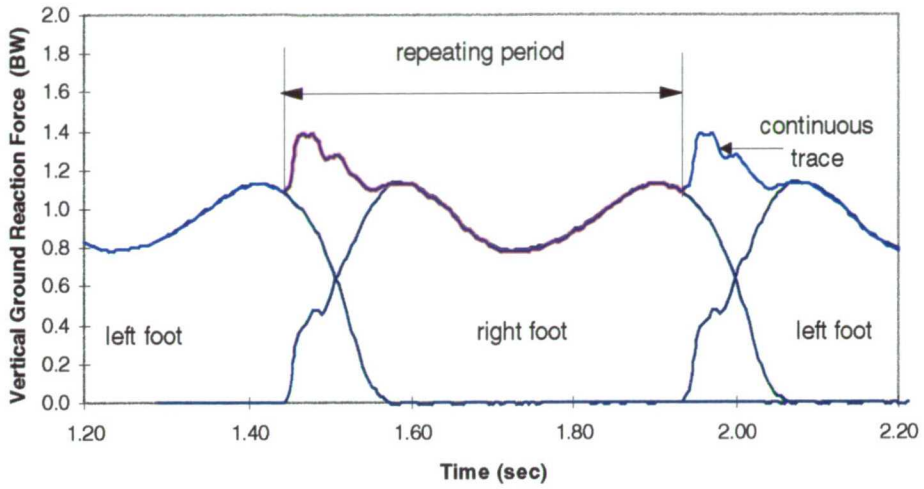

Figure 124 Continuous force time history trace (pace 1.85 Hz).

9.8.1.1 Translational results

To predict the continuous trace from the marker positions required writing a kinematics/kinetics program that used the markers positions as input. Although there were no markers on the left side limbs, it was assumed the left side produced the same force contribution as the right. In the final summing of the force contributions for each limb, the right side segments were used to represent the left side segments by introducing a phase shift in the time sequencing of exactly half the walking period.

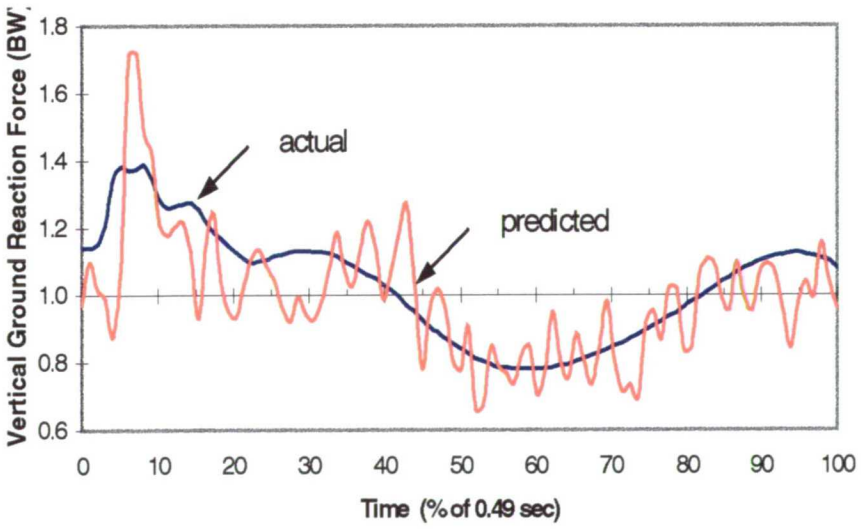

Figure 125 Predicted vertical GRF for walking using the translational approach (no filtering applied).

Figure 125 shows the predicted vertical ground reaction force for the walking gait shown in Figure 122. The smooth background curve is the actual trace and represents the "repeating period" shown in Figure 124. The jagged curve was the predicted trace using positional data in its raw, unfiltered form. Keeping in mind the results of Bobbert *et al.* [1991], this rough prediction was expected.

9.8.1.2 Rotational results

The program was also capable of predicting the vertical GRF based on the rotational approach described in section 9.7.4. By seeding the calculation with the translational kinematics for the right toe, the predicted vertical GRF for the same walking gait is shown in Figure 126.

The results show a far greater variation, especially in the first 20% of the cycle, than that calculated for the translational approach. However, this was not entirely unexpected as the segmental angles were calculated using the positional data from of two joint markers which are both fluctuating with the sinusoidal movement of the skin. Any "out of phase" movement between the markers would lead to large fluctuation in the limb angles. Both the translational and rotational results need to be subjected to data filtering to improve the predicted fit to the actual trace.

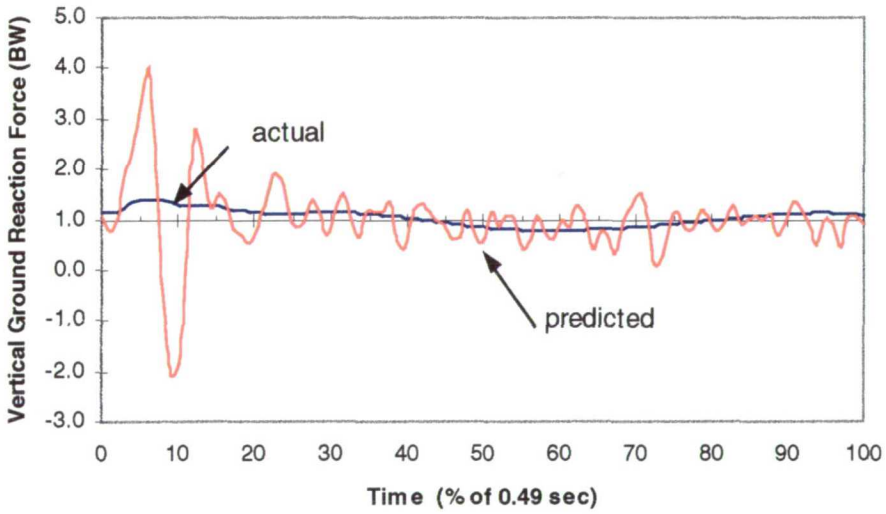

Figure 126 Predicted vertical GRF for walking using the rotational approach (no filtering applied).

9.8.2 Effects of Using a Single Low Pass Filter on All Data

Bobbert *et al.* [1991] discussed the need to filter the marker position data to reduce the sinusoidal accelerations induce by the movement of the skin (on which the markers are attached) relative to the centre of mass of the limb. In their final predictions they opted to filter the knee, ankle, and foot markers at 50 Hz, the hip marker at 20 Hz and the remaining upper body markers at 15 Hz. This combination of data filtering gave the best results for Bobbert's running gaits, but would it produce the best results for walking and negotiating stairs? Figure 127 shows the results of translational approach calculations filtered at various cut-off frequencies.

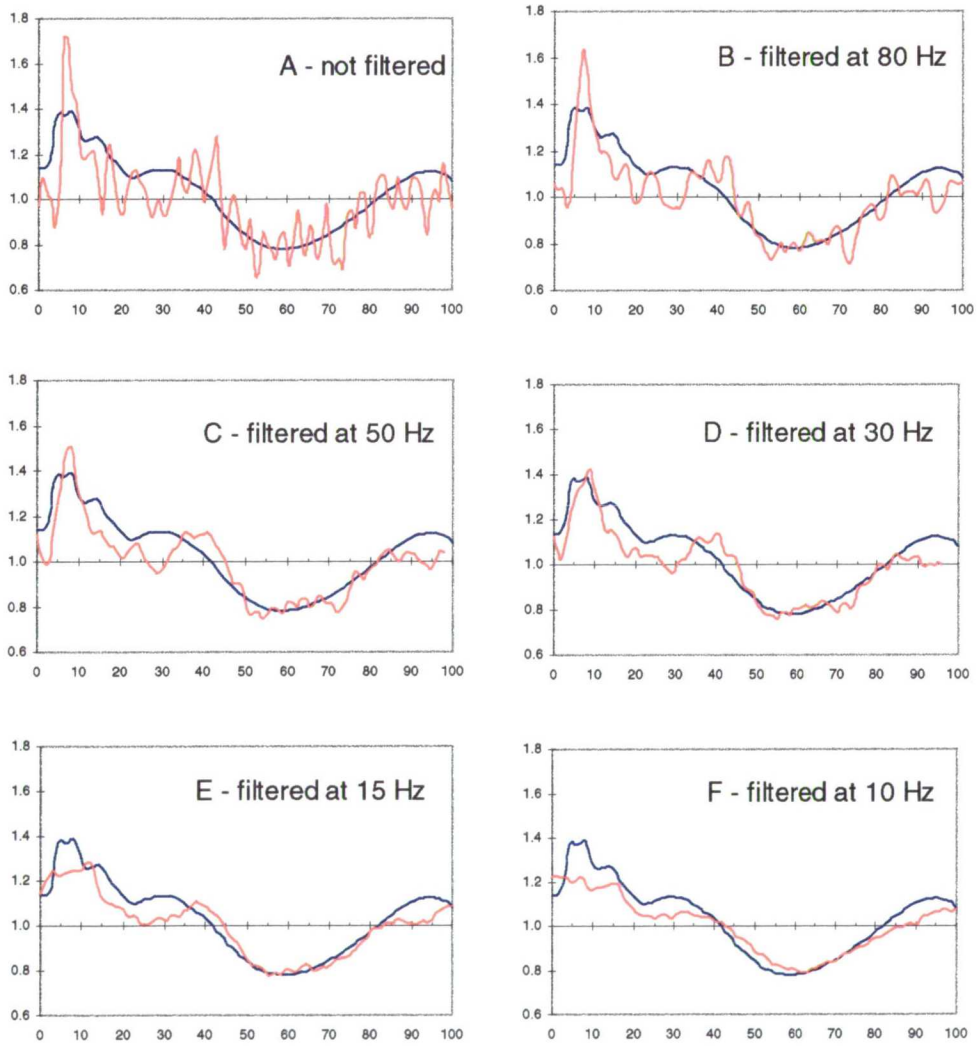

Figure 127 Results of filtering all marker position data using a translational approach a) no filter, reference plot b) 80 Hz, c) 50 Hz, d) 30 Hz, e) 15 Hz, and f) 10 Hz.

The last two figures (E and F) show a close approximation to the measured data in the last 60% of the gait cycle. However, the reduced cut-off frequency also removed the initial peak. Raising the cut-off to 50 or even 30 Hz (C or D) recovered the initial peak but also caused deterioration in the prediction of the latter 60%. Like in Bobbert *et al.* [1991] the best fit will be a combination of filtering values applied to individual marker data.

When the rotational approach was used with the same cut-off frequencies the results are as shown in Figure 128 (the scale has not been changed to allow comparisons with the translational approach).

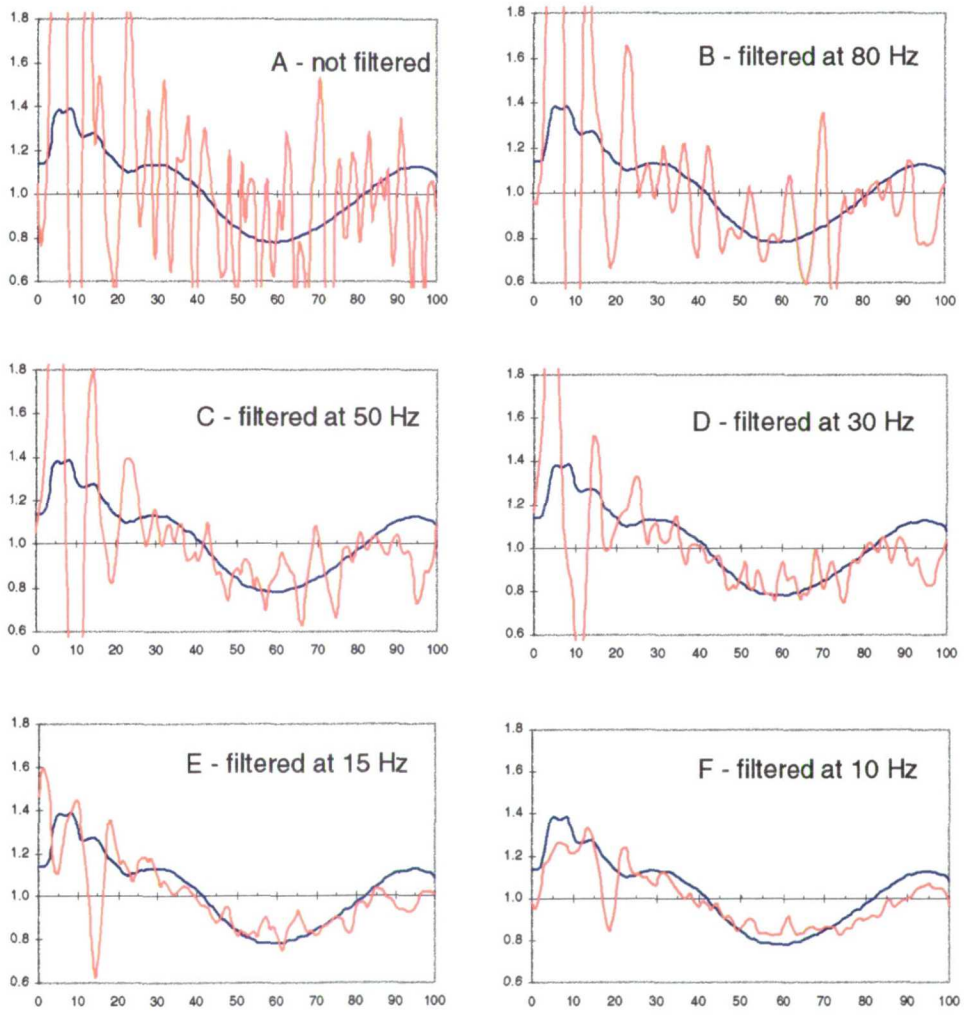

Figure 128 Results of filtering all marker position data using a rotational approach a) no filter, reference plot b) 80 Hz, c) 50 Hz, d) 30 Hz, e) 15 Hz, and f) 10 Hz.

Following the rotational approach produced unrealistic predictions until the marker data was filtered at 10 Hz. This plot (F) produced a close result except for

a dip in the prediction occurring at approximately 20% of the gait cycle. Analysing the angular acceleration data for all body segments indicated this dip was created (and exaggerated) by a rapid change in the angular acceleration of the lower leg (see Figure 129). Viewing the body kinematics at this point indicated the acceleration change occurred when the knee flexed between 65ms and 120ms after initial heel impact. Due to the calculation method used in the rotational approach, the effect of this spike was passed on to trunk, neck, upper arms and lower arms. This process exaggerated the effects of the spike and caused a large dip on the predicted GRF.

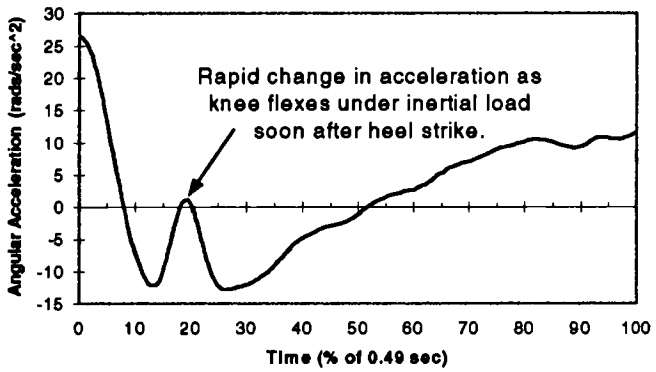

Figure 129 Angular acceleration of the stance lower leg occuring during the gait cycle.

A way to remove this effect was to substitute the translational accelerations for the rotational accelerations at the hip. This process initialised the rotation of the trunk with the translational accelerations of the hip. Hence, the rotational approach calculation was seeded with the translational accelerations of both the toe and hip markers. The results are shown in Figure 130. The trace is very similar to the fully translational result shown in Figure 127-F.

9.8.3 Effects of Using a Single Low Pass Filter on Individual Data Sets

The vertical GRF predicted from the translational approach needed to be filtered to attain reasonable results (as discussed in section 9.8.2). Like in Bobbert *et al.* [1991] the filtering process can be tailored by filtering the individual marker data with different cut-off frequencies. Figure 131 show attempts at selecting the combinations that best predicted the measured vertical ground reaction force.

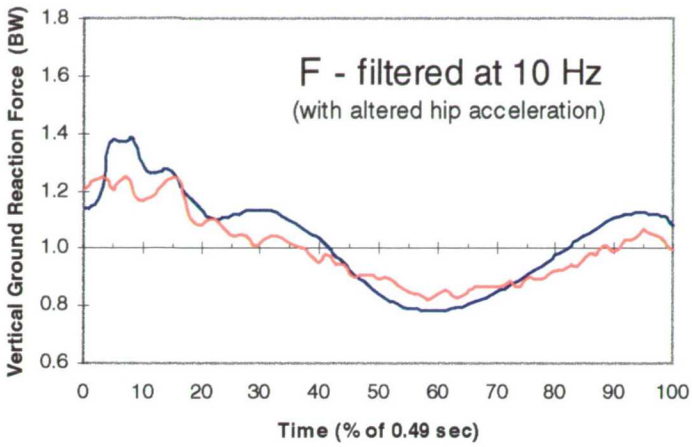

Figure 130 Predicted vertical GRF calculated from a rotational approach.

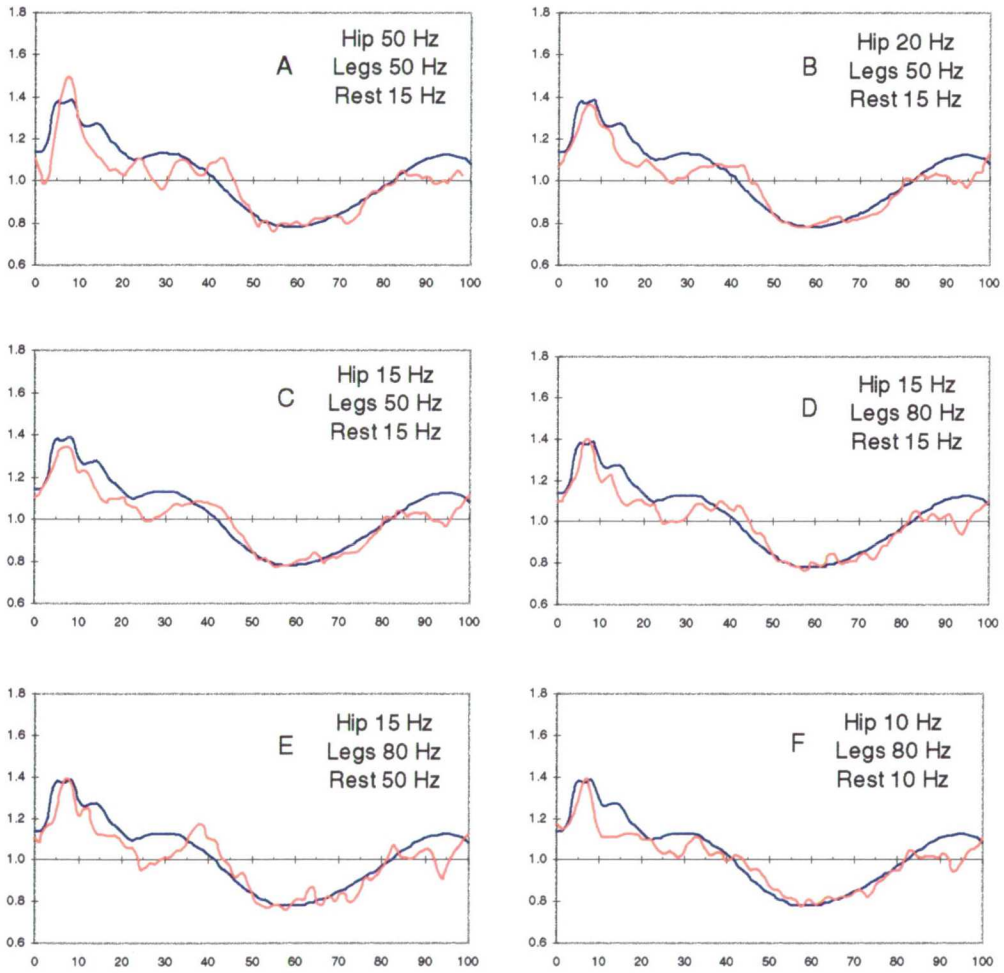

Figure 131 Effects of varying the cut-off frequency for different marker data on the vertical GRF predicted by the translational approach.

Figure 131-B is the predicted result using the same combination of cut-off frequencies as recommended in Bobbert. By placing ± 10% error bands on the actual trace (see Figure 132) it can be seen that nearly all of the predicted trace

falls within the boundary and in fact a large portion of the predicted trace falls within ± 5%. The trouble spots occurred along the gait cycle around 15% (error -13%), 25% (error -12%), and 95% (error -14%). Similar if not slightly better results were also obtained from Figure 131-C although the trace did not fully predict the height of the initial peak.

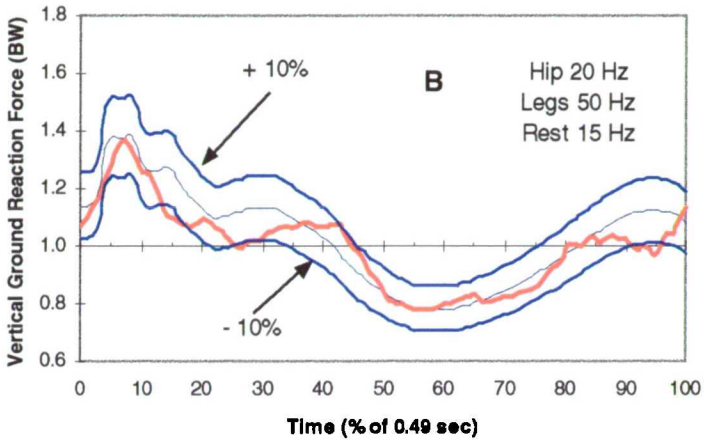

Figure 132 10% error bands placed on Figure 131-B.

Bobbert reported errors of 10% or less for the predicted vertical GRF traces for running. This is consistent with the work presented here. Therefore it is clear that the same combination of filtering used for running produced arguably the best results for walking.

Following the rotational approach (with allowances for the translational substitution of the hip data) required a different choice of cut-off frequencies. As presented in Figure 130, a low pass filter of 10 Hz produced a very close result although the height of the initial peak was somewhat under predicted. By altering the cut-off frequency near 10 Hz, a number of predicted vertical GRF plots were made (see Figure 133).

An interesting note which was clear from the data was that altering the cut-off frequency for the legs had a far greater influence on the overall predicted trace than that seen for the translational approach. This would suggest that even small increases in the cut-off frequency (above 10 Hz) allowed large variations in the angular accelerations of the leg segments to develop. Of the six plots, C and F produce the best results.

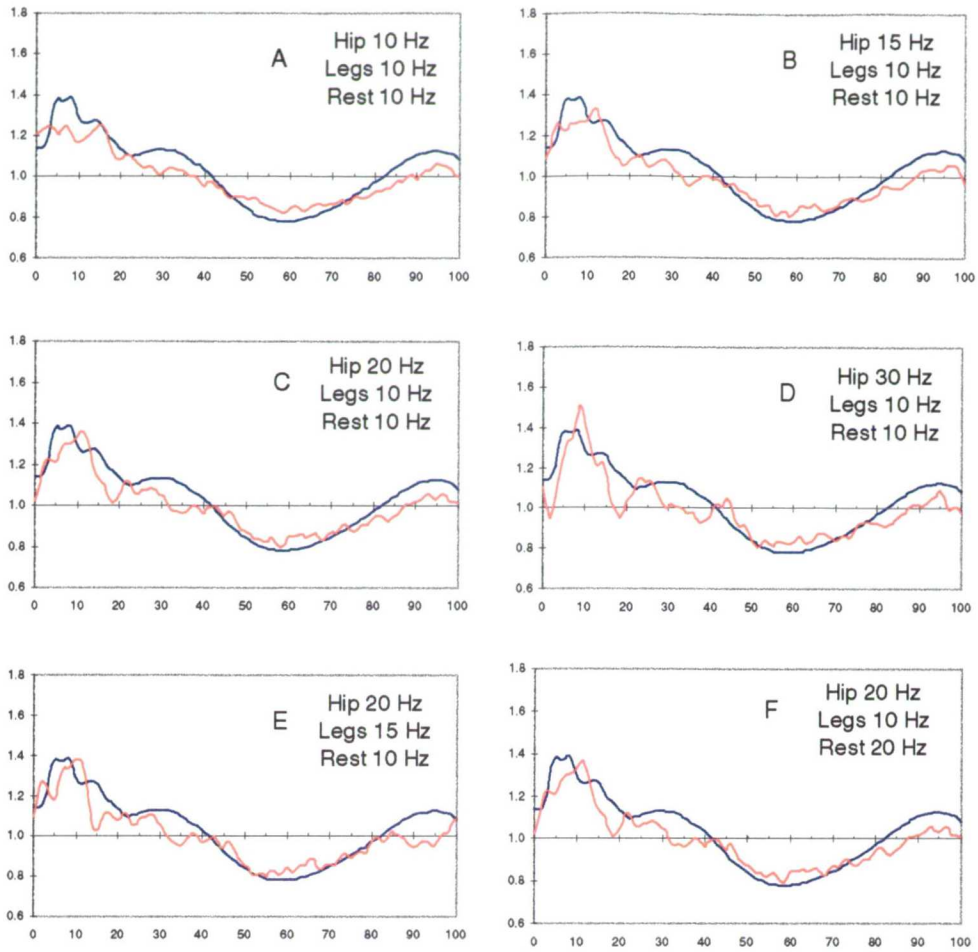

Figure 133 Effects of varying the cut-off frequency for different marker data on the vertical GRF predicted by the rotational approach.

After placing ± 10% error bands Figure 133-F mostly all of the predicted values fall within the boundary (see Figure 134). The trouble spots occurred along the gait cycle around 5% (error -12%), 18% (error -14%) and 32% (error -14%). The figure did show a significant improvement in the predicted values between 90% and 100% of the gait cycle over the translational approach.

It can be argued which calculation approach and which combination of filtering produced the best predictions. Further "refined" filtering may produce even better results. To gain an understanding of the composition of the predicted traces the next section is devoted to studying the individual segmental contributions of the predicted traces.

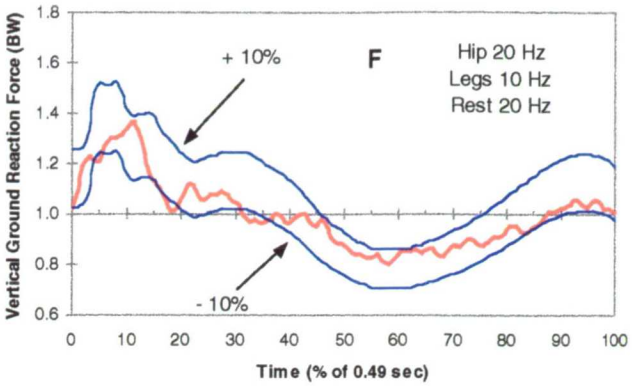

Figure 134 10% error bands on Figure 133-F.

9.8.4 Segmental Contributions to the Predicted Vertical GRF

The vertical forces predicted in Figure 131-A,B, and D (following the translational approach) have been broken down into component segmental contributions (see Figure 135, Figure 136 and Figure 137 respectively). As expected, the trunk accounted for a large majority of the force in all plots owning to its large mass (nearly 50% of the body mass, see section 9.7.1). The largest contributors after the trunk were the upper leg (both stance and swing) and the head/neck. These segments also had larger masses relative to the remaining body parts hence, increasing their contribution to the overall force prediction

Also interesting was the distribution of the individual contributions. In all three figures the stance leg (including the foot) provided a majority of its contribution in the first 10% of the gait cycle. This occurred because the floor acted as a "brake" to the downward inertia of the leg just after contact with the floor. Hence, the predicted force is the reaction of the floor against this downward inertia. The swing leg on the other hand, provided most of its contribution around 35% and 90% of the gait cycle. The remaining components showed very little fluctuations in their contributions. This would seem to justify the collection of the head, arms, and trunk (HAT) into a single segment as discussed in papers from section 9.5.

It is also interesting to see how the individual contributions changed with alterations to the cut-off frequency. Note the large reduction in the predicted hip force (around 7% of gait cycle) when the filter was reduced from 50 Hz to 20 Hz.

Yet, reducing the filter even further from 20 Hz to 15 Hz had very little effect. This may indicate that using a cut-off frequency above 20 Hz induces erroneous accelerations into predicted value for the hip. The contribution of the leg segments also showed some affects when the cut-off frequency was raised from 50 Hz to 80 Hz. One can see small changes in the trace shapes, although not as pronounced as the hip.

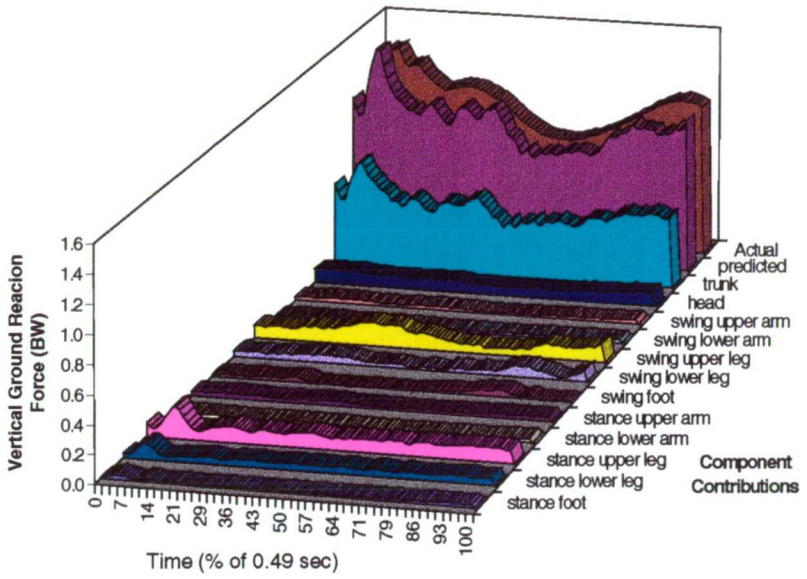

Figure 135 Segmental contribution to the predicted vertical ground reaction force from Figure 131-A (hip 50Hz, legs 50Hz, rest 15Hz).

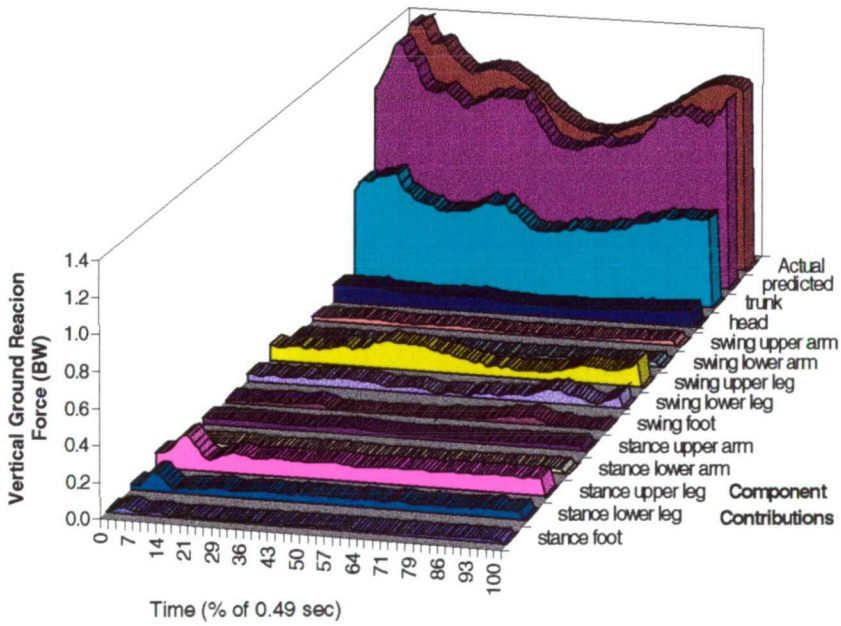

Figure 136 Segmental contribution to the predicted vertical ground reaction force from Figure 131-B (hip 20Hz, legs 50Hz, rest 15Hz).

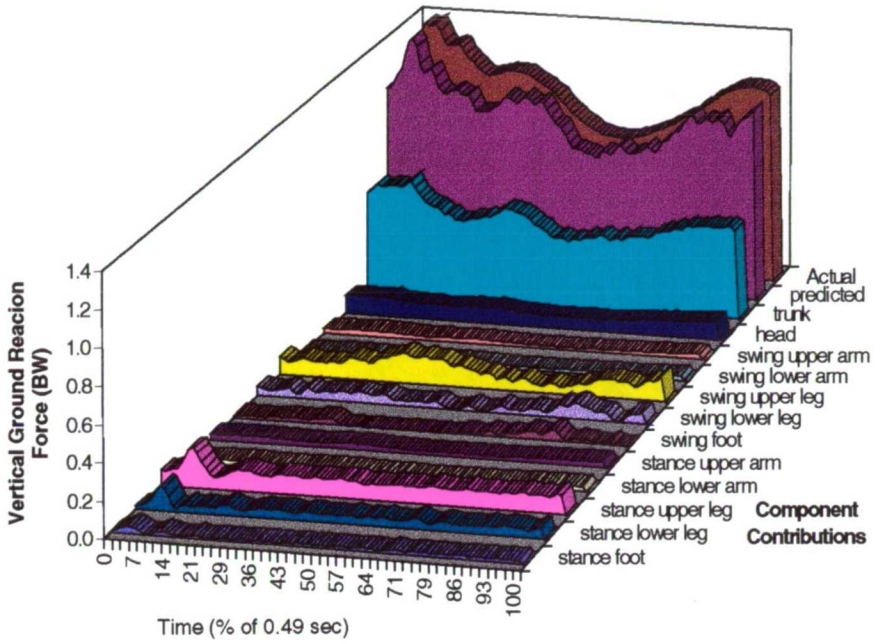

Figure 137 Segmental contribution to the predicted vertical ground reaction force from Figure 131-D (hip 15Hz, legs 80Hz, rest 15Hz).

The vertical GRF's predicted in Figure 133-A,E, and F (following the rotational approach) have been broken down into component segmental contributions (see Figure 138, Figure 139 and Figure 140 respectively). Again, the trunk accounted for a large majority of the force in all plots with the next largest contributor being the upper leg (both stance and swing) and the head/neck.

The improved prediction of the force between 90% and 100% of the gait cycle (as discussed in the previous section) came mainly from the contribution of the swing upper leg. Comparing Figure 138 and Figure 139 show a significant increase in the swing leg contribution when the cut-off frequency was lowered from 15 Hz to 10 Hz. The trunk contribution however, was severely decreased at the initial hump when the cut-off frequency was lower from 20 Hz to 15 Hz. Another point was the influence of the knee flex seen in the stance upper and lower leg contributions. When the cut-off frequency was increased from 10 Hz to 15 Hz, the dip at 20% of the gait increased significantly. As before, there was little fluctuation in the contribution of the arms and head justifying the collection of the head, arms, and trunk into a single HAT segment.

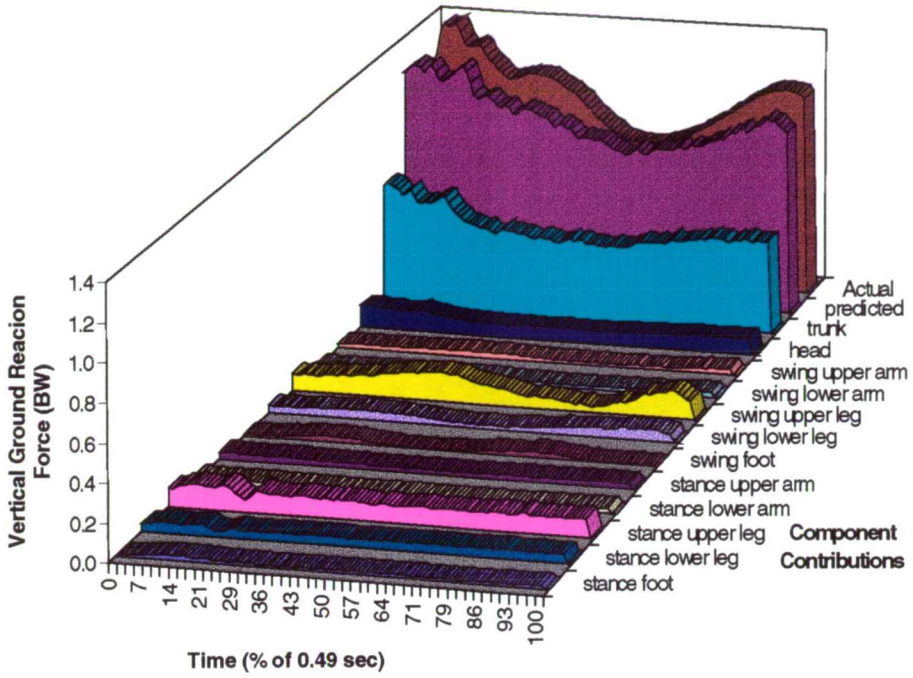

Figure 138 Segmental contribution to the predicted vertical ground reaction force from Figure 133-A (hip 10Hz, legs 10Hz, rest 10Hz).

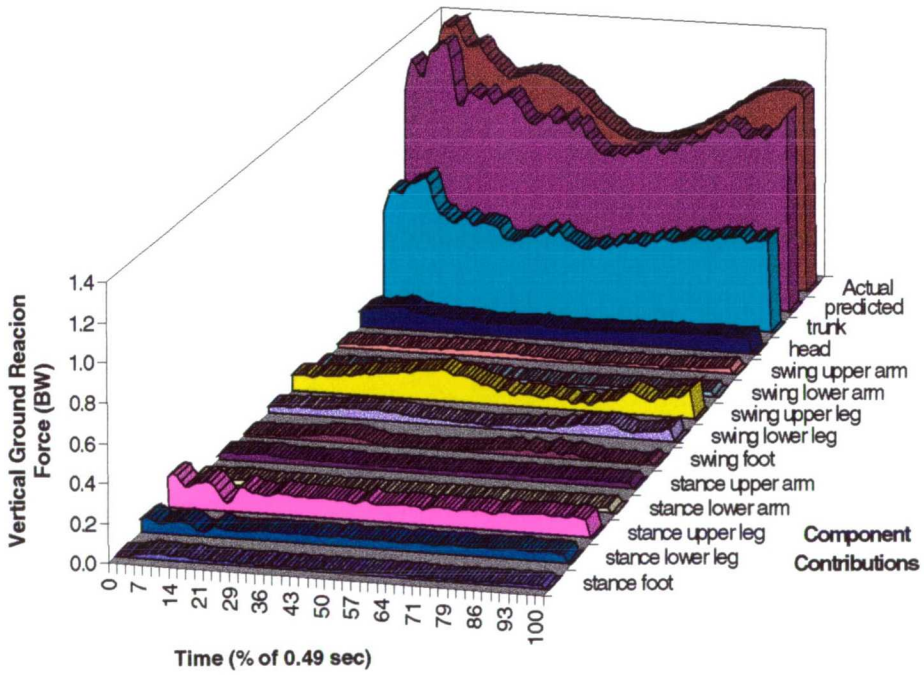

Figure 139 Segmental contribution to the predicted vertical ground reaction force from Figure 133-E (hips 20Hz, legs 15Hz, rest 10Hz).

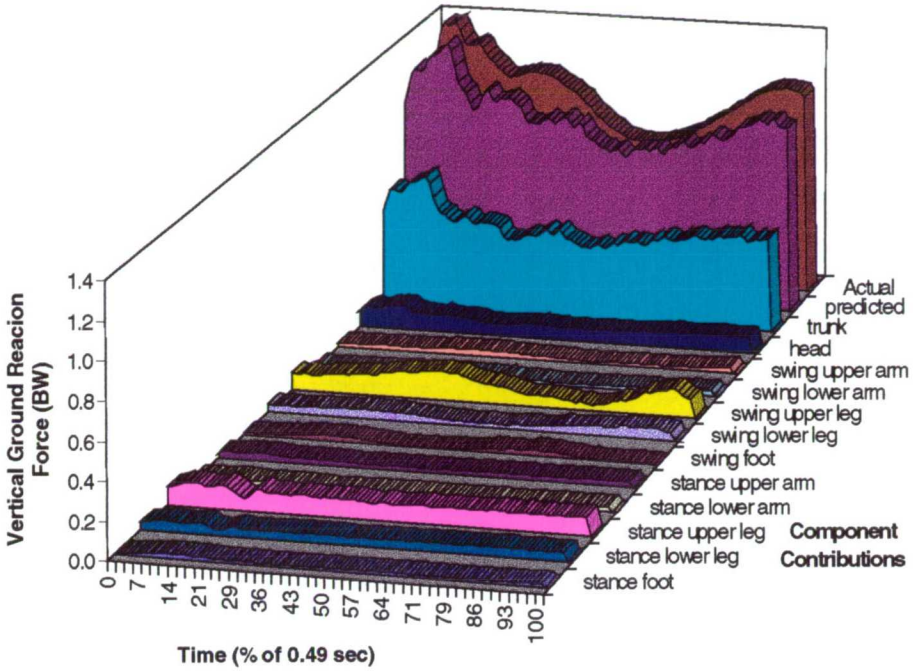

Figure 140 Segmental contribution to the predicted vertical ground reaction force from Figure 133-F (hip 20Hz, legs 10Hz, rest 20Hz).

9.8.5 Predictions of Vertical GRF's for Other Walking Gait Traces

The same procedures used in the translational and rotational approachs have been applied to two other walking traces, shown as Figure 141 and Figure 142.

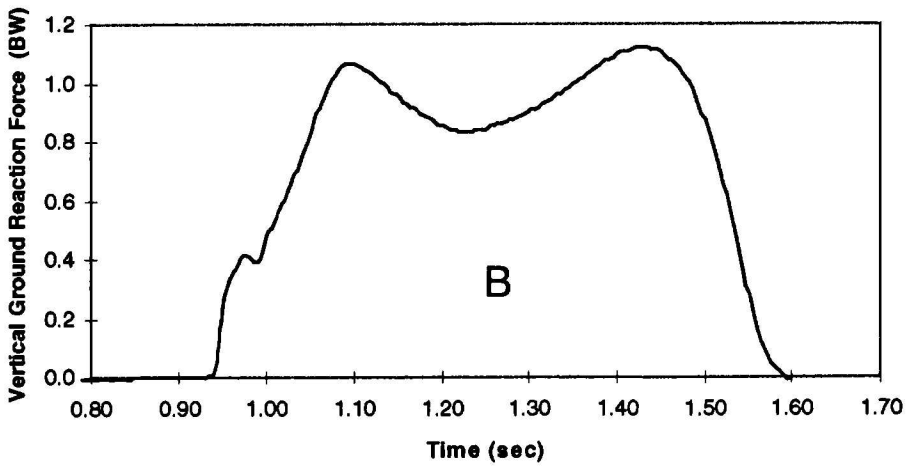

Figure 141 Force-time history form a second walking trace at approximately 2 Hz.

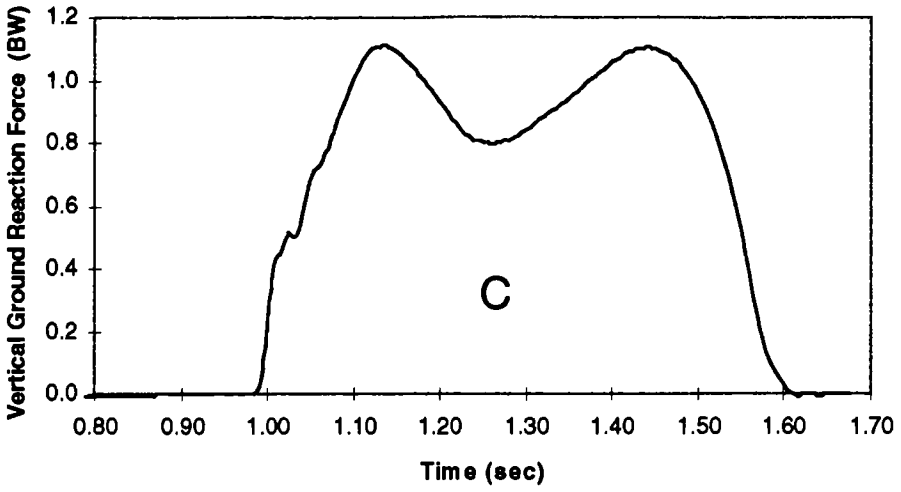

Figure 142 Force-time history for a third walking trace at approximately 2 Hz.

The marker data corresponding to the traces have been filtered with the same cut-off values used previously. Figure 143 presents the 3 predicted vertical GRF's traces for plots B and C using a translational approach calculation.

The first two plots B1 and C1, used the filtering values which produced the best results for the previous walking trace. In this case, the traces did not fully predict the heights of the first peak although they were only 5% out. By increasing the hip cut-off frequency from 20 Hz to 30 Hz (plots B3 and C3), the peak were accurately predicted. This would suggest that the translational approach can be used for a range of loading conditions from walking to running if the cut-off frequencies are maintained at 20-30 Hz for the hip, 50 Hz for the legs and 15 Hz for the rest of the marker data. This being the case, these filter values were also appropriate to predict vertical GRF's for ascending and descending staircases as these force traces mimic those produced from walking and running. One cause for concern in all plots was the failure of the predicted traces to closely match the actual values in the 90% to 100% region of the gait cycle. A possible reason for this was elaborated on in section 9.9 "Discussion".

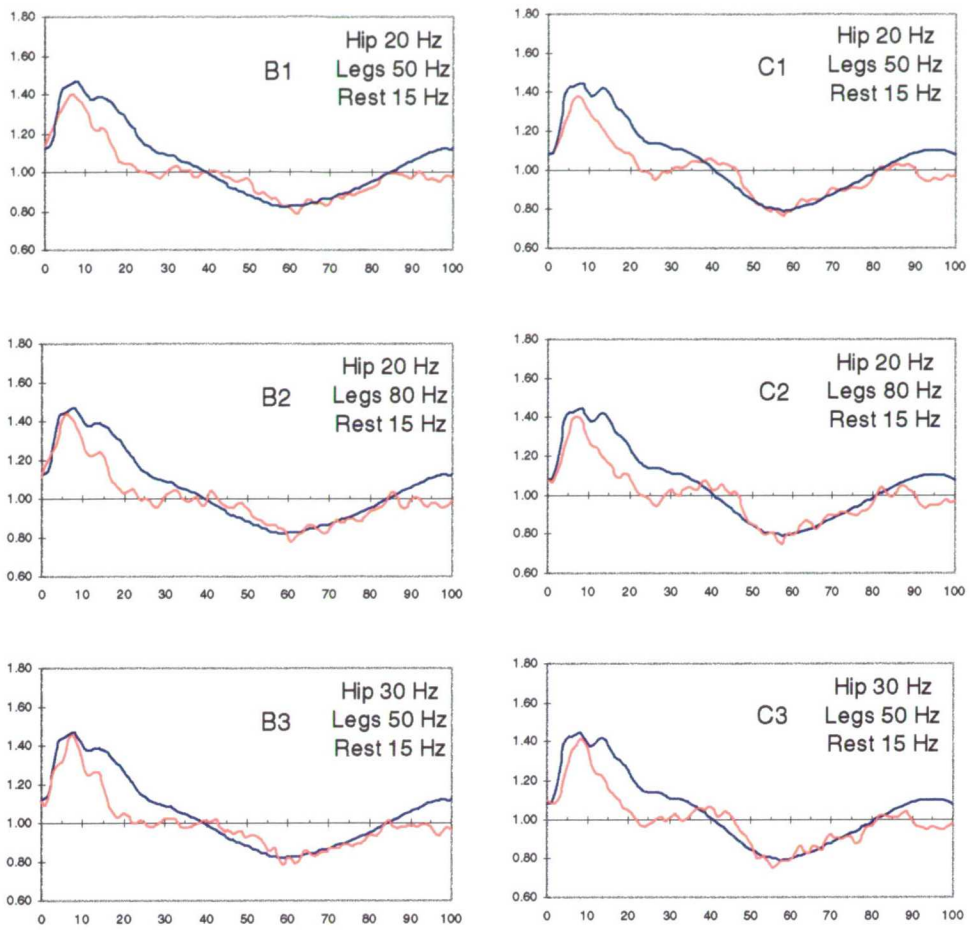

Figure 143 Predicted traces compared with actual traces for "B and C" (translational approach).

Figure 144 presents the 3 predicted vertical GRF's traces for plots B and C using a rotational approach calculation. All plots (with the possible exception of B2) are very poor in their prediction of the actual force trace. Yet, these filtering values predicted good results for the previous walking trace. It is likely that the rotational approach is very sensitive to the filtering values and each loading situation requires a unique set of cut-off frequencies to obtain the most accurate prediction. If this is the case, it would suggest that the rotational approach is too sensitive to use for general loading situation.

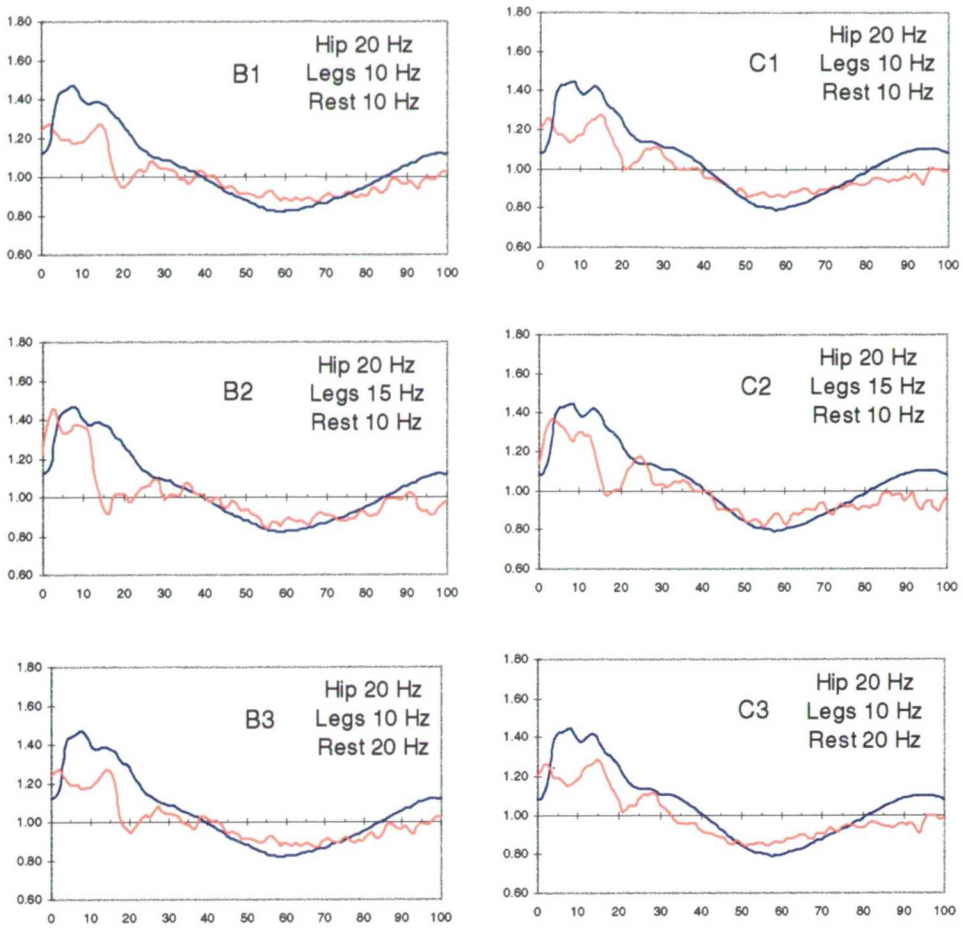

Figure 144 Predicted traces compared with actual traces for "B and C" (rotational approach).

9.8.6 Prediction of Vertical GRF's for Stair Ascending and Descending

A small staircase was constructed (4 stairs) in the CODA laboratory to capture the positional data as a subject ascended and descended the stairs. The force plate could not be incorporated into the staircase because of space limitations hence, measured vertical ground reaction force data did not accompany the staircase trials. This should not be viewed as a problem however, since results based on walking and running trials have show that reasonable predictions can be made following a translational approach.

Figure 145 shows the predicted vertical GRF for a subject walking down a staircase at 2.2 Hz with the marker data filtered at 15 and 50 Hz. The traces appear rough when compared to the walking results but are in line with the oscillations presented in Bobbert *et al.* [1991]. As discussed in the previous

section, the actual trace would be somewhere between these predicted results using the cut-off frequencies of 30 Hz for the hip, 50 Hz for the leg and 15 Hz for the arms, shoulder and head. Figure 146 presents the predicted vertical GRF's for 4 different descending trials (blue) using the aforementioned filtering values. The underlying trace (red) is a typical continuous force time history trace for a subject descending a staircase at a footfall rate of 2.1 Hz.

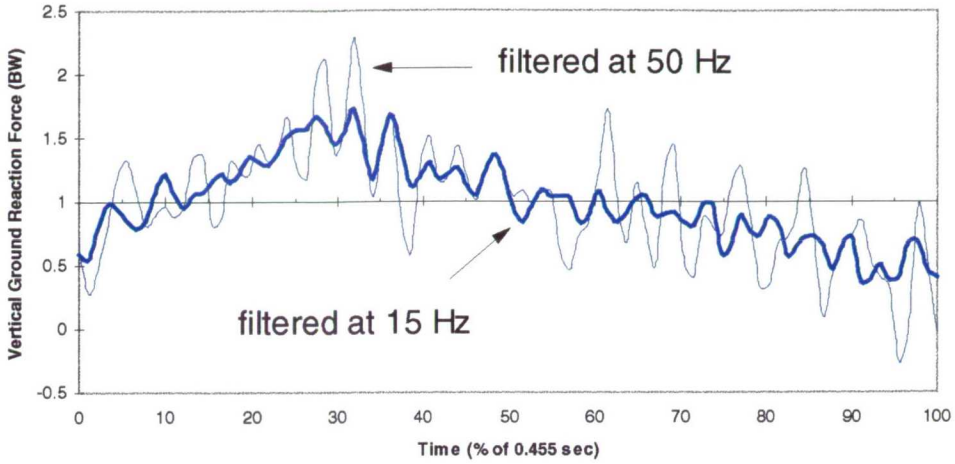

Figure 145 Predicted vertical GRF's for a subject walking down a staircase at a footfall rate of 2.2 Hz.

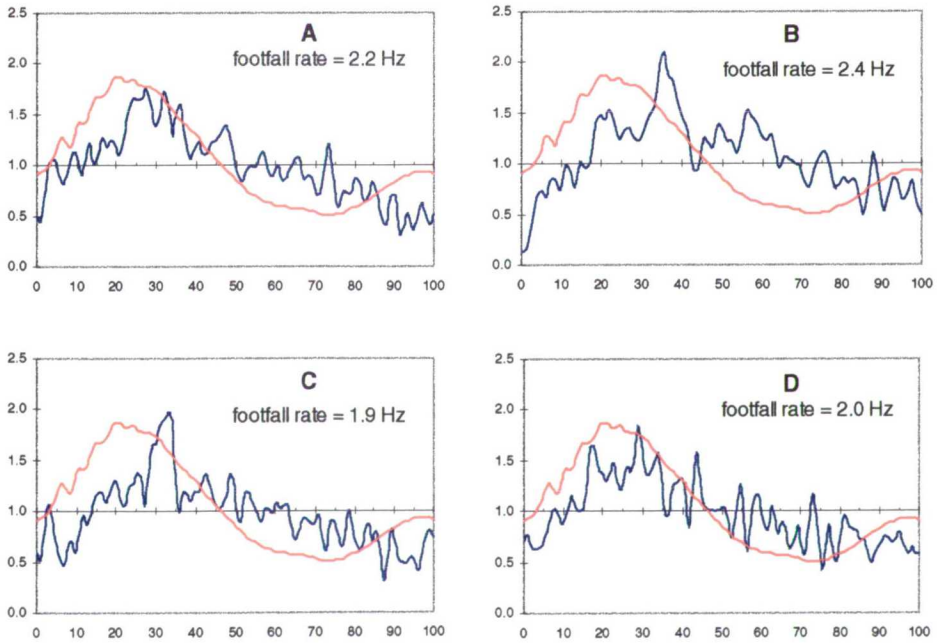

Figure 146 Predicted vertical GRF's from 4 different sets of marker data for descending a staircase.

Looking at the actual and predicted traces, one can make broad comparisons as to their shape. All plots start below the 100% body weight line and the height of the first peak is roughly the same. After the first peak, all plots descend below the 100% body weight line and end below the 100% body weight line. One negative point was the failure of the predicted traces to show a definitive trough.

Figure 147 presents the predicted vertical GRF's for 4 different descending trials (blue) using the aforementioned filtering values. The underlying trace (red) is a typical continuous force time history trace for a subject ascending a staircase at a footfall rate of 1.9 Hz.

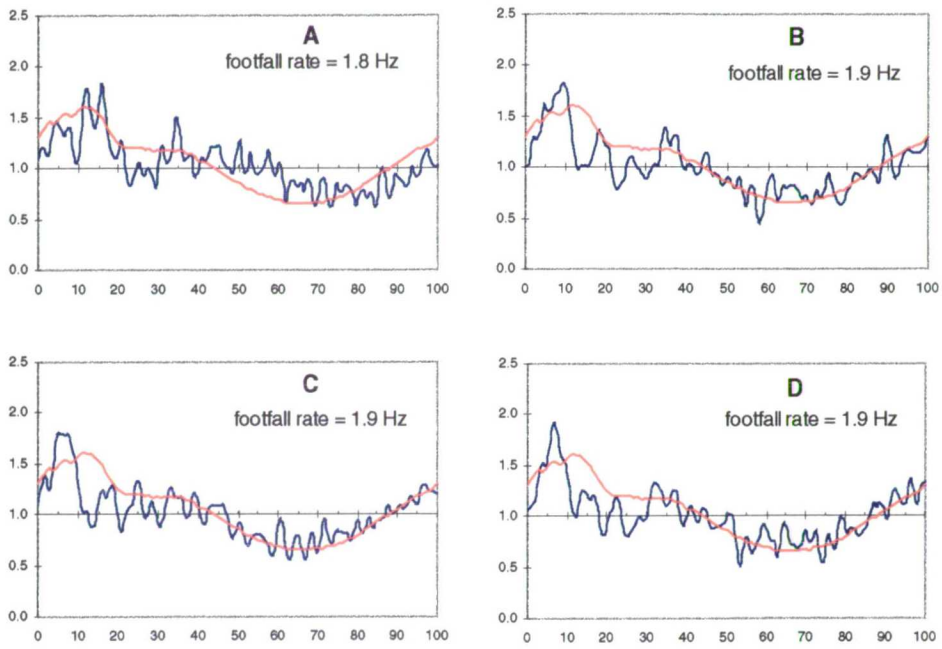

Figure 147 Predicted vertical GRF's from 4 different sets of marker data for ascending a staircase.

The actual vertical GRF closely resembles the traces seen for walking. As explained in section 6.4.1, when ascending a staircase at footfall rates less than approximately 2.2 Hz it was very likely the method of ascent would be a slow, one step at a time, walking action. Hence, the trace typically had two peaks with the second peak either equal to or slightly larger than the first.

When comparing the predicted and the actual (typical) trace a close resemblance can be seen. All traces start at approximately the same value then climb to an initial first peak. The plots then decrease to a trough at approximately the same

values until moving back up and finishing above the 100% body weight line. As with the walking predictions, the second peak located around the 30% mark was roughly predicted.

Although it is not possible to assess the percentage error of the predicted traces to the typical traces, it does appear the that the predicted values were reasonably close to what might be expected for the footfall rates used. Perhaps, the best indication as to the accuracy of the results can be made by determining the harmonic values from the predicted force traces and comparing them to the values calculated from experimental results. By doing so, one can see how closely the initial harmonics are predicted.

9.8.7 Harmonic Components from Predicted Vertical GRF's During Walking and Ascending/Descending Stairs.

Much effort was made in Chapter 5 and 6 to show that significant harmonic amplitudes calculated from typical vertical GRF traces only exist up to the fourth or fifth harmonic (typically) and that the trace itself can be accurately predicted using only the first 10 harmonics or less. Therefore, to compare the actual and predicted vertical GRF's presented in this chapter, the first 10 harmonics were calculated and presented in a summary table (see Table 23). The shaded cells represent values calculated via the rotational approach.

The first 24 results are the harmonic amplitudes calculated from the predicted traces of the continuous plot shown in Figure 124. Looking specifically at the results for Figure 131 and Figure 133, the average first harmonic amplitude was 0.17. This value is approximately 23% smaller than the actual value of 0.22 with the difference being attributed to the less than perfect fit of the predictions in the 10% to 30% and 80% to 100% ranges of the gait cycle. The third and fifth harmonic values, on the other hand, are approximately 50% to 75% larger than the actual values. The remaining harmonics all follow the actual values without any major deviations. The predictions from Figure 143 also show the same patterns discussed above.

The predictions from the stair ascending and descending are much rougher than those for walking and as such the Fourier analysis shows significant harmonic

amplitudes beyond the 10 harmonic. If one looks at the results from the typical traces and assumes the same pattern as above, the first harmonic value is assumed to be 20% to 30% lower the actual values.

9.9 DISCUSSION

This chapter has built on the work of Bobbert, Miller and Nissinen and Thornton-Trump and Daher in the area of predicting vertical ground reaction forces from body segment positional data. Positional data gathered from the Stanmore work (detailed in Chapter 8), coupled with the anthropometric data of Clauser *et al.* [1969], had been used in a Newtonian approach to predict the vertical ground reaction forces during walking and ascending / descending stairs.

In the final discussions of Bobbert *et al.* [1991], they comment on their inability to remove the sinusoidal oscillations of the markers as the skin moved relative to the bones and other tissue during the running gait. Perhaps, these small oscillations were not as significant as Bobbert suggested. When one thinks of the centre of mass of any limb, it is typically governed by the position of the muscle mass and to a lesser extent the position of the bone. The muscle mass is not stationary and will move relative to the bone(s) on which it is attached. Therefore (as pointed out by Bobbert), the oscillations experienced by the centre of mass will lie somewhere between the oscillation of the muscle and the oscillation of the bone. If the movement of the skin also falls into this category, then perhaps the oscillations of the skin might mimic the oscillation of the limb centre of mass. Regardless to whether this is true, one can say with authority that the success of the vertical ground force prediction relies on the ability of the markers positions to accurately predict the motions of the centre of mass.

A second potential source of error, although a small one, was the assumption that the left side limbs produced the same motions as the right side limbs with a phase shift of half the footfall rate. Assuming the entire body felt the initial "shock" as the right heel struck the ground but the shock died out very quickly. The shock would be felt by the left side limbs which, at that time, were just completing the toe push-off portion the walking gait. If the shock died out quickly, when the substitution was made for the motions of the left side with the motions of the right side, taking place half a stride length in the future, the shock oscillations are

no longer present and therefore the initial shock would not exist when one should. If this were true however, the difference would likely be insignificant for two reasons. The mass of the arm and leg as a whole is small when compared to the rest of the body. Even a moderate increase in accelerations would not make a significant impact to the overall ground reaction force. Secondly, any induced oscillations of the left leg due to the right heel impact will likely be damped out very quickly as the left leg is still touching the ground during the right heel strike.

The results of the walking VGRF predictions showed a very close approximation to the actual VGRF's with the traces typically within 10% and the peak values being accurately predicted. The results of the ascending / descending VGRF predictions could not be compared with actual measurements, however, comparisons with typical VGRF traces near the same footfall rates showed good correlation for ascending traces but poor correlation for descending traces. One possible reason for this wass that during descents, much higher impact loads occurred suggesting greater movement of the limb centres of gravity, relative to the markers (especially for the trunk) than that which occurred for ascending. If this was true than accurately predicting the movements of the centres of gravity from marker data may be greatly flawed. Prediction of the correct movements is vital for an accurate prediction of the VGRF. Therefore, based on the work in this chapter, it is expected that one could predict the VGRFs for walking and slow ascents only, following the techniques used in this work.

The harmonic amplitudes were very sensitive to the shapes of the footfall traces. On average the predicted first harmonic values for the predicted walking traces were 20% to 40% lower. The second and fourth predicted harmonics showed very good correlation while the third and fifth predicted harmonic were an average of 50% higher. Direct comparisons could not be made for the ascending and descending traces because the actual force time histories were not captured during the tests. However comparisons with typical traces tended to be as inaccurate as for walking traces. Therefore, the methods used in this work fail to give an accurate indication of the harmonic components for both walking and negotiating stairs.

Figure Number	Pace (Hz)	Harmonic Amplitudes as a Fraction of Subject Weight									
		1	2	3	4	5	6	7	8	9	10
Figure 124 (actual)	**2.04**	**0.22**	**0.02**	**0.04**	**0.04**	**0.02**	**0.01**	**0.01**	**0.01**	**0.01**	**0.01**
Figure 127-A	2.04	0.17	0.03	0.09	0.07	0.04	0.04	0.04	0.03	0.02	0.04
Figure 127-B	2.04	0.17	0.03	0.08	0.07	0.04	0.04	0.04	0.03	0.02	0.03
Figure 127-C	2.04	0.17	0.03	0.08	0.07	0.03	0.03	0.03	0.02	0.02	0.02
Figure 127-D	2.04	0.18	0.03	0.08	0.06	0.03	0.03	0.02	0.02	0.01	0.01
Figure 127-E	2.04	0.18	0.03	0.07	0.03	0.02	0.00	0.00	0.01	0.00	0.01
Figure 127-F	2.04	0.17	0.03	0.04	0.01	0.00	0.01	0.01	0.01	0.01	0.01
Figure 128-A	2.04	0.18	0.01	0.07	0.11	0.16	0.17	0.17	0.22	0.28	0.29
Figure 128-B	2.04	0.18	0.01	0.06	0.11	0.16	0.16	0.16	0.20	0.25	0.25
Figure 128-C	2.04	0.19	0.02	0.07	0.10	0.15	0.15	0.13	0.16	0.19	0.18
Figure 128-D	2.04	0.19	0.02	0.07	0.10	0.13	0.13	0.10	0.11	0.12	0.09
Figure 128-E	2.04	0.18	0.02	0.05	0.06	0.07	0.04	0.01	0.02	0.04	0.05
Figure 128-F	2.04	0.17	0.01	0.02	0.03	0.04	0.03	0.02	0.01	0.01	0.03
Figure 131-A	2.04	0.17	0.03	0.07	0.05	0.04	0.03	0.03	0.03	0.02	0.02
Figure 131-B	2.04	0.17	0.03	0.07	0.05	0.03	0.02	0.01	0.02	0.01	0.00
Figure 131-C	2.04	0.18	0.03	0.07	0.04	0.03	0.01	0.01	0.01	0.01	0.00
Figure 131-D	2.04	0.17	0.03	0.07	0.04	0.03	0.01	0.02	0.02	0.01	0.00
Figure 131-E	2.04	0.18	0.03	0.08	0.06	0.03	0.01	0.02	0.01	0.01	0.02
Figure 131-F	2.04	0.17	0.02	0.05	0.03	0.03	0.02	0.02	0.02	0.01	0.01
Figure 133-A	2.04	0.17	0.01	0.02	0.03	0.04	0.03	0.02	0.01	0.01	0.03
Figure 133-B	2.04	0.17	0.03	0.04	0.02	0.03	0.02	0.00	0.01	0.01	0.01
Figure 133-C	2.04	0.17	0.03	0.05	0.02	0.04	0.03	0.01	0.00	0.01	0.01
Figure 133-D	2.04	0.17	0.03	0.05	0.03	0.05	0.06	0.03	0.02	0.02	0.01
Figure 133-E	2.04	0.17	0.03	0.06	0.03	0.05	0.02	0.01	0.01	0.01	0.01
Figure 133-F	2.04	0.17	0.03	0.05	0.02	0.04	0.03	0.01	0.00	0.01	0.01
Figure 142-B (actual)	**2.02**	**0.25**	**0.05**	**0.05**	**0.03**	**0.02**	**0.01**	**0.02**	**0.02**	**0.01**	**0.01**
Figure 143-B1	2.02	0.17	0.06	0.08	0.04	0.04	0.02	0.01	0.01	0.01	0.01
Figure 143-B2	2.02	0.17	0.06	0.08	0.05	0.04	0.02	0.02	0.01	0.01	0.01
Figure 143-B3	2.02	0.16	0.06	0.08	0.05	0.04	0.02	0.01	0.01	0.01	0.01
Figure 144-B1	2.02	0.13	0.04	0.05	0.03	0.01	0.01	0.04	0.03	0.02	0.01
Figure 144-B2	2.02	0.15	0.06	0.08	0.06	0.06	0.04	0.01	0.02	0.02	0.02
Figure 144-B3	2.02	0.13	0.04	0.05	0.03	0.01	0.01	0.04	0.03	0.02	0.01
Figure 142-C (actual)	**2.08**	**0.24**	**0.03**	**0.06**	**0.04**	**0.02**	**0.01**	**0.01**	**0.02**	**0.01**	**0.01**
Figure 143-C1	2.08	0.16	0.02	0.09	0.05	0.04	0.01	0.01	0.01	0.01	0.00
Figure 143-C2	2.08	0.16	0.02	0.09	0.05	0.04	0.02	0.01	0.02	0.01	0.00
Figure 143-C3	2.08	0.16	0.02	0.10	0.05	0.04	0.01	0.01	0.01	0.01	0.01
Figure 144-C1	2.08	0.15	0.04	0.04	0.02	0.00	0.02	0.03	0.03	0.02	0.01
Figure 144-C2	2.08	0.16	0.04	0.06	0.05	0.05	0.03	0.00	0.02	0.03	0.02
Figure 144-C3	2.08	0.16	0.05	0.03	0.02	0.00	0.02	0.03	0.03	0.02	0.01
Figure 146 (typical trace)	**2.11**	**0.61**	**0.14**	**0.06**	**0.04**	**0.01**	**0.00**	**0.01**	**0.01**	**0.01**	**0.01**
Figure 146-A	2.20	0.40	0.17	0.02	0.07	0.08	0.02	0.02	0.02	0.04	0.07
Figure 146-B	2.44	0.42	0.14	0.07	0.09	0.11	0.07	0.12	0.08	0.01	0.07
Figure 146-C	1.94	0.37	0.13	0.04	0.06	0.02	0.09	0.09	0.04	0.02	0.07
Figure 146-D	1.98	0.35	0.13	0.05	0.01	0.01	0.04	0.04	0.06	0.06	0.03
Figure 146 (typical trace)	**1.91**	**0.39**	**0.07**	**0.06**	**0.04**	**0.02**	**0.01**	**0.01**	**0.01**	**0.01**	**0.01**
Figure 147-A	1.77	0.24	0.14	0.08	0.06	0.07	0.04	0.05	0.01	0.03	0.05
Figure 147-B	1.89	0.27	0.10	0.11	0.08	0.05	0.04	0.08	0.05	0.05	0.05
Figure 147-C	1.89	0.28	0.10	0.09	0.05	0.05	0.06	0.06	0.05	0.04	0.06
Figure 147-D	1.87	0.26	0.12	0.10	0.07	0.05	0.02	0.08	0.06	0.02	0.03

Table 23 The first fifteen harmonic amplitude values calculated from actual and predicted vertical GRF's (shaded rows represent predictions following a rotational approach).

REFERENCES

Beckett, R., and Chang, K. (1968). *An Evaluation of the Kinematics of Gait by Minumum Energy.* Journal of Biomechanics. Vol.1. pp.147-159.

Bobbert, M.F., Schamhardt, C., and Nigg, M. (1991). *Calculation of Vertical Ground Reaction Force Estimates During Running from Positional Data.* Journal of Biomechanics. Vol.24. No.12. pp.1095-1105.

Bobbert, M.F., Yeadon, M.R., and Nigg, M. (1992). *Mechanical Analysis of the Landing Phase in Heel-Toe Running.* Journal of Biomechanics. Vol.25. No.3. pp.223-234.

Brand, R.A., Crowninnshield, R.D., Wittstock, C.E., Pedersen, D.R., Clark, C.R., and van Krieken, F.M. (1982). *A Model of Lower Extremity Muscular Anatomy.* Journal of Biomech. Engng. Vol.104. pp.304-310.

Bresler, B. and Grankel, J.P. (1950). *The Forces and Moments in the leg During Level Walking.* ASME Transactions. Vol.22. pp.27-36.

Cappozzo, A., Leo, T. and Pedotti, A. (1975). *A General Computation Method for the Analysis of Human Locomotion.* Journal of Biomechanics. Vol.8. pp.307-320.

Cavagna, G.A., Thys, H., and Zamboni, A. (1979). *The Sources of External Work in Level Walking and Running.* Journal of Physiology. Vol.262. pp.639-657.

Clauser, C.E., McConville, J.T. and Young, J.W. (1969). *Weight, Volumn and Center of Mass of Segments of the Human Body.* Wright-Patterson Air Force Base, OH (ARML-TR-69-70). pp.59-60.

Cunningham, D.M. (1950). *Components of Floor Reactions During Walking.* Prosthetic Devices research Project I.E.R., Rept. Series II, Issue 14. University of California, Berkely.

Dempster, R. (1971). *Space Requirements for the Seated Operator.* W.A.D.C. Technical Report. pp.55-159.

Dempster, R. and Gaughran, G.R.L. (1967). *Properties of Body Segments based on Size and Weight.* American Journal of Anatomy. Vol.120. pp.33-54.

Dowling, J.J. and Vamos, L. (1995). *Identification of Kinetic and Temporal Factors Related to Vertical Jump Performance..* Journal of Applied Biomechanics. Vol.9. pp.95-110.

Eng, J.J. and Winter, D.A. (1995). *Kinetic Analysis of the Lower Limbs during Walking: What Information Can be Gained From a Three-dimensional Model?* Journal of Biomechanics. Vol.28. No.6. pp.753-758.

Hamill, J. and Knutzen, K.M. (1995). Biomechanical Basis of Human Movement. Williams & Wilkins. London.

Hardt, D.E. and Mann, R.W. (1980). *A Five Body-Three Dimensional Dynamic Analysis of Walking.* Journal of Biomechanics. Vol.13. pp.455-457.

Huston, R.L., Passerello, C.E., Hessel, R.E., and Harlow, M.W. (1976). *On Human Body Dynamics..* Annals of Biomedical Engineering. Vol.4. pp.25-43.

Jackson, K.M. (1979). *Fitting of Mathematical Functions to Biomechanical Data.* IEEE Transactions on Biomedical Engineering, BME-26 Vol.2. pp.122-124.

Ju, Ming-shaung and Mansour, J.M. (1988). *Simulation of the Double Limb Support Phase of Human Gait..* Journal of Biomechanical Engineering. Vol.110. pp.223-229.

Koopman, B., Grootenboer, H.J., and de Jongh, H.J. (1995). *An Inverse Dynamics Model for the Analysis Reconstruction and Prediction of Bipedal Walking..* Journal of Biomechanics. Vol.28. No.11. pp.1369-1376.

Light, L.H., McLellan, G.E. and Klennerman, L. (1980). *Skeletal Transients on Heel Strike in Normal Walking with Different Footwear.* Journal of Biomechanics. Vol.13. pp.477-480.

McGhee, R.B., Koozekanni, S.H., Gupta, S., and Cheng, T.S. (1976). *Automatic Estimation of Joint Forces and Moments in Human Locomotion from Television Data.* Proceedings of the IV IFAC Symposium on Identification and Parameter Estimation. USSR.

Miller, D.I. and Nissinen, M.A. (1987). *Critical Examination of Ground Reaction Force in the Running Forward Somersault.* International Journal of Sport Biomechanics. Vol.3. pp.189-206.

Murray, M.P., Drought, A.B. and Kory, R.C. (1964). *Walking Patterns of Normal Men..* Journal of Bone Joint Surgery. Vol.46A. pp.335-360.

Murray, M.P., Kory, R.C., Clarkson, R.H. and Sepic, S.B. (1966). *Comparison of Free and Fast Speed Walking Patterns of Normal Men.* American Journal of Physical Mechanics. Vol.45. pp.8-24.

Murray, M.P. (1968). *Gait as a Total Pattern of Movement.* American Journal of Physical Mechanics. Vol.48. pp. 290-333.

Onyshro, S. and Winter, D.A. (1980). *A Mathematical Model for the Dynamics of Human Locomotion.* Journal of Biomechanics. Vol.13. pp.361-368.

Pandy, M.G. and Berme, N. (1988). *A Numerical method for Simulating the Dynamics of Human Walking..* Journal of Biomechanics. Vol.21. No.12. pp.1043-1051.

Pierrynowski, M.R., Winter, D.A., and Norman, R.W. (1980). *Mechanical Energy Transfer in Treadmill walking.* Ergonomics. Vol.24. pp.1-14.

Scott, S.H. and Winter, D.A. (1991). *Galocrural and Talocalcaneal Joint Kinematics and Kinetics During the Stance Phase of Walking.* Journal of Biomechanics. Vol.24. pp.743-752.

Seireg, A. and Arvikar, R.J. (1975). *The Prediction of Muscular Load Sharing and Joint Forces in the Lower Extremities During Walking.* Journal of Biomechanics. Vol.8. pp.89-102.

Thornton-Trump, A.B. and Daher, R. (1975). *The Prediction of reaction Forces from Gait Data.* Journal of Biomechanics. Vol.8. pp.173-178.

White, S.C. and Winter, D.A. (1985). *Mechanical Power Analysis of the Lower Limb Musculature in Race Walking.* International Journal of Sports Biomechanics. Vol.1. pp.15-24.

Williams, K.R. and Cavanagh, P.R. (1983). *A Model for the Calculation of Mechanical Power During Distance Running.* Journal of Biomechanics. Vol.16. pp.115-128.

Winter, D.A. (1979). *A New Definition of Mechanical Work Done in Human Movement.* Journal of Applied Physiology. Vol.46. pp.79-83.

Winter, D.A. (1983). *Moments of Force and Mechanical Power in Jogging.* Journal of Biomechanics. Vol.16. pp.91-97.

CHAPTER TEN 10

FINAL DISCUSSIONS

10 DISCUSSIONS AND FUTURE RESEARCH

10.1 EPSRC PROJECT OBJECTIVES

This work was produced with funding provided by the Engineering and Physical Research Council (EPSRC). In the "Case for Support" put forward it was stated that the purpose of the study was to address gaps in the design and analysis techniques applicable to flexible staircases. To achieve the purpose of the study, 6 objectives were listed which could be the focus of the study. They were:

1) collect experimental data on human footprint loading of staircases,
2) verify and enhance this data using analytical techniques,
3) evaluate both experimentally and analytically, the effect of multi-person excitation,
4) investigate footprint-structure interaction using computer modelling techniques for flexible staircases,
5) gather data and evaluate the acceptable vibration levels which are appropriate to staircases,
6) where necessary, make recommendations about design procedures for such structures.

These objectives were modified somewhat during the research. The discussions which follow summarise the substantial work completed in this theses and how it related to the original purpose of the work.

10.2 EXPERIMENTAL WORK CONDUCTED ON THE FLAT

The first objective was to gather experimental data on footprint (footfall) loading on staircases. It was assumed that this data should also be compared with data from footprint loading on floors. As part of the process of determining the

variation in harmonic loading between persons walking on a staircase with persons walking on a floor (flat), a series of "yard stick" measurements were made with subjects walking along a raised platform and stepping onto a calibrated force plate. The output voltage traces from the force plate was recorded by a data acquisition system and stored on a laptop computer. The sampling rate chosen for the work was 200 Hz or approximately 3 times the highest frequency expected. The range of footfall rates varied between 1 and 3 Hz with over 1000 individual traces recorded from 40 subjects.

Each subject started at the beginning of the platform, and walked at a comfortable "natural" stride following the tones generated from an electronic metronome. As they approached the force plate their stride length was measured just before and just after contact. These lengths were averaged, then divided by the subject's height and recorded as a normalised stride length for that particular test. It was noted that the stride lengths changed considerably as a function of the footfall rate with an average value of 0.46 or 46% of the subject's height.

Figure 148 is a plot of the first harmonic results as calculated from all footfall traces. The scatter was reduced by dividing the harmonic values for each test by the subject's normalised stride length and then multiplying by the average normalised stride length (0.46). This produced a plot of average first harmonic amplitude verses footfall rate. The results had a mean that tended to follow a third order polynomial (see Figure 149). However, due to randomness of the data above 2.2 Hz, the upper end should be used with caution. Below 2.2 Hz, the equation for the polynomial can be used with confidence, especially in the range of average footfall rates, 1.7 to 2.1 Hz. The ±2 sigma (σ) limit extends ±32% from the mean.

Second harmonic values were considerably lower than the first harmonic. As seen in Figure 150, the average amplitude was approximately 0.06. The remaining third and fourth harmonic values were even smaller (<0.03) and by the fifth harmonic the amplitudes were approximately zero.

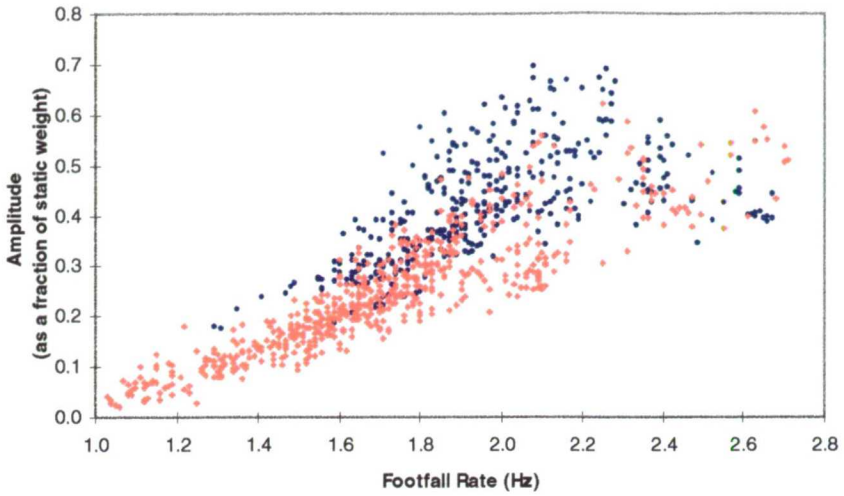

Figure 148 All first harmonic data from walking tests.

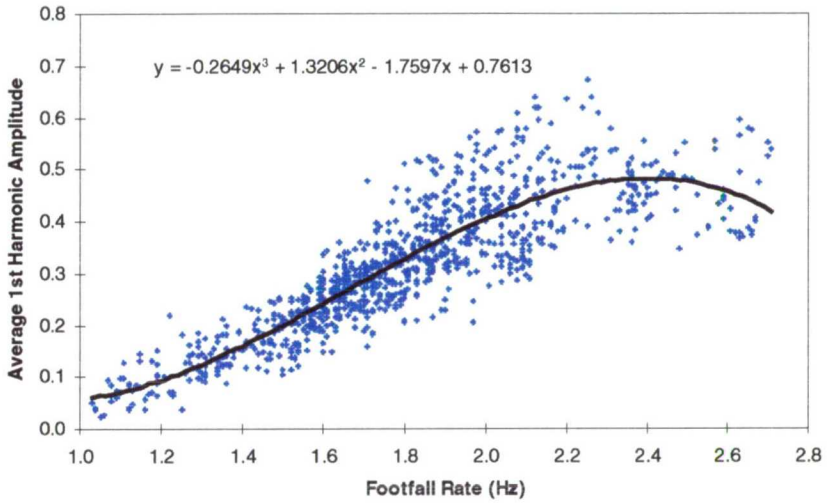

Figure 149 Third order polynomial fit to the first harmonic data.

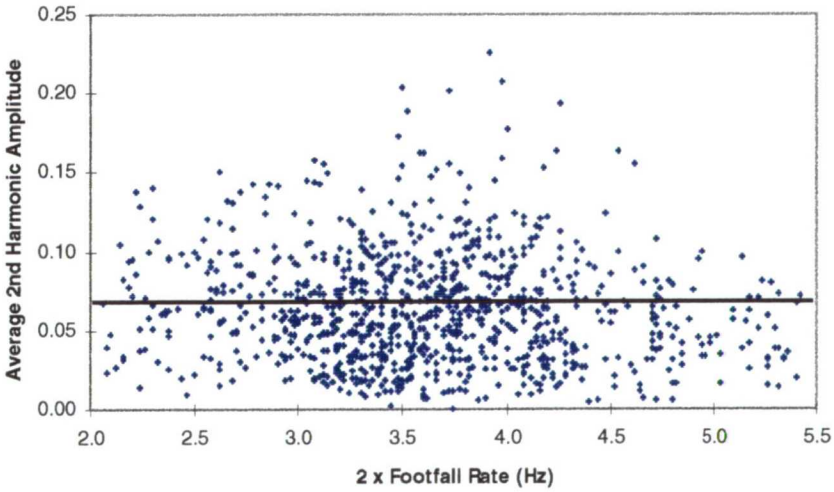

Figure 150 All second harmonic data from walking tests.

These results have been incorporated into a new method for calculating peak acceleration limits on simply supported footbridges (or floors). Presently, peak accelerations are calculated using the expressions in BS5400. These expressions use a fixed fundamental (first) harmonic amplitude of 0.26 or 26% of body weight and do not consider contributions from higher harmonics. Rainer *et al.* [1988] introduced a new approach for predicting peak accelerations at resonance on simply supported footbridge spans based on a 'dynamic amplification factor'. Their expression is given below.

$$a_p = (2\pi f_o)^2 \frac{\alpha P}{k} \Phi$$

where a_p = maximum peak acceleration at resonance
f_o = natural frequency of the footbridge (Hz),
α = harmonic amplitude as fraction of body weight,
P = subject body weight,
k = measured stiffness of span at centre,
Φ = dynamic amplification factor (DAF).

Rainer' formula allowed a user to vary the harmonic amplitudes thus allowing the calculation of the peak accelerations due to higher harmonics. However, their method had two drawbacks: the DAF's were obtained from a series of separate curves (supplied by Rainer) and the harmonic amplitudes must be known by the user at the natural frequency of the footbridge.

In Chapter 5, a new expression was introduced, as given below, which could be incorporated directly into a spreadsheet or computer program since it did not require data obtained *directly* from the Rainer curves and the harmonic amplitudes were automatically predicted based on the natural frequency of the footbridge equalling the footfall rate.

$$a_p = (2\pi f_o)^2 \frac{FHA_m P}{k} \left\{ Cr_{(0.005)} - \left(a\xi^{-b} \right) * (\xi - 0.005) \right\}$$

where a_p = maximum peak acceleration at resonance,
f_o = natural frequency of footbridge (Hz),
FHA_m = mean first harmonic amplitude,
P = subject body weight,
k = measured stiffness of span at centre,
$Cr_{(0.005)}$ = critical damping ratio curve at 0.005,
ξ = critical damping ratio for footbridge,

a, b = expressions for constants.

The latter half of the equation, namely,

$$\left\{Cr_{(0.005)} - \left(\left(a\xi^{-b}\right) * \left(\xi - 0.005\right)\right)\right\}$$

is a mathematical formulation which calculates the value of the DAF based on Rainer's curves. The FHA_m was calculated using the third order polynomial equation given in Figure 149 while $Cr_{0.005)}$, a and b were calculated using further expressions detailed in Chapter 5. The only inputs required are the natural frequency of the footbridge and the weight of the subject. This approach provides designers with a simple and more accurate method for predicting peak accelerations at resonance than found in BS5400. This work was in accordance with objectives of the study.

10.3 EXPERIMENTAL WORK CONDUCTED ON STAIRS

Testing was conducted on a purpose built staircase which was altered between inclinations of 22° to 33°. The staircase was located outdoors at University College London and incorporated seven steps with the fourth or middle step replaced by the force plate used in the floor testing. A false step was placed over the force plate to disguise its presence. The analysis equipment was the same as that used for the floor testing and is described in Chapter 5.

The sampling rate chosen for the experiments was 200 Hz and over 500 individual traces were recorded from 25 subjects. All footfall traces were normalised to subject body weight and all subjects participating in the stair testing also participated in the floor testing.

For each test, the subject was asked to ascend or descend the staircase using one stair per step. By having the force plate as the fourth step, it allowed the subjects to attain a natural rhythm before they contacted the plate. It was decided to forgo the electronic metronome and allow the subjects to choose the footfall rate for each test. Each subject was also asked to comment on what footfall rate felt the most comfortable as they ascended and descended the staircase. This request

produced two values; one while 'walking' up or down the stairs and a second while 'running'.

Unlike on the floor, the stride length when negotiating stairs is fixed by the geometry of the staircase. Therefore the harmonic results were only normalised to the subject's weight. Figure 151 is a plot of the first harmonic values while ascending.

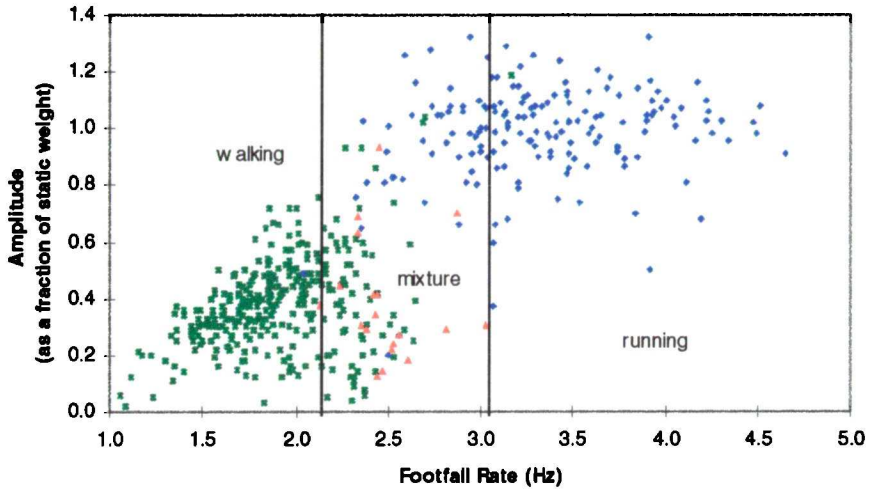

Figure 151 First harmonic values for ascending stairs.

Three distinct regions appear in the plot. The area labelled 'walking' refers to the method of ascent which dominates this area, i.e. each subject walked up the stairs hitting the balls of their feet first then touching down their heels briefly before lifting them again and pushing off with the toes. The area labelled 'running' was dominated by traces from subjects running up the stairs only using the balls of their feet. The 'mixture' area was a region of indecision. Footfall traces in this area varied tremendously in shape and hence produce very different harmonic results. All subjects felt that near 2 Hz was the most comfortable footfall rate at which to walk up the stairs and near 3.3 Hz was the most comfortable rate at which to run up. Attempting to walk or run in the mixture region made most subjects feel 'uncomfortable' and was not normally a footfall rate they would use to ascend the stairs. Figure 152 is a plot of the typical footfall traces found in the three regions.

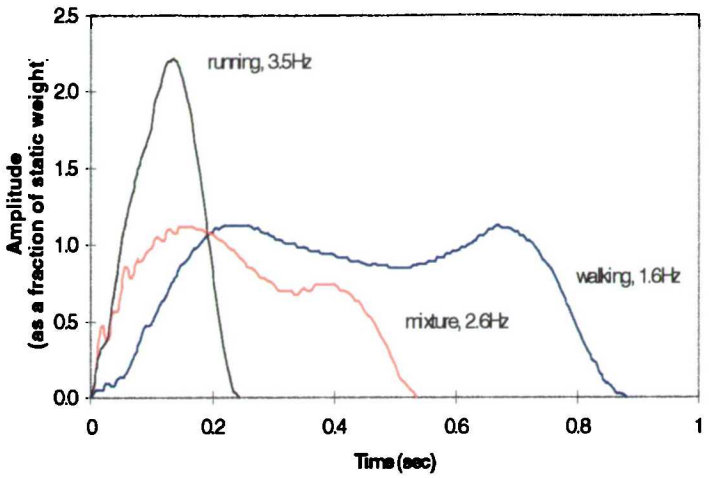

Figure 152 Typical footfall traces found in ascending data.

Unlike the floor data, it was unclear where a mean line should be drawn through the first harmonic data. It was clear however, that the upper value exceeded 1.0 which was substantially higher than that seen for the flat testing. Perhaps even more disturbing were the magnitudes of the second harmonics (see Figure 153). These values were substantially higher than those calculated for the floor testing with an average amplitude around 0.13 as compared with 0.07. The third and fourth harmonics also had significant magnitudes of approximately 0.07 and 0.04, respectively. The fifth and higher harmonics were virtually zero.

Figure 154 is a plot of the first harmonic values calculated from the descending traces. Like the ascending tests, the results could be roughly broken into three regions. Below 2.3 Hz the subjects walked down the stairs hitting the balls of their feet first, then touched down their heels briefly before raising them to push off with their toes. Above 3.3 Hz the subjects tended to run down the stairs using the balls of their feet. In the mixture region the subjects were comfortable either walking or running down the stairs. The subjects also stated that they were comfortable descending at nearly all footfall rates. Figure 155 is a plot of the typical footfall traces found in the three regions.

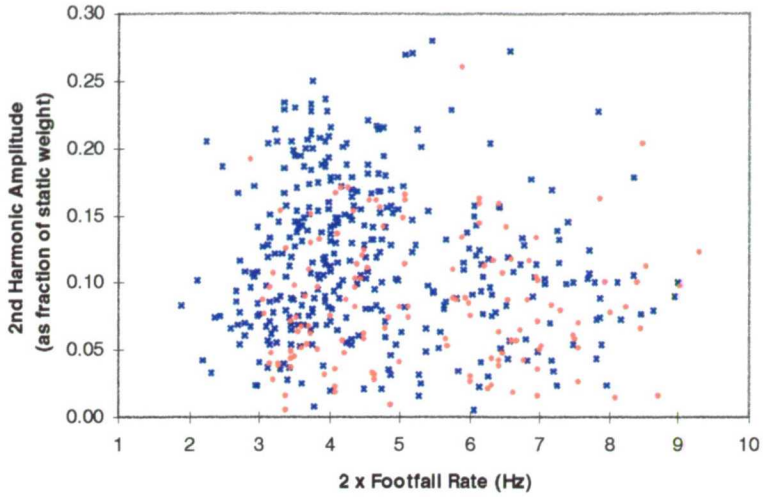

Figure 153 Second harmonic values for ascending stairs.

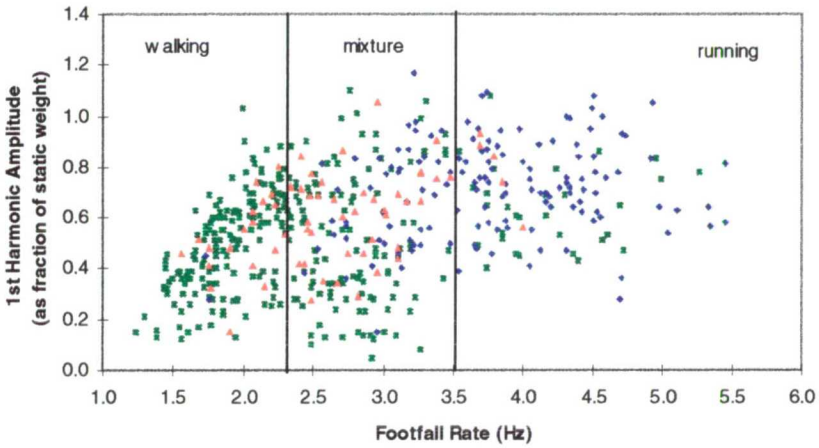

Figure 154 First harmonic values for descending stairs.

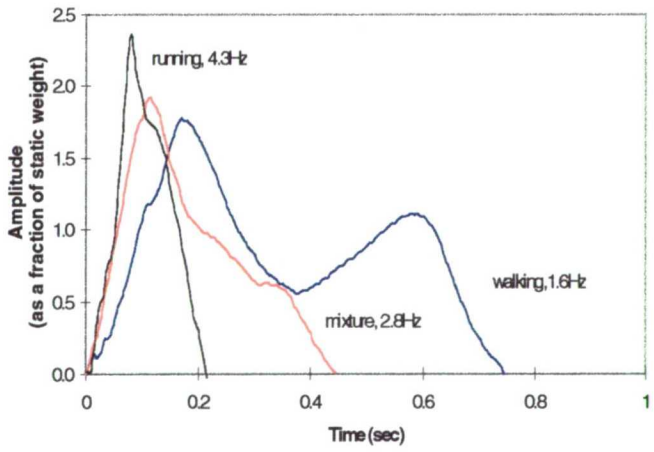

Figure 155 Typical footfall traces found in descending data.

Figure 156 is a plot of the second harmonic values for the descending data. The second harmonics on average were significantly higher than ascending traces with an average amplitude around 0.19. The third and fourth harmonics also had

significant magnitudes of approximately 0.08 and 0.04, respectively. The fifth and higher harmonics were virtually zero.

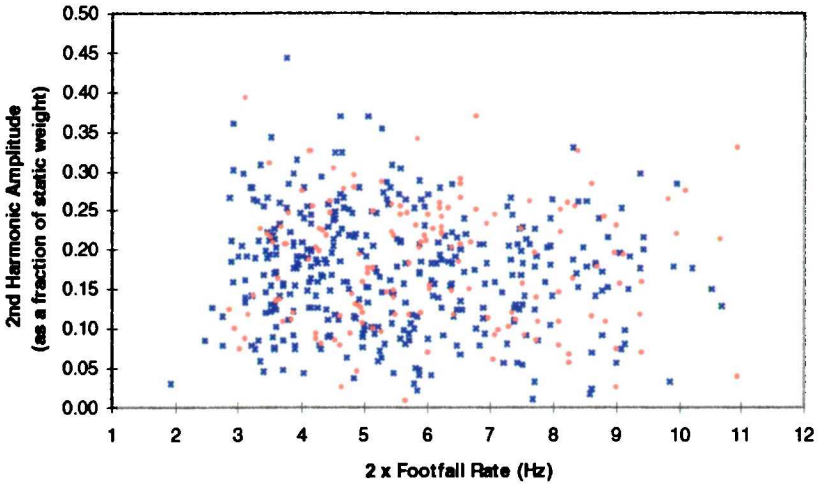

Figure 156 Second harmonic values for descending stairs.

During a descent, the weight is transferred quickly from one leg to the other, which creates a deeper hollow between the humps in the trace. The greater the distance between the hollow and the humps, the greater the second harmonic value. Comparing the 'walking' traces from Figure 152 and Figure 155, both traces were generated at the same footfall rate yet the shapes were very different.

The results of this work provided clear evidence that experience gained from floors and footbridges was highly inappropriate to use for staircases. The mean dynamic loads experienced during ascending and descending were found to be 1.3 and 2.1 times the subject body weight respectively, compared with 1.2 for walking on a floor. The peak dynamic loads were found to be 2.5 and 3.0 times the subject body weight for ascending and descending respectively, compared with only 1.7 for walking on a floor. Overall, ascending and descending traces produced first harmonic values nearly 2.5 times greater at 3.3Hz than that experienced on a floor at 2.0 Hz whilst second harmonic values were up to 3 times greater at 2.0 Hz. The third and forth harmonic values were also approximately 2 to 3 times greater but remained low with values rarely greater than 0.10.

10.4 EVALUATION OF GROUP LOADING

Bishop *et al.* [1995] conducted a Monte Carlo simulation of a number of subjects descending a staircase at identical footfall rates. This simulation was duplicated in this study and expanded to include 3 potential group loading conditions. The first was a group ascending or descending with widely spaced footfall rates. The second was a group ascending or descending with closely spaced footfall rates. The third was identical to Bishop's work with a group ascending or descending with the same footfall rate. The raw data used for all simulations were selected from the experimental work conducted on the stairs.

To simulate a group ascending or descending with widely spaced footfall rates a collection of 9 footfall traces were selected with rates varying by approximately 0.25 Hz. The traces were added together with randomly selected phase shifts forming a combined trace. The combined signal was subjected to an FFT calculation to produce a spectrum of harmonic amplitudes. This simulation was repeated thousands of times to produce an average harmonic spectrum. The final results showed that no change on the original (average) first harmonic amplitude occurred. This was the same result Ellingwood and Tallin [1984] predicted for groups walking across a floor.

To simulate a group ascending or descending with closely spaced footfall rates a collection of 9 footfall traces were selected with a variation across their rates of 10%. The traces were added together with a phase shift varying between 0 and 2π to form a combined signal. The traces were also added together with a phase shift varying between 0 and π. This was to simulate a characteristic observed on actual staircase i.e. as congestion increased the phase shifts between subjects decreased. This typically applied to smaller groups of less than 10 persons. The results of thousands of simulations are shown in Figure 157. As indicated on the plot, the average first harmonic value prior to the simulations was 0.37. After the simulations the results were 0.70 with phase shifts varying between 0 and 2π and 1.10 with phase shifts varying between 0 and π. This simulation work showed that groups with closely spaced footfall rates could produce magnification factors between 2 and 3.

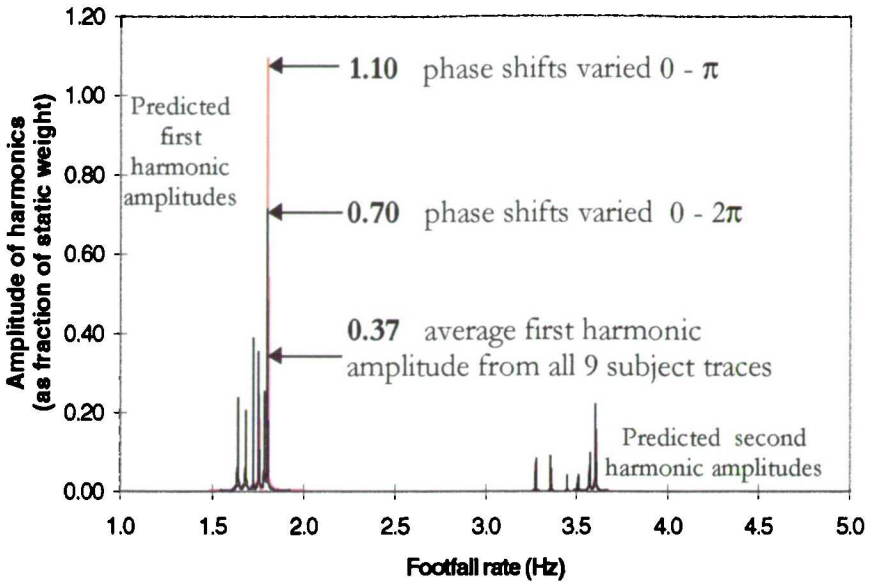

Figure 157 Average spectral results for closely spaced footfall rates.

To duplicate the work of Bishop *et al.* [1995], four groups of subjects were chosen consisting of 4, 9, 18 and 27 traces all with the same footfall rates. After the combined traces were formed a harmonic analysis was conducted to find the first harmonic amplitudes. The amplitudes were divided by the average first harmonic value from the original traces to produce an enhancement factor. The results were then converted into a probability density function (pdf). For each analysis a million simulations were conducted to produce smooth pdf curves. As seen in Figure 158 the most likely enhancement factors varied between 1.6 for a group of 4 and 4 for a group of 27.

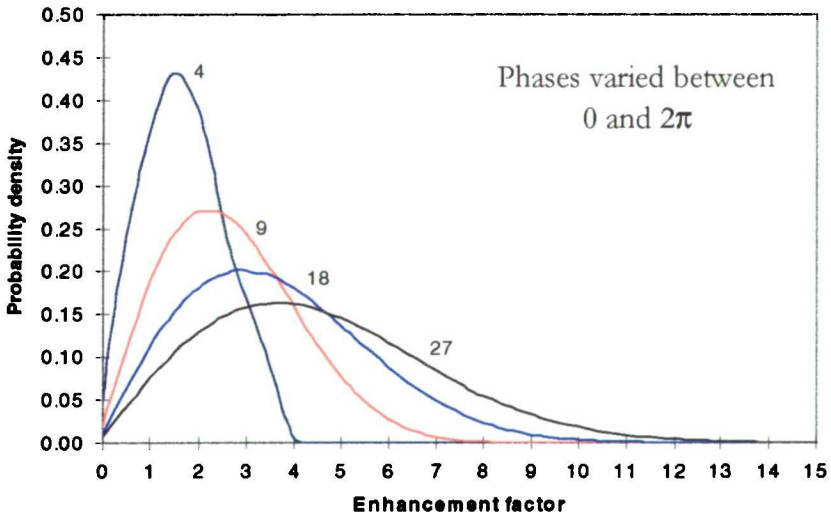

Figure 158 Probability density functions of enhancement factors on first harmonics (phase shifts 0 to 2π).

The enhancement factors for the larger groups do not take into consideration the increased damping effects induced onto the staircase which would likely reduce the enhancement factors by as much as 50% (as mentioned in Bishop *et al.*[1995]). The analysis was also conducted varying the phase shifts between 0 and π for the 4 and 9 subject groups. Results shown in Figure 159 indicate most likely enhancement factors of 3 for a group of 4 and 6 for a group of 9.

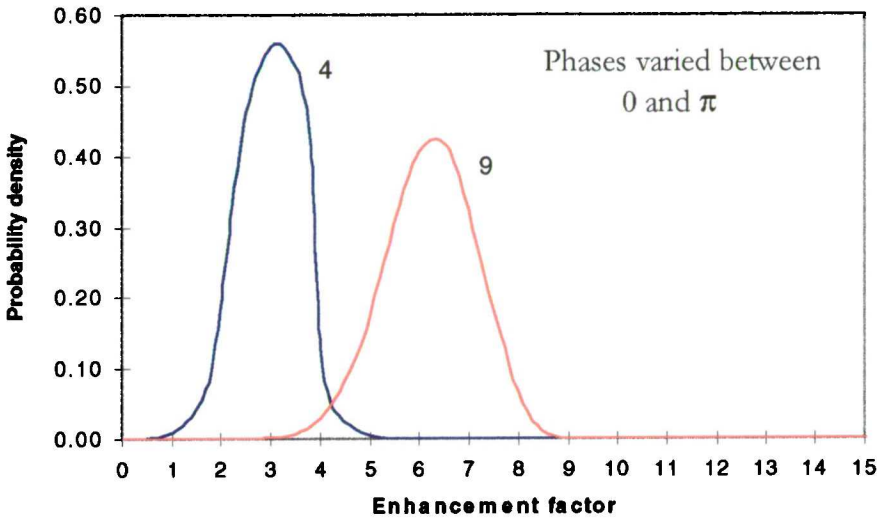

Figure 159 Probability density functions of enhancement factors on first harmonics (phase shifts 0 to π).

10.5 PREDICTING VERTICAL GROUND REACTION FORCES FROM GAIT DATA

As part of the study, an analytical analysis was conducted to verify experimental results. The analysis followed the work of Bobbert *et al.*[1991] with a correction to account for the double support phase during walking and ascending / descending stairs (see Chapter 9 for details).

The analysis required body segment positional data as well as anthropometric data on limb characteristics (i.e. size and mass) like that presented in Dempster and Gaughran [1967]. The positional data was gathered at the Stanmore Orthopaedics Centre during several days of testing with a CODA system (see Chapter 8). As part of the testing, a subject was wired with LED's at the head, shoulder, elbow, wrist, hip, knee, ankle, heel, and toe. As the subject walked past the CODA system sets of Cartesian co-ordinates were captured for each LED at a sampling rate of 200 Hz. Simultaneously, the impact forces were also recorded with the

same force plate used in the experiments on the flat and on the stairs. Positional data was also recorded on a 4 step staircase erected in the Stanmore laboratory.

The positional data was post-processed to calculate linear and angular velocities and accelerations which were used in a Newtonian approach (force = mass x acceleration) to calculate the vertical ground reaction forces. As part of the post-processing, digital filtering was used to diminish the sinusoidal oscillations found in the data due to the skin moving relative to the underlying tissue. The accuracy of the predictions relied on the ability of the LED's to predict the movements of the centres of gravity of the limbs. Figure 160 is an example of a predicted trace compared with an actual continuous force-time history trace for walking at 2.1 Hz. The low pass filtering required to produce this trace was 20 Hz on the hip co-ordinates, 50 Hz on the leg co-ordinates and 15 Hz on the remaining co-ordinates.

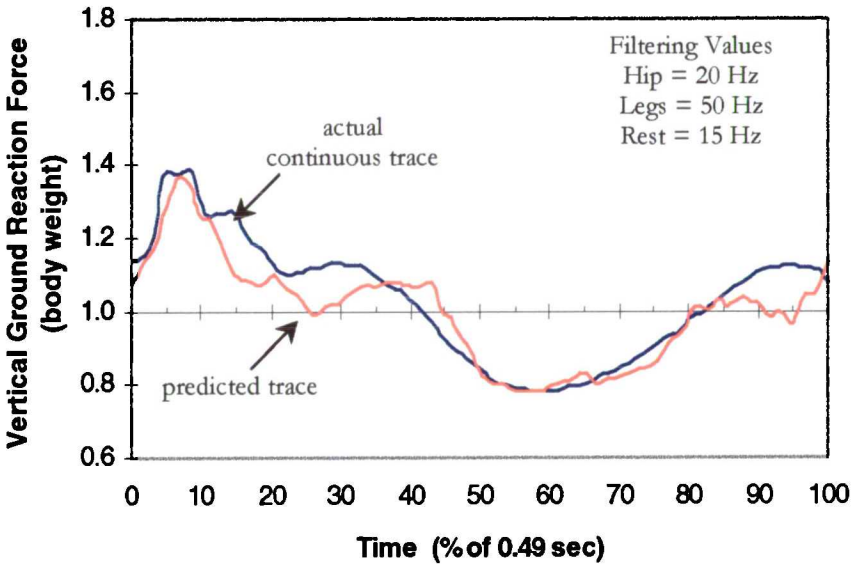

Figure 160 Continuous trace compared with predicted trace.

The results of the walking trials typically generated predicted traces within 10% of the actual traces with the peak values accurately predicted. After calculating the harmonics for both traces the first harmonic amplitudes were typically 20% to 25% lower while the second and fourth harmonics were accurately predicted. The third and fifth harmonics were typically 50% larger than the actual, however, they remained small, typically less than 0.10. For the staircase testing the predicted traces were compared with typical continuous traces having the same footfall rates. Again, the results showed close approximation to the actual traces. These

findings indicated that vertical ground reaction forces can be satisfactorily predicted without the use of a force plate.

10.6 DISCUSSION

During the fulfilment of this thesis, original work was conducted in several key areas. Chapter 5 details the extensive force plate testing on a horizontal platform. The data collected reflects the largest investigation of human loading on floors found in the available literature. The third order polynomial expressions calculated from the first harmonic data provides unique programmable expressions for the structural and biomechanical engineer. An example of their application was the development of a new expression (based on Rainer *et al.*[1988]) for calculating peak vertical acceleration in simply supported floors and footbridges. The harmonic results were summarised and presented in Kerr and Bishop [1997].

Chapter 6 details the extensive force plate testing conducted on a custom built staircase. Once again, the data collected reflects the largest investigation of human loading of stairs found in the available literature. The raw data as well as the calculated harmonics clearly show much higher values than found during floor testing. The information produced in this chapter provides proper guidance for staircase designers as to the loads and harmonics expected during ascending and descending stairs. . The harmonic results were summarised and presented in Kerr and Bishop [1997].

Chapter 7 details the extensive Monte Carlo simulation work which provides clear evidence that group loading conditions will magnify the forces induced on a staircase. This result is the complete opposite of the non-existent group loading effects experienced on floors. This information, combined with the data in Chapter 6, provides the designer with further guidance as to the loads and harmonics expected on staircases.

Chapter 9 provides the analytical link to the experimental results from Chapter 5 and 6. This was done by altering the Newtonian approach, used in nearly all available literature, to account for the double support phase encountered during walking and ascending / descending stairs. This unique approach allowed the

prediction of loads and harmonic values based on body segment positional data collected during testing at Stanmore Hospital. The modelling work predicted very good force-time histories for walking and ascending. Unfortunately, the descending force-time histories as well as the harmonic predictions for walking and negotiating stairs showed poor correlation with actual results.

The substantial increases in peak load, harmonic amplitudes and group loading effects should concern structural engineers since the push for aesthetically pleasing structures is continuing to reduce fundamental natural frequencies. This thesis has shown that any staircase having a natural frequency less than 10 Hz may be dynamically responsive to pedestrians and produce unacceptable levels of vibration.

Further research should also be conducted into quantifying acceptable vibration levels for these structures. Preliminary research has shown that the topic of acceptable vibration levels is extremely complicated and warrants a detailed and lengthy study of its own.

REFERENCES

Bishop, N.W.M., Willford, M., and Pumphrey, R. (1993). *Multi-Person Excitation of Modern Slender Staircases.* Engineering for Crowd Safety. Elsevier Science Publishers. Amsterdam. Pp.399-408.

Bobbert, M.F., Schamhardt, C., and Nigg, M. (1991). *Calculation of Vertical Ground Reaction Force Estimates During Running from Positional Data..* Journal of Biomechanics. Vol.24. No.12. pp.1095-1105.

Bobbert, M.F., Yeadon, M.R., and Nigg, M. (1992). *Mechanical Analysis of the Landing Phase in Heel-Toe Running.* Journal of Biomechanics. Vol.25. No.3. pp.223-234.

Dempster, R. and Gaughran, G.R.L. (1967). *Properties of Body Segments based on Size and Weight.* American Journal of Anatomy. Vol.120. pp.33-54.

Ellingwood, B. and Tallin, A. (1984). *Structural Serviceability: Floor Vibrations.* Journal of Structural Engineering. Vol.110. No.2.

Kerr, S.C. and Bishop, N.W.M. (1997). *Human Induced Loading of Flexible Staircases.* Innovation in Civil and Structural Engineering. Mouchel Centenary Conference Proceedings. ISBN 0-948749-50-4 Pp. 311-318.

Rainer, J.H., Pernica, G., and Allen, D.E. (1988). *Dynamic Loading and Response of Footbridges.* Canadian Journal of Civil Engineering. Vol.15. Pp.66-71.

APPENDIX A

A

COMPUTER PROGRAMS

Flowchart for Harmonic.cpp Program

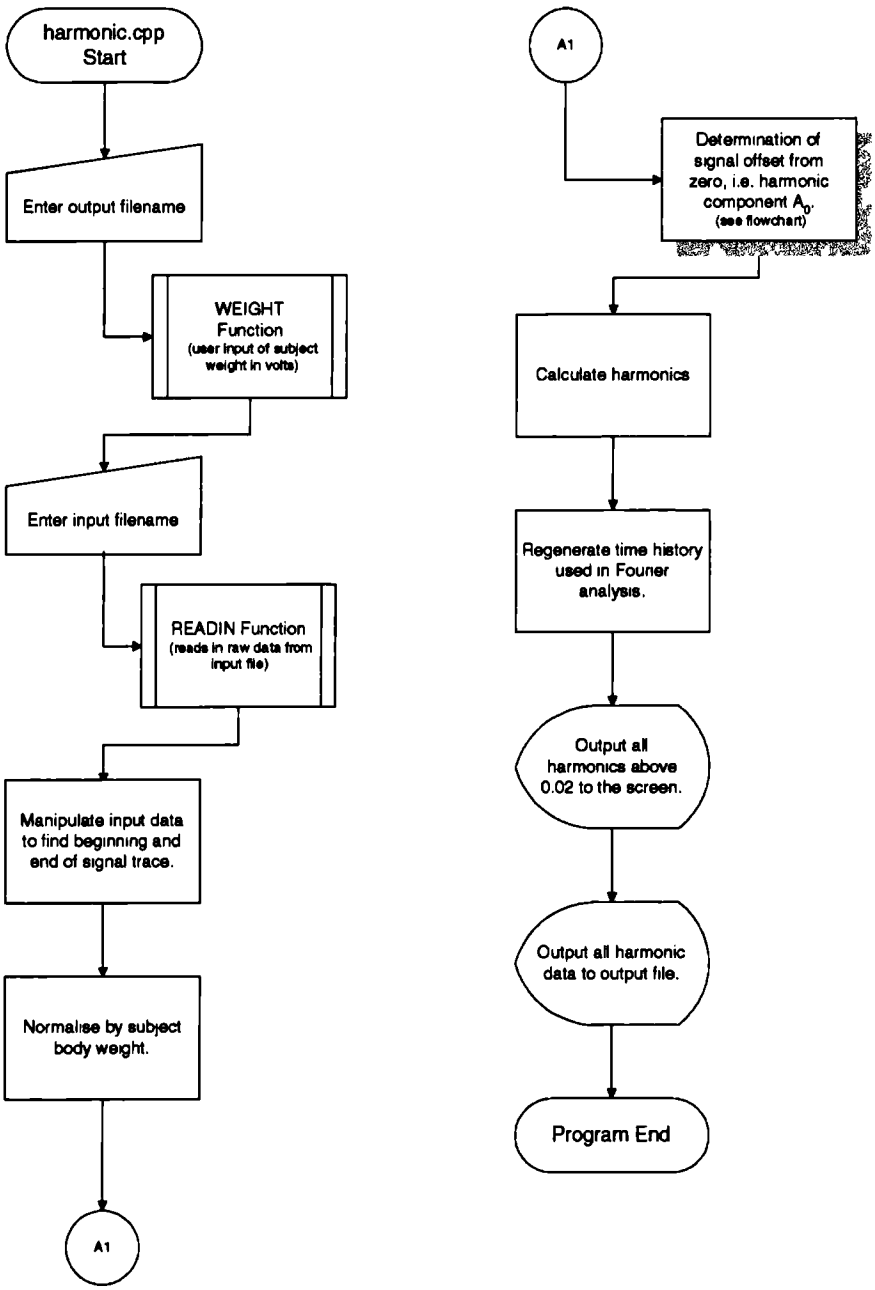

Azero Process

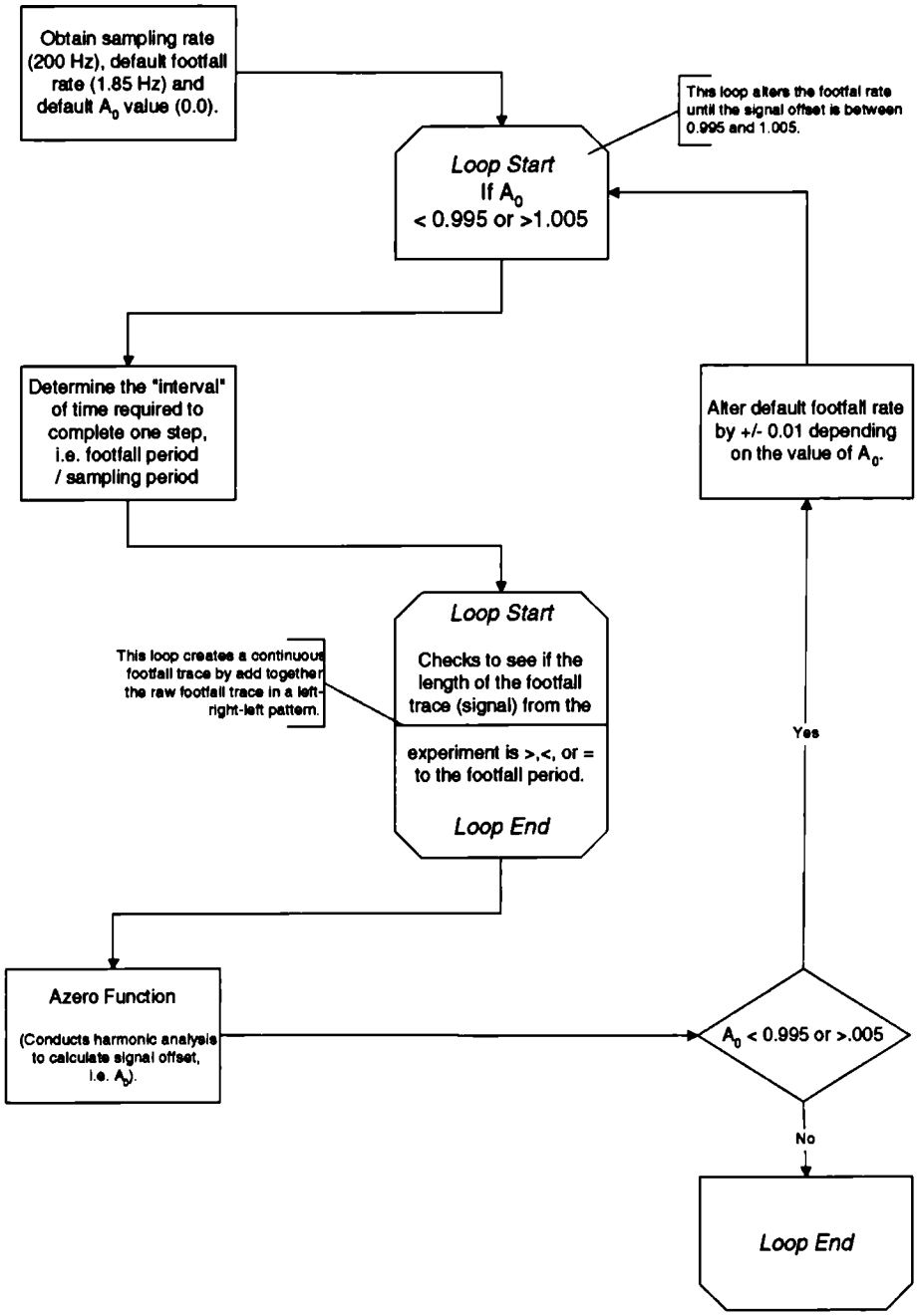


```
//*************************************************************************
//        Signal Regeneration and Harmonic Calculation Program
//        harmonic.cpp
//        Version 1.0         25/11/96
//        Version 2.0         10/01/97
//        Takes input from an nCode DAC file binary format
//        and generates a continuous signal trace assuming the average value of the
//        signal trace equals the subjects body weight. It then calculates the signal
//        harmonics using Fourier analysis.
//*************************************************************************


#include <iostream.h>
#include <fstream.h>
#include <iomanip.h>
#include <stdio.h>
#include <stdlib.h>
#include <string.h>
#include <math.h>
```

```
//char *INPUT_FILE ();                                          //INPUT FILE function
float GET_WEIGHT();                                             // GET WEIGHT function
float (*READIN(char *path))[2];                                 // READIN function
float MAXMIN(float input[][2],int first,int last,int opt);      // MAXMIN function
float AZERO(float thistory[600][2],int interval,float stept);   // AZERO function

float (*input)[2];
float thistory[600][2]={0.0};
float numpts={0.0};
float samplef={0.0}, samplet={0.0};
float stepf={1.80}, stept={0.0};
float zerooff={0.0};
float Azero={0.0};
char *path;
int interval,numpoints;
int first={0}, last={0};

int main ()
 {
        char output[80]= 2stair.asc ;
        //cout<<"Enter the output file name => ';                //  opening an output file
        //cin>>output;

        ofstream outfile(output,ios::app);
        float weight;
        weight=GET_WEIGHT();

        char subdir[10];//="14_5_97";
        char slash[2]= "\\';
        char intro[5];//="717n";
        int opt;//={2};
        int opt1;//={2};
        int exnum={0};
        int exclude[30];
        int largest;//={2};
        int beg={0}, end={0};
        int count={0};
        int i={0},j={0},k={0},n={0};

        char *new_fnum[30]={"\0","\0","\0","\0","\0","\0","\0","\0","\0","\0",
                            "\0","\0","\0","\0','\0','\0","\0","\0","\0",
                            "\0','\0','\0","\0","\0","\0","\0 ,'\0","\0","\0 ,
                            };

        char *fnum[30]={"0101.dac","0201.dac","0301.dac","0401.dac",
                        "0501.dac","0601.dac","0701.dac","0801.dac",
                        "0901.dac","1001.dac","1101.dac','1201.dac',
                        "1301.dac","1401.dac","1501.dac","1601.dac",
                        "1701.dac","1801.dac","1901.dac","2001.dac',
                        "2101.dac","2201.dac",'2301.dac', 2401.dac",
                         2501.dac","2601.dac", 2701.dac , 2801.dac",
                        "2901.dac","3001.dac",        };

        char path[80]="c:\\usr\\kerr\\walkfile\\";
        cout<<"\nThe path to the data files is assumed to be "<<path;
        cout<<'\n\nEnter the sub-directory to the data files (ie 9_12_96).    ';
        cin>> subdir;
        cout<<'\nEnter the first part of the data files (ie 124n)   ";
        cin>> intro;
        cout<<"\nThe data files are assumed to end with  01.dac'    ";
        cout<<"\n\nWhat is the largest file number (ie 5, 10, 20, etc ...)    ";
        cin>> largest;
        cout<<"\nDo you wish to use all "<<largest<<" files (1) or exclude some (2)."
                <<"\nEnter a number                                                  ";
        cin>> opt;

        switch (opt)
        {
        case 1:
                for(i=0;i<largest;i++)
                        new_fnum[i]=fnum[i];
                break;
        case 2:
                cout<<'\nDo you wish to exclude a range of files (1) or individual files (2).\nEnter a number
        ";
                cin>> opt1;
                switch (opt1)
                {
                case 1:
                        cout<<'\nEnter the first file number in your range (ie 1, 4, 10, etc...)        ;
                        cin>> beg;
                        cout<< \nEnter the last file number in your range to exclude\n'
                                <<'(Cannot be the same as the first).                                  ";
                        cin>> end;

                        for(i=0;i<(largest-(end-beg));i++)
                        {
                                if(i==(beg-1))
                                {
                                        j+=((end-beg)+1);
                                        count++;
                                        continue;
                                }
                                new_fnum[i-count]=fnum[j];
                                j++;
                        }
                        break;

                case 2:
```

```
                cout<<'\nHow many files do you wish to exclude.   ";
                cin>> exnum;
                for(i=0;i<exnum;i++)
                {
                        cout<< \nEnter a file number (ascending order)    ";
                        cin>>  exclude[i];
                }


                for(i=0;i<largest;i++)
                {
                        if(i==(exclude[j+count i]-1))
                        {
                                j++;
                                count++;
                                continue;
                        }
                        new_fnum[i-count]=fnum[j];
                        j++;
                }
                break;
        }
        break;
}


strcat(path,subdir);
strcat(path,slash);
strcat(path,intro);

char fname[30][80];

for(n=0;n<(largest-(end-beg)-exnum);n++) if(strlen(new_fnum[n])==8)
{
        strcpy(fname[n],path);
        strcat(fname[n],new_fnum[n]);

        input=READIN(fname[n]);
        numpts=input[0][0];
        samplef=input[0][1];


        for (i=1;i<=numpts;i++)
        {
                input[i-1][0]=input[i][0];
                input[i-1][1]=input[i][1];
        }


        zerooff=(input[0][1]+input[1][1])/2;
        for (j=0;j<=1;j++)
        {
                for (i=0;i<numpts;i++)        // rough zeroing of data
                {
                        input[i][1]-=zerooff;
                }

                for (i=0;i<numpts;i++)// finds the first and last data point of the "camel hump"
                {

                        if((input[i][1]<=0.05)&&(input[i+1][1]>0.05)&&(input[i+10][1]>0.1))
                                first=i;
                        else
                        {
                        if((input[i][1]>0.1)&&(input[i+1][1]<=0.1)&&(input[i+10][1]<=0.1))
                                last=i+5;
                        }
                }
                zerooff=input[first][1];      // fine zeroing ...
        }

        //last=numpts-10;
        for (i=0;i<=numpts;i++)
        {

                input[i][1]/=weight;          // normalizes input values by body weight
                input[i][0]=-first*(1/samplef)+i*(1/samplef);//set input[first][0] equal to time zero
        }
        float temp=input[first][0];

        for (i=numpts;i<(2*numpts+10);i++)               //  pad out input with extra zeros
        {                                                //  just over double the trace length
                input[i][0]=input[i-1][0]+(1/samplef);
                input[i][1]=0.0;
        }
        //*****************************************
        //        AUTOMATION LOOP BEGINS
        //        For iterating Azero until it is 1.00


        float thistory[600][2]={0.0};
        autoloop:
        if(Azero<0.995 || Azero>1.005)
        {

        samplet=1/samplef;                    /* sampling period and frequency */
        stept=1/stepf;
        interval=int(stept/samplet);/* first X points before overlap begins i.e. input[interval][0] */
        numpoints=3*interval;/* for generating 3 steps of information for final time history trace */
```

```
        if((input[last][0]-input[first][0])>stepf)       /* overlap ... cals all points except last */
        {
                for(i=0;i<=interval;i++)
                {
                        thistory[i][0]=input[i+first][0]+stepf;
                        thistory[i][1]=input[first+i][1]+input[first+interval+i+1][1]
                         +((input[first+interval+i][1]-input[first+interval+i+1][1])
                         *(input[first+interval+i+1][0]-thistory[i][0]))
                         /(input[first+interval+i+1][0]-input[first+interval+i][0]);
                }
        }

        if((input[last][0]-input[first][0])<stepf) /* no overlap ... cals all points except last */
        {
                for(i=0;i<=interval;i++)
                {
                        thistory[i][0]=input[first+i][0]+stepf;
                        thistory[i][1]=input[first+i][1];
                }
        }

        if((input[last][0]-input[first][0])==stepf) /* concurrent ... cals all points except last */
        {
                interval=interval-1;
                for(i=0;i<=interval;i++)
                {
                        thistory[i][0]=input[first+i][0]+stepf;
                        thistory[i][1]=input[first+i][1];
                }
        }

        for(i=interval+1;i<numpoints;i++)        /* produces the rest of the time history by repeating the
                                                 points calculated previously */
        {
                thistory[i][0]=thistory[i-(interval+1)][0]+stepf;
                thistory[i][1]=thistory[i-(interval+1)][1];
        }


        Azero=AZERO(thistory,interval,stepf);   // calls AZERO function

        if((Azero-1)>=0.005)
                stepf-=0.01;
        else if((Azero-1)<(-.005))
                stepf+=0.01;
        goto autoloop;
        }

        //      AUTOMATION LOOP ENDS
        //*****************************************


 ************************************************************************************************
// This section calculates A and B for the first (sample freq / 2) harmonics (Fourier Coefficient)
//  It combines A and B into coefficient C plus a phase shift.

        const double pi=3.141592654;
        double A[200]={0.0}, B[200]={0.0}, C[200]={0.0}, phase[200]={0.0};
        double Atemp, Btemp, Ctemp;
        double thistoryregen[600]={0.0};
        double har={0.02};

        A[0]=Azero;

        for(i=1;i<((interval+1)/2);i++)         // calculates (samplef/stepf/2) harmonics
        {
                for(j=0;j<=interval;j++)
                {
                        Atemp=(thistory[j][1]*cos(2*pi*stepf*i*thistory[j][0]))
                                *(thistory[j+1][0]-thistory[j][0]);
                        A[i]+=Atemp;
                        Btemp=(thistory[j][1]*sin(2*pi*stepf*i*thistory[j][0]))
                                *(thistory[j+1][0]-thistory[j][0]);
                        B[i]+=Btemp;
                }
                A[i]=A[i]*(2/stepf);
                B[i]=B[i]*(2/stepf);
                C[i]=sqrt(A[i]*A[i]+B[i]*B[i]);
                phase[i]=atan(fabs(B[i]/A[i]))*(180/pi);
        }

        //=============================================
        // Regenerates the time signal from the harmonics

        for (i=0;i<numpoints;i++)
        {
                for (j=1;j<5 /*((interval+1)/2)*/;j++)
                {
                        Ctemp=A[j]*cos(2*pi*stepf*j*thistory[i][0])+
                                B[j]*sin(2*pi*stepf*j*thistory[i][0]);
                        thistoryregen[i]+=Ctemp;
                }
                thistoryregen[i]=thistoryregen[i]+Azero;
        }

        ofstream thout("thregen2.out );
        for (i=0;i<numpoints;i++) thout<<thistory[i][0]<<          "<<thistory[i][1]<<"
<<thistoryregen[i]<<"\n ;
```

```
                cout<<setprecision(2)<<setiosflags(ios::fixed);
                cout<<"\n\n"<<fname[n]<< \n\n"
                << First hump at '<<MAXMIN(input,first,last,1)<<' "<< Min is  <<MAXMIN(input,first,last,2)
                <<          <<"Last hump at  <<MAXMIN(input,first,last,3)<< \n\n'<< Overall max is
                "<<MAXMIN(input,first,last,4)
                << \n\n ;
                cout<<"Azero is "<<A[0]<<'    "<< Pace is  <<stepf<< \n\n ;

                for (i=1;i<=25;i++)
                {
                        if(C[i]>har)
                                cout<< A"<<i<<" = "<<A[i]<<   "<< B"<<i<<  =  <<B[i]<<"     "
                                        <<"C"<<i<<  =  <<C[i]<<        <<"phase <<i<<" =
                                        <<setprecision(0)<<setiosflags(ios::fixed)<<phase[i]<<  degs\n
                                        <<setprecision(2)<<setiosflags(ios::fixed);
                }
                char file[30][80];
                strcpy(file[n],intro);
                strcat(file[n],new_fnum[n]);

                outfile <<setprecision(2)<<setiosflags(ios::fixed)<<file[n]<<"         <<weight
                <<"       "<<MAXMIN(input,first,last,1)<<"        "<<MAXMIN(input,first,last,2)
                <<"       "<<MAXMIN(input,first,last,3)<<"        "<<stepf
                <<setprecision(2)<<setiosflags(ios::fixed)
                <<"       "<<C[1]<<"          "<<C[2]<<"          <<C[3]<<'          "<<C[4]<<          "
                <<setprecision(0)<<setiosflags(ios::fixed)<<phase[1]<<"     "
                <<phase[2]<<"       "<<phase[3]<<"      '<<phase[4]<< \n ;


        Azero=0.0;
        }

        outfile.close();


        return 0;

}

//============================================================================
//      GET_WEIGHT
//      Requests the subjects weight in volts
//============================================================================

float GET_WEIGHT()
{
        float weight;

        cout<<"\nEnter the weight in volts. => ";
        cin>>weight;
        //weight=1.6;
        cout<<"\n\n';

        return weight;
}

//============================================================================
//      READIN Function
//      Reads in a binary DAC file from nCode. These DAC and actually the converted
//      ADM files from the data acquisition stuff.
//
//============================================================================
#include <iostream.h>
#include <fstream.h>

float (*READIN(char *path))[2]
{
        float n[1000]={0};
        float inputt[800][2]={0.0};
        float numpts;
        float srate;
        int i={0};
        int count={0};
        ifstream in(path,ios::in | ios::binary);          // opening the input file
        if(!in)

        in.read((unsigned char *) &numpts, sizeof numpts);
        in.read((unsigned char *) &srate, sizeof srate);
        in.seekg(512,ios::beg);

        while(in.read((unsigned char *) &n, sizeof n));

//      float (*inputt)[2]= new float [numpts][2];

        inputt[0][0]=numpts;
        inputt[0][1]=srate;
        inputt[1][0]=0.0;

        for(i=0;i<50;i++)
        {
                if(n[i]==0.0) count++;
        }

        inputt[1][1]=n[count];

        for (i=(count+1);i<numpts;i++)
        {
                inputt[i-(count-1)][0]=inputt[i-(count)][0]+(1/srate);
                inputt[i-(count-1)][1]=n[i];
        }
```

```
        in.close;

        return inputt;

}


//=============================================================================
//      MAXMIN Function
//      Calculates the following depending on OPT :
//              opt=1     finds max value of first hump in single foot fall trace
//              opt=2     finds min value between first and second hump
//              opt=3     finds max value of second hump in single foot fall trace
//              opt=4     finds overall max value in single foot fall trace
//=============================================================================

float MAXMIN(float input[][2], int first, int last, int opt)
{
        int i;
        int band=((last-first)/8);
        float output=(0);

        switch(opt)
        {
        case 1:
                for (i=(first+band);i<=(first+3*band);i++)
                {
                        if(input[i][1]>output)
                        output=input[i][1];
                }
                break;
        case 2:
                output=1.0;
                for (i=(first+3*band);i<=(last-3*band);i++)
                {
                        if(input[i][1]<output)
                        output=input[i][1];
                }
                break;
        case 3:
                for (i=(last-3*band);i<=(last-band);i++)
                {
                        if(input[i][1]>output)
                        output=input[i][1];
                }
                break;
        case 4:
                for (i=first;i<=last;i++)
                {
                        if(input[i][1]>output)
                        output=input[i][1];
                }
                break;
        }

        return output;
}

// ============================================================================
//      AZERO Function
//      This function calculates A zero Fourier coefficient i.e. body weight
//=============================================================================

float AZERO(float thistory[600][2],int interval,float stept)
{
        int i;
        float Azero=(0.0);
        float striparea=(0.0);
        float totalarea=(0.0);

        for(i=0;i<=interval;i++)
        {
                striparea=((thistory[i][1]+thistory[i+1][1])/2)*(thistory[i+1][0]-thistory[i][0]);
                totalarea=totalarea+striparea;
        }
        Azero=(totalarea/stept);

        return Azero;
}
```

Flowchart for ms_thistory.cpp Program

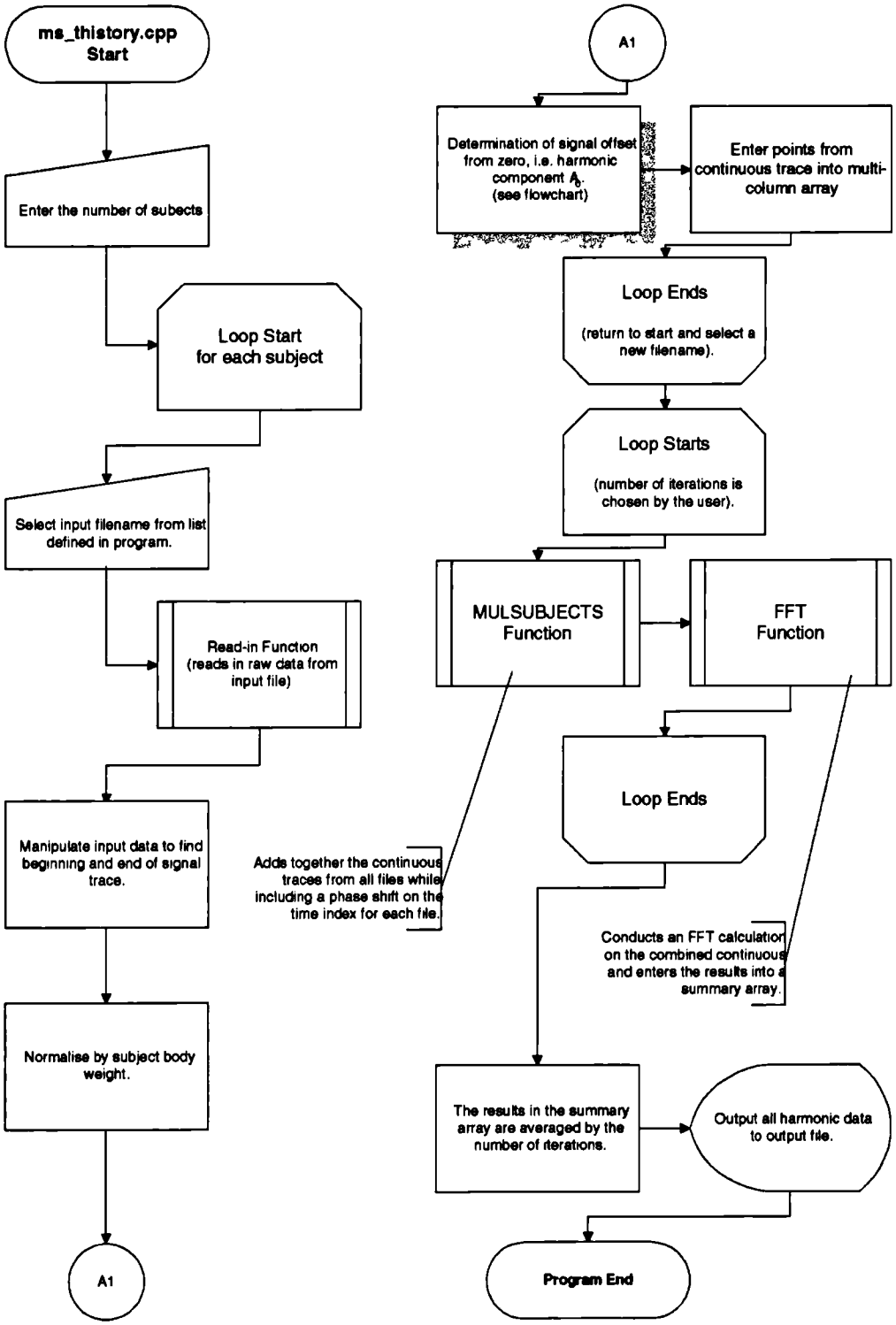

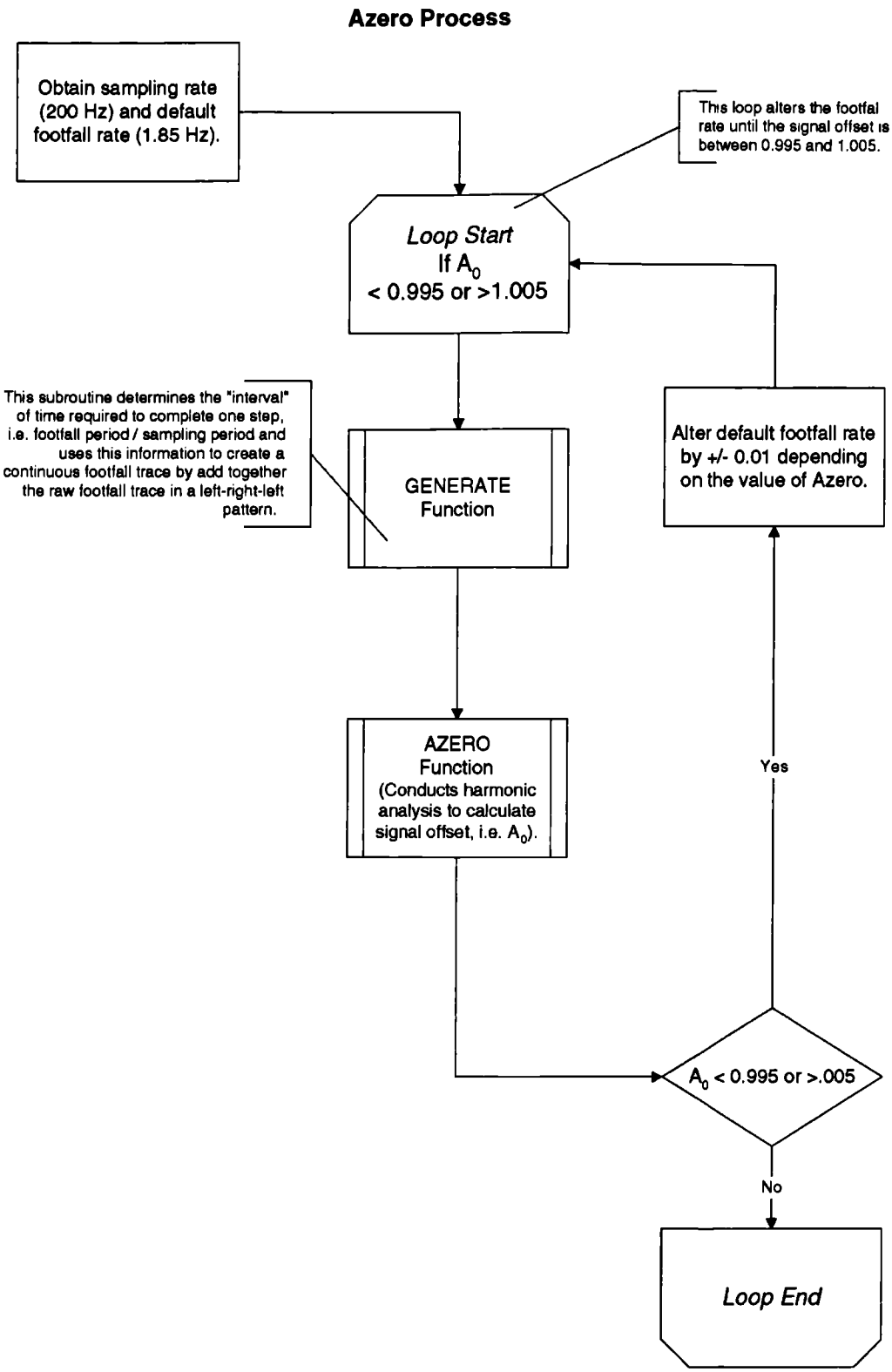
Azero Process
Obtain sampling rate (200 Hz) and default footfall rate (1.85 Hz).
This loop alters the footfal rate until the signal offset is between 0.995 and 1.005.
Loop Start
If A_0 < 0.995 or >1.005
This subroutine determines the "interval" of time required to complete one step, i.e. footfall period / sampling period and uses this information to create a continuous footfall trace by add together the raw footfall trace in a left-right-left pattern.
GENERATE Function
Alter default footfall rate by +/- 0.01 depending on the value of Azero.
AZERO Function (Conducts harmonic analysis to calculate signal offset, i.e. A_0).
Yes
A_0 < 0.995 or >.005
No
Loop End

```
//*****************************************************************************
//      Multi - Subject Time History Creation
//      ms_thistory.cpp        Original        7/2/97
//                             Vr. 2.0        29/6/97
//      Reads in many DAC files and adds them together with a phase shift to create
//      a single summated time history.  Then performs an FFT calculation for every
//      iteration and produces a single column of FFT magnitude points with a sample
//      rate of 40.96 cycles/second (use this number in nCode's ATD program).
//*****************************************************************************
#include <iostream.h>
#include <fstream.h>
#include <iomanip.h>
#include <stdio.h>
#include <stdlib.h>
#include <string.h>
#include <math.h>
#include <time.h>
#include "tal_lib.h"

float *READIN(char *fname);

float AZERO(float *thistory,int interval,float stept);

float *GENERATE(float input[],float stepf,float samplef,int first,int last);
void MULSUBJECTS(float *combined_thistory,float (*multi_thistory)[1200],float
samplet,int subnum,int interarray[]);

float temp1[1200]={0.0};
float input[600]={0.0};
float *raw_data=0;
float *thistory=0;
float multi_thistory[27][1200]={0.0};
float numpts[27]={0.0};
float samplef={0.0},samplet={0.0};
float stepf={2.0},stept={0.0};
float zerooff={0.0};
float Azero={0.0};
float ABCout={0.0};
int interarray[27]={0};
int interval,numpoints;
int first={0}, last={0};
int subnum={0};
int i,j,n,mm;

int const NN={131072};

float fin_thistory[131072]={0.0};
float count[131072]={0.0};

char fname[27][80] =//{"c:\\usr\\kerr\\walkfile\\30degu\\a3u0401.dac"};
                      {"c:\\usr\\kerr\\walkfile\\30degu\\c1u0501.dac",
                      "c:\\usr\\kerr\\walkfile\\30degu\\a3u0501.dac",
                      "c:\\usr\\kerr\\walkfile\\30degu\\a3u0401.dac",
                      "c:\\usr\\kerr\\walkfile\\30degu\\a2u0501.dac",
                      "c:\\usr\\kerr\\walkfile\\30degu\\d1u0401.dac",
                      "c:\\usr\\kerr\\walkfile\\30degu\\a2u0801.dac",
                      "c:\\usr\\kerr\\walkfile\\30degu\\a7u0501.dac",
                      "c:\\usr\\kerr\\walkfile\\30degu\\a7u1101.dac",
                      "c:\\usr\\kerr\\walkfile\\30degu\\a1u0701.dac",
                      "c:\\usr\\kerr\\walkfile\\30degu\\a2u0901.dac",
                      "c:\\usr\\kerr\\walkfile\\30degu\\c2u0201.dac",
                      "c:\\usr\\kerr\\walkfile\\30degu\\c7u0301.dac",
                      "c:\\usr\\kerr\\walkfile\\30degu\\c6u0401.dac",
                      "c:\\usr\\kerr\\walkfile\\30degu\\a7u0201.dac",
                      "c:\\usr\\kerr\\walkfile\\30degu\\a3u1001.dac",
                      "c:\\usr\\kerr\\walkfile\\30degu\\b8u0201.dac",
                      "c:\\usr\\kerr\\walkfile\\30degu\\a8u0301.dac",
                      "c:\\usr\\kerr\\walkfile\\30degu\\a2u1001.dac",
                      "c:\\usr\\kerr\\walkfile\\30degu\\d3u1401.dac",
                      "c:\\usr\\kerr\\walkfile\\30degu\\a2u0601.dac",
                      "c:\\usr\\kerr\\walkfile\\30degu\\b5u0201.dac",
                      "c:\\usr\\kerr\\walkfile\\30degu\\c7u0101.dac",
                      "c:\\usr\\kerr\\walkfile\\30degu\\d1u1601.dac",
                      "c:\\usr\\kerr\\walkfile\\30degu\\d1u0101.dac",
                      "c:\\usr\\kerr\\walkfile\\30degu\\a1u0501.dac",
                      "c:\\usr\\kerr\\walkfile\\30degu\\d1u0301.dac",
                      "c:\\usr\\kerr\\walkfile\\30degu\\a3u0601.dac"};

float weight[27]=     {1.33,2.72,2.72,1.7,1.58,1.7,1.54,1.54,1.57,
```

```
                    1.70,1.53,1.45,1.80,1.54,2.72,1.33,1.72,1.70,
                    1.70,1.70,1.81,1.45,1.58,1.58,1.57,1.58,2.72};

//float weight[27]={2.72};


int main ()
 {
       subnum=9;                      // ENTER THE NUMBER OF SUBJECTS!

       float *outputdata;
       outputdata=new float[NN];
       complex16 *ff;
       ff=new complex16[NN];

       for(n=0;n<subnum;n++)
       {
              Azero=0.0;
              raw_data=READIN(fname[n]);
              numpts[n]=raw_data[0];
              samplef=raw_data[1];

              for(i=0;i<600;i++) input[i]=0.0;      // reset input array

              for (i=2;i<numpts[n]+4;i++)
              {
                     input[i-2]=raw_data[i];
              }

              zerooff=(input[1]+input[2])/2;        // rough zeroing of data

              for (i=0;i<numpts[n];i++)     input[i]-=zerooff;

              for (i=0;i<numpts[n];i++)     // finds the first and last data points
              {                             // of the "camel hump"

                     if((input[i]<=0.05)&&(input[i+1]>0.05)&&(input[i+10]>0.1))
                     first=i;
                     else if((input[i]>0.1)&&(input[i+1]<=0.1)&&(input[i+10]<=0.1))
                     last=i+5;
              }

              zerooff=input[first];                 // fine zeroing ...

              for (i=0;i<numpts[n];i++)  input[i]/=weight[n];      //normalizes input
                                                                   values by body weight




       //*************************************************************************
       //      AUTOMATION LOOP BEGINS
       //      For iterating Azero until it is 1.00

              autoloop:
              if(Azero<0.995 || Azero>1.005)
              {
                     samplet=1/samplef;
                     // sampling period and frequency
                     stept=1/stepf;
                     interval=int(stept/samplet);
                     // first X points before overlap begin, input[interval][0]
                     thistory=GENERATE(input,stepf,samplef,first,last);
                     // calls GENERATE function
                     Azero=AZERO(thistory,interval,stept);
                     // calls AZERO function

                     for(i=0;i<1200;i++)  temp1[i]=thistory[i];
                     // The above line is here so I can look at thistory
                     // at this intermediate step.
                     if((Azero-1)>=0.005)          stepf-=0.01;
                     else if((Azero-1)<(-.005))    stepf+=0.01;

                     goto autoloop;
              }


              //      AUTOMATION LOOP ENDS
```

```
        //*************************************************************************

                interarray[n]=interval; //needed to get proper phase in MULTISUBJECTS
                for(i=0;i<1200;i++)    multi_thistory[n][i]=temp1[i];

        }

        time_t tnow;

        srand(time(&tnow));

        float (*pmth)[1200]=0;
        pmth=multi_thistory;
        for(i=0;i<NN;i++)ff[i].x=0.0;          // fin_thistory[i]=0.0;

        int iteration;
        iteration=100;
        for (mm=0;mm<iteration;mm++)
        {
                cout<<'\niteration     '<<mm;
                //combined_thistory=MULSUBJECTS(pmth,samplet,subnum,interarray);
                MULSUBJECTS(outputdata,pmth,samplet,subnum,interarray);

                for(i=0;i<NN;i++)
                {
                        ff[i].x=outputdata[i];
                        ff[i].y=0.0;
                }

                FFT1(ff,NN,1);                 //conducts IFFT

                for(i=0;i<NN;i++) fin_thistory[i]=sqrt(ff[i].x*ff[i].x+ff[i].y*ff[i].y);
                for(i=1;i<NN;i++)
                {
                        fin_thistory[i]/=(fin_thistory[0]*0.5);
                        fin_thistory[i]=fin_thistory[i]*subnum;
                        count[i]+=fin_thistory[i];
                }
                count[0]=0.0;
        }
        for(i=0;i<NN;i++)      count[i]/=iteration;

        cout<<'\n\n';
        //for(i=0;i<NN;i++) fin_thistory[i]/=iteration;


        ofstream outfile('27_0pi.asc');//open ASCII file for combined time history



        for(i=0;i<4000;i++)
        {
        outfile <<setprecision(4)<<setiosflags(ios::fixed)<<i*(samplef/NN)<<'       '
                        <<setprecision(5)<<setiosflags(ios::fixed)<<count[i]<<'\n';
        }
        outfile.close;

        cout<<'\nAll finished!\n';

        delete [] outputdata;
        delete [] ff;

        return 0;

}
//=============================================================================
//      READIN Function
//      Reads in a binary DAC file from nCode. These DAC and actually the converted
//      ADM files from the data acquisition stuff.
//
//=============================================================================

float *READIN(char *fname)
{
        float n[1000]={0};
        float inputt[600]={0.0};
        float numpt;
        float srate;
        int i={0};
        int count={0};
```

```
        ifstream in(fname,ios::in | ios::binary);    // opening the input file
        if(!in)

        in.read((unsigned char *) &numpt, sizeof numpt);
        in.read((unsigned char *) &srate, sizeof srate);
        in.seekg(512,ios::beg);

        while(in.read((unsigned char *) &n, sizeof n));

        inputt[0]=numpt;
        inputt[1]=srate;

        for(i=0;i<50;i++)  if(n[i]==0.0) count++;    // checks to see if any zero at the
        beginning

        for (i=(count+2);i<numpt+2;i++)  inputt[i-count]=n[i-2];// copies fine input to
        array inputt

        in.close;

        return inputt;
}

//============================================================================
//      GENERATE Function
//      Reads in array "input" and regenerated a continuous time history
//============================================================================

float *GENERATE(float input[],float stepf,float samplef,int first,int last)
{
        float shistory[1200]={0.0};

        samplet=1/samplef;            // sampling period and frequency
        stept=1/stepf;
        interval=int(stept/samplet);  // first X points before overlap
        begins(input[interval])

        if((last-first)*samplet>stept)// OVERLAP ... cals all points
        {
                for(i=0;i<interval;i++)
                {
                        shistory[i]=input[first+i]+input[first+interval+i+1]
                           +((input[first+interval+i]-input[first+interval+i+1])
                           *((first+interval+i+1)*samplet-((i+first)*samplet+stept)))
                           /((first+interval+i+1)*samplet-((first+interval+i)*samplet));
                }
        }

        if((last-first)*samplet<stept)// NO OVERLAP ... cals all points except last
        {
                for(i=0;i<interval;i++)
                {
                        shistory[i]=input[first+i];
                }
        }

        if((last-first)*samplet==stept)// CONCURRENT ... cals all points except last
        {
                for(i=0;i<=interval;i++)  shistory[i]=input[first+i];
        }


        return shistory;
}



// ============================================================================
//      AZERO Function
//      This function calculates A zero Fourier coefficient i.e. body weight
//============================================================================

float AZERO(float *thistory,int interval,float stept)
{
        int i;
        float Azero={0.0};
        float striparea={0.0};
        float totalarea={0.0};

        for(i=0;i<interval-1;i++)
```

```
        {
                striparea=((thistory[i]+thistory[i+1])/2)*samplet;
                totalarea+=striparea;
        }
        Azero=(totalarea/stept);

        return Azero;
}

// ============================================================================
//      MULSUBJECTS Function
//      Multiple subjects function ... used to reconfigure the thistory array from
//      that of one subject A to that of a many subject A's
//============================================================================

//float *MULSUBJECTS(float (*multi_thistory)[1200],float samplet,int subnum,int
interarray[])
void MULSUBJECTS(float *combined_thistory, float (*multi_thistory)[1200],float
samplet,int subnum,int interarray[])

{
        int phase={0}, offset={0};
        int i,j;
        int count={0};
//      float trace[27][131072]={0.0};
//      float com_thistory[131072]={0.0};

        float (*trace)[27];
        trace=new float[NN][27];
        float *com_thistory;
        com_thistory=new float[NN];

        for (i=0;i<NN;i++)com_thistory[i]=0.0;

        for (i=0;i<subnum;i++)
        {
                count=1;
                float random=rand();
                phase=(random/32767)*(interarray[i]);
                offset=0;
                for (j=0;j<NN;j++)
                {
                        if((j+phase)==count*interarray[i])
                        {
                                offset=count*interarray[i];
                                count++;
                        }
                        trace[j][i]=multi_thistory[i][j+phase-offset];
                }

        }


        for (j=0;j<NN;j++)
        {
                for (i=0;i<subnum;i++)  com_thistory[j]+=trace[j][i];
                combined_thistory[j]=com_thistory[j];
        }

        delete [] com_thistory;
        delete [] trace;

        //return com_thistory;
        return ;
}
```

Flowchart for tforce.cpp Program

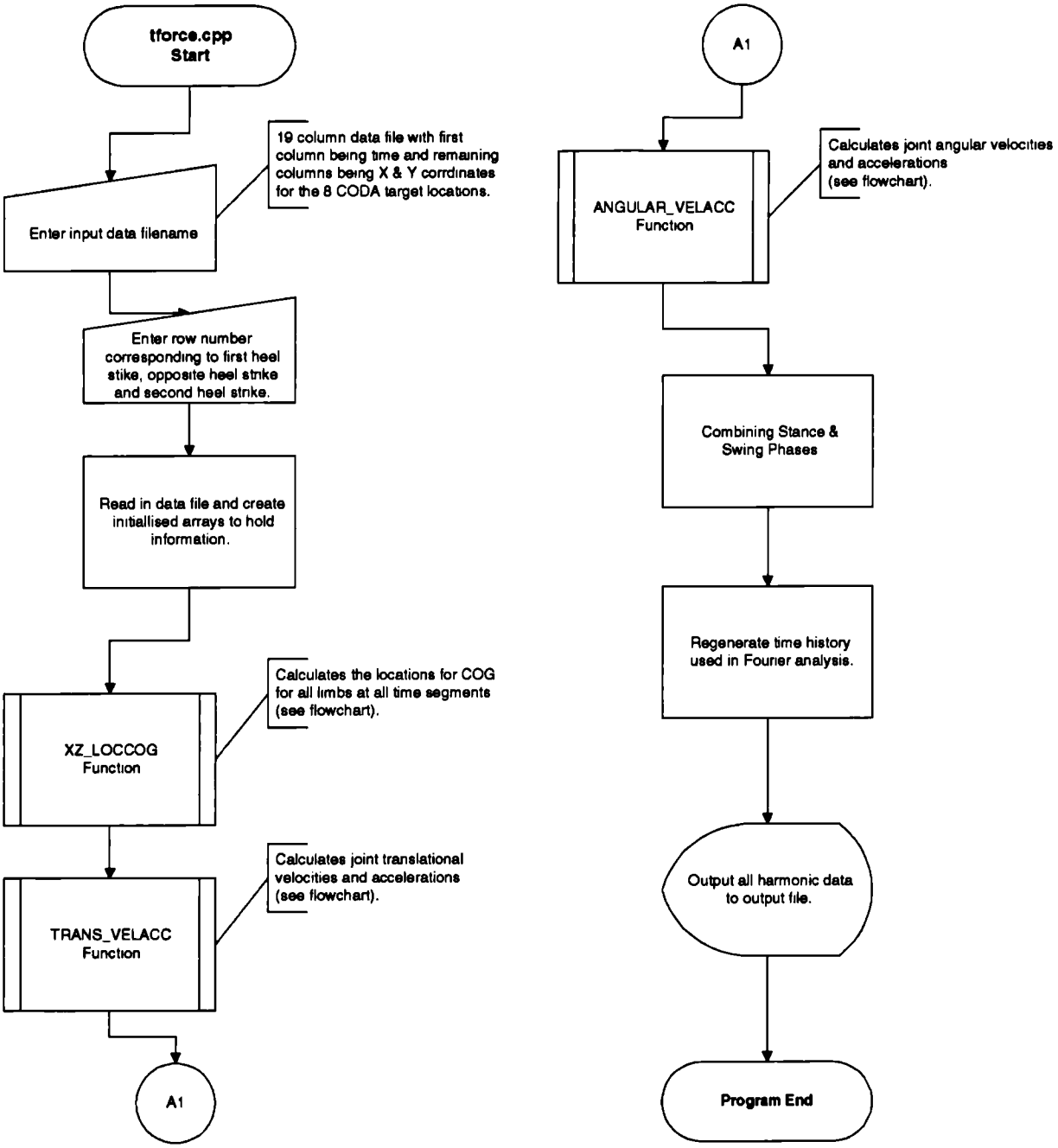

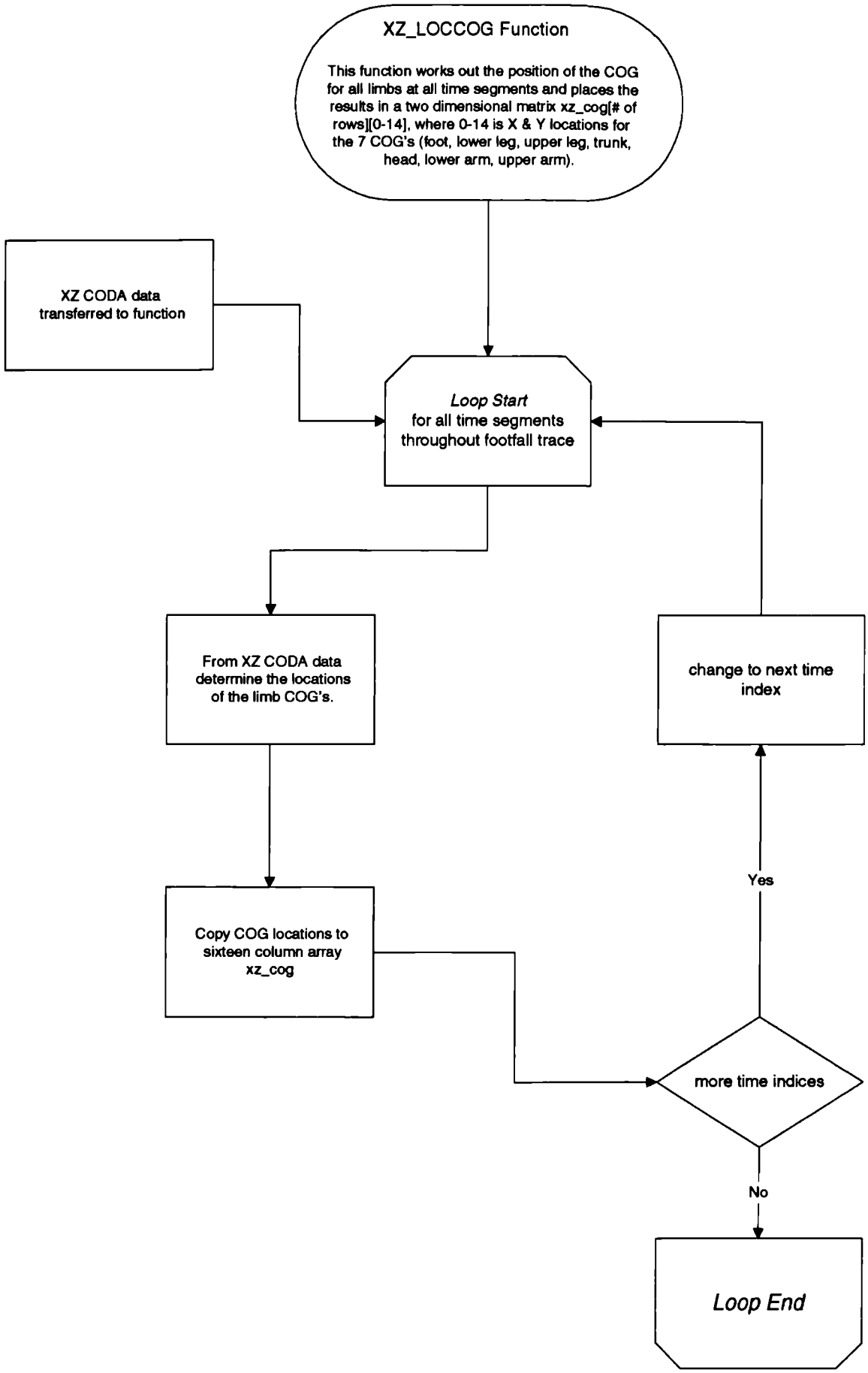
XZ_LOCCOG Function
This function works out the position of the COG for all limbs at all time segments and places the results in a two dimensional matrix xz_cog[# of rows][0-14], where 0-14 is X & Y locations for the 7 COG's (foot, lower leg, upper leg, trunk, head, lower arm, upper arm).
XZ CODA data transferred to function
Loop Start
for all time segments throughout footfall trace
From XZ CODA data determine the locations of the limb COG's.
change to next time index
Copy COG locations to sixteen column array xz_cog
Yes
more time indices
No
Loop End

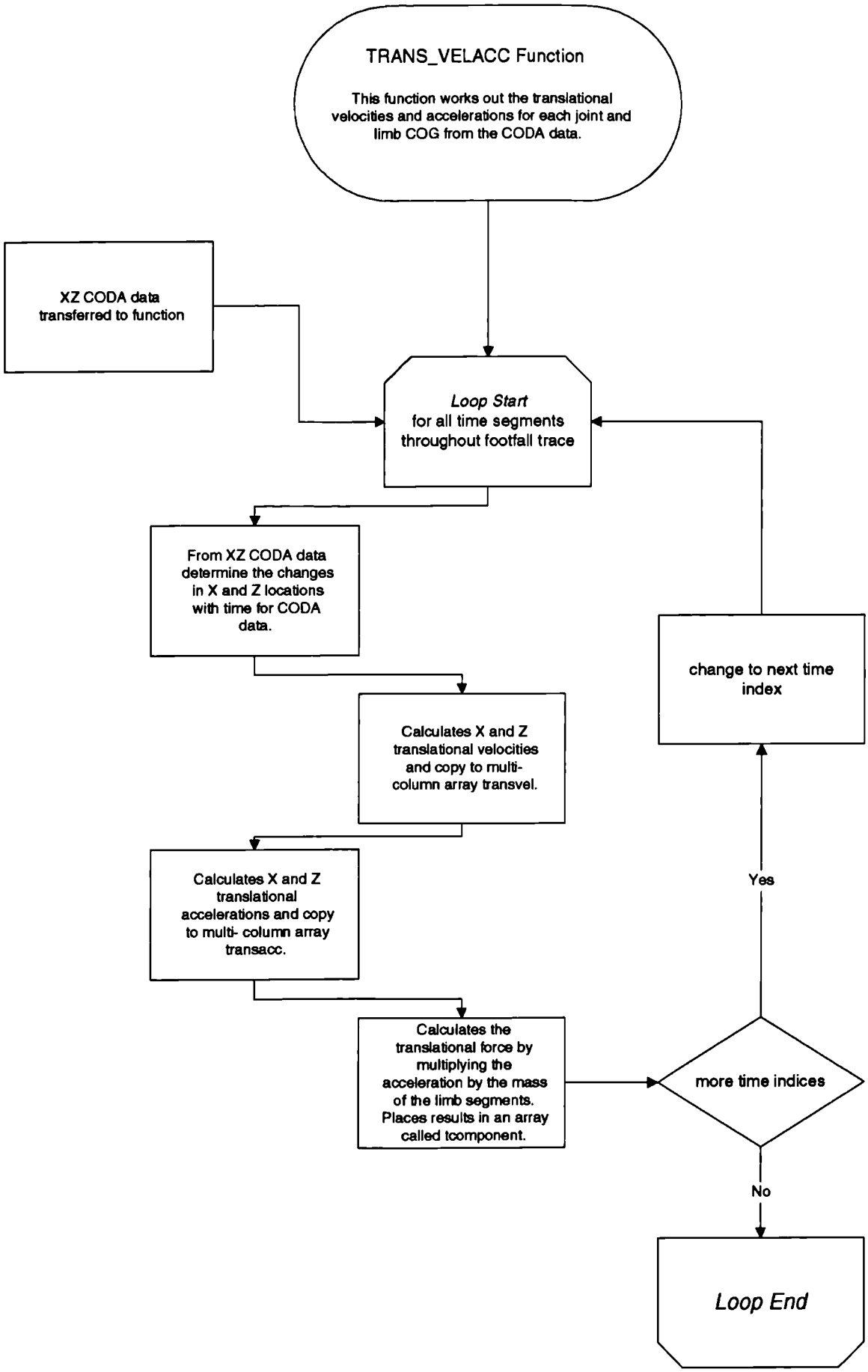
TRANS_VELACC Function
This function works out the translational velocities and accelerations for each joint and limb COG from the CODA data.
XZ CODA data transferred to function
Loop Start
for all time segments throughout footfall trace
From XZ CODA data determine the changes in X and Z locations with time for CODA data.
Calculates X and Z translational velocities and copy to multi-column array transvel.
Calculates X and Z translational accelerations and copy to multi- column array transacc.
Calculates the translational force by multiplying the acceleration by the mass of the limb segments. Places results in an array called tcomponent.
more time indices
Yes
No
change to next time index
Loop End

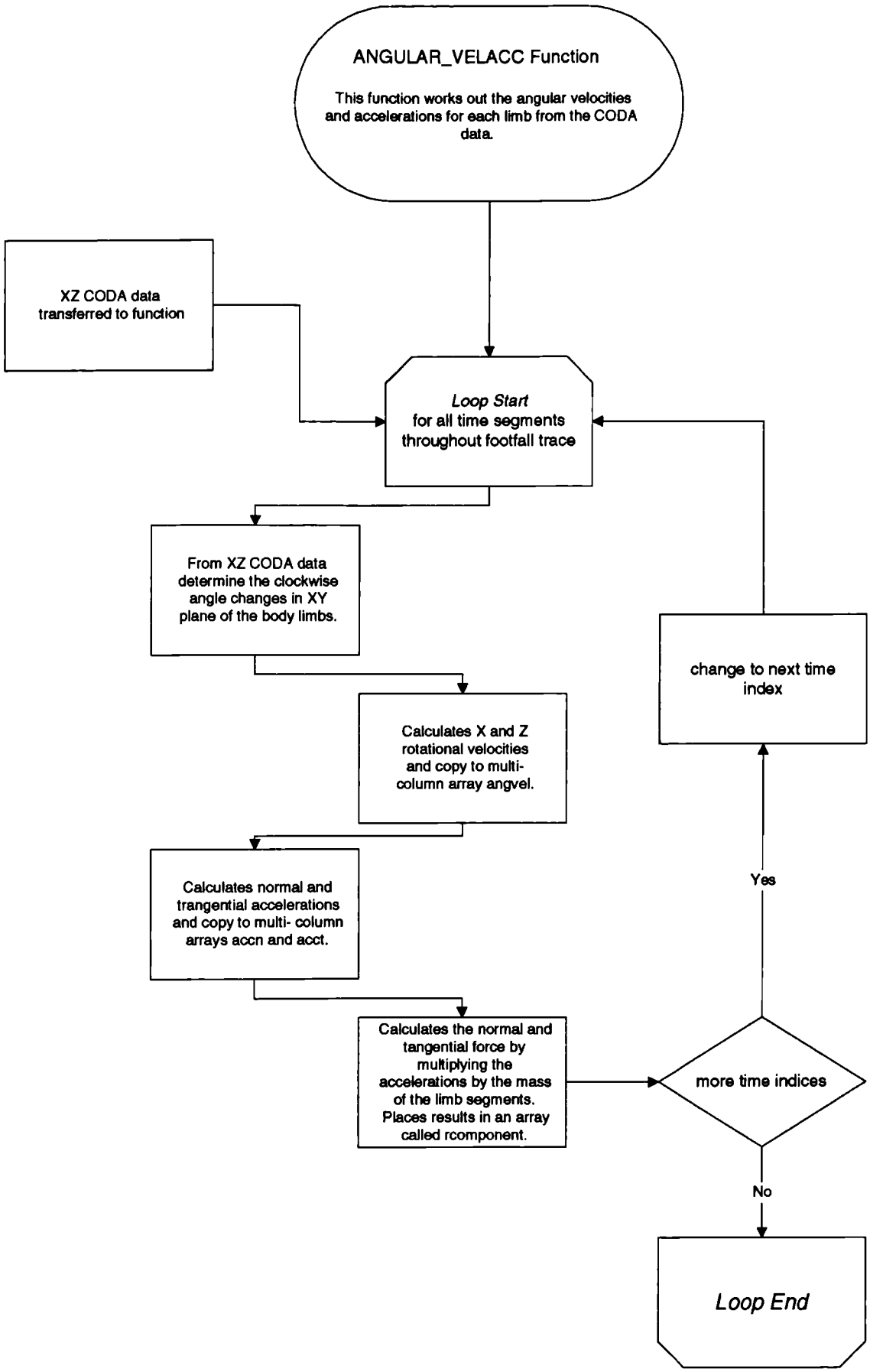
ANGULAR_VELACC Function
This function works out the angular velocities and accelerations for each limb from the CODA data.
XZ CODA data transferred to function
Loop Start
for all time segments throughout footfall trace
From XZ CODA data determine the clockwise angle changes in XY plane of the body limbs.
Calculates X and Z rotational velocities and copy to multi-column array angvel.
Calculates normal and trangential accelerations and copy to multi- column arrays accn and acct.
Calculates the normal and tangential force by multiplying the accelerations by the mass of the limb segments. Places results in an array called rcomponent.
more time indices
Yes
No
change to next time index
Loop End

```
//*****************************************************************************
//      Total Analytical Force Calculation
//      tforce.cpp
//      Vr. 1.0 25/8/97
//      Reads in an nineteen column (1st column is time) of body X and Y coordinates
//      and uses them to calculated the force at each centre of gravity for trans-
//      lational and rotational motions of each limb.
//*****************************************************************************

#include <iostream.h>
#include <fstream.h>
#include <iomanip.h>
#include <stdio.h>
#include <stdlib.h>
#include <string.h>
#include <math.h>
#include <time.h>

#define PI 3.1415926535f

char data_file[80];//="b5_1550b.dat";        // Change file name here
int i=0,j=0;
int fhs=0;
int shs=0;
int ohs=0;

void XZ_LOCCOG(float (*xz_cog)[17],float (*data)[28],int lastrow);
void TRANS_VELACC(float tforce[],float (*xz_cog)[17],float (*data)[28],float
(*tcomponent)[13],float (*transvel)[28],float (*transacc)[28],int lastrow);
void ANGULAR_VELACC(float rforce[],float (*data)[28],float (*rcomponent)[13],float
(*transacc)[28],float (*angvel)[8],float (*angacc)[8],float (*cogaccAB)[8],int lastrow);


int main()
{
        cout<<"\n\nWhat is the name of your data file?       ";
        cin>>data_file;
        cout<<"\n\nWhich row does right heel strike start (FHS)?           ";
        cin>>fhs;
//      fhs = 63;               //for stair down 8
//      fhs = 42;               //for walkfor5
        cout<<"\nWhich row does left heel strike start (OHS)?             ";
        cin>>ohs;
//      ohs = 164;              //for stair down 8
//      ohs = 140;
        cout<<"\nWhich row does second right heel strike start (SHS)?      ";
        cin>>shs;
//      shs = 265;              //for stair down 8
//      shs = 238;
        int count=0;
        float (*g)[28];         // reads in data file
        g = new float [500][28];
        ifstream infile(data_file);
        while(!infile.eof())
        {
                for (j=0;j<28;j++) infile>>g[i][j];
                for (j=1;j<28;j++) g[i][j] /=1000.0f; // change from mm to m
        //      for (j=1;j<28;j+=3)    g[i][j] =-g[i][j];     // for new files changes
        sign of X (CODA LHR to RHR)
                for (j=2;j<28;j+=3)    g[i][j] =-g[i][j];     // for old files changes
        sign of Y (CODA LHR to RHR)
                i++;
                count++;
        }

        count -=2;

        float (*transacc)[28];          // creates global array to hold trans acc
        transacc = new float [count][28];

        float (*transvel)[28];          // creates global array to hold trans vel
        transvel = new float [count][28];

        float (*angacc)[8];             // creates global array to hold rotational acc
        angacc = new float [count][8];

        float (*angvel)[8];             // creates global array to hold rotational vel
        angvel = new float [count][8];

        float (*cogaccAB)[8];           // acceleration of A with respect to B
        cogaccAB = new float [count][8];
```

```
        float (*xz_cog)[17];   // creates global array to hold COG locations (X & Y)
        xz_cog = new float [count][17];

        float *rforce;
        rforce = new float [count];

        float *tforce;
        tforce = new float [count];

        float (*rcomponent)[13];
        rcomponent = new float [count][13];

        float (*tcomponent)[13];
        tcomponent = new float [count][13];

        for (i=0;i<count;i++)                          //initialise array
        {
                tforce[i] = rforce[i] = 0.0f;
                for(j=0;j<8;j++) angvel[i][j]=0.0f,angacc[i][j]=0.0f,cogaccAB[i][j]=0.0f;
                for(j=0;j<17;j++) xz_cog[i][j]=0.0f;
                for(j=0;j<28;j++) transvel[i][j]=0.0f,transacc[i][j]=0.0f;
        }

        for(i=0;i<count;i++)                           // set first column
        {                                              // equal to data file time column
                xz_cog[i][0]=g[i][0];
                transvel[i][0]=g[i][0];
                transacc[i][0]=g[i][0];
                rcomponent[i][0]=tcomponent[i][0]=g[i][0];
        }

        // Calculate the locations of the COG's for all time segments
        XZ_LOCCOG(xz_cog,g,count);

        // Calculate the joint translational velocities and accelerations
        TRANS_VELACC(tforce,xz_cog,g,tcomponent,transvel,transacc,count);

        // Calculate the segment rotational velocities and accelerations
        ANGULAR_VELACC(rforce,g,rcomponent,transacc,angvel,angacc,cogaccAB,count);



        // ============================================================================
        // COMBINING STANCE PHASE AND SWING PHASE

        // Heel strike for the oppsite foot occurs at 'shs/2' or ohs
        // therefore, overlap the force traces for legs and arms by
        // shs/2 and add together.

/*      for (i=fhs;i<ohs;i++)
        {
                for (j=5;j<15;j++) force[i][j] += force[i+(ohs-fhs)][j];
        }

        for (i=fhs;i<ohs;i++)
        {
                for (j=5;j<15;j++) tforce[i][j] += tforce[i+(ohs-fhs)][j];
        }
*/
        //============================================================================


        //============================================================================
        // OUTPUT TO FILE OUTPUT.ASC
/*
        int width=8;
        float totalf = 0.0f;

        ofstream outfile('output.asc',ios::app);
        outfile<<'     THIS IS THE FORCE OUTPUT AT LIMB COG FOR THE Y DIRECTION\n\n';
        outfile<<setw(4)<<'Row';
        outfile<<setw(width)<<'Time'<<setw(width)<<'Hd-Sh'<<setw(width)<<'Sh-Hp'
                <<setw(width)<<'Sh-Eb'<<setw(width)<<'Eb-Wr'<<setw(width)<<'Hp-Kn'
                <<setw(width)<<'Kn-Ak'<<setw(width)<<'Hl-To'<<setw(width)<<'TOTAL';
        outfile<<'\n\n';
*/
    ofstream outfile('output.asc',ios::app);
        int width=8;
        for (i=fhs-1;i<ohs;i++)
        {
```

```
                outfile <<setiosflags(ios::fixed);
        //      for
                (j=0;j<13;j++)outfile<<setw(width)<<setprecision(3)<<tcomponent[i][j];
        //      for
                (j=0;j<13;j++)outfile<<setw(width)<<setprecision(3)<<rcomponent[i][j];
                outfile <<setw(width)<<setprecision(3)<<g[i][0];
                outfile <<setw(width)<<setprecision(3)<<tforce[i];
        //      outfile <<setw(width)<<setprecision(3)<<rforce[i];
                outfile<<'\n';
        }
        outfile <<'\n';
/*      for (i=0;i<count;i++)
        {
                outfile <<setw(4)<<i;
                outfile <<setiosflags(ios::fixed);
                outfile <<setw(width)<<setprecision(3)<<g[i][0];
                for (j=0;j<8;j++) outfile<<setw(width)<<setprecision(3)<<angvel[i][j];
                outfile<<'\n';
        }
*/
//      outfile.close();

/*      ofstream out('velacc.asc',ios::app);
        out     <<setiosflags(ios::fixed);
        for (i=0;i<28;i++) out<<setw(8)<<i;
        out<<'\n';
//      for(i=0;i<shs;i++)
//      {
//              out     <<setw(8)<<i;
//              for (j=0;j<28;j++) out<<setw(8)<<setprecision(3)<<transacc[i][j];
//              out<<'\n';
//      }
//      out<<'\n\n';
        for(i=0;i<shs;i++)
        {
                out     <<setw(8)<<i;
                for (j=0;j<28;j++)      out<<setw(8)<<setprecision(3)<<velocity[i][j];
                out<<'\n';
        }
        out.close();
*/

        delete [] g;
        delete [] transvel;
        delete [] transacc;
        delete [] angvel;
        delete [] angacc;
        delete [] cogaccAB;
        delete [] xz_cog;

        return 0;
}


//-------------------------------------------------------------------------
//      XZ_LOCCOG function
//
//      This function works out the position of the COG for all limbs at all time
//      segments and places the results in a two dimensional matrix
//      xz_cog[# of rows][0-14].  0-14 is X & Y locations for the 7 COG's.
//      (foot, lower leg, upper leg, trunk, head, lower arm, upper arm)
//-------------------------------------------------------------------------

void XZ_LOCCOG(float (*xz_cog)[17],float (*data)[28],int lastrow)
{
        float delta_x=0.0f;
        float delta_z=0.0f;

        for (i=0;i<lastrow;i++)
        {
                // neck
                delta_x = data[i][25]-data[i][16];
                delta_z = data[i][27]-data[i][18];
                xz_cog[i][1]= data[i][25]- 0.43f * delta_x;
                xz_cog[i][2]= data[i][27]- 0.43f * delta_z;

                // upper arm
                delta_x = data[i][16]-data[i][19];
                delta_z= data[i][18]-data[i][21];
                xz_cog[i][3]= data[i][16]- 0.48f * delta_x;
```

```
                xz_cog[i][4]= data[i][18]- 0.48f * delta_z;

                // lower arm
                delta_x = data[i][19]-data[i][22];
                delta_z= data[i][21]-data[i][24];
                xz_cog[i][5]= data[i][19]- 0.41f * delta_x;
                xz_cog[i][6]= data[i][21]- 0.41f * delta_z;

                // trunk
                delta_x = data[i][16]-data[i][13];
                delta_z= data[i][18]-data[i][15];
                xz_cog[i][7]= data[i][16]- 0.54f * delta_x;
                xz_cog[i][8]= data[i][18]- 0.54f * delta_z;

                // upper leg
                delta_x = data[i][13]-data[i][10];
                delta_z= data[i][15]-data[i][12];
                xz_cog[i][9]= data[i][13]- 0.41f * delta_x;
                xz_cog[i][10]= data[i][15]- 0.41f * delta_z;

                // lower leg
                delta_x = data[i][10]-data[i][4];
                delta_z= data[i][12]-data[i][6];
                xz_cog[i][11]= data[i][10]- 0.44f * delta_x;
                xz_cog[i][12]= data[i][12]- 0.44f * delta_z;

                // segment from ankle to heel
                delta_x = data[i][4]-data[i][7];
                delta_z= data[i][6]-data[i][9];
                xz_cog[i][13]= data[i][4]- 0.50f * delta_x;
                xz_cog[i][14]= data[i][6]- 0.50f * delta_z;

                // foot
                delta_x = data[i][7]-data[i][1];
                delta_z= data[i][9]-data[i][3];
                xz_cog[i][15]= data[i][7]- 0.47f * delta_x;
                xz_cog[i][16]= data[i][9]- 0.47f * delta_z;
        }

        return;
}


//-------------------------------------------------------------------------------
//      TRANS_VELACC function
//
//      This function works out the translational velocities and accelerations
//      for each joint and limb COG from the input data.
//-------------------------------------------------------------------------------

void TRANS_VELACC(float tforce[],float (*xz_cog)[17],float (*data)[28],float
(*tcomponent)[13],float (*transvel)[28],float (*transacc)[28],int lastrow)
{
        float delta_x=0.0f;
        float delta_z=0.0f;
        float delta_t=0.01f;

        for(i=2;i<lastrow;i++)
        {
                for (j=3;j<28;j+=3)
                {
                        delta_x = data[i][j-2]-data[i-2][j-2];
                        delta_z= data[i][j]-data[i-2][j];
                        transvel[i-1][j-2] = delta_x/delta_t;
                        transvel[i-1][j]   = delta_z/delta_t;

                        if(i==2) continue;
                        else if (i==3) continue;

                        transacc[i-2][j-2] = (transvel[i-1][j-2] - transvel[i-3][j-
                        2])/delta_t;
                        transacc[i-2][j]   = (transvel[i-1][j] - transvel[i-
                        3][j])/delta_t;
                }
        }

        // ============================================================
        //  Working out the force due to the vertical linear accelerations
        //      on the limb centre of gravities.
        // ============================================================
```

```
        // limb weight as a fraction of the total body mass
        // total body mass of 0.102kg gives a weight of 1 N due to gravity
        // numbers from Clauser instead of Dempster for trial run
        const float bodymass    = 0.102f;
        const float wt_head_neck = 0.084f * bodymass;
        const float wt_trunk = 0.500f * bodymass;
        const float wt_uarm = 0.028f * bodymass;
        const float wt_larm = 0.023f * bodymass;
        const float wt_uleg = 0.100f * bodymass;
        const float wt_lleg = 0.043f * bodymass;
        const float wt_foot = 0.014f * bodymass;

        float (*cogvel)[17];
        cogvel = new float [lastrow][17];
        float (*cogacc)[17];
        cogacc = new float [lastrow][17];

        for (i=0;i<lastrow;i++)       //initialise array
        {
                for(j=0;j<17;j++) cogvel[i][j]=cogacc[i][j]=0.0f;
        }

        for(i=2;i<lastrow;i++)
        {
                for (j=2;j<17;j+=2)
                {
                        delta_x = xz_cog[i][j-1]-xz_cog[i-2][j-1];
                        delta_z= xz_cog[i][j]-xz_cog[i-2][j];
                        cogvel[i-1][j-1] = delta_x/delta_t;
                        cogvel[i-1][j]   = delta_z/delta_t;

                        if(i==2) continue;
                        else if (i==3) continue;

                        cogacc[i-2][j-1] = (cogvel[i-1][j-1] - cogvel[i-3][j-1])/delta_t;
                        cogacc[i-2][j]   = (cogvel[i-1][j] - cogvel[i-3][j])/delta_t;
                }
        }
        int offset = 0;
        for (i=0;i<lastrow;i++)
        {
                if(i+101>=lastrow) offset=2*101;
                tforce[i]=      wt_head_neck * (cogacc[i][2] + 9.81f)+
                                wt_uarm         * (cogacc[i][4] + 9.81f)+
                                wt_larm         * (cogacc[i][6] + 9.81f)+
                                wt_trunk        * (cogacc[i][8] + 9.81f)+
                                wt_uleg         * (cogacc[i][10] + 9.81f)+
                                wt_lleg         * (cogacc[i][12] + 9.81f)+
                                wt_foot         * (cogacc[i][16] + 9.81f)+
                                wt_uarm         * (cogacc[i+98-offset][4] + 9.81f)+
                                wt_larm         * (cogacc[i+98-offset][6] + 9.81f)+
                                wt_uleg         * (cogacc[i+98-offset][10] + 9.81f)+
                                wt_lleg         * (cogacc[i+98-offset][12] + 9.81f)+
                                wt_foot         * (cogacc[i+98-offset][16] + 9.81f);
        }

        offset=0;
        for (i=0;i<lastrow;i++)
        {
                if(i+98>=lastrow) offset=2*98;
                tcomponent[i][1]=wt_head_neck * (cogacc[i][2] + 9.81f);
                tcomponent[i][2]=wt_uarm * (cogacc[i][4] + 9.81f);
                tcomponent[i][3]=wt_larm * (cogacc[i][6] + 9.81f);
                tcomponent[i][4]=wt_trunk * (cogacc[i][8] + 9.81f);
                tcomponent[i][5]=wt_uleg * (cogacc[i][10] + 9.81f);
                tcomponent[i][6]=wt_lleg * (cogacc[i][12] + 9.81f);
                tcomponent[i][7]=wt_foot * (cogacc[i][16] + 9.81f);
                tcomponent[i][8]=wt_uarm * (cogacc[i+98-offset][4] + 9.81f);
                tcomponent[i][9]=wt_larm * (cogacc[i+98-offset][6] + 9.81f);
                tcomponent[i][10]=wt_uleg * (cogacc[i+98-offset][10] + 9.81f);
                tcomponent[i][11]=wt_lleg * (cogacc[i+98-offset][12] + 9.81f);
                tcomponent[i][12]=wt_foot * (cogacc[i+98-offset][16] + 9.81f);
        }

        return;
}


//-------------------------------------------------------------------------
//      ANGULAR_VELACC function
//
```

```
//      This function works out the angular velocities and accelerations
//      for each limb segment from the input data.
//-------------------------------------------------------------------------

void ANGULAR_VELACC(float rforce[],float (*data)[28],float (*rcomponent)[13],float
(*transacc)[28],float (*angvel)[8],float (*angacc)[8],float (*cogaccAB)[8],int lastrow)
{
        float delta_x=0.0f;
        float delta_z=0.0f;
        float delta_t=0.01f;
        float limb_length[8]={0.0f};
        float cog_length[8]={0.0f};

        float (*theta)[8];
        theta = new float [lastrow][8];
        float (*delta_theta)[8];
        delta_theta = new float [lastrow][8];
        float (*accn)[8];
        accn = new float [lastrow][8];
        float (*acct)[8];
        acct = new float [lastrow][8];
        float (*accAB)[8];
        accAB = new float [lastrow][8];
        float (*cogaccn)[8];
        cogaccn = new float [lastrow][8];
        float (*cogacct)[8];
        cogacct = new float [lastrow][8];

        for (i=0;i<lastrow;i++)
        {
                for (j=0;j<8;j++)
                {
                        theta[i][j]=0.0f;
                        delta_theta[i][j]=0.0f;
                        accn[i][j]=0.0f;
                        acct[i][j]=0.0f;
                }
        }


        for(i=0;i<lastrow;i++)
        {
                // neck
                delta_x = data[i][25]-data[i][16];
                delta_z = data[i][27]-data[i][18];
                limb_length[0]=sqrt(delta_x*delta_x + delta_z*delta_z);
                cog_length[0]=0.57*limb_length[0];
                if (delta_x==0.0) delta_x +=0.0001f;          // avoids division by zero
                theta[i][0]= float(atan(delta_z/delta_x));
                if ((delta_x>0.0)&&(delta_z>0.0)) theta[i][0] = PI-theta[i][0];

                else if ((delta_x>0.0)&&(delta_z<0.0)) theta[i][0] = PI-theta[i][0];
                else if ((delta_x<0.0)&&(delta_z<0.0)) theta[i][0] = 2*PI-theta[i][0];
                else if ((delta_x<0.0)&&(delta_z>0.0)) theta[i][0] = -theta[i][0];

                // upper arm
                delta_x = data[i][19]-data[i][16];
                delta_z= data[i][21]-data[i][18];
                limb_length[1]=sqrt(delta_x*delta_x + delta_z*delta_z);
                cog_length[1]=0.48*limb_length[1];
                if (delta_x==0.0) delta_x +=0.0001f;          // avoids division by zero
                theta[i][1]= float(atan(delta_z/delta_x));
                if ((delta_x>0.0)&&(delta_z>0.0)) theta[i][1] = PI-theta[i][1];

                else if ((delta_x>0.0)&&(delta_z<0.0)) theta[i][1] = PI-theta[i][1];
                else if ((delta_x<0.0)&&(delta_z<0.0)) theta[i][1] = 2*PI-theta[i][1];
                else if ((delta_x<0.0)&&(delta_z>0.0)) theta[i][1] = -theta[i][1];

                // lower arm
                delta_x = data[i][22]-data[i][19];
                delta_z= data[i][24]-data[i][21];
                limb_length[2]=sqrt(delta_x*delta_x + delta_z*delta_z);
                cog_length[2]=0.41*limb_length[2];
                if (delta_x==0.0) delta_x +=0.0001f;          // avoids division by zero
                theta[i][2]= float(atan(delta_z/delta_x));
                if ((delta_x>0.0)&&(delta_z>0.0)) theta[i][2] = PI-theta[i][2];

                else if ((delta_x>0.0)&&(delta_z<0.0)) theta[i][2] = PI-theta[i][2];
                else if ((delta_x<0.0)&&(delta_z<0.0)) theta[i][2] = 2*PI-theta[i][2];
                else if ((delta_x<0.0)&&(delta_z>0.0)) theta[i][2] = -theta[i][2];
```

```
        // trunk
        delta_x = data[i][16]-data[i][13];
        delta_z= data[i][18]-data[i][15];
        limb_length[3]=sqrt(delta_x*delta_x + delta_z*delta_z);
        cog_length[3]=0.46*limb_length[3];
        if (delta_x==0.0) delta_x +=0.0001f;          // avoids division by zero
        theta[i][3]= float(atan(delta_z/delta_x));
        if ((delta_x>0.0)&&(delta_z>0.0)) theta[i][3] = PI-theta[i][3];

        else if ((delta_x>0.0)&&(delta_z<0.0)) theta[i][3] = PI-theta[i][3];
        else if ((delta_x<0.0)&&(delta_z<0.0)) theta[i][3] = 2*PI-theta[i][3];
        else if ((delta_x<0.0)&&(delta_z>0.0)) theta[i][3] = -theta[i][3];

        // upper leg
        delta_x = data[i][13]-data[i][10];
        delta_z= data[i][15]-data[i][12];
        limb_length[4]=sqrt(delta_x*delta_x + delta_z*delta_z);
        cog_length[4]=0.59*limb_length[4];
        if (delta_x==0.0) delta_x +=0.0001f;          // avoids division by zero
        theta[i][4]= float(atan(delta_z/delta_x));
        if ((delta_x>0.0)&&(delta_z>0.0)) theta[i][4] = PI-theta[i][4];

        else if ((delta_x>0.0)&&(delta_z<0.0)) theta[i][4] = PI-theta[i][4];
        else if ((delta_x<0.0)&&(delta_z<0.0)) theta[i][4] = 2*PI-theta[i][4];
        else if ((delta_x<0.0)&&(delta_z>0.0)) theta[i][4] = -theta[i][4];

        // lower leg
        delta_x = data[i][10]-data[i][4];
        delta_z= data[i][12]-data[i][6];
        limb_length[5]=sqrt(delta_x*delta_x + delta_z*delta_z);
        cog_length[5]=0.56*limb_length[5];
        if (delta_x==0.0) delta_x +=0.0001f;          // avoids division by zero
        theta[i][5]= float(atan(delta_z/delta_x));
        if ((delta_x>0.0)&&(delta_z>0.0)) theta[i][5] = PI-theta[i][5];

        else if ((delta_x>0.0)&&(delta_z<0.0)) theta[i][5] = PI-theta[i][5];
        else if ((delta_x<0.0)&&(delta_z<0.0)) theta[i][5] = 2*PI-theta[i][5];
        else if ((delta_x<0.0)&&(delta_z>0.0)) theta[i][5] = -theta[i][5];

        // segment from heel to the ankle
        delta_x = data[i][4]-data[i][7];
        delta_z= data[i][6]-data[i][9];
        limb_length[6]=sqrt(delta_x*delta_x + delta_z*delta_z);
        cog_length[6]=0.0f;
        if (delta_x==0.0) delta_x +=0.0001f;          // avoids division by zero
        theta[i][6]= float(atan(delta_z/delta_x));
        if ((delta_x>0.0)&&(delta_z>0.0)) theta[i][6] = PI-theta[i][6];

        else if ((delta_x>0.0)&&(delta_z<0.0)) theta[i][6] = PI-theta[i][6];
        else if ((delta_x<0.0)&&(delta_z<0.0)) theta[i][6] = 2*PI-theta[i][6];
        else if ((delta_x<0.0)&&(delta_z>0.0)) theta[i][6] = -theta[i][6];

        // foot
        delta_x = data[i][1]-data[i][7];
        delta_z= data[i][3]-data[i][9];
        limb_length[7]=sqrt(delta_x*delta_x + delta_z*delta_z);
        cog_length[7]=0.47*limb_length[7];
        if (delta_x==0.0) delta_x +=0.0001f;          // avoids division by zero
        theta[i][7]= float (atan(delta_z/delta_x));
        if ((delta_x>0.0)&&(delta_z>0.0)) theta[i][7] = PI-theta[i][7];

        else if ((delta_x>0.0)&&(delta_z<0.0)) theta[i][7] = PI-theta[i][7];
        else if ((delta_x<0.0)&&(delta_z<0.0)) theta[i][7] = 2*PI-theta[i][7];
        else if ((delta_x<0.0)&&(delta_z>0.0)) theta[i][7] = -theta[i][7];
}

//  Calculates the angular velocity for each segment
for (i=2;i<lastrow;i++)
{
        for (j=0;j<8;j++)
        {
                delta_theta[i-1][j] = theta[i][j]-theta[i-2][j];
                if (theta[i][j]-theta[i-2][j]>(3*2*PI/4)) delta_theta[i-1][j] = -
                (2*PI-delta_theta[i-1][j]);
                if (theta[i][j]-theta[i-2][j]<(-3*2*PI/4)) delta_theta[i-1][j] =
                2*PI+delta_theta[i-1][j];
                angvel[i-1][j] = delta_theta[i-1][j]/delta_t;
        }
}

// Calculates the angular acceleration for each segment
```

```
        for (i=3;i<lastrow;i++)
        {
                for (j=0;j<8;j++)
                {
                        angacc[i-1][j] = (angvel[i][j] - angvel[i-2][j])/delta_t;
                }
        }


        // *===================================================================
        //      Computing the normal and tangential acceleration  at the joints
        //      like in Bobbert's paper (1992)  equation 3 pp.225
        //
        // *===================================================================

        for (i=2;i<lastrow;i++)
        {
                for (j=0;j<8;j++)
                {
                        accn[i][j] =
                        limb_length[j]*(angvel[i][j]*angvel[i][j])*sin(theta[i][j]);
                        acct[i][j] = limb_length[j]*angacc[i][j]*cos(theta[i][j]);
                        accAB[i][j]=  acct[i][j]-accn[i][j];
                }
        }

//      ofstream outfile("output.asc",ios::app);
//      int width=8;
//      for (i=41;i<140;i++)
//      {
///             outfile<<setiosflags(ios::fixed);
//              outfile<<setw(width)<<setprecision(3)<<data[i][0];
//              outfile<<setw(width)<<setprecision(3)<<theta[i][4]
//                              <<setw(width)<<setprecision(3)<<angvel[i][4]
//                              <<setw(width)<<setprecision(3)<<angacc[i][4]
//                              <<setw(width)<<setprecision(3)<<acct[i][4]
//                              <<setw(width)<<setprecision(3)<<accn[i][4]
//                              <<setw(width)<<setprecision(3)<<accAB[i][4]
//                              <<setw(width)<<setprecision(3)<<transacc[i][15]
//                              <<setw(width)<<setprecision(3)<<transacc[i][12];
//      //      outfile<<setw(width)<<setprecision(3)<<transacc[i][12]
//      //                      <<setw(width)<<setprecision(3)<<transacc[i][6]
//      //                      <<setw(width)<<setprecision(3)<<cogaccAB[i][5];
//      //      for
(j=0;j<13;j++)outfile<<setw(width)<<setprecision(3)<<rcomponent[i][j];
//
//              outfile<<"\n";
//      }
        // *====================
        //      Computing the normal and tangential vertical acceleration  at the COG,s
        //
        // *====================
        for (i=2;i<lastrow;i++)
        {
                for (j=0;j<8;j++)
                {
                        cogaccn[i][j] =
cog_length[j]*(angvel[i][j]*angvel[i][j])*sin(theta[i][j]);
                        cogacct[i][j] = cog_length[j]*angacc[i][j]*cos(theta[i][j]);
                        cogaccAB[i][j]=  cogacct[i][j]-cogaccn[i][j];
                }
        }

        // ===================================================================
        //      Working out the force due to the normal
        //      and tangential vertical accelerations
        //      on the limb centre of gravities.
        // ===================================================================

        // limb weight as a fraction of the total body mass
        // total body mass of 0.102kg gives a weight of 1 N due to gravity
        const float bodymass    = 0.102f;
        const float wt_head_neck = 0.084f * bodymass;
        const float wt_trunk = 0.500f * bodymass;
        const float wt_uarm = 0.028f * bodymass;
        const float wt_larm = 0.023f * bodymass;
        const float wt_uleg = 0.100f * bodymass;
        const float wt_lleg = 0.043f * bodymass;
        const float wt_foot = 0.014f * bodymass;

        int offset = 0;
```

```
/*      for (i=0;i<lastrow;i++)
        {
                if(i+98>=lastrow) offset=2*98;
                rforce[i]=      wt_head_neck * (cogaccAB[i][0]+transacc[i][18] + 9.81f)+
                        wt_uarm         * (cogaccAB[i][1]+transacc[i][21] + 9.81f)+
                        wt_larm         * (cogaccAB[i][2]+transacc[i][24] + 9.81f)+
                        wt_trunk        * (cogaccAB[i][3]+transacc[i][15] + 9.81f)+
                        wt_uleg         * (cogaccAB[i][4]+transacc[i][12] + 9.81f)+
                        wt_lleg         * (cogaccAB[i][5]+transacc[i][6] + 9.81f)+
                wt_foot         * (cogaccAB[i][7]+transacc[i][3] + 9.81f)+
                wt_uarm         * (cogaccAB[i+98-offset][1]+transacc[i][21] + 9.81f)+
                wt_larm         * (cogaccAB[i+98-offset][2]+transacc[i][24] + 9.81f)+
                wt_uleg         * (cogaccAB[i+98-offset][4]+transacc[i][12] + 9.81f)+
                wt_lleg         * (cogaccAB[i+98-offset][5]+transacc[i][6] + 9.81f)+
                wt_foot         * (cogaccAB[i+98-offset][7]+transacc[i][3] + 9.81f);
}
*/
//      for (i=0;i<lastrow;i++)       rforce[i]=accAB[i][5];


        for (i=0;i<lastrow;i++)
        {
                accAB[i][7] += transacc[i][3];
                accAB[i][5] += transacc[i][6];
                accAB[i][4] += transacc[i][12];//*/accAB[i][5];
                accAB[i][3] += /*transacc[i][15];//*/accAB[i][4];
                accAB[i][0] += accAB[i][3];
                accAB[i][1] += accAB[i][3];
                accAB[i][2] += accAB[i][1];
        }
        for (i=0;i<lastrow;i++)
        {
                cogaccAB[i][7] += transacc[i][3];
                cogaccAB[i][5] += transacc[i][6];
                cogaccAB[i][4] += transacc[i][12];//*/accAB[i][5];
                cogaccAB[i][3] +=/* transacc[i][15];//*/accAB[i][4];
                cogaccAB[i][0] += accAB[i][3];
                cogaccAB[i][1] += accAB[i][3];
                cogaccAB[i][2] += accAB[i][1];
        }

        for (i=0;i<lastrow;i++)
        {
                if(i+98>=lastrow) offset=2*98;
                rforce[i]=      wt_head_neck * (cogaccAB[i][0] + 9.81f)+
                                wt_uarm         * (cogaccAB[i][1] + 9.81f)+
                                wt_larm         * (cogaccAB[i][2] + 9.81f)+
                                wt_trunk        * (cogaccAB[i][3] + 9.81f)+
                                wt_uleg         * (cogaccAB[i][4] + 9.81f)+
                                wt_lleg         * (cogaccAB[i][5] + 9.81f)+
                                wt_foot         * (cogaccAB[i][7] + 9.81f)+
                                wt_uarm         * (cogaccAB[i+98-offset][1] + 9.81f)+
                                wt_larm         * (cogaccAB[i+98-offset][2] + 9.81f)+
                                wt_uleg         * (cogaccAB[i+98-offset][4] + 9.81f)+
                                wt_lleg         * (cogaccAB[i+98-offset][5] + 9.81f)+
                                wt_foot         * (cogaccAB[i+98-offset][7] + 9.81f);
        }

        offset = 0;
        for (i=0;i<lastrow;i++)
        {
                if(i+98>=lastrow) offset=2*98;
                rcomponent[i][1]=wt_head_neck * (cogaccAB[i][0] + 9.81f);
                rcomponent[i][2]=wt_uarm * (cogaccAB[i][1] + 9.81f);
                rcomponent[i][3]=wt_larm * (cogaccAB[i][2] + 9.81f);
                rcomponent[i][4]=wt_trunk * (cogaccAB[i][3] + 9.81f);
                rcomponent[i][5]=wt_uleg * (cogaccAB[i][4] + 9.81f);
                rcomponent[i][6]=wt_lleg * (cogaccAB[i][5] + 9.81f);
                rcomponent[i][7]=wt_foot * (cogaccAB[i][7] + 9.81f);
                rcomponent[i][8]=wt_uarm * (cogaccAB[i+98-offset][1] + 9.81f);
                rcomponent[i][9]=wt_larm * (cogaccAB[i+98-offset][2] + 9.81f);
                rcomponent[i][10]=wt_uleg * (cogaccAB[i+98-offset][4] + 9.81f);
                rcomponent[i][11]=wt_lleg * (cogaccAB[i+98-offset][5] + 9.81f);
                rcomponent[i][12]=wt_foot * (cogaccAB[i+98-offset][7] + 9.81f);
        }

/*      for (i=0;i<lastrow;i++)
        {
                if(i+98>=lastrow) offset=2*98;
        rcomponent[i][1]=wt_head_neck * (cogaccAB[i][0]+transacc[i][18] + 9.81f);
        rcomponent[i][2]=wt_uarm * (cogaccAB[i][1]+transacc[i][21] + 9.81f);
```

```
        rcomponent[i][3]=wt_larm * (cogaccAB[i][2]+transacc[i][24] + 9.81f);
        rcomponent[i][4]=wt_trunk * (cogaccAB[i][3]+transacc[i][15] + 9.81f);
        rcomponent[i][5]=wt_uleg * (cogaccAB[i][4]+transacc[i][12] + 9.81f);
        rcomponent[i][6]=wt_lleg * (cogaccAB[i][5]+transacc[i][6] + 9.81f);
        rcomponent[i][7]=wt_foot * (cogaccAB[i][7]+transacc[i][3] + 9.81f);
        rcomponent[i][8]=wt_uarm * (cogaccAB[i+98-offset][1]+transacc[i][21] + 9.81f);
        rcomponent[i][9]=wt_larm * (cogaccAB[i+98-offset][2]+transacc[i][24] + 9.81f);
        rcomponent[i][10]=wt_uleg * (cogaccAB[i+98-offset][4]+transacc[i][12] + 9.81f);
        rcomponent[i][11]=wt_lleg * (cogaccAB[i+98-offset][5]+transacc[i][6] + 9.81f);
        rcomponent[i][12]=wt_foot * (cogaccAB[i+98-offset][7]+transacc[i][3] + 9.81f);
        }
*/
        return;
}
```

```
        rcomponent[i][3]=wt_larm * (cogaccAB[i][2]+transacc[i][24] + 9.81f);
        rcomponent[i][4]=wt_trunk * (cogaccAB[i][3]+transacc[i][15] + 9.81f);
        rcomponent[i][5]=wt_uleg * (cogaccAB[i][4]+transacc[i][12] + 9.81f);
        rcomponent[i][6]=wt_lleg * (cogaccAB[i][5]+transacc[i][6] + 9.81f);
        rcomponent[i][7]=wt_foot * (cogaccAB[i][7]+transacc[i][3] + 9.81f);
        rcomponent[i][8]=wt_uarm * (cogaccAB[i+98-offset][1]+transacc[i][21] + 9.81f);
        rcomponent[i][9]=wt_larm * (cogaccAB[i+98-offset][2]+transacc[i][24] + 9.81f);
        rcomponent[i][10]=wt_uleg * (cogaccAB[i+98-offset][4]+transacc[i][12] + 9.81f);
        rcomponent[i][11]=wt_lleg * (cogaccAB[i+98-offset][5]+transacc[i][6] + 9.81f);
        rcomponent[i][12]=wt_foot * (cogaccAB[i+98-offset][7]+transacc[i][3] + 9.81f);
        }
*/
        return;
}
```